Biodegradable pulsatile release technologies for viral vector based vaccinations

Thesis submitted for the degree of Doctor of Philosophy in Infection, Immunology & Translational Medicine

Michaelmas 2018

Supervisor: Prof. Adrian V.S. Hill

Christos Krastev

Magdalen College

Student number: 628044

Word count: ~35200 (excluding bibliography, figures and tables)

Abstract

Vaccines are arguably the greatest public health intervention of modern era medicine. Most vaccines, in order to be effective require multiple doses. This is disadvantageous as there is an increasing trend towards non-compliance with subsequent doses. Viral vectored vaccines represent arguably the next generation of vaccines but they too often require a heterologous prime-boost approach such as the use of Adenoviral-MVA vectors. This thesis describes work utilising biodegradable microparticulate and non-microparticulate technologies to attempt to transform vaccination regimes from multiple into one single injection. Both technologies were tested using the heterologous Adenoviral-MVA prime-boost regime. A novel and virus-tailored encapsulation using the solvent triacetin and qPCR-based quantification methodology is proposed for the microencapsulation of MVA virus in biodegradable PLGA or PLA microparticles. Immunogenicity studies comparing routine prime-boost using 2 injections compared to single-dose administration of soluble Adenovirus with encapsulated MVA virus in PLA microparticles, showed comparable immune responses after 8 weeks. However true pulsatile release kinetic based on T-cell and antibody response kinetics was not observed. When experimentally tested with malarial sporozoite challenge the same formulation failed to provide comparable protective immune responses with a single immunisation after 5 weeks. Further work is still required to manufacture more uniform and reproducible formulations. This work is a significant improvement in the field of viral vector encapsulation in solid polymeric matrices, which could benefit not only human vaccination but also veterinary, including fish vaccination, improving quality of life, reducing public health costs and ultimately saving more lives.

Acknowledgements

I would like to thank God for guiding me through and providing me with external strength to complete this work. Secondly, the encouragement from my whole family: Rado, Agathi and Ioanna.

Thirdly, I would like to express my gratitude to my supervisor Adrian Hill who was understanding and to Adam Walters for guidance.

I would like to thank all the members of the Jenner Institute but in particular Ahmed Salman for his help with in vivo imaging and challenge studies.

Lastly, I would like to thank my funding body the Wellcome Trust for the opportunity to come to Oxford.

Table of contents

1 Chapter 1: Introduction 16

1.1 Vaccine immunisation schedules and coverage 16

1.2 Microencapsulation technology for single dose vaccinations 17

1.2.1 Historical overview of vaccine microencapsulation 18

1.2.2 Biodegradable polymers 18

1.2.3 PLGA and PLA polymers for microparticle production 19

1.2.4 Microparticulate PLGA carriers for vaccines 20

1.2.5 Preparation techniques for microparticles 21

1.3 The human immune system 25

1.3.1 Innate immune system 25

1.3.2 Adaptive immune system 27

1.3.3 How vaccines work 39

1.3.4 Adjuvants in vaccinations 41

1.3.5 Conjugate vaccines 42

1.3.6 Virus-like particles (VLPs) 43

1.3.7 Self-amplifying mRNA vaccines 44

1.3.8 Viral vector vaccines 44

1.4 Malaria 47

1.4.1 Malaria life cycle 47

1.4.2 Malaria vaccine intervention using viral vectors 49

1.4.3 Controlled release MP sytems for malaria vaccine development 50

1.5 DPhil thesis aims 51

2 Chapter 2: Materials & Methods 53

2.1 Materials 53

2.1.1 Reagents 53

2.2 Cell culture 54

2.3 Murine standardised quantitative whole IgG ELISA 54

2.4 Animal work 55

2.4.1 Mouse immunisation 55

2.4.2 Viral vectored vaccines 56

2.4.3 Mouse peripheral blood mononuclear cells (PBMCs) collection and preparation 56

2.4.4 Mouse splenocyte preparation 57

2.4.5 Ex-vivo IFN-γ PBMC ELISPOT assay 57

2.4.6 Ex-vivo IFN-γ spleen ELISPOT assay 58
2.4.7 PBMCs intracellular cytokine (ICS) staining 58
2.4.8 Splenocyte ICS staining 60
2.4.9 Plaque assay for MVA virus 60
2.4.10 Scanning Electron microscopy (SEM) 61
2.4.11 Transmission Electron microscopy (TEM) 61
2.4.12 TEM immunostaining for MVA virus 62
2.4.13 Intraparticle MVA distribution 62
2.4.14 Lyophilisation (freeze drying) 62
2.4.15 In vivo imaging 63
2.4.16 Production of infectious chimeric parasite in sporozoite form 63
2.4.17 Blood smear preparation with Giemsa staining 64
2.4.18 Challenge of immunised experimental mice with PfLSA1 sporozoites 64
2.4.19 In vitro MVA release assay from microparticles 65
2.4.20 Microencapsulation of BSA-FITC in PLGA or PLA microparticles using dichloromethane (DCM) as solvent 65
2.4.21 Microencapsulation of BSA-FITC in PLGA:PLA MPs using DCM as solvent 66
2.4.22 Microencapsulation of MVATIPeGFP virus in PLGA MPs using DCM as the solvent 66
2.4.23 Microencapsulation of MVA virus in polymeric MPs using triacetin as the solvent ... 67
2.4.24 Characterisation of MP size and surface morphology 67
2.4.25 Determination of encapsulation efficiency of BSA-FITC in MPs 67
2.4.26 Critical points for survival of MVA virus after exposure to solvents, sonication or lyophilisation 68
2.4.27 Measurement of NaOH lysed MVA virus using protein assay 68
2.4.28 Data analysis 69
2.4.29 Flowcytometry analysis 69
2.4.30 Electrospraying processing of MVA virus 69
2.4.31 MVA virus bulk and purification 70
2.4.32 Sterility test for bulked up MVA viruses 71
2.4.33 Free-flow electrophoresis (FFE) 72
2.4.34 Quantitative PCR (qPCR) for MVA 72
2.4.35 Primer design 72
2.4.36 Viral DNA extraction 74
2.4.37 qPCR setup 74
2.4.38 SYBR green based qPCR protocol 75
2.4.39 Taqman probe based qPCR protocol 76

3 Chapter 3: MVA virus encapsulation & quantification 78
3.1 Introduction 78
3.2 Vaccine encapsulation into polymeric microparticles 80
3.3 BSA-FITC loaded microparticles.....80
3.4 MVA encapsulation processing stability studies 84
3.5 MVA extraction strategies for quantification of infectious virions 95
3.5.1 Molecular weight based separation.....96
3.5.2 Chemical and enzymatic extraction 98
3.6 Ultracentrifugation and separation on sucrose gradient based on buoyancy 100
3.7 Ultracentrifugation and separation based on buoyancy in water-free environment in pure triacetin.....102
3.8 Separation based on surface polarity.....105
3.9 Discussion 108
4 Chapter 4: Development of a qPCR based protocol for quantification of infectious encapsulated MVA 118
4.1 Introduction 118
4.2 Universal viral quantification methods 119
4.3 Quantification of encapsulated MVA with qPCR.....120
4.4 Quality controls for qPCR methodology.....126
4.5 Discussion 129
5 Chapter 5: Microparticle preparation, optimisation & characterisation 137
5.1 Introduction 137
5.2 Quantification of encapsulated viral content.....137
5.3 Microparticle batch optimisation and characterisation 138
5.4 Intraparticle location of MVA virus after encapsulation 146
5.5 Discussion 147
6 Chapter 6: In vivo & in vitro studies with MP technology.....152
6.1 Introduction 152
6.2 In vivo immunogenicity studies 152
6.3 In vivo MP biodistribution and real time release kinetics using in vivo imaging...159
6.4 Proof-of-concept immunogenicity study: single injection vs routine double injection 166

6.5 In vivo protective efficacy of single injection technology with sporozoite challenge 171
6.6 In vitro release kinetics of MP batches 175
6.7 MVA encapsulation by electrospraying 177
6.8 Discussion 180
7 Chapter 7: Thesis summary, future prospects & conclusion 191
7.1 Microparticulate delivery system for MVA virus 191
7.1.1 In vitro studies 191
7.1.2 In vivo studies using encapsulated MVA 192
7.2 Future prospects 195
7.2.1 Microparticulate delivery of MVA in Adenovirus-MVA prime boost regime (Chapters 5&6) 195
7.3 Overall conclusion 196
8 References 198

Table of Figures

Figure 1.1 Chemical structure of PLGA and its hydrolysis process 19
Figure 1.2 Different microcapsule architectures 21
Figure 1.3 Single emulsion solvent evaporation method for microencapsulation 22
Figure 1.4 Double emulsion solvent evaporation methods for microencapsulation 23
Figure 1.5 A simplified overview of dendritic cell (DC)-mediated antigen specific CD4+ and CD8+ T-cell clonal expansion. 28
Figure 1.6 Model for development of human T-cell memory 33
Figure 1.7 Classical MHC-class I presentation 36
Figure 1.8 Classical MHC-class II presentation 37
Figure 1.9 Schematic overview of how vaccines work 40
Figure 1.10 Overview of vaccinia production cycle 46
Figure 1.11 Life cycle of Plasmodium species 49
Figure 3.1 Graphical thesis concept for a single administration prime-boost regime 81
Figure 3.2 Preparation of microparticles by double emulsion solvent evaporation 82
Figure 3.3 Microparticle morphology 83
Figure 3.4 Quantification of bioactive MVA with plaque assay 85
Figure 3.5 Stability of MVA virus during encapsulation procedure in the absence of PLGA polymer 87
Figure 3.6 In vivo immunogenicity from MVA exposed to solvents, homogenisation and lyophilisation 90
Figure 3.7 Particle size analysis using Accusizer diffractometer 92
Figure 3.8 Diagnostic TEM images of negatively stained MVA virus exposed to DCM and triacetin solvents 93
Figure 3.9 Updated MP formulation procedure for bioactive MVA virus 94
Figure 3.10 Morphology of triacetin based MPs and DCM based MPs 95
Figure 3.11 Attempted extraction procedures to separate encapsulated MVA virus from PLGA polymer and measure infectious virus 97
Figure 3.12 Detection limit of titrated NaOH lysed MVA virus using BCA and micro-BCA assays .. 99
Figure 3.13 Separation of encapsulated MVA from PLGA polymer using ultracentrifugation in sucrose gradient 101
Figure 3.14 Separation of encapsulated MVA from PLGA polymer using ultracentrifugation in pure triacetin 103
Figure 3.15 Free flow electrophoresis (FFE) procedure overview 106
Figure 3.16 Separation of encapsulated MVA from PLGA polymer using Free Flow electrophoresis (FFE) 107
Figure 4.1 Quantitative PCR (qPCR) for determination of encapsulated MVA virus within MP batch 121
Figure 4.2 Establishment of a robust qPCR primer/probe set targeting the E9L DNA polymerase region of MVA virus 123
Figure 4.3 Standard curves for quantification and titration of encapsulated MVA viruses in polymeric MPs 125
Figure 4.4 Establishment of quality controls before planned qPCR work 127
Figure 4.5 Determination on which standard curve preparation procedure to use for proposed qPCR work 128
Figure 5.1 Images of the first 4 MP batches from Table 5.2 141
Figure 5.2 Updated MP procedure with encapsulation efficiencies (EE%) for different polymer formulations 143
Figure 5.3 SEM Morphology of optimised triacetin based MPs 144

Figure 5.4 Effect of long vs short exposure to EtOH on MVA bioactivity and MVA intraparticle distribution 145
Figure 6.1 Scheme to dissect the humoral immune response generated from MVA-loaded MP technology 153
Figure 6.2 In vivo humoral immunogenicity for MVA-loaded MPs only without Adenovirus prime 155
Figure 6.3 T-cell gating strategy 156
Figure 6.4 Characterisation of CD4+ T-cell responses induced following administration of MVA-loaded MPs in mice 157
Figure 6.5 Characterisation of CD8+ T-cell responses induced following administration of MVA-loaded MPs in mice 158
Figure 6.6 Limit of detection (LOD) for luciferase signal for in vivo imaging system 160
Figure 6.7 In vivo imaging following intramuscular administration of MVA luciferase-loaded MPs (Part I - PBS) 162
Figure 6.8 In vivo imaging following intramuscular administration of MVA luciferase-loaded MPs (Part II - PLGA) 162
Figure 6.9 In vivo imaging following intramuscular administration of MVA luciferase-loaded MPs (Part III - PLA) 163
Figure 6.10 In vivo imaging following intramuscular administration of MVA luciferase-loaded MPs (Part IV - Summary) 164
Figure 6.11 Repeat in vivo imaging following intramuscular administration of MVA luciferase-loaded MPs 165
Figure 6.12 Proof-of-concept immunogenicity experiment replacing the prime-boost regime with MVA-loaded MPs 168
Figure 6.13 Characterisation of CD4+ T-cell responses induced following administration of MVA-loaded MPs in mice for proof-of-concept experiment 170
Figure 6.14 Characterisation of CD8+ T-cell responses induced following administration of MVA-loaded MPs in mice for proof-of-concept experiment 171
Figure 6.15 Characterisation of CD4+ T-cell responses induced following administration of MVA-loaded MPs, pre-challenge in mice. 173
Figure 6.16 Characterisation of CD8+ T-cell responses before challenge and survival curve after challenge. 174
Figure 6.17 Cumulative release profiles of MVATIPeGFP from MPs and bioactivity of MVA in acidic environments 177
Figure 6.18 Electrospraying method for MVA encapsulation 178

Table of Tables

Table 1.1 UK's immunisation schedule for 2018-2019 16
Table 2.1 Commercially available reagents used during thesis 53
Table 2.2 Viral vectors used throughout thesis 56
Table 2.3 Primer/probe sets used in this thesis 76
Table 3.1 Immunogenicity from MVA exposed to solvent, homogenisation and lyophilisation 88
Table 4.1 Most commonly used viral quantification protocols 120
Table 5.1 Formula for determination of MVA content in MPs 138
Table 5.2 Table of optimisation steps for encapsulation efficiency with varying processing conditions 140
Table 6.1 Vaccination regime for MVA-loaded MPs only without Adenovirus prime 154
Table 6.2 Vaccination regime for determination of LOD of luciferase signal for IVIS 200 imaging system 159
Table 6.3 Vaccination regime for biodistribution of MVA-loaded MPs 161
Table 6.4 Vaccination regime for repeat in vivo biodistribution of MVA-loaded MPs 164
Table 6.5 Vaccination regime for proof-of-concept immunogenicity experiment 166
Table 6.6 Vaccination schedule for challenge experiment 172

List of Abbreviations

29g	29 gauge
Ab	Antibody
ACK	Ammonium chloride potassium
AcN	Acetonitrile
Adenovirus	Ad
Ag	Antigen
ANOVA	Analysis of Variance
AP	Alkaline phosphatase
APC	Antigen presenting cell
ASPA	Animals Scientific Procedures Act
ATCC	American Type Culture Collection
Balb/c mice	'Bagg Albino c' mice
BCA assay	Bicinchoninic acid assay
bp	Base pair
BSA	Bovine serum albumin
class II-associated invariant chain peptide	CLIP
CMC	Carboxymethylcellulose
Conventional DC	cDC
CRM	Cross-reacting material

CTLs	Cytotoxic T-lymphocytes
DCM	Dichloromethane
DCs	Dendritic cells
DMEM	Dulbecco's modified Eagle's media
DNA	Deoxyribonucleic acid
EDTA	ethylenediaminetetraacetic acid
EEV	Extracellular enveloped virus
eGFP	Enhanced green fluorescent protein
EHDA	Electrohydrodynamic atomisation
ELISA	Enzyme-linked immunosorbent assay
ELISPOT	Enzyme-linked immunosorbent spot
Encapsulation Efficiency	EE
ER	Endoplasmic reticulum
EtA	Ethyl Acetate
EtOH	Ethanol
Fc	Fragment constant
FCS	Foetal calf serum
FFE	Free-flow electrophoresis
FITC	Fluorescein isothiocyanate
follicular helper T-cells	Tfh
Fork-head box P3	FOXP3
GA	Glycolic acid
GM-SCF	Granulocyte-macrophage colony stimulating factor
HMW	High molecular weight
HPV	Human Papilloma virus
HRP	Horseradish peroxidase
i.m.	intramuscularly
i.u.	Infectious units
i.v.	intravenously
ICS	Intracellular staining
IEV	Intracellular enveloped virus
IFN-γ	Interferon-γ
IgG	Immunoglobulin G
IL	Interleukin
IMV	Intracellular mature virus
Invariant chain	Ii

ISAV	Infectious salmon anemia virus
kV	kiloVolt
LA	Lactic acid
LD_{50}	Lethal Dose 50
Limit of detection	LOD
LMW	Low molecular weight
LSA1	Liver stage antigen 1
M	Molar
mA	Milliampere
mAb	Monoclonal antibody
MHC	Major Histocompatibility Complex
MICA	MHC class I chain-related sequence A
Minor Groove Binding	MGB
ml	millilitre
mM	millimolar
MPs	microparticles
MRI	Magnetic Resonance Imaging
mRNA	Messenger RNA
mTorr	milliTorr
MVA	Modified Vaccinia Ankara
Mw	Molecular weight
N_2 gas	Nitrogen gas
NK	Natural Killer
NKG2D	Natural killer group 2D
nm	nanometre
NTC	No template control
OMPC	Meningococcal outer membrane protein complex
P.berghei	*Plasmodium berghei*
P.f.	Plasmodium falciparum
PAMPs	Pathogen-associated molecular patterns
PbCSP	*P. berghei* circumsporozoite protein
PBMC	Peripheral blood mononuclear cell
PBS	Phosphate buffered saline
PCR	Polymerase chain reaction
PEG	Polyethylene glycol
PfCSP	*P. Falciparum* circumsporozoite protein

PfLSA1	*Plasmodium falciparum* liver stage antigen 1
pfu	Plaque forming units
PHA	Phytohemagglutinin
PLA	Polylactic acid
Plasmacytoid DC	pDC
PLGA	Polylactic glycolic acid
PRRs	Pattern recognition receptors
PTFE	Polytetrafluoroethylene
PVA	Polyvinyl alcohol
PvCSP	*P. vivax* circumsporozoite protein
qPCR	Quantitative polymerase chain reaction
RBCs	Red blood cells
regulatory T-cells	Treg
RNA	Ribonucleic acid
ROS	Reactive oxygen species
rpm	Revolutions per minute
RT	Room temperature
s	second
SAM	Self-amplifying mRNA
SEM	Scanning electron microscopy
SFU	Spot forming unit
SIV	Simian immunodeficiency virus
SPADNS	2-(P-sulfophenylazo)-1,8-dihydroxy-3,6-naphthalene disulfate
T_{CM}	Central memory T-cell
TCR	T-cell receptor
TEA	Triethanolamine
T_{Eff}	Effector T-cell
TEM	Transmission electron microscopy
T_{EM}	Effector memory T-cell
Tm	Melting temperature
TMB	3,3’5,5’ Tetramethylbenzidine
TNF-α	Tumour necrosis factor alpha
Transforming growth factor beta	TGF-β
TRAP	Thrombospondin-related adhesion protein
trasporter associated with antigen processing-1/-2	TAP-1, TAP-2

T_{SCM}	Stem cell memory T-cell
UV	Ultraviolet
vDNA	Viral Deoxyribonucleic acid
VLPs	Virus-like particles
VV	Vaccinia virus
WHO	World Health Organisation
μm	micrometre
ρ	density

Introduction

1 Chapter 1: Introduction

One of the greatest scientific chapters in human history was the impact of immunisation on global human and veterinary health. The success in developing vaccines for many life-threatening diseases such as smallpox, polio, rubella, with crowning glories being the eradication of smallpox in humans[1] and rinderpest for cattle[2], has led to the decision to consider vaccines as the greatest public health intervention for the 20th century[3]. From Edward Jenner's empirical use of an animal pox virus[4], to Louis Pasteur's usage of attenuated microorganisms demonstrated with anthrax in sheep and then rabies virus in humans and animals[5], to modern genetic engineering for vaccine development[6] and viral vectored vaccines[7], the field of vaccinology has evolved tremendously over the ages.

1.1 Vaccine immunisation schedules and coverage

As of August 2018 the recommended immunisation for the UK[8], which varies from country to country, is comprised of several vaccines that are administered over time in multiple doses as shown in Table 1.1. Frequencies between each dose for each vaccine vary from few weeks, to months or even years.

Vaccine	Frequency of doses
Inactivated poliovirus	2, 3, 4 months
Hepatitis B virus	2, 3 , 4 months
Human Papilloma virus	Females age 12-13 years 3 doses at 0, 1 and 2 or 6 months
Measles, mumps, rubella	12-13 months, 3 years and 4 months
Rotavirus	2, 3 months
Meningococcal group C	3, 12-13 months, around 14 years
Pneumococcal disease	2, 4, 12-13 months
Heamophilus influenza type b	2, 3, 4, 12-13 months
Diptheria, tetanus, pertussis	2, 3, 4 months, 3.5 years and around 14 years (DT only)

Table 1.1 UK's immunisation schedule for 2018-2019

Despite possessing a number of effective developed vaccines against a broad spectrum of diseases and a steady yearly increase in vaccine coverage worldwide, according to the WHO

vaccine preventable diseases still have a toll of around 1.5 million childhood deaths each year[9]. The reason for these deaths is not just lack of vaccine effectiveness but also lack of adequate vaccine administration worldwide especially in third world countries. The uptake of all 3 doses of diphtheria, tetanus and pertussis vaccine (DTP3) is used by the WHO to measure vaccine coverage nationwide. Worldwide, 86% of children are fully immunised against diphtheria, tetanus and pertussis after receiving all 3 doses of DTP vaccine. The rest, 14%, are either unimmunised or under-immunised, having receiving only one dose of DTP rather the full 3 doses, but both remain at risk of infection with these disease agents (WHO immunisation data). When stripped down, this problem has been identified as a noncompliance issue with immunisation schedules. In developed countries something as simple as missing or delaying vaccination appointments or lack of education about the potential of vaccinations are contributing to this problem[10]. In developing countries, factors are more practical such as limited access to healthcare, general lack of resources and habitation of remote areas[11,12]. A contributing factor that is independent of the developmental status of a nation is the outbreak of war/conflicts and refugee status, with a recent example being in Syria where vaccine compliance fell dramatically and a vaccine preventable polio outbreak occurred in spring 2017[13]. Unfortunately, the requirement of vaccines for multiple booster injections in order to provide robust and durable immunity, impede the successful implementation of nationwide vaccination programmes and disease eradication efforts.

1.2 Microencapsulation technology for single dose vaccinations

Controlled release microparticle-based technology is currently considered as an option for achieving robust and durable immunity after only one injection, rather than multiple which is the current practice[14]. This microparticle-based technology could potentially eliminate the repeated need for booster shots, by reducing the number of administered immunisations and

thus the need of regular clinic visits[15], thereby increasing compliance rates throughout the world irrespective of national developmental status or related contributing factors. Biodegradable microparticles encapsulating the booster vaccine would be administered once and stay in the body as a depot, alongside the soluble priming vaccine. The biodegradable microparticles would in turn release the vaccine over time either by continuous or pulsatile release kinetics, mimicking the repeated immunisation approach currently used in the clinic[16].

1.2.1 Historical overview of vaccine microencapsulation

Over the past 4 decades researchers have strived to develop polymeric biodegradable microcapsule technologies capable for providing immunity after a single injection[17]. Polylactic-co-glycolic acid (PLGA) based microparticles have been extensively studied due to their FDA-approved biocompatibility status[18] and adjustable release kinetics[19]. Early attempts in the 1990s and 2000s with PLGA microparticles encapsulating tetanus toxoid for pulsatile release delivery suggested that immune responses comparable or even superior to the standard prime and boost approach might be achievable[19,20].

1.2.2 Biodegradable polymers

Biodegradable polymers are either naturally occurring or man-made (synthetic) in origin. Once in vivo, they are degraded chemically or enzymatically or both, releasing non-toxic by-products which are removed by normal metabolic pathways. Such materials used today are categorised as follows: 1) synthetic polymers, which are mostly hydrophobic in nature such as: polyanhydrides, α-hydroxy acids which include PLGA, and others; 2) natural polymers which include inorganic substances like hydroxyapatite (commonly used in tissue engineering) or sugars like chitosan, alginate and hyaluronic acid[21,22].

1.2.3 PLGA and PLA polymers for microparticle production

PLGA is a copolymer of polylactic acid (PLA) and polyglycolic acid (PGA) united by an ester bond (Figure 1.1). In water, hydrolytic biodegradation of PLGA occurs via de-esterification (hydrolysis of the ester bonds), breaking it down to its monomeric polymers PLA and PGA. Lactic acid then enters the Krebs cycle whereby it's removed from the body as carbon dioxide and water, whereas glycolic acid is excreted directly via the kidneys or also enters the Krebs cycle similarly to lactic acid[23].

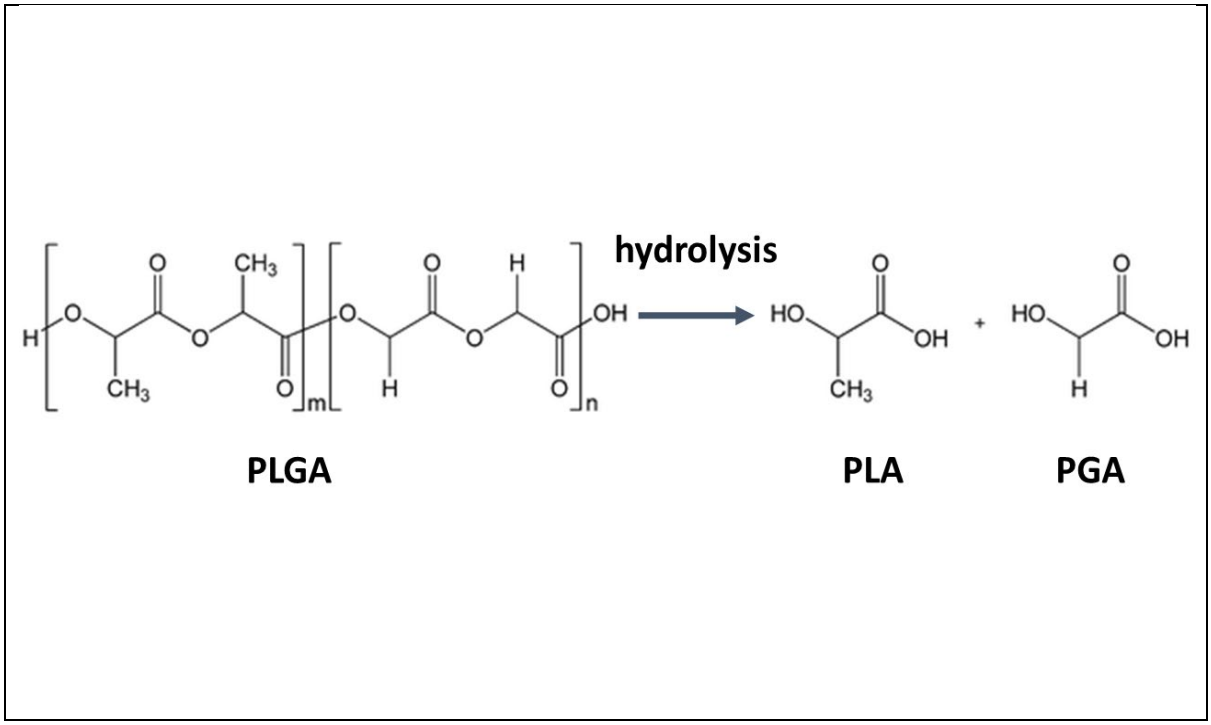


Figure 1.1 Chemical structure of PLGA and its hydrolysis process

Depending on the intrinsic ratio of PLA and PGA used for the polymerisation of PLGA, PLGA inherits different configurations reported in terms of the monomers used (i.e. PLGA 65:35 means a copolymer with intrinsic ratio of 65% lactic acid and 35% glycolic acid). Presence of methyl side group in PLA (Figure 1.1) renders it more hydrophobic than PGA and hence lactic acid-rich (ratio PLA>PGA) PLGA is overall less hydrophilic, absorbs less water and in terms of microparticle production, such microparticles degrade more slowly[24]. PLGA polymer is

preferred over its monomeric counterparts, because it can be easily manipulated and provide more control on the releasing behaviour from microparticles[14]. Properties such as: molecular weight (Mw) in kDa (the higher Mw, the longer it takes to degrade, the intrinsic ratio between PLA and PGA (affecting water penetration and hydrolysis) and ester capping (as opposed to allowing a free carboxylic acid group), influence not only the encapsulation and release of the vaccine but also the biodegradation rate of the polymer itself[25]. Interestingly a bi-directional relationship exists between the drug being encapsulated and the polymer, where the type of drug plays a role in the biodegradation of the polymer, and hence affects its release rate[26].

1.2.4 Microparticulate PLGA carriers for vaccines

Within the microencapsulation field, there are inconsistencies when micro-formulations are described, which can be confusing to anyone unfamiliar with the field[27]. By definition, the term 'microparticle' refers to a particle having sizes from 1μm to 1000μm[28]. Under the umbrella term of microparticles, 'microspheres' refer to spherically shaped microparticles, whereas 'microcapsules' refer to microparticles whose core is made from a material different to the exterior material that encases it. Cores can range from solid state, to liquid and even gas[27] (Figure 1.2).

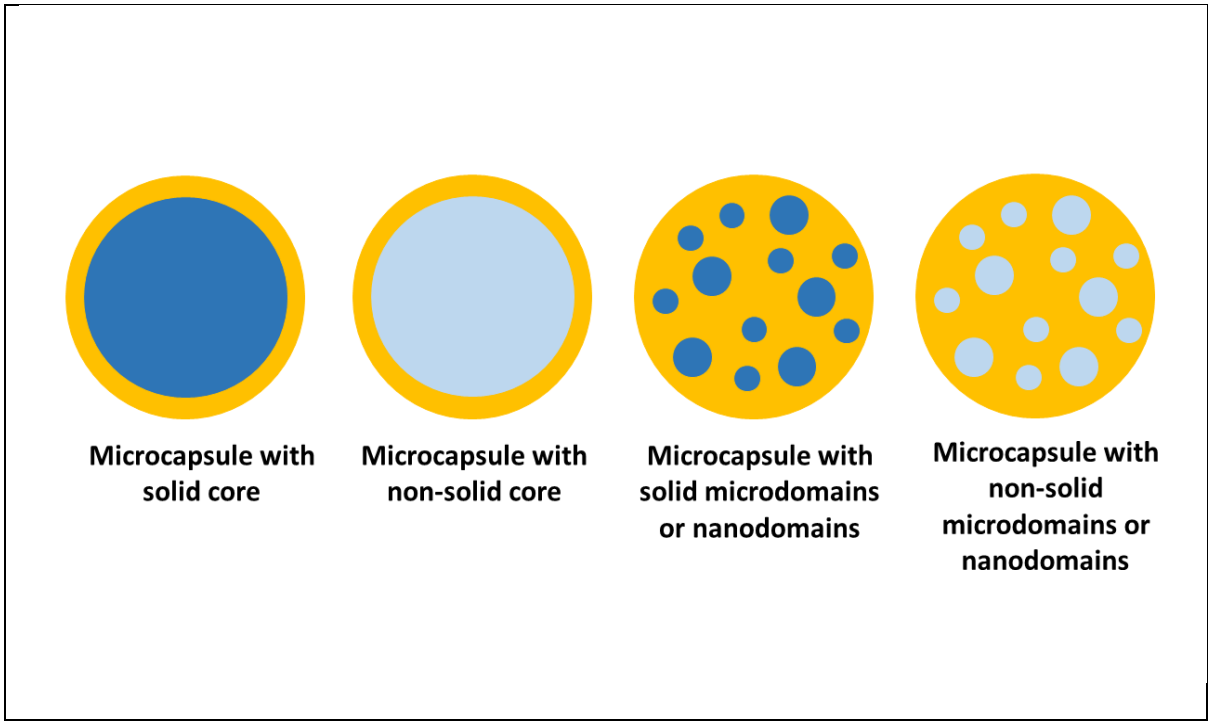


Figure 1.2 Different microcapsule architectures

1.2.5 Preparation techniques for microparticles

There is a plethora of techniques available for the fabrication of microparticles for parenteral usage in controlled release applications. The most frequently used methods are namely: 1) solvent evaporation method; 2) phase separation (coacervation); 3) spray drying and 4) ionic gelation. They are all far from ideal, each having their own advantages and disadvantages but overall the holy grail of the microencapsulation is to encapsulate any protein/drug/vaccine without reducing its bioactivity and improve their shelf life[29].

1.2.5.1 Solvent evaporation method (single emulsion)

The single emulsion solvent evaporation method is characterised by an oil-in-water (O/W) emulsification. PLGA polymer is dissolved in a volatile solvent like dichloromethane (DCM) and then the drug/vaccine is added to this solution to be dispersed. This mixture is then emulsified either by agitation, homogenization or sonication in water containing a stabiliser like polyvinyl alcohol (PVA). Then the solvent is allowed to evaporate or extracted under

reduced atmospheric pressure, leading to the solidification of the oil droplets. An overview of the process is shown in Figure 1.3. This method is most suitable for water insoluble substances like steroids[24].

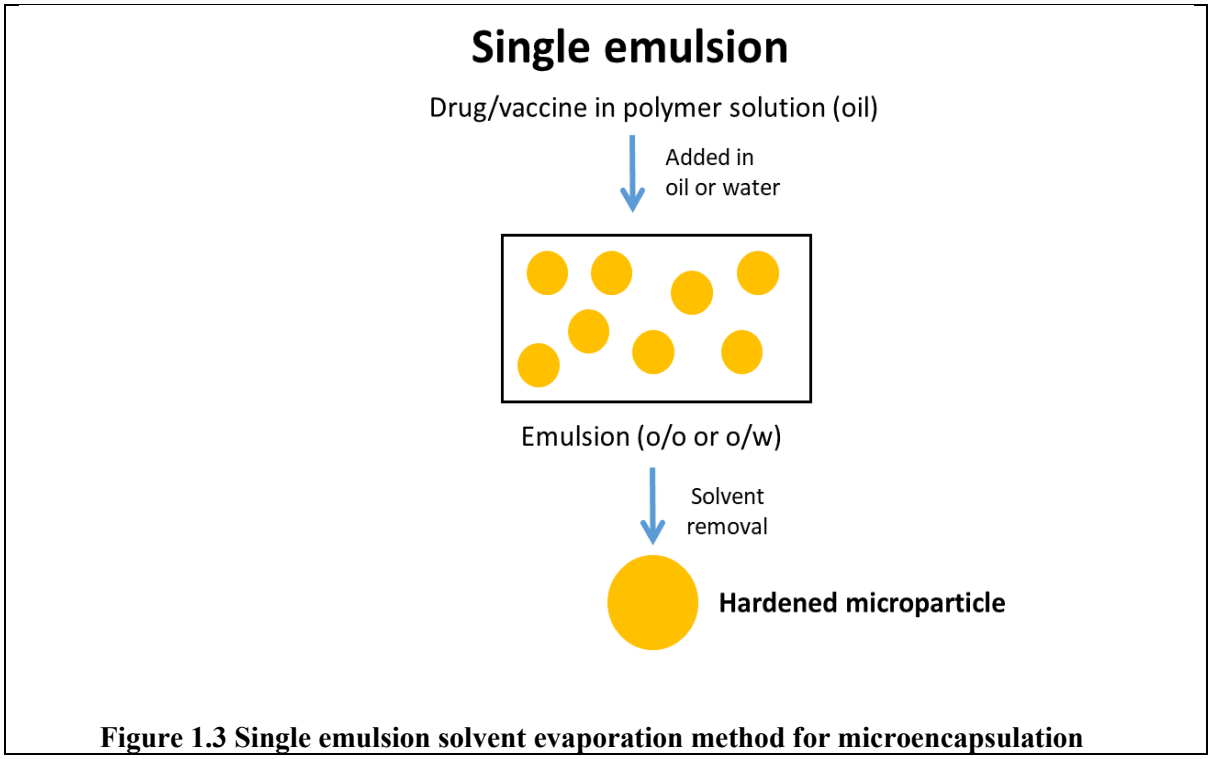


Figure 1.3 Single emulsion solvent evaporation method for microencapsulation

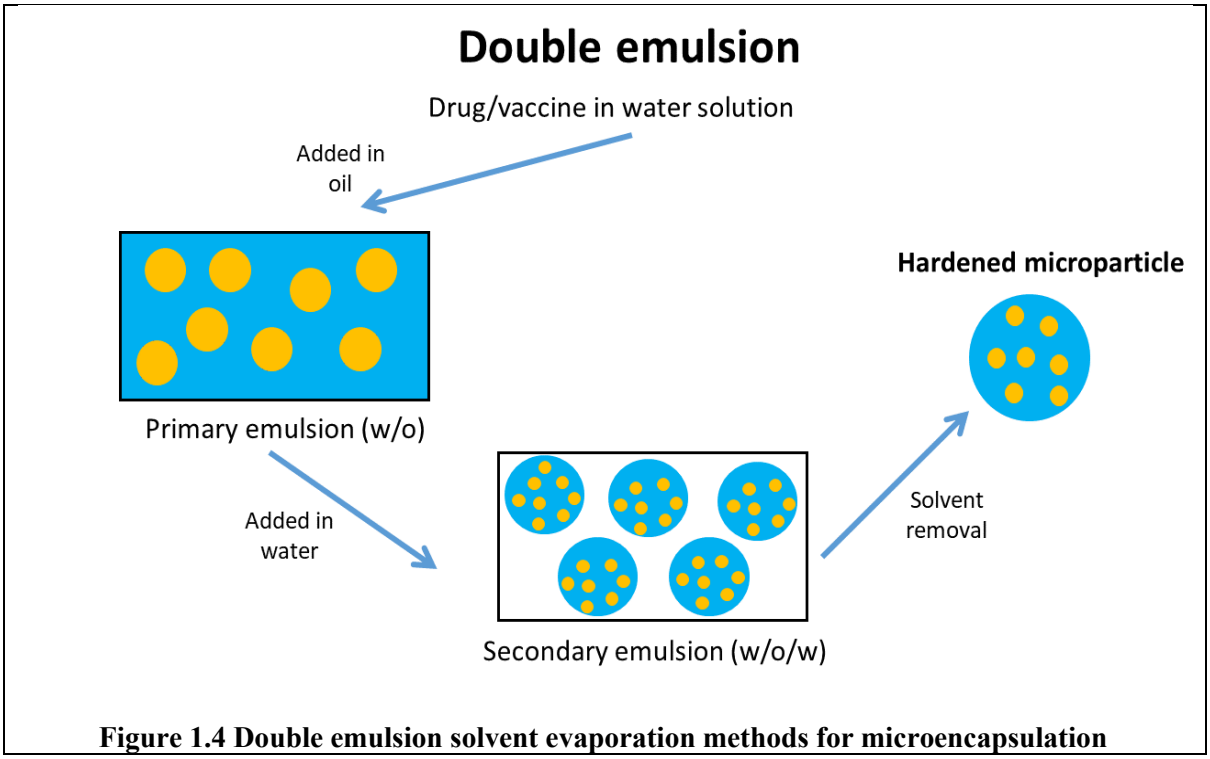


Figure 1.4 Double emulsion solvent evaporation methods for microencapsulation

1.2.5.2 Solvent evaporation method (double emulsion)

Double (or multiple) emulsion is characterised by a water-in-oil-in-water (W/O/W) emulsification. In contrast to single emulsion, this protocol is best suited for encapsulation of water-soluble substances like proteins and vaccines[24]. The drug/vaccine is dissolved in water (water phase) and then this solution is added to the organic (oil) phase containing the dissolved PLGA and/or PLA with the help of solvent. This forms the first water-in-oil emulsion. This primary emulsion is then added to a PVA containing solution which is then emulsified again forming the secondary and final emulsion: water-in-oil-in-water emulsion. Similar to the single emulsion, the solvent is removed leading to injectable hardened microparticles. An overview of this process is shown in Figure 1.4.

1.2.5.3 Phase separation (coacervation) by non-solvent addition

The term 'coacervation' (Latin verb *coacervus* =pile) was coined in the 1930s to describe macromolecular aggregation (or phase separation) by partial desolvation of fully solvated macromolecules[30]. Microparticles are produced by dispersing the aqueous solution containing the drug into organic polymer solution, followed by phase separation by adding a 2nd organic solvent in which the polymer is not soluble (non-solvent). Adding a non-solvent like silicone oil results in the precipitation (coacervate) of the polymer around the drug/vaccine forming microparticles. However microparticles produced with this method have a broad size distribution making them unsuitable for clinical use and such microparticles tend to aggregate extensively[31].

1.2.5.4 Spray drying

In spray drying PLGA polymer is dissolved in a suitable solvent and drug/vaccine is added into the polymer solution. Conceptually the process is very simple. First, the polymeric mixture is loaded into a syringe and pumped at a constant rate with the help of a syringe pump. This is pumped through an electrified nozzle inside an enclosed case filled with inert gas. Once at the nozzle tip, droplets are propelled away and while they are in flight the volatile solvent evaporates, resulting in solid microparticles. Microparticles are finally retrieved in a collector container[32,33].

1.2.5.5 Ionic gelation/crosslinking

Instead of using synthetic PLGA polymer, naturally occurring alginate polymer is used to manufacture alginate microparticles. Alginate is a polysaccharide obtained from marine algae[34]. With this method microparticles are produced by dropwise addition of the drug/vaccine loaded alginate solution into an aqueous calcium chloride solution. Calcium ions diffuse into the alginate, triggering ionic gelation. This forms a 3-dimensional matrix of ionically-crosslinked alginate microparticles entrapping the drug/vaccine[35,36].

1.3 The human immune system

To understand how vaccines work and how this microencapsulation technology could influence the immunological outcome by directly interacting with its different cellular constituents, it is useful to understand first how the human body responds when fighting an infectious agent. Humans possess an evolutionary descendant protective mechanism providing resistance to bacteria, parasites, viruses and fungi[37]. The human immune system is categorised into two complementary systems known as the innate and adaptive immune system. The innate system relies on innate receptors having broad specificity against unique microbial molecular signatures while the adaptive immune system relies on receptors with a restricted range of specificity[38]. Together, both arms of the immune system provide a complex network of cells, which when combined provide a resistive barrier against harmful intruders.

1.3.1 Innate immune system

When microorganisms enter the human body they are quickly detected by germline encoded pattern recognition receptors (PRRs), which recognise conserved signatures of microbes intracellularly and extracellularly and indicate an infection[39]. Once detected, these pathogen-associated molecular patterns (PAMPs)[40], allow the innate immune system to distinguish non-self from self-molecules and activate the adaptive immune responses to non-self molecules - a model first proposed by Charles Janeway[41].

1.3.1.1 Innate immune cells

The innate immune system is comprised of a network of cells, each having unique effector functions and are characterised by the presence or absence of phagocytic ability. Non-phagocytic cells are namely natural killer (NK) cells, eosinophils, basophils and mast cells. Mast cells contain granules of potent inflammatory mediators such as histamine, prostaglandins and leukotrienes which are released upon pathogen detection[42], whilst eosinophils also contain cytotoxic granules with inflammatory mediators and are implicated in host resistance against

helminths[43] (parasites). Basophils circulate throughout the body and are also sources of inflammatory mediators attracting phagocytic cells by chemotaxis and vascular permeability[44]. Lastly, NK cells can directly kill tumour or virally infected cells, hence their name, and express both activating and inhibitory receptors to distinguish self from non-self. Whilst they are able to secrete inflammatory cytokines, their granules contain perforin and granzymes, and can be utilised to directly lyse pathogens and infected cells by triggering apoptosis (cell death)[45].

In comparison, phagocytes include macrophages, neutrophils and dendritic cells (DCs), capable of internalising whole microorganisms and particles (≥0.5μm) resulting in their destruction[46]. Phagocytosis/opsonisation is an important and effective way to clear pathogens during the innate immune response. Macrophages and their precursors (monocytes) upon tissue damage or infection are rapidly recruited to the tissue area, where they differentiate into tissue-specific macrophages with different functions and contribute to the repair of the tissue and senescent cells[47]. Neutrophils on the other hand, in addition to their broad armamentarium present in their granules containing serine proteases, microbicidal and anti-toxin substances, can generate reactive oxygen species (ROS), resulting in rapid pathogen killing[48]. Finally, yet importantly, DCs are regarded as the most specialised and crucial cell type for immunity connecting and orchestrating both the innate and adaptive immune systems by interacting with cells from both networks. They are the only antigen-presenting cell (APC) able to stimulate naïve T-cells[49]. The general idea of induced inflammation caused by these innate cells is that not only it removes cellular debris and pathogens, but it also facilitates the transport of antigen by DC migration through the afferent lymphatics to draining lymph nodes[49]. When a pathogen is engulfed, pathogen antigen (Ag) is processed into peptides, then loaded and presented in the context of Major Histocompatibility Complex (MHC) class I or II molecules[49]. Ag-loaded DCs then upregulate the expression of chemokine receptor CCR7 through a maturation process of

the DC, which triggers the chemokine migration of Ag-loaded DCs from tissue to the draining lymph nodes[50]. However once at the lymph node, antigen presentation to naïve T-cells is not enough to induce their differentiation: that is why costimulatory molecules like CD80, CD86 and CD40 are upregulated on the APC surface to interact with the CD28L and CD40L on the surface of the naïve T-cells[51].

1.3.2 Adaptive immune system

In contrast to innate immunity, the adaptive immune system maximises and specifically targets the immune response towards the infection, while minimizing unnecessary collateral damage. This is dependent on randomly generated antigen receptors via somatic recombination, which are clonal in nature and have limitless specificity potential[38]. It has been estimated that lymphocyte receptor diversity repertoire has at least 1 million possible clonotype combinations[52], which is much larger than the total number of genes of the human genome[53] (~20,000). Adaptive immunity is dictated by T-cells and B-cells which upon stimulation, expand and differentiate into specialised cells to produce Ag-specific responses. Once the invading pathogen is eliminated, the majority of the adaptive cells die and leave behind long-term memory cell subsets, which will mediate a fast and protective immune response upon re-infection[54]. Primarily, vaccines target these specific T-cell and B-cell populations in order to stimulate them and elicit a targeted immune response.

1.3.2.1 T-lymphocytes

The mediator molecule of T-cell activation and Ag- recognition is the T-cell receptor (TCR), whose α and β chains recognise Ag peptides on APCs in the context of MHC class I or II molecules[55]. Once naïve T-cells are presented Ag-peptide through the TCR with the presence of costimulatory signals from the APC, T-cell activation occurs which leads to cell proliferation and clonal TCR selection[54]. Specialised T-cells responses are tailored to the invading pathogen and depending on the microenvironment's cytokine profile, the type of APC and the TCR

signal, 2 main categories of T-cells are generated: CD4+ 'helper' T-cells and 'cytotoxic' CD8+ T-cells[54,55].

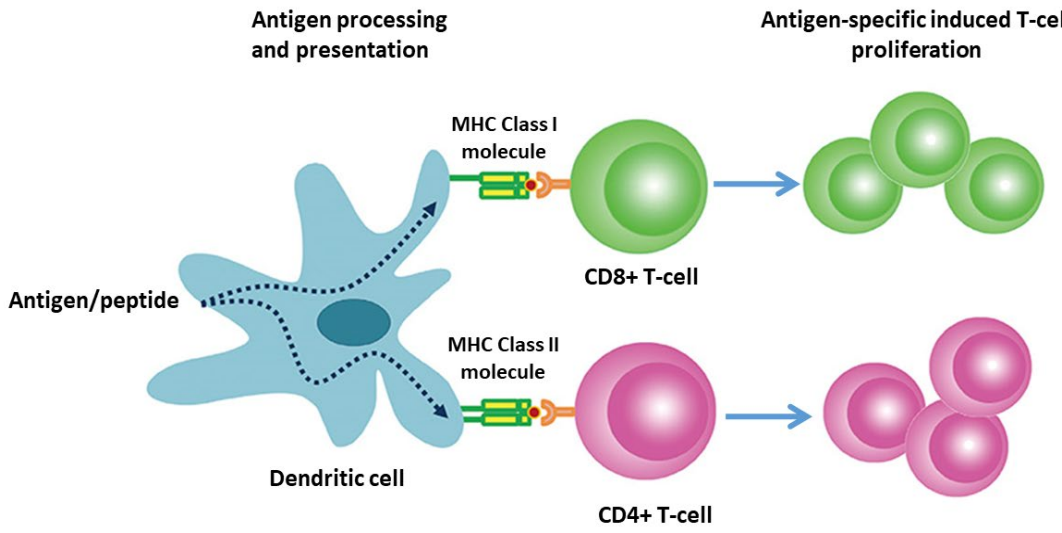


Figure 1.5 A simplified overview of dendritic cell (DC)-mediated antigen specific CD4+ and CD8+ T-cell clonal expansion.
Foreign antigen is taken up by DCs, processed into peptides and presented on MHC class I or II molecules. DCs then interact with CD8+ T-cells via antigen presented on MHC class I molecules, whereas antigen presented on MHC class II molecules allow interaction with CD4+ T-cells. With the help of co-stimulatory molecules present on the activated DC's cell surface both T-cell subset are induced to proliferate and generate an antigen specific response. Adapted and modified from Ra *et al*[56].

1.3.2.2 CD4+ T-lymphocytes

CD4+ T-cells are referred to as T-helper (Th) cells because they support the induced immune response with cytokine and chemokine production and secretion. Cytokines activate nearby innate and adaptive immune cells while chemokines recruit new immune cells to the infection site[57]. In 1986 Mosmann[58] and Coffman[59] initiated the elucidation of the CD4+ T-lymphocyte immunology by characterising the pattern of cytokines they produced and establishing the dogma of the Th1 and Th2 cell subsets. Interleukin-12 (IL-12) and IFN-γ are critical for the development of Th1 cells[60] and in turn Th1 cells secrete IFN-γ, Tumour necrosis factor (TNF)-

α and β, which are particularly effective in protecting against intracellular pathogens that grow inside macrophages[61]. Similarly, Th2 cells were characterised as producers of IL-4, IL-5 and IL-13 and established to partake towards immunity to parasites and allergic immune responses[62].

We now know that T-cell subsets are more heterogeneous than we once thought and since the 1980s, new T-cell clonal lineages have been identified which are actively studied. Each subset has their own cytokine release patterns and effector roles and shown to not only promote immune responses like the Th9, Th17, Th22 and follicular helper (Tfh) T-cells, but also keep the system in check like the immunosuppressive regulatory T-cells (Treg)[63]. For example, Th9 cells which require TGF-β to mature in comparison to Th2 cells, provide immunity against helminth parasites and they predominantly secrete IL-9 which enhances immune cell infiltration into infected sites[64]. Treg cells on the other hand, release IL-10 and TGF-β and are characterised by the constant upregulation of the fork-head box 3 (FOXP3) transcription factor in order to assert their immunoregulatory function on other cells[65].

1.3.2.3 CD8+ T-lymphocytes

CD8+ T-cells or also known as cytotoxic T-lymphocytes (CTLs) or lately Tc1, contribute to the resistance against viral, bacterial and protozoan pathogens with their capacity to kill directly infected cells[66]. Direct target cell lysis occurs via 2 distinct mechanisms[67]: 1) CD8+ T-cell granule exocytosis containing perforin/granzymes and 2) induction of programmed cell death by FasL-Fas interaction. Both mechanisms induce the target cell's own apoptotic death by activating the caspase cascade[68]. CD8+ T-cells primarily secrete IFN-γ and TNF as well as chemokines to recruit macrophages and neutrophils to the site of infection[69]. In the setting of an immunisation, CD4+ T-cells are necessary for the induction of a primary CD8+ T-cell immune response robust in magnitude and functionality[70].

Depending on the cellular microenvironment and inter-cellular interactions, CD8+ T-cells can adopt similar subset profiles seen in CD4+ T-cells and become Tc2, Tc9, Tc17 or even CD8+ Tregs[71]. For example, Tc2 cells kill predominantly via the perforin/granzyme pathway and also produce IL-4, IL-5 and IL-13 like their CD4+ Th2 cells counterparts[72]. CD8+ Tregs are IL-15 dependent, secrete IL-10, IL-16, TGF-β, CCL4 and ultimately complement the function of their respective CD4+ Tregs by inhibiting APCs and Tfh cells and killing activated CD4+ T-cells[73,74].

1.3.2.4 γδ T-cells

In addition to the lymphocytes mentioned above having an α and β chain TCR, a distinct lymphocyte population has been discovered whose TCR is made of γ and δ chains, hence their name: γδ T-cells. It is now known that 2 main γδ T-cell subsets exist in humans: the Vδ1 T-cells present in the thymus, peripheral organs and mucosal surfaces as well the Vδ2 T-cells present prominently in the circulatory system[75]. In comparison to the αβ T-cells, γδ T-cells can recognise Ag directly and are not restricted in recognising Ag presented with an MHC molecule[76]. They can recognise unconventional Ags like natural small mycobacterial Ags, byproducts of polyisoprenoid biosynthesis and stress molecules like MICA, which is the ligand of the NKG2D receptor present on the γδ T-cell surface[77–79]. Because of the presence of the innate NKG2D receptor and the γδ TCR, γδ T-cells display adaptive and innate immunoproperties and present a link between the two immune systems. Activated γδ T-cells were shown to have cytotoxic abilities with the usage of the perforin & granzyme pathways or by engaging death receptors on target cells, especially tumor cells[80]. Furthermore, their secretory profile includes proinflammatory IFN-γ and TNF-α cytokines[75], IL-10 cytokine which is used to regulate proliferating activated CD8+ T-cell populations [81] as well as IL-17 which recruits neutrophils and monocytes from the bone marrow and kickstarts an inflammatory response at the site of infection[82]. Lastly, γδ T-cells also exhibit Ag-presenting

capacity and can prime αβ T-cells by presenting processed peptides from microbes, apoptotic cells or tumour cells and even induce the maturation of DCs with TNF-α secretion[83].

Using experimental animal infection models it was observed that cytokine secreting γδ T-cells appeared days before an αβ T-cell response was even developed and that these were the most critical early producers[84]. This was found to be in agreement with the clinical setting, where γδ T-cells are present in heightened proportions early during infections[85]. These immunological properties could play a critical role in designing better cancer immunotherapies[86] and better vaccine responses. Most recently, absence of γδ T-cells during experimental murine vaccination with irradiated sporozoites impaired protective CD8+ responses, indicating their significance, whilst in the first PfSPZ vaccine trial the frequency of Vδ2 γδ T-cells was significantly increased[87].

1.3.2.5 NKT cells and MAIT cells

Another unconventional minor lymphocyte group are the Natural Killer T (NKT)-cells. They possess TCRs of limited diversity and are characterised by their ability to recognise foreign microbial and self lipids/glycolipids presented with the help of Cd1 molecule, a non-polymorphic MHC-like molecule[88]. These Cd1 restricted cells are typically categorised into: a) Type 1 NKT cells or invariant NKT which own a conserved invariant TCRα chain with a limited recognition repertoire TCRβ chain and are activated by the antigen α-galactosylceramide and b) Type 2 NKT cells which don't possess the conserved invariant TCRα chain but instead have a broader recognition repertoire of TCRαβ chains and they are α-galactosylceramide resistant[89]. When they are activated and depending on the surrounding microenvironment, NKT cells can mirror the Th-cell subset activity with their iNKT1, iNKT2 and iNKT17 sybtypes and the associated cytokine secretion profiles, which in turn can either promote or suppress the strength of the mounted immune response[90]. It is agreed that the

existence of NKT cells serves to protect the host from infections and also contributes to the immunosurveilance of foreign organisms[91,92].

Similarly, mucosal associated invariant T (MAIT) cells also have an invariant conserved TCRα chain, distinct though from the NKT and a modest number of TCRβ chains[93]. They are also restricted to another non classical MHC-I like molecule, called MR1, which enables them to recognise byproducts of vitamin B2 synthesis present in most microbial and yeast organisms, thus allowing their detection[94]. MAIT cells are abundant in mucosal surfaces and organs within the gut periphery and contribute to foreign antimicrobial defences, in addition to regulating the commensal flora[95]. More specifically they are able to kill bacterially infected cells through perforin and granzyme molecules[96] and augment the establishment of a robust adaptive immune response by secreting IFN-γ, TNF-α and IL-17[97].

Due to the fact that both NKT and MAIT cells can stimulate an extensive array of immune responses as well as potentially provide immunological memory[95], both cell types are under active investigation to specifically target them and improve vaccine efficacy for both human and animal diseases[98–100].

1.3.2.6 T-cell immunological memory

T-cell memory refers to the heightened immune response seen after antigen experience with the generation and persistence of memory T-cells whose frequencies dynamically change throughout the human lifetime. During an infection there is a 10^5 fold increase in the generation of Ag-specific T-cells from a naïve T-cell population[101]. These then differentiate into effector T cells and some of them become Ag-specific memory T-cells[54]. Finally these long-lived memory T-cells persist in the body in heterogeneous memory subsets and orchestrate the protective immune responses upon re-exposure of the same infectious agent[102]. Although still debatable, a progressive linear differentiation model exists explaining the origin of terminal

effector T-cells, which depends on TCR signal strength and/or T-cell activation status upon Ag re-exposure[103,104]. This model is explained in Figure 1.6.

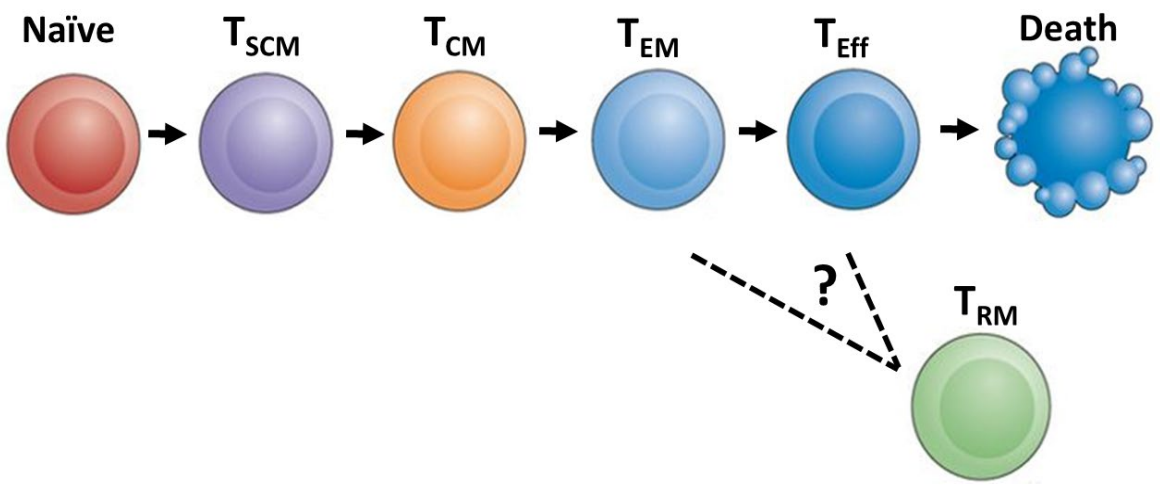


Figure 1.6 Model for development of human T-cell memory
Successive development from naïve activated T-cells: stem cell memory (T_{SCM}), central memory (T_{CM}) and effector memory (T_{EM}) all of which are circulatory. Effector (T_{Eff}) T-cells are terminally differentiated cells and a number of them die after increased Ag exposure. Tissue resident memory (T_{RM}) T-cells migrate to different organ sites through chemotaxis and they are thought to originate either from T_{EM} or T_{Eff} precursor subtype. Modified from *Farber et al* [105].

1.3.2.7 B-cells and antibody production

An effective antibody (humoral) response involves the participation of B-cells which secrete antibodies. Upon activation either with T-cell help, or less effectively independently, B-cells undergo somatic hypermutation and class switching, leading to the production of high affinity antibodies against the Ag they recognise[106]. During activation B-cells differentiate into short lived plasma cells and after the pathogen is eliminated a small percentage is transformed into memory B-cells[106]. When the same pathogen Ag is re-encountered memory B-cells

differentiate into plasma cells and produce large quantities of immunoglobulins (Ig) which in reality are the secreted form of the B-cell receptor.

1.3.2.8 Antigen presentation

A distinctive feature of T-cell activation is the requirement to recognise specific Ag bound on MHC restrictive molecules. To achieve this, both MHC class I and class II molecules need to bind Ag-derived peptides (fragments) onto their binding groves, which is realised via different processing routes. Classically, CD4+ T-cells respond only to antigenic peptides derived from exogenous Ag scavenged by APCs and associated with MHC class II molecule in the presence of costimulatory signals[107]. In comparison naïve CD8+ T-cells specifically respond only to endogenous cytosolic Ag from self-proteins, viruses, intracellular bacteria and tumours which are associated with MHC class I molecules[108].

The MHC-class I Ag-presentation pathway is present in all nucleated cells and acts as a probing mechanism for CD8+ T-cells to surveil the intracellular proteomic content at any time[109]. With the catabolic activity of the proteasome, peptide fragments are generated from foreign endogenous proteins via enzymatic degradation and these peptides are shuttled to the endoplasmic reticulum (ER). This transporation is mediated by the heterodimeric trasporter associated with antigen processing-1 (TAP1) and TAP2. At the ER, the 8-10 aminoacid long peptides & TAP1/2 complex are bridged together with the MHC-class I heavy chain dimer & β_2-microglobulin complex via the action of the tapasin, calreticulin and thiol oxidoreductase ERp57[110]. Once complete, the MHC-class I-peptide complex is translocated to the cell surface via the Golgi network and secretory pathway for recognition by CD8+ T-cells[109]. This process is shown in Figure 1.7.

MHC-class II-Ag complexes on the other hand are mostly found on the surface of APCs including DCs, B-cells, macrophages, thymic cortical and medullary epithelial cells, however

non-APC cells (fibroblasts, epithelial and endothelial cells, keratinocytes) are also able to induce MHC-class II-Ag expression on their cell surfaces under immunoregulatory IFN-γ stress signal[111]. Captured exogenous Ag reaches vesicular endosomal and/or lysosomal compartments via macropinocytosis, clathrin-mediated or fluid phase endocytosis and phagocytosis[112]. MHC-class II heterodimer molecules consist of α and β subunits and similarly to class I molecules assemble in the ER. There, the MHC-class II α/β chains engage with the chaperone molecule invariant chain (Ii), which stabilises the complex and contains an endosomal target and retention motif which targets the Ii-MHC class II complexes to endosomal and/or lysosomal compartments[113]. Through a series of orchestrated proteolytic cleavages mediated by cathepsin S, the Ii is degraded to a small 3 kilodalton (kDa) fragment called the class II-associated invariant chain peptide (CLIP), which is lodged in the peptide binding groove of the MHC-class II molecule[114]. CLIP must then be removed from the binding groove and exchanged with peptides of variable length from the available Ag derived peptide pool that was co-created during the endosomal proteolytic pathway. The final Ag peptide exchange into the binding groove, is catalysed by HLA-DM[115], which increases the rate of release of CLIP from the MHC-class II molecule at a specialised organelle called the MIIC[110]. Following these events which are depicted in Figure 1.8, MHC-class II-peptide complexes are destined to the cell surface for surveillance by CD4+ T-cells.

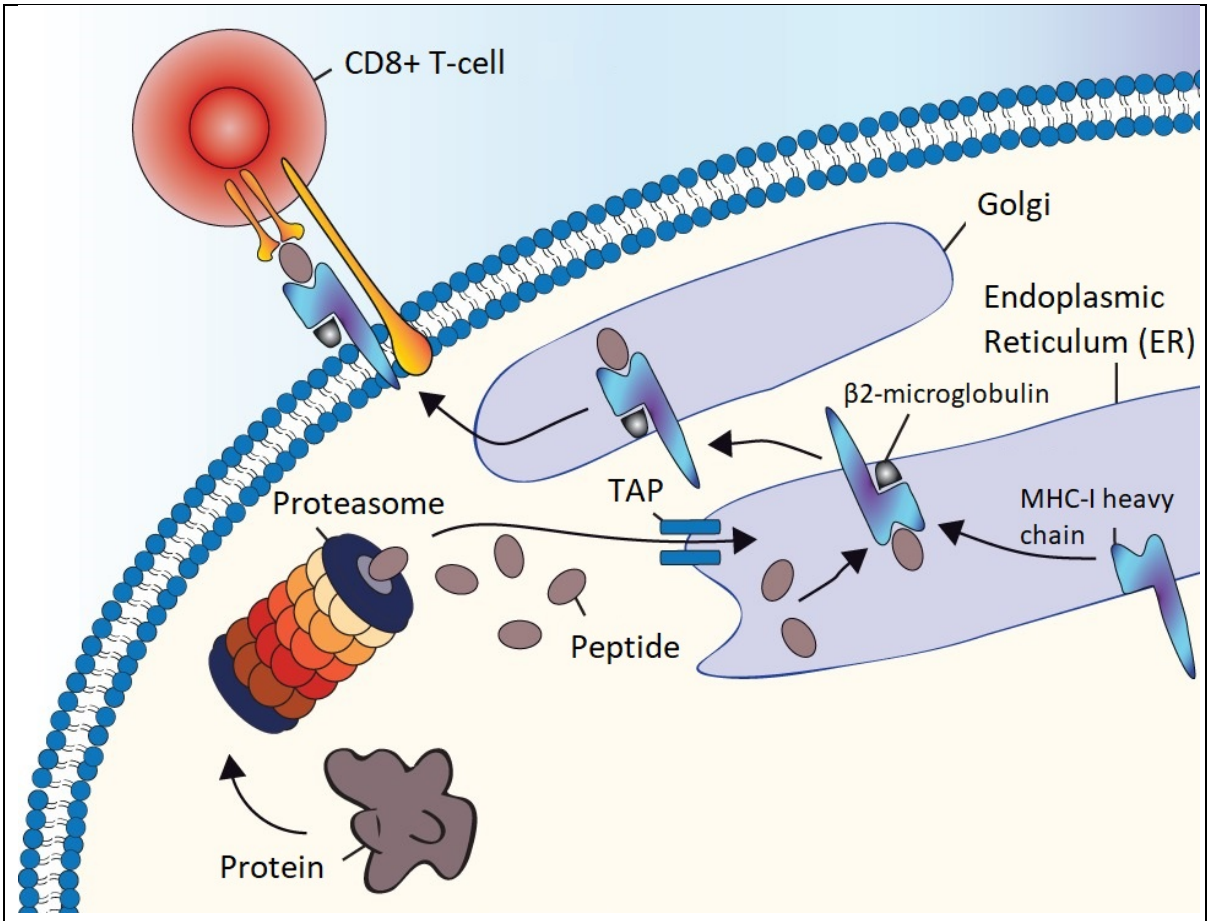


Figure 1.7 Classical MHC-class I presentation
Cytoplasmic Ag is degraded in the proteasome allowing the generation of short 8-10 aminoacid long peptides that are then transported to the endoplasmic reticulum (ERD) via the trasporter assoaciated with antigen processing-1/-2 (TAP1/2). At the ER, peptides are loaded onto nascent MHC-class I heavy chain molecules linked with β2-microglobulin, and then translocated via the Golgi network to the cell surface to be surveyed by the CD8+ T-cells. Image adapted and modified from *Murrat P & Tellam J.*[116]

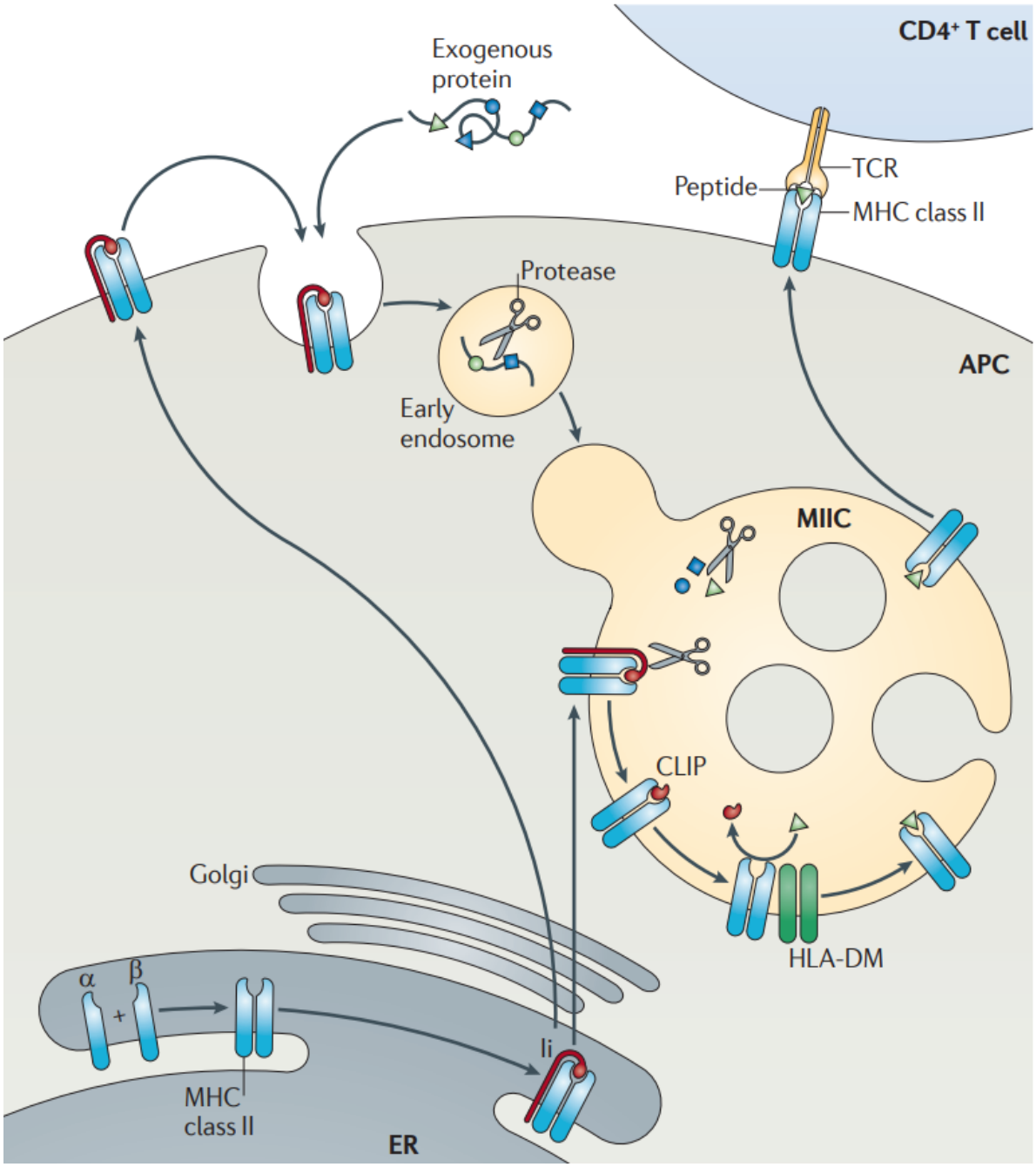


Figure 1.8 Classical MHC-class II presentation
Exogenous Ag is recruited into the APC via the endocytis pathway. MHC class II molecules which are made of 2 heterodimeric α and β chains are assembled first in the endoplasmic reticulum (ER) and stabilised with the invariant chain (Ii) chaperone. This complez is then transported via the Golgi to a specialised organelle called the MIIC. Once at the MIIC, proteases degrade both endocytosed Ag and the Ii, resulting in a pool of variable length peptides and the class II associated Ii peptide (CLIP), which stays within the peptide binding grove of the MHC-class II molecule. Then CLIP is exchanged for peptide with the catalytic activity of HLA-DM and the nascent peptide-loaded MHC-class II molecule is transported to the cell surface to be presented to CD4+ T-cells. Adapted from *Neefjes et al* [117].

However, there are few exceptions to this classical MHC Ag presentation dogma. It has been observed that extracellular antigens can in fact be loaded and presented on MHC class I molecules by APCs and stimulate CD8+ T-cell immunity, by a process now known as cross-presentation[118]. Multiple APCs have the capacity to cross-present Ag but human DCs, which are divided into conventional DCs (cDC) and plasmacytoid (pDCs) are believed to be the major cross-presenting cells in vivo[119]. There are two main cross-presentation pathways, which work together or in isolation: the TAP-independent vacuolar pathway and the TAP-dependent endosome-to-cytosol pathway. In the first pathway, endolysosomal proteases are used to degrade internalised Ag and generate peptides that are loaded on MHC-class I molecules recycled from the cell membrane[110]. The second pathway, precursor Ags are transferred from endosomes into the cytoplasm, where they are fed directly into the MHC-class I presentation pathway after stepwise cleavage by proteasomes into peptides and transported by TAP[120].

In a similar fashion, loading and presentation of intracellular Ags with MHC-class II molecules is possible with the involvement of autophagy[121]. Autophagy (macroautophagy) is a dynamic process, which allows cells to recycle cytoplasmic material and organelles during normal conditions, under cellular stress or deprivation as well as under immunostimulatory cues[122]. Cytoplasm is sequestered into double membraned structures called autophagosomes which fuse with lysosomes and all their content is degraded by the lysosomal apparatus and ultimately this allows access of endogenous Ags to the MIIC and the MHC class II loading machinery[122]. It has been shown that autophagy can assist in packaging Ags from donor cells as well as modulating the endosomes in DCs, therefore enhancing the cross-presentation process[121].

In combination, both cross-presentation and autophagy processes are not only important for ensuring normal immunological physiology. They can assist in Ag presentation and promote immunity, since they are the only pathways that can help with the detection of viral or other

infections that solely occur in cells other than APCs e.g. neurons and glial cells, by gathering foreign Ags when immunostimulatory 'danger' signals are released into the cellular microenviroment from nearby infected or dying cells[118].

1.3.3 How vaccines work

As previously discussed, the basic notion behind vaccination revolves around the ability of the immune system to respond faster and more vigorously upon re-exposure to the same pathogen, which is known as immunological memory[123]. A vaccine is a biological preparation/product that stimulates immunity to a particulate disease, by activating the threat detection system of the immune system which is based on Ag epitope recognition. Components of innate immunity will bind to the vaccine and help in its engulfment by APCs. In turn these APCs will process the vaccine and present the Ag epitope with MHC protein on their surfaces[124]. Depending on the type of antigen, different mechanisms will be activated ultimately leading to the generation of immune memory cell populations and an overview is shown in Figure 1.9. If the Ag is of viral origin, then it will typically be presented mainly in the context of MHC class I molecule and presented via the APCs to CD8+ T-cells, triggering a cell-mediated immunity[125]. If the Ag is of bacterial and/or parasitic origin, however, it will more likely be presented predominantly by APCs on MHC class II molecules triggering an antibody-mediated immune response.

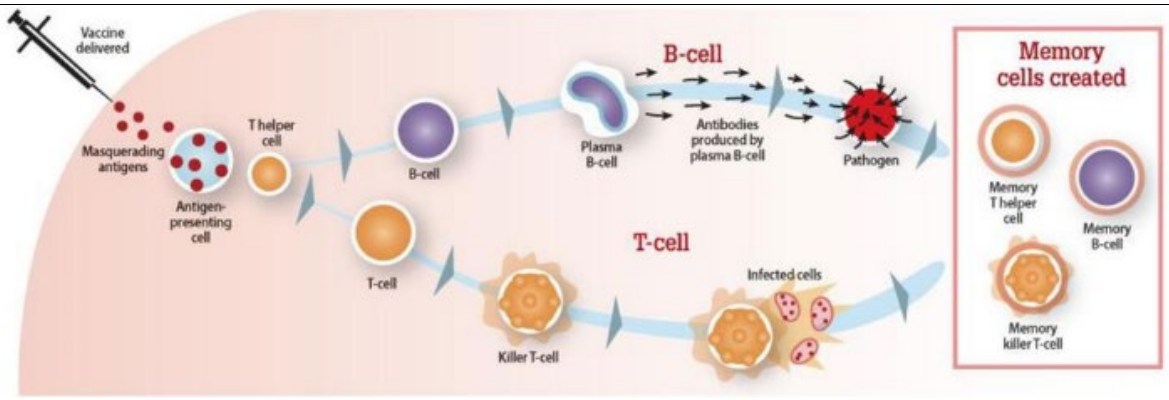


Figure 1.9 Schematic overview of how vaccines work.
Vaccines stimulate several immune cells by providing antigens from pathogens. Antigen presenting cells encounter, digest and then display the antigen on their surface so that it gets recognised by CD4+ T-helper cells. These antigen specific T-helper cells send chemical messengers to B-cells and killer CD8+ T-cells, which activate them. Once stimulated by the same antigen and the chemical signals from CD4+ T- helper cells, B-cells and killer T-cells proliferate and become antigen-specific specialised immune cells, which can produce antigen-specific neutralising antibodies or kill infected cells respectively. A portion of these T-helper, B- and killer T-cells transform into memory populations which respond faster and more efficiently against future infection by the same antigen. Adapted from History of Vaccines Organisation[126].

This artificial active form of immunisation, which stimulates immune responses without the symptoms of an active disease, includes several types of vaccines[127]. Live attenuated vaccines such as measles, mumps and chickenpox, contain laboratory-weakened versions of the original infectious agents[128]. Live attenuated vaccines can mount qualitively and quantitively equal immune response similar to fighting the natural disease and can generate memory responses sufficient for lifelong immunity after a single dose[127]. Inactivated vaccines like polio (i.e. IPV) or most seasonal influenza vaccines, are produced by inactivating the original infectious agent with heat, chemicals and/or radiation. In comparison to live attenuated vaccines with their intrinsic adjuvanticity, inactivated vaccines do not provide as equally potent immunity as live attenuated vaccines and generally need repeating doses over time[129]. With inactivated vaccines, although all infection-associated antigens are present and antibody responses are directed to the whole repertoire of antigens separately, not all of these antigens are critical for causing

disease[127]. Additionally they do not promote the generation of cytotoxic T-cells, suited for intracellular pathogen and viral clearance. Furthermore inactivated vaccines are not particularly potent to sensitise the adaptive immune, hence why they are co-administered with adjuvants and/or with frequent booster shots to bypass this issue[127]. Toxoid vaccines like the tetanus vaccine, create immunity targeted to toxins produced by the infectious agent rather the agent itself and also require repeated booster shots to provide ongoing protection[127]. Subunit vaccines like the recombinant Hepatitis B vaccine and *Haemophilus influenzae b*, include one specific epitope or small antigen from the pathogen rather than many, which are recognised by either B-cells or T-cells triggering an immune response. Finally, with the advent of molecular biology, recombinant viral vector vaccines which are also subunit vaccines, are now considered as an attractive alternative to the traditional vaccine types. Attenuated viruses are able to introduce DNA or RNA into body cells and induce effectively both humoral and cell-mediated responses[130].

1.3.4 Adjuvants in vaccinations

As just mentioned, inactivated and subunit vaccines lack intrinsic adjuvanticity therefore synthetic or natural adjuvants are incorporated in order to induce, enhance or prolong the immune response after immunisation. Often referred to as ‘‘the immunologists’ dirty little secret’’[41], depending on the adjuvant being employed and the target pathogen, the immune response can be shaped as needed e.g. invoke cellular immunity or humoral or both[131]. Broadly speaking, adjuvants are divided into 2 categories: 1) immunostimulatory adjuvants, that directly influence cells of both innate and adaptive immune systems and 2) delivery vehicles, which optimise the Ag-presentation to the immune system via Ag-trapping/depot effect or controlled/slow release, or at the same time also deliver other immunostimulants or even act themselves as immunostimulatory adjuvants[124,132]. Apart from the depot effect, other adjuvant

mechanisms of action could include any combination of the following: recruitment of APCs and other immune cells at the site of injection[133], activation of the inflammasome[134], enchanced Ag-uptake and presentation, subsequent cytokine/chemokine production, increased expression of MHC I&II molecules and APC maturation[135]. For example, AS01, a liposome-based adjuvant containing MPLS and QS21 immunopotentiators leads to increased generation of activated Ag-loaded monocytes and MHC-II^{++} bearing DCs[136], whilst Montanide ISA™ 51, a water-in-oil emulsion of mineral oil and mannide mono-oleate emulsifier acts as an Ag-depot sustaining Ag exposure and pivoting potent cytotoxic T-cell responses[137]. Other examples of clinically approved adjuvants include: MF59 used in seasonal influenza vaccines, AS04 used in Hepatitis B and HPV vaccines and AF03 squalene-emulsion based adjuvant used in pandemic influenza vaccines[138]. Apart from these traditional adjuvants, lipid-based immune stimulating complexes (ISCOMs)[139], liposomes[140], carbon nanotubes[141], virus-like particles (VLPs)[142] and even biodegradable polymeric nanoparticles/microparticles[132,143,144] are indeed promising and could be co-administered in the future as vaccine adjuvants to promote a mature immune response. It is interesting to note that polymeric vaccine adjuvants (matrices and nano/microparticles), are attractive targets for replacing standardly used adjuvants because of their tunable properties such as surface charge, hydrophobicity, degradability, chemical composition and finally the ability to functionalise them e.g. target them to APC with the help of antibodies or coat them with immunostimulatory molecules[145].

1.3.5 Conjugate vaccines

Bacterial meningitidis is caused primarily by 3 polysaccharide encapsulated pathogens: pneumococci, meningococci and *Haemophilus influenzae type b*[146]. Early bacterial capsular polysaccharides-based vaccines showed inadequate immune response in young children and although antibodies were produced due to having repetitive B-cell epitopes but no

corresponding T-cell epitopes, no long-term memory was formed[147,148]. As their name suggests, to overcome the lack of T-cell response, a conjugation technology is used to link the capsular polysaccharides with protein carriers[149]. This coupling event invokes an enchanced and more complete immunogenicity with the cooperation of T-cell and B-cell populations, higher amounts of antibodies and anamnestic immune responses[146,150,151]. Today, the following protein carriers are being used in licensed conjugated polysaccharide vaccines: tetanus toxoid, cross-reacting material 197 $(CRM)_{197}$, *H.influenzae* protein D, diphtheria toxoid and meningococcal outer membrane protein complex (OMPC)[152]. Historically, the introduction of these protein carriers into childchood immunisation schedules led to a successful campaign preventing invasive and non-invasive bacterial meningitidis worldwide[146,152].

1.3.6 Virus-like particles (VLPs)

With the emergence of molecular biology, the idea of using non-infectious virus particles as protective vaccines came to fruition. Virus-like particles (VLPs) are supramolecular bio-nanostructures made from virion-building proteins, which can self-assemble to form viral capsids devoid of any infective viral genetic material, making them a safe vaccine platform[153]. Due to this non-infective property and structural native resemblance to the infectious particles, VLP vaccines have superb immunogenicity due to their repetitive surface structure, stimulating both humoral and cellular immune responses against human and veterinary illnesses[154,155]. VLPs can be mass-produced in a range of expression systems including yeast, bacteria, plants, insect and mammalian cells and at the moment academic and industry partners aim to maximise their production rates whilst lowering production costs[156]. The exterior surfaces of VLPs can be further decorated with chemical or genetic fusion techniques by grafting foreign epitopes onto the VLP surface, forming chimeric VLPs, as well as exploiting the inner surfaces of VLPs to deliver adjuvants or antigens[157]. In addition, chimeric VLPs include VLPs which are made

from viral subunits of one virus while the envelope proteins are donated by a second virus[158]. This could pave the way for tissue-targeted delivery of VLPs, where the envelope proteins or the capsid proteins or both, could be engineered to target specific tissue receptors[158].

1.3.7 Self-amplifying mRNA vaccines

A particular innovation in the field of genetic immunisation is the usage of self-amplifying mRNA (SAM) vaccines, which are virally derived and engineered alphavirus genomes[159]. They are characterised by their ability of Ag-encoding RNA template self-amplification in the host cytoplasm by taking advantage of the cellular translational apparatus for Ag production in order to culminate in a targeted adaptive immune response[160,161]. SAM vaccines are 9kb long and contain cassettes encoding the inserted Ag of interest and proteins facilitating RNA replication[162]. They possess great safety profiles as they do not interact nor integrate into the host genome[163] and are instrinsically self-adjuvanting because they are detected by the host's intracellular nucleic-sensing machinery[162]. In addition, they are scalable with a low associated production cost and can activate both humoral and cellular arms of immunity, thus making them an great alternative to subunit and live attenuated vaccines[164].

1.3.8 Viral vector vaccines

Viral vector vaccines are a promising vaccine platform for delivery of vaccine antigens from an infectious agent due to their ability to express those antigens and induce robust antibody titres as well as Ag-specific cellular immune responses, without the need for exogenous adjuvants. The first published report using a developed recombinant virus, was a vaccinia viral vector in 1984 expressing Hepatitis B surface antigen and conferred protection against viral challenge[165]. Since then several viral vectors have been explored as delivery systems for heterologous immunogens including adenoviruses, adeno-associated viruses, alphaviruses, herpesviruses and others[166], while cytomegalovirus, measles virus and vesicular stomatitis

virus are the newest members of this family currently in clinical trials and/or about to be licenced[167].

1.3.8.1 Adenovirus-viral based vaccines

Adenoviruses are characterised by an icosahedral non-enveloped capsid (70-100nm) encasing a nucleoprotein core containing a double-stranded DNA genome[168] (30-40k bp). They can be manipulated to incorporate foreign DNA up to 8k bp size and they have the ability to grow in high titres during cell culture, thus can be manufactured easily, safely and inexpensively[169]. Adenoviruses can directly transduce and activate DCs forcing them to increase secretion of cytokines, chemokines and upregulate their costimulatory molecules on their surface and contribute to more efficient antigen presentation to other immune cells[170]. They can also induce transgene product specific CD4+, CD8+ T-cells or in the case of correctly folded proteins, induce B-cell specific responses[171]. Adenoviral vectors have been applied to a wide range of diseases including malaria[172], HIV[173] and most recently for Ebola[174,175].

1.3.8.2 Poxvirus-based vaccines

Due to the success of vaccinia vectored vaccines in the eradication of smallpox, poxviruses have been used intensely for vaccine applications due to their safety profile. Vaccinia virus (VV) is a lipid enveloped DNA virus with dimensions of 360 x 270 x 250 nm[176] and member of the *Orthopoxvirus* genus of the *Poxviridae* family[177]. It possesses a large double stranded DNA genome of about 180-200 kb, which enables the insertion of >10kbp of heterologous DNA for vaccine transgene induction purposes[178].

For the purposes of this thesis it is also necessary to gain an understanding of vaccinia's production cycle. Unlike other DNA viruses, vaccinia have their own transcription machinery allowing self-sufficient replication in the cytoplasm[179]. Infectious intracellular mature virus (IMV) are formed in the cytoplasm and mostly remain within the cell until lysis. A portion of

IMV move and cover themselves with double layer membrane from either endosomes or the Golgi network and transform into intracellular enveloped virus (IEV). IEV then migrates to the cell surface via the microtubule network where they bud off while acquiring another layer of lipid bilayer to form the extracellular enveloped virus (EEV) which disseminates to nearby cells[180]. An overview of the vaccinia production cycle is shown in Figure 1.10.

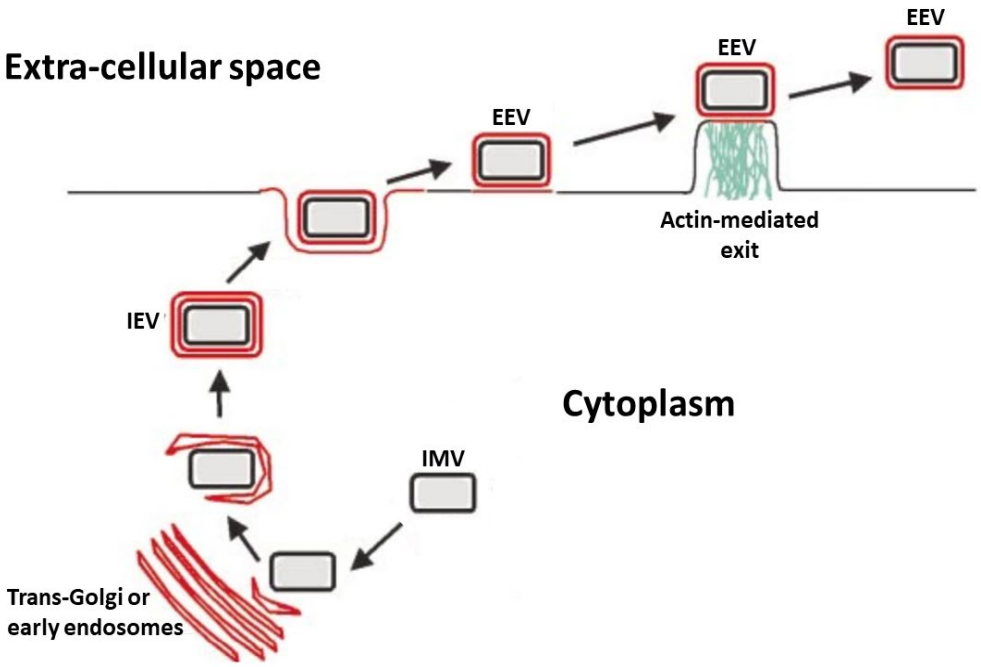


Figure 1.10 Overview of vaccinia production cycle
Intracellular mature virions (IMV) are manufactured within the cytoplasm in viral factories. A portion of IMV move to the Trans-Golgi network where they wrap themselves by double membrane either from the Golgi or early endosomes, forming the intracellular enveloped virions (IEV). IEV move to the cell surface via microtubules, where the outermost layer of IEV fuses with the cell surface membrane. Then an actin-mediated event pushes the virion outside the cell forming the extracellular enveloped virion (EEV). Adapted and modified from Smith et al[179].

Modified vaccinia Ankara (MVA) virus is an attenuated derivative of VV, which was obtained from a donkey pox lesion in Ankara (Turkey) – hence its name, passing it over 570 times in primary chicken embryo fibroblasts during the 1950s and 1960s[181]. When compared to the parental VV, MVA virus was rendered replication-deficient in humans by loss of 13% of its

genome[181]. For this reason MVA was prefered for administering a recombinant vaccinia vaccine to immunocompromised individuals in HIV trials, rather than administering a replicating viral vector[182]. Recombinant MVA viral vector has been used to deliver the immunodominant *Mycobacterium tuberculosis* antigen 85A[183] and also to deliver an multi-epitope string from *P.falciparum* fused to the thrombospondin-related adhesion protein[184] (TRAP).

1.4 Malaria

Despite our in-depth understanding of the human immune system and global efforts to rationalise and improve the design of modern vaccines to eradicate disease, malaria remains one of the most pernicious infectious diseases and a leading cause of mortality in tropical regions. In 2016, 216 million malaria cases happened worldwide with 90% of cases happening in the African region, followed by the South-East Asia (7%) and eastern Mediterranean region[185] (2%). Despite more than 6 decades of research there is no licenced vaccine against malaria[186]. Malaria is caused by protozoan parasites of the genus *Plasmodium* and this infectious agents is transmitted by infected female Anopheles species mosquitoes when they bite[187]. In humans there are 5 Plasmodium species that cause malaria: *P.falciparum, P.vivax, P.malariae, P.ovale* and *P.knowlesi*, of which *P.falciparum* and *P.vivax* are the most prevalent[188].

1.4.1 Malaria life cycle

The malarial life cycle starts with the bite of an infected female Anopheles mosquito, which transmits infectious motile sporozoites from the mosquito's salivary glands and injected directly into the dermis or the human circulatory system[187]. These sporozoites reach the liver infecting hepatocytes, replicate intracellularly and develop into schizonts which then become merozoites. Once this step is finished, merozoites are released into the blood invading

erythrocytes and begin the asexual replication cycle. Merozoites mature first into trophozoites and then develop into schizonts. After the matured schizonts and erythrocytes die, more waves of merozoites are released into the bloodsteam, which step is responsible for the associated symptoms seen with malaria disease[189]. A small proportion of the invading merozoites develop into either female or male gametocytes, which initiates the sexual cycle. These gametocytes are taken up by another mosquito during a blood meal and once ingested they fuse to form a zygote and then ookinetes inside the mosquito's midgut[187]. These ookinetes then mature into oocysts which produce sporozoites which move to the salivary gland of the newly infected mosquito in order to be injected into a new human host and thus complete the life cycle of the plasmodium species. An overview of this process is shown in Figure 1.11. Because the malarial parasite is found most of the time intracellularly either inside hepatocytes or erythrocytes, it can in part escape from immune system detection. In turn, the complex life cycle of plasmodium hinders the development of a successful malaria vaccine. As if this wasn't enough, plasmodium actively employs avoidance mechanisms. It constantly changes some of its key surface antigens[190], has high levels of polymorphism in its antigens and the genome encodes multiple copies of antigenically different but functionally similar proteins[191,192].

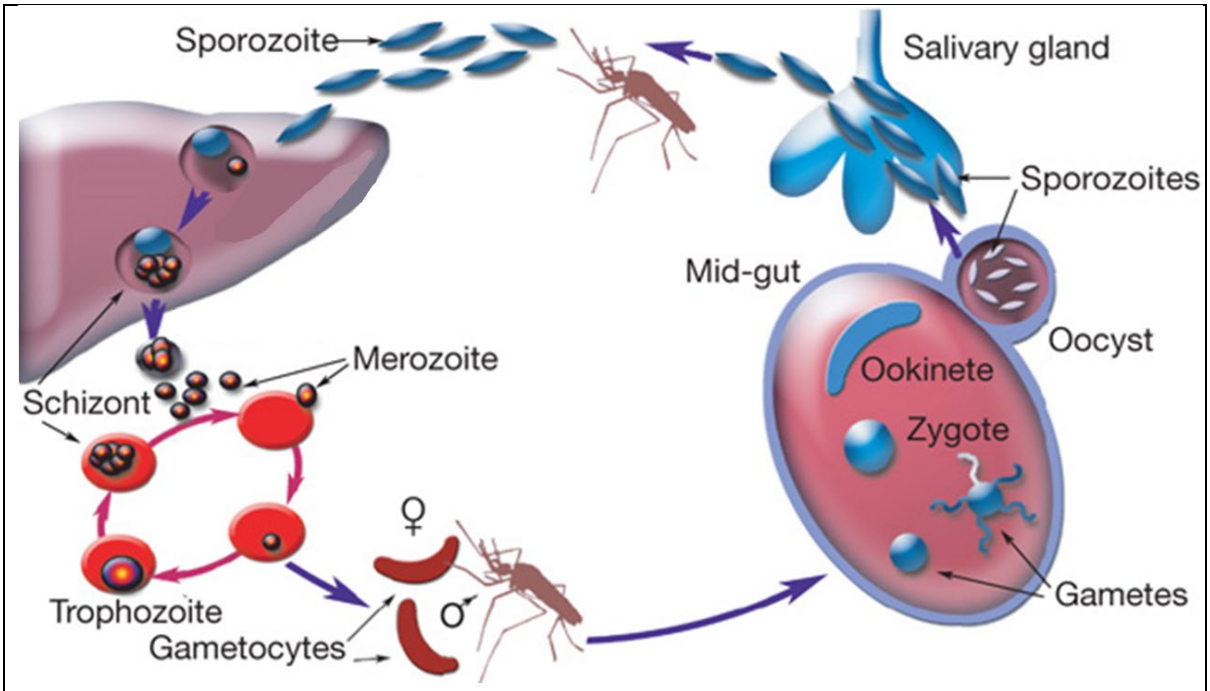


Figure 1.11 Life cycle of Plasmodium species
Infection takes place when infected mosquitos bite the human host injecting sporozoites. Sporotoizes infect hepatocytes and mature into schizonts, which then release merozoites which in turn infect erythrocytes. Trophozoites mature into schizonts again, releasing even more merozoites to infect more cells. A portion of merozoites differentiate into gametocytes, which are then taken up by another mosquito. While in the mid-gut of the mosquito, gametes generate zygotes, which become motile (ookinetes) and transform into oocysts. These proliferate and release sporozoites which are finally deposited in the salivary glands of the mosquito which will then feed off a new human host. Image adapted and modified from Winzeler E[193].

1.4.2 Malaria vaccine intervention using viral vectors

From a vaccine design point of view, cell mediated immune response has been proposed as a promising strategy to target the intracellular live form of the falciparum parasite. It has been shown experimentally in mice that vaccine induced CD8+ T-cells targeting a malarial epitope can provide protection against parasite challenge[194]. Thus an attractive strategy would be to focus on inducing a CD8+ cytotoxic T-cell response. As previously mentioned in the introduction CD8+ T-cells only recognise processed antigen presented via the MHC class I mechanism. Recombinant viral vectors are able deliver the malarial antigen in the form of DNA, transducing the target cell. Infected cells in turn efficiently display the processed

malarial antigen via the MHC class I molecule directly to CD8+ T-cells, or transduced infected cells can be phagocytosed themselves by APCs like DCs, which will also activate the CD8+ T-cells. Therefore, usage of viral vectors is currently a highly ranked strategy for induction of cytotoxic CD8+ T-cells in large part based on comparisons of the cellular immunogenicity to a range of different subunit vaccine types.

1.4.3 Controlled release MP sytems for malaria vaccine development

In the setting of malaria vaccination, controlled release systems have been explored with polymeric microparticles encapsulating: 1) recombinant malaria antigens such as PfCSP in PLA and polycaprolactone MPs in rabbits[195], PfCSP or PbCSP in PLA and/or PLGA MPs tested in murine models[196–198] and PvCSP in lipid enveloped PLGA MPs; 2) peptides such as Pb9 in PLGA MPs[199] or SPf66 in PLGA MPs[200] both tested in mouse models or SPf66 peptide in PLGA MPs tested in monkeys[201]. All these studies showed that controlled release MP systems were capable of inducing and sustaining higher Ab responses and/or inducing proliferative cytotoxic T-cell responses.

1.5 DPhil thesis aims

Recently, it has been recognised that there is an unmet clinical need for vaccine compositions having controlled release of viral vectors or providing single dosage to eliminate the need for re-immunisation as required in traditional vaccines[202].

Therefore, this thesis set out to address both challenges mentioned above by developing a technology that would allow a pulsatile release for single vaccine dosage of encapsulated viral vectors. The thesis had the following 5 general aims:

1. Encapsulate MVA virus in polymeric microparticles and quantify encapsulated content using infectious units as the readout.
2. Demonstrate immunogenicity arising from an encapsulated MVA virus.
3. Compare immunogenicity from single injection microparticle technology with encapsulated MVA to a standard unencapsulated MVA boost in an adenovirus-MVA prime-boost setting.
4. Investigate protective efficacy in a murine malarial challenge model using the technology developed.

Chapter 2
Materials & Methods

2 Chapter 2: Materials & Methods

2.1 Materials

2.1.1 Reagents

Table 2.1 Commercially available reagents used during thesis

Material	Supplier	Catalogue Number
GFP protein	Merck/Millipore	14-392
Anti-GFP protein	Millipore	06-896
Goat antimouse HRP	Sigma Aldrich	A5278
0.5ml insulin syringe/needle	BD Biosciences	587412
MAIP Elispot Plates	Millipore	MAIPS4510
Anti-mouse IFN-γ mAb	Mabtech	3321-3-1000
PureLink viral DNA/RNA mini kit	ThermoFisher Scientific	12280050
70μm cell strainer	Falcon	352350
Golgi Plug	BD Biosciences	555029
FIX/PERM	BD Biosciences	555029
PERM/WASH	BD Biosciences	555029
BCA assay	ThermoFisher Scientific	23227
DNAReleasy	Anachem	95016898
MicroAmp 96 well plates	ThermoFisher Scientific	N8010560
Polycarbonate ultracentrifuge tubes	Beckman Coulter	362305
Agarose	Sigma Aldrich	A9539
Ethanol	Sigma Aldrich	32213
Smart Ladder DNA marker	Eurogentec	MW-1700-10
NUNC Maxisorp 96-well plates	ThermoFisher Scientific	DIS-971-030J
ArC Amine reactive beads	Invitrogen	A10628
Anti-vaccinia virus Ab	Abcam	Ab156854
U-bottom plates 96-well	VWR International	734-0027
Penicillin/streptomycin (100U)	Sigma Aldrich	P-0781
Fetal Calf serum	Sigma Aldrich	F-2442
DMSO	Sigma Aldrich	D2650
Cell strainers (70μm)	ThermoFischer	22363548
24-well tissue culture plates	Appleton Woods	BC012
15ml centrifuge trubes	ThermoFisher Scientific	FB55950
50ml centrifuge tubes	Greiner	227261
Anti-mouse TNFa- FITC	eBioscience	11-7321-81
Anti-mouse CD8- PerCPCy5.5	eBioscience	11-7321-80
Anti-rat anti-hamster Igκ compensation beads	BD Bioscience	552845
Anti-mouse IFN-γ - APC	eBioscience	11-7321-54
Aqua- Amcyan live dead	Lifetechnologies	LF 257
Anti-mouse CE107a –PE	eBioscience	11-732-85
PLGA 50:50 Mw 30-60k	Sigma Aldrich	P2191
PLGA ester terminated Mw 50-75k	Sigma Aldrich	430471

PLA Mw 18-28k	Sigma Aldrich	719935
Triacetin 99%	Sigma Aldrich	240885
Taqman mastermix	ThermoFisher	4440038
SYBR mastermix	ThermoFisher	4367659

2.2 Cell culture

DF-1 chicken embryo fibroblasts (ATCC) passage numbers 10 to 30, were cultured overnight at a density of $5x10^5$ cells/well in a 24-well plate, at 37˚C under a 5% CO_2 atmosphere in a fully humidified incubator. Dulbecco's modified Eagle's media (DMEM) were supplemented with 2% or 10% (v/v) foetal calf serum (FCS), 100 units/ml penicillin, 100µg/ml streptomycin, 4mM L-glutamine, 1x non-essential amino acids and 2mM sodium pyruvate. After 24 hours the 10% FCS medium was removed, cells were washed once with Phosphate buffered saline (PBS) and 2% (v/v) FCS DMEM was added for infectivity assays.

2.3 Murine standardised quantitative whole IgG ELISA

Mice were prewarmed in a heatbox at 37°C for 10 minutes before lateral tail vein was pricked and blood was collected in heparin-coated microcuvettes. Blood was stored overnight at 4°C and sera were collected after centrifuging at 12000x g for 10 minutes. To detect mouse total IgG to eGFP, 96-well NUNC Maxisorp plates were coated at a concentration of 1µg/ml GFP and left overnight at 4°C (100µl/well). Next day, plates were flicked out and washed once with PBS containing 0.05% Tween (PBS/Tween). Plates were then blocked with 200µl/well 1% BSA/PBS solution for 1 hour at 37°C followed by 3 washes with PBS/Tween wash solution. Standards and vaccinated test sera were all diluted in 1% BSA/PBS and then added to each plate for 1 hour at 37°C. Plates were covered with aluminium foil during this step. The standard was prepared from commercially anti-GFP monoclonal antibody (Millipore) starting from 800ng/ml concentration and then serially diluted 2-fold in duplicate. Dilution series of vaccinated mouse sera samples (10-fold starting from 1:500 down to 1:50000) were added to the plates in duplicate. Plates were washed 3 times with PBS/Tween before the addition of goat

anti-mouse HRP conjugated antibody (Sigma) diluted 1:2000 in 1% BSA/PBS and incubated for 1 hour at RT while being covered. The antibody dilution was determined with a checkerboard titration. Finally, plates underwent a final 5x wash with PBS/Tween and bound antibodies were detected with the addition of 50µl/well of TMB substrate solution warmed to RT. Plates were developed for exactly 2 minutes and the reaction was stopped with the addition of 50µl/well 1M H_2S0_4. Absorbance was measured at 450nm wavelength with Varioskan Scan plate reader machine (ThermoFischer) and antibody titres were extrapolated based on the standard curve. Values taken for the extrapolation were the ones where the samples were diluted enough to fall on the linear part of the anti-GFP standard curve.

2.4 Animal work

Balb/c mouse strain (Harlan Laboratories, UK) was utilised for the experimental purposes described in this thesis undertaken at Oxford University. All mouse procedures were performed in compliance to the UK's Home Office Animals Scientific Procedures Act (ASPA) 1986. Animals were housed under sterile conditions at the Wellcome Trust Centre of Human Genetics Functional Genomics Facility (FGF) and any experimental procedures were done in accordance to UK's Home Office terms and conditions under Project License PPL 30/2889. Balb/c mice used age and sex matched within each experiment. Lastly, animals had free access to food and water whilst maintained in a 12-hour alternating light and dark cycle.

2.4.1 Mouse immunisation

Mice were immunised using a 0.5ml insulin syringe/needle (29g) and vaccine formulations were administered intramuscularly (i.m.) into the gastrocnemius leg muscle. Mice were anesthetised before each immunisation using inhalation anaesthetic of 3.5% isoflurane in pure oxygen with a delivery rate of 1.5 L/min until loss of paw withdrawal reflex. To ensure similar depth of vaccine penetration within the muscle mass of all vaccinated groups, cylindrical tubing

was cut to suitable size and placed around syringe needle before injection, to stop syringe penetrating at different depths. All immunisation doses, vaccine formulations and time intervals are all explained in the main text and figure legends.

2.4.2 Viral vectored vaccines

All viral vectors were diluted in PBS for vaccinations. Adenoviral vectors were dosed in 10^8 infectious units (i.u.) whilst MVA viral vectors were dosed in 10^6 plague forming units (pfu).

Virus	Antigen encoded
Adenovirus Chimpanzee vector type 63 (Ad63)	TIPeGFP
Adenovirus human vector type 5 (AdHu5)	TIPeGFP
Adenovirus Chimpanzee vector type 63 (Ad63)	LSA1
MVA virus	TIPeGFP
MVA virus	Luciferase
MVA virus	LSA1

Table 2.2 Viral vectors used throughout thesis

2.4.3 Mouse peripheral blood mononuclear cells (PBMCs) collection and preparation

Mice were pre-warmed in a heatbox at 37°C for 10 minutes before lateral tail vein was pricked and blood was collected in dropwise fashion into 300µl 10mM EDTA/PBS in sterile 1.5ml Eppendorf tubes. Red blood cells (RBCs) were lysed by adding 1ml ACK lysis buffer and inverting the tube several times. Cells were mixed well and centrifuged at 1073x g for 4 minutes. The red supernatants were then removed and the process was repeated until a definite white pellet was visible. Cells were briefly span down to collect leftover supernatant without disturbing the PBMC pellet. Finally, pellets were resuspended in 300µl complete DMEM media until they were needed for downstream immunological assays like IFN-γ ELISPOT and intracellular (ICS) staining. PBMCs were counted using a CASY counter using appropriate cell size settings and PBMC cell concentrations were recorded for back-calculation of number of cells seeded per each well.

2.4.4 Mouse splenocyte preparation

Mice were sacrificed by cervical dislocation and post-mortem spleens were harvested by dissection and collected in sterile PBS. Spleens were mechanically disrupted using the flat end of a 5ml syringe plunger before being passed through a 70µm cell strainer in PBS to prepare single cell suspensions into a 50ml Falcon tube, topped up to 20ml with PBS. Samples were subsequently centrifuged for 5 minutes at 500x g. Red blood cells (RBCs) were removed by first removing the supernatants, and adding 5ml ACK lysis buffer to the cell pellet whilst gently shaking for 4 minutes before adding 25ml PBS. Splenocytes were then centrifuged again and resulting cell pellets were resuspended in 5ml complete DMEM medium after passing through a 70µm for a last time to remove the 'ghost' fat tissue cell debris. Splenocytes were counted using a CASY counter using appropriate cell size settings and splenocyte cell concentrations were adjusted to $1x10^7$ cells/ml using complete DMEM medium for the downstream use in ex-vivo IFN-γ ELISPOT and intracellular staining assays.

2.4.5 Ex-vivo IFN-γ PBMC ELISPOT assay

MAIP plates were coated with 50µl of anti-mouse IFN-γ mAb diluted to 5µg/ml concentration in carbonate-bicarbonate coating buffer and left overnight at 4°C. Plates were coated with 100µl complete DMEM medium for minimum 1 hour at 37°C. PBMCs were prepared as described in section **Error! Reference source not found.** and then 50µl of PBMCs were plated in duplicate and serially diluted 2-fold down the ELISPOT plates. To gauge the IFN-γ response of our vaccinated subjects, 50µl of Pb9 peptide at 1µg/ml final plating concentration was added to stimulated wells whilst complete medium without any peptide was added to unstimulated wells. PHA (lectin) was utilised for its potent T-cell activating ability and used a positive control in the ELISPOT assay whilst an SIV gag peptide (irrelevant peptide) was used as a negative control peptide for the assay. Once the appropriate peptides were added to the corresponding wells, plates were incubated for 20 hours at 5% CO_2 atmosphere in a fully

humidified incubator. Plates were then washed 6x times with PBS and incubated at room temperature for 2 hours with 50µl/well of biotinylated rat anti-mouse IFN-γ mAb diluted to 1µg/ml concentration in PBS. Plates were then washed again 6x times with PBS and incubated at room temperature for 1 hour with 50µl/well of streptavidin alkaline phosphatase diluted to 1µg/ml concentration in PBS. Plates were washed 6x times with PBS making sure that plates are dry before addition of colour development buffer. Plates were then developed for 15 minutes by adding 50µl of BioRad AP development buffer. Developed spots were counted using an ELISPOT reader (AID iSpot Reader Spectrum – Autoimmun Diagnostika, Germany), ensuring that all plates are read with the same camera settings. Number of cells added per well was back-calculated using the cell concentration numbers counted from CASY counter. Results were expressed as spot forming units (SFU) per 10^6 PBMC after subtraction of background responses of media only unstimulated wells from those measured in peptide stimulated wells.

2.4.6 Ex-vivo IFN-γ spleen ELISPOT assay

ELISPOT plates were prepared as in section 2.4.5 and splenocytes were prepared as in section 2.4.4. After splenocyte cell concentrations were adjusted to $1x10^7$ cell/ml, 50µl were mixed with the corresponding stimulating peptides. Plates were handled and developed as in section 2.4.5. Results were expressed as SFU per 10^6 splenocytes after subtraction of background responses of media only unstimulated cells from those measured in peptide stimulated wells.

2.4.7 PBMCs intracellular cytokine (ICS) staining

To characterise the percentage of cytokine producing $CD4^+$ and $CD8^+$ T lymphocytes from the vaccinated groups, a single suspension of PBMC was prepared as described earlier in section 2.4.3. 150µl of PBMCs were incubated with 50µl of stimulatory or unstimulatory mixtures in 96-well round bottom plates. The stimulatory mixture contained Pb9 and Pb15 peptides specific to the antigen vaccinated with at a final concentration of 1µg/ml and 2µg/ml

respectively, plus 1:1000 Golgi plug (BD biosciences) plus anti-CD107α mAb at a 1:450 concentration for the staining of CD107α expression. PBMCs were allowed to incubate for 6 hours and after the incubation, plates were stored overnight at 4°C. Following day cells were centrifuged at 800x g for 3 minutes and supernatants were discarded. Cells were washed once with 100µl PBS with a viability dye (Live/Dead fixable Aqua dead cell stain kit, ThermoFisher) diluted to 1:1000 dilution in PBS and added to cells for 30 minutes at 4°C protected from light. Cells were washed again with 100µl PBS, centrifuged at 800x g and resuspended in 100µl 1% BSA/PBS. Cells were washed twice with 100µl 1%BSA/PBS before the addition of the extracellular staining antibodies. After stimulation Fc receptors were blocked with anti-mouse CD16/CD32 (Fc block) and cells were labelled with fluorescently conjugated Abs: anti-mouse CD4-Pacific Blue, CD8-PerCPCy5.5 (eBiosciences). PBMCs were surface stained with 50µl of the aforementioned cocktail of antibodies in 1% BSA/PBS for 30 minutes at 4°C in the dark. Following surface staining PBMCs were washed with 150µl of 1% BSA/PBS and then fixed with 100µl of FIX-PERM (BDBiosciences) for 8 minutes. PBMCs were subsequently washed and permeabilised twice with 100µl of PERM/WASH (BDBiosciences) and stained intracellularly with 50µl of anti-mouse IFN-γ-APC and TNF-α-FITC (eBiosciences) diluted in PERM/WASH for 30 minutes at 4°C. Following intracellular staining, PBMCs were washed three times with 150µl of PERM/WASH followed by 2 washes with 100µl of 1% BSA/PBS and resuspended in 80µl of 1% BSA/PBS for immediate acquisition on an LSRII flow cytometer (BD Sciences). If the flowcytometer was not available immediately, PBMCs were resuspended instead in 80µl of 1% BSA/PBS/formalin solution and stored overnight until acquisition. Fluorescence data were analysed using FlowJo software 10 (Treestar). Background responses in unstimulated cells were subtracted from the stimulated cells with the corresponding vaccinating Ag prior to analysis. As a positive control for the ICS staining to

stimulate production of IFN-γ, polyclonal stimulators phorbol myristate acetate (PMA) and ionomycin were used at 50 ng/ml and 500 ng/ml concentration respectively. A negative control of an irrelevant peptide SIV gag was used at 200 ng/ml.

2.4.8 Splenocyte ICS staining

To dissect the $CD4^+$ and $CD8^+$ T cell cytokine producing populations after vaccination, a single suspension of splenocytes was prepared from post mortem spleen as described in section 2.4.4. 150µl of splenocytes were added to 96 well round bottom plates and mixed with the appropriate stimulatory peptides. Splenocytes were handled and fluorescence was acquired in a similar way as described in section 2.4.7.

2.4.9 Plaque assay for MVA virus

In order to quantify the fitness of the MVA virus after exposure to different chemicals or incubation times or simply titrate and quantify the amount infectious virus after bulking up, plaque assays were executed using MVA-GFP expressing virus. DF-1 cells were utilised to titrate the MVA. 24 well plates or 96 well plates were seeded 1 day prior use with $4x10^5$ cells/well or $1x10^5$ cells/well and plates were incubated at 37˚C under a 5% CO_2 atmosphere in a fully humidified incubator for 18 hours until they reached a 90% confluency. After removing the complete DMEM media from the wells, 150µl of complete DMEM media containing 2% FCS were added to the cells until the titration point. Viral dilutions of each treatment group were prepared in a separate V-bottom plate in 10-fold dilutions. Virus samples were vortexed for 5 seconds to ensure a thoroughly mixed suspension. Once the viral dilution series was made media was aspirated and 100µl of the appropriate viral dilutions were added to the cells. To evenly disperse the virus plate was rocked backwards and forwards five times and from side to side another 5 times. Plates were incubated for 1.5 hours at 37˚C under a 5% CO_2 atmosphere in a fully humidified incubator and following the completion of incubation,

the media containing the virus was aspirated and replaced with 200µl for 96 well plates or 400µl for 24 well plates of Carboxymethylcellulose/complete media with 2% FCS overplay per well. Plates were then placed back at 37˚C under a 5% CO_2 atmosphere in a fully humidified incubator for 30 hours before visible plaque were counted by either visual scoring or taken electronic images using the ELISPOT machine with the FITC filter channel.

2.4.10 Scanning Electron microscopy (SEM)

The surface morphology and shape of the polymeric microparticles was examined using a Zeiss 300 FEG-SEM system. In brief, lyophilised microparticles were re-hydrated, centrifuged at 12045x g to remove trehalose, then 20µl suspension of microparticles were plated onto SEM aluminium stubs fitted with double adhesive carbon conducting tape. Specimens were first placed in a desiccator until fully dried and then moved in a sputter coater (QT Timed gold Quorum) to be coated with conductive gold layer for 1 minute with a 4 nm/min coating rate, for a final 3.8-4 nm coat thickness. Images were captured at 3kV accelerating voltage due to microparticles being reactive to anything higher than 3kV compromising their structural stability while imaging was conducted.

2.4.11 Transmission Electron microscopy (TEM)

For structural visualisation of MVA virus after exposure to different chemicals, TEM images were acquired. 10µl of MVA treated viral solutions were added onto grids. Grids were stained for 10 minutes with 2% aqueous uranyl acetate, followed by passing over 5 drops of water and then stained again for another 10 minutes with Reynold's lead citrate and washed again with passing over 5 water drops. Grids were then imaged using a Tecnai12/FEI operated at 100kV accelerating voltage utilising a digital CCD camera (Ultrascan US1000).

2.4.12 TEM immunostaining for MVA virus

To stain MVA against its multimerisation domain A27L, an anti-vaccinia mouse A27L antibody was used (Abcam, UK). Droplets containing MVA virions (10µl) were added onto TEM grids and blocked with 0.2% BSA solution for 10 minutes. Grids were washed by passing 5 drops of water and incubated with A27L antibody diluted in either 1:20, 1:100 or 1:200 dilutions in block solution for 30 minutes. A27L antibody was washed again with 5 drops of water before incubating the grids with an anti-mouse secondary antibody containing gold nanoparticles for 30 minutes. A last wash with PBS followed by deionised water to remove phosphate ions was done before grids were treated for TEM visualisation as described in Section 2.4.11 (above) with uracyl acetate acting also as fixative solution for MVA virus.

2.4.13 Intraparticle MVA distribution

To visualise the intraparticle distribution of encapsulated genetically engineered fluorescent MVA virus expressing a GFP molecule fused with the D8 transmembrane protein, a fluorescent Leica microscope was utilised. Microparticles were washed with water to remove trehalose and 20µl of suspended microparticles placed onto microscopic glass slides. Coverslips were placed on top of the samples (0.22µm thickness) and edges of coverslip were sealed and coverslip fasten on the glass slide with nailpolish to prevent any water evaporation. The GFP molecule was excited at 488nm and MPs were visualised and imaged.

2.4.14 Lyophilisation (freeze drying)

Once the microparticulate batches have been manufactured in order to improve their longterm stability, freeze-drying was performed which resulted in dry and structurally intact products. After being washed with dH_2O, MPs were spun down at 2000x g and resuspended in 2ml of water and transferred in glass freeze-drying vials. Trehalose was then added as a cryoprotectant to a final concentration of 15% (w/v). Before lyophilisation, samples were flash-frozen using dry ice and denatured alcohol. Samples were shaken gently to evenly disperse the MPs and

avoid sedimentation while being flash-frozen. For lyophilisation a VirTis® Advantage Plus freeze-drying system was utilised. After flash-freezing, MP batches were added to the pre-chilled chamber of VirTis® at -40°C for 30 minutes. Condenser temperature was set at -45°C and vacuum was initiated at 100 mTorr after first incubation. Primary drying was carried out with the following steps: i) 5 hours at -45°C with 50 mTorr vacuum ii) 30 minutes at -30°C with 50 mTorr vacuum and iii) 5 hours minutes at -10°C for 50 mTorr. Secondary drying consisted of 6 hours at 20°C with 100 mTorr vacuum. Samples were then stored at 4°C until needed. Weights of freeze-drying vials were measured before and after lyophilisation and the total weight of dried sample was calculated as the difference in weight of the vial before and after lyophilisation with the microparticle batches.

2.4.15 In vivo imaging

Vaccinated mice with encapsulated MVA-luciferase doses were imaged using the IVIS system (PerkinElmer, UK) in order to track bioactivity of MVA, its release rate and the microparticulate biodistribution of the encapsulated MVA-luciferase virus. Mice were anaesthetised and injected subcutaneously with 50µl of 50mg/ml luciferin substrate. After 8 minutes post luciferin injection, mice were imaged for 2 minutes. Bioluminescence from the expressed viral luciferase was quantified using the Living Image 4.2 image analysis software (PerkinElmer, UK) and expressed as the total photon flux emitted per second.

2.4.16 Production of infectious chimeric parasite in sporozoite form

Chimeric parasites were kindly provided by Dr. Ahmed Salman. Frozen *P.berghei* expressing the PfLSA1 antigen were thawed from liquid nitrogen and injected in 100µl volume intra-peritoneally into 5 naïve mice. After 6 days parasitaemia was determined by viewing Geimsa stained thin blood films. The parasitic infected mice were anaesthetised and placed onto pots of starved 5 days old female *Anopheles stephensi* mosquitoes for 10 minutes so that they get a

blood meal. The infected mosquitos with the *P.berghei* PFLSA1 antigen were maintained at 20°C in a humidified incubator and fed with free access to fructose solution. Following 20 days post-feed, infected mosquitos were sacrificed and their salivary glands were dissected under a microscope to obtain infectious sporozoites. Salivary glands were homogenised on ice and sporozoites were resuspended in sterile complete DMEM media and counted using a haemocytometer. Motility of sporozoites under phase contrast microscope was used to confirm fitness of sporozoites.

2.4.17 Blood smear preparation with Giemsa staining

Tail snip was performed and a drop of mouse blood was placed on a glass slide to prepare thin blood smear. Blood smears were allowed to completely air dry, then fixed by dipping in pure methanol and finally stained for 1 hour with 5% Giemsa stain diluted in dH_2O. Slides were then washed and allowed to air dry once again at room temperature before it was finally viewed with a light microscope at 100x magnification under oil immersion.

2.4.18 Challenge of immunised experimental mice with PfLSA1 sporozoites

To evaluate the efficacy of the encapsulated MVA PfLSA1 versus the unencapsulated normal prime boost approach, vaccinated and naïve control groups were injected intravenously with 1000 sporozoites into the lateral tail vein after 1 week post boost vaccination with unencapsulated MVA. Mice were monitored daily after 5 days post infection via thin blood films. The moment blood smears were positive with parasites and confirmed from 3 consecutives days, mice were humanely culled. Based from these blood smears and their current parasitic loads, linear regression analysis allowed the calculation of the time needed for the mouse to reach 1% parasitaemia and plot them in a graph. If however, after 14 days blood smears were negative post-infection, mice were categorised as ‘fully protected’ and were then culled.

2.4.19 In vitro MVA release assay from microparticles

After determining how many infectious MVA virions there are per milligram of lyophilised material, all tested batches were matched in terms of dry weight to have the same starting amount of encapsulated MVA virus. MVA-GFP virus was encapsulated for these studies. Microparticles were washed once with dH_2O to remove traces of trehalose and each batch was tested in duplicate and resuspended in 1ml of PBS in sterile Eppendorf tube and placed into a benchtop shaker incubator at 37°C and 200rpm. Supernatants were collected weekly by spinning the tubes at 12045x g, removing the supernatant and then replenishing with fresh PBS. Collected supernatants were then used to measure release of infectious MVA virions using plaque assay as the readout, and handled as described as in section 2.4.9.

2.4.20 Microencapsulation of BSA-FITC in PLGA or PLA microparticles using dichloromethane (DCM) as solvent

BSA-FITC loaded PLGA or PLA microparticles (MPs) of varying polymer composition were fabricated using a solvent evaporation method known as the double emulsion method with some modifications. Briefly, BSA-FITC (5mg) were dissolved in 60µl PBS – first aqueous solution (W_1) – and was added to polymer (100mg) dissolved in DCM (1ml) – oil solution (O). The mixture was emulsified by probe sonication (model XL-2000 Misonix, Microson™, setting 2) for 30 seconds to form the first inner emulsion (W_1/O). Immediately, this W_1/O emulsion was poured into 10ml of 1% PVA aqueous solution and mixed vigorously with a homogenizer (model PT-1200e Apolytron™) at maximum speed (2500 rpm) for 3 minutes. Then the resulting double emulsion ($W_1/O/W_2$) was poured into a 100ml evaporating flask and connected to a rotary evaporator (model Rotavapor® R-210, Buchi™) for the removal of DCM under reduced atmospheric pressure. PLGA MPs were washed 3 times with dH_2O by centrifugation at 2000x g (X-12R Allegra). MPs were then reconstituted with trehalose

cryprotectant at a final concentration of 15% (w/v), flash frozen and then lyophilised using VisTris AdVantage (SP Scientific).

2.4.21 Microencapsulation of BSA-FITC in PLGA:PLA MPs using DCM as solvent

Similarly BSA-FITC was encapsulated into PLGA:PLA MPs having a 1:3 ratio between the 2 polymers. For the 1:3 ratio batch, 150mg of PLGA and 50mg of PLA were used. BSA-FITC was dissolved in PBS as before and added to the PLGA polymer in DCM followed by a 30 seconds sonication to form the W_1/O emulsion. This emulsion was then added to the dissolved PLA polymer in DCM and was also sonicated for 30 seconds to form a $W_1/O_1/O_2$ emulsion. Finally this was poured into 10ml 1% PVA aqueous solution to form a $W_1/O_1/O_2/W_2$ and treated as in section 2.4.20.

2.4.22 Microencapsulation of MVATIPeGFP virus in PLGA MPs using DCM as the solvent

MVA virus expressing a model antigen, TIPeGFP, was produced and purified by Vector Core facilities (Jenner Institute, University of Oxford). TIP is an epitope string consisting of murine T-cell epitopes including Pb9 from the circumsporozoite protein of *P.berghei* and Pb15 from *M.Tuberculosis* antigen 85A[203]. TIP is fused to the N-terminus of enhanced GFP.

10^7 pfu of MVA TIPeGFP was added into 50µl of PBS forming the first aqueous phase. 100mg of PLGA polymer was used each time dissolved in DCM. The aqueous phases were then added to the dissolved polymer and was homogenised or sonicated for 30 seconds. This was then transferred into 10ml of 1% PVA aqueous solution and mixed vigorously with a homogenizer at a maximum speed for 3 minutes. Then the resulting double emulsion ($W_1/O/W_2$) was poired into a 100ml evaporating flask and connected to a rotary evaporator to remove the DCM solvent under reduced pressure. MVA-loaded MPs were washed 3 times with PBS with centrifugation at 2000x g and finally MPs were then flash-frozen and lyophilised for longterm storage.

2.4.23 Microencapsulation of MVA virus in polymeric MPs using triacetin as the solvent

10^7 pfu of different MVA viruses were added into 50ml to form the first aqueous phase. Polymer concentration was 100mg/ml dissolved in triacetin. The aqueous phases containing the MVA was added to the dissolved polymer and homogenised at maximum speed for 30 seconds. This first emulsion was then added into 1% PVA aqueous solution to form the double emulsion. The volume of 1% PVA in initial experiments was 10ml but in the final stages of the project this was changed to 50ml of 1% PVA to ensure that the triacetin solvent was fully removed into the aqueous phase resulting in the hardening of the triacetin-based MPs, since triacetin is only 6% water miscible. MVA loaded microparticles were then washed 3x times with water and treated the same way as in above section and lyophilised.

2.4.24 Characterisation of MP size and surface morphology

After lyophilisation BSA-FITC loaded and MVA-loaded MPs were mounted onto microscope slides for visualisation. All images of MPs were acquired using a Leica DM500 optical microscope at 40x magnification. Images were then analysed using Image Prosight software.

Particle size analysis for all MPs was performed by laser diffraction analysis using an Accusizer. MPs were uniformly dispered in distilled water using a magnetic stirrer while being measured.

2.4.25 Determination of encapsulation efficiency of BSA-FITC in MPs

To determine BSA-FITC loading efficiency, 10mg of lyophilised BSA MPs were lysed using 500µl of 1M NaOH overnight at 37°C in a 200rpm shaking incubator. Samples were neutralised with 500µl of 1M HCl and the amount of supernatant was then quantified using the Bicinchoninic acid (BCA) assay, (ThermoFischer, UK). A standard curve using BSA dilutions, was used to interpolate the BSA content from each supernatant and calculate the theoretical amount of BSA-FITC per mg of lyophilised material for the whole batch. The FITC excitation

range did not interfere with the excitation range used for the BCA readout according to manufacturers guidelines.

2.4.26 Critical points for survival of MVA virus after exposure to solvents, sonication or lyophilisation.

i) Solvents: 10^6 pfu of MVA-GFP virus were added to sterile Eppendorf tubes. Then an array of different solvents each at 100µl volumes: acetone, DMSO, DCM, AcN, were added to tubes were vortexed for 30 seconds. Then 2ml of PBS were added to each tube to dilute the solvent and solvents were removed by negative pressure using SpeedVac concentrator for 1 hour. MVA virus was added to DF-1 cells and titrated according to section 2.4.9.

ii) Sonication: 10^6 pfu of MVA-GFP virus were added to 1ml of PBS. Samples were either sonicated using a probe sonicator (model XL-2000 Misonix, Microson™, setting 2) or homogenised (model PT-1200e Apolytron™ at maxium speed -25000 rpm) for 30 seconds. MVA virus was then added to DF-1 cells and titrated according to section 2.4.9.

iii) Lyophilisation: 10^6 pfu of MVA virus were mixed with different excipients, and then lyophilised using VirTris AdVantage (SP Scientific). After lyophilisation, batches were rehydrated with 1ml PBS and MVA viruses were added to DF-1 cells and titrated according to section 2.4.9.

2.4.27 Measurement of NaOH lysed MVA virus using protein assay

To measure protein content, the BCA protein assay was used according to the manufacturer's instructions and performed on 96 well black microtitre plates. For standard curve, known amounts of MVA starting from 10^8 pfu/ml and the subsequent 2-fold dilutions, were lyophilised and then lysed overnight with 500µl 1M NaOH and neutralised with 500µl 1M

HCl. This way the standard curve of known viral amount, has undergone the same treatment that the encapsulated MVA has gone through after NaOH hydrolysis. Standards were done in triplicate.

2.4.28 Data analysis

Results are shown as the mean plus standard deviation. Data were analysed by one-way Analysis of Variance (ANOVA) followed by Bonferroni's multiple comparison post-hoc test. Differences between treatment groups were considered significant if the p value was less than 0.05. Error bars correspond to standard deviation. Statistical analysis was done using the Prism 6 software package (GraphPad software Inc, USA).

2.4.29 Flowcytometry analysis

Flowcytometry data were collected using LSR II flowcytometer and then analysed using FlowJo version 10 (Tree Star, USA).

2.4.30 Electrospraying processing of MVA virus

An EHDA system was used to assess the effect of electrospraying on virus viability after exposure to high voltages. Such high voltages are routinely used in electrospray-based manufacturing methods for production of uniform polymeric microparticles[204]**.** A high voltage source (0-30kV output, amperage 0-4 mA) was connected via metallic clips and wires to a single stainless steel needle assembly and a ground electrode to create an electric field inside an airtight acrylic chamber. The chamber was filled with N_2 gas to provide a combustion-free inert atmosphere throughout the experiments. Experimental MVA solutions (1ml) were fed into the chamber using polytetrafluoroethylene (PTFE) tubing using plastic 10ml syringes (BD PlasticTM,VWR,UK) mounted on a programmable syringe pump (Harvard Apparatus PHD2000, Harvard Apparatus LTD, UK) which controlled the flow rate input into the EHDA system. Once the chamber was filled with inert gas and the appropriate voltages have been set

and applied, the virus solutions were pumped at a constant rate through the electrified needle and then collected in a sterile 10ml glass vial. Upon completion, the tubing system and needle were flushed with 10ml of pure ethanol followed by 10ml PBS. After electrospraying recovered viral samples were assessed for viral infectivity using plaque assays.

2.4.31 MVA virus bulk and purification

Desired MVA viruses (MVA-D8-GFP) were multiplied initially after infecting a confluent monolayer of DF-1 cells in a T75 flask with 2% FCS (v/v) complete DMEM media for 3 days at 37˚C incubator, as a premaster seed flask. In parallel, a T175 multilayered hyperflask was seeded with DF-1 cells with complete 10% FCS (v/v) DMEM media and incubated until it has reached a 90% confluency. Cells from the T75 flask were harvested mechanically with a cell scraper, placed in falcon tube, flash-frozen and thawed 3 times in order to release the produced MVA viruses from within the DF-1 cells. This cell supernatant was then used to infect the confluent T175 hyperflask after being mixed in 500ml of 2% FCS DMEM followed by a 5 day incubation at 37˚C. Cells from the infected hyperflask, were harvested with cell scrapers and pooled into a 250ml conical bottle, which was then spun for 10 minutes at 670x g to pellet the cells. From this point onwards all cell pellets and supernatants were kept on ice. The supernatant from the hyperflask was carefully added to 2x sterile 250ml flat-bottom bottles and were kept on ice. Then the pelleted cells were resuspended in 2ml 10mM Tris pH 9 buffer, transferred to a 15ml Falcon tube and lyses with 3 freeze-thawing cycles with vigorous vortexing in between. Then the respuspended cell pellet was pelleted at 670x g for 5 min and finally the supernatant was taken and added to the previously collected 500ml supernatant in the 2x 250ml bottles. These 2 bottles were spun for 40 minutes at 26000x g at 4˚C with an Avanti centrifuge, and supernatants were discarded, leaving a large pellet, which was then resuspended into 2ml 10mM Tris pH 9 and mixed hard by vortexing.

To further purify the pellet, which contains the bulked up MVA viruses and other sub-cellular organelles a 36% semi-purification method was used. The ultracentrifuge buckets were thoroughly cleaned in a biological safety cabinet before usage by cleaning the lids with 10% (v/v), then spraying with 70% EtOH, turned upside down to let the EtOH be evaporated and then wiping down with paper. This was done to ensure that no cross-contamination of previously bulked up MVA viruses occurs.

Autoclaved thick walled polycarbonate ultracentrifuge tubes (Beckman Coulter) were filled with 2ml of 36% (w/v) sucrose cushion solution and then 1ml of sample was loaded gently on top of it with a Pasteur pipette. After this step, tubes were spun down in a fixed angle rotor with Optima TLX at 7000x g at 4˚C for 2 hours with medium speed acceleration and deceleration settings, so that the sucrose cushion doesn't get disturbed. The supernatant which includes sucrose mixed with cell impurities was removed by firstly removing the top upper layer, ensuring that this does not contact the purified pellet at the base of the tube and then by removing 1ml at a time in order to not disturb the purified pellet containing the MVA viruses. The pellet was then resuspended in 1ml of 10Mm Tris pH 9 buffer, vortexed and small aliquots were done and stored at -80˚C until further use. The bulked up MVA batch was tested for sterility and then plaque assays were performed to determine the viral titre.

2.4.32 Sterility test for bulked up MVA viruses

The sucrose cushioned purified MVA viruses were tested for sterility from any contaminating bacteria or fungi that might have been introduced during the bulking up procedure. Lysogeny broth (LB) nutrient rich broth was used to test for the presence of growing contaminating microorganisms. LB broth was autoclaved and kept sterile at all times. A 10µl sample from the purified aliquoted virus was added to LB media and incubated in a shaking incubator at 37˚C for 3 days. A shoe sole swap was inoculated into LB medium as a positive control. Non-

inoculated sterile LB medium was used as a negative control. Finally, a sample aliquot from the Tris buffer used to resuspend the pelleted MVA viruses was also tested. Presence of a cloudy medium after 3 days of incubation signified contamination.

2.4.33 Free-flow electrophoresis (FFE)

Free-flow electrophoresis strategy was explored to attempt and separate MVA from dissolved polymeric matrix due to differences in charge of the polymer and virus. FFE is a matrix-free electrophoretic separation technique. A FFE chamber setup comprised of a continuous zone electrophoresis with a 0.5mm spacer and a 250mM sucrose/ 10mM triethanolamine/100mM Acetic acid buffer system at pH 7 for both the stabilisation buffer and electrode buffer.The run parameters used were 800V and 120mA. Sample was injected at 1.5ml/hour into the FFE chamber and after separation based on their isoelectric point it was collected in 96 fractions in total in a 96 deep well plate.

2.4.34 Quantitative PCR (qPCR) for MVA

2.4.35 Primer design

Primers, designed from scratch with stringent criteria using Primer3 software (http://primer3.ut.ee/), were selected to recognise the conserved sequence encoding the DNA polymerase of MVA virus (E9L gene – Copenhagen designation). This ~3k bp DNA sequence is an ortholog to the Vaccinia virus Western Reserve (WR) strain (VACWR065) DNA polymerase gene with a UniProt ascension number P06856. Primers were designed to conform with IDT's online guidelines (https://www.idtdna.com/pages/decoded/decoded-articles/pipet-tips/decoded/2013/10/21/designing-pcr-primers-and-probes).

For primer design: 1) Primer size was selected to be from 18 to 23 bases with melting temperature (Tm) between 60 and 64°C and ideal of 62°C. 2) The Tm of both primers were set to be 1°C or 2°C maximum different from each other so that both primers bind at the same time

and efficiently amplify the amplified product (amplicon). 3) Amplicon size (PCR product) was set to be within the range of 75-150 bp size. 4) Lastly, the GC content of the primer assay was set to be between 35-65% with an ideal of 50%, which allows a degree of complexity while having a unique sequence. 5) On the Primer3 settings we made the primers even more stringent with a maximum allowable length of a mononucleotide repeat to be 3 rather 5 using the Max Poly-X function; example AAA instead of AAAAA. 6) Returned software generated primers that contained regions of 4 or more consecutive G residues were not selected.

For internal Taqman-based probe design (oligo): 1) Generated probe was set to be in the region between the 2 primers but should not overlap with a primer binding site located on the same DNA strand. 2) Oligo size was set to be from 20-30 bp with an optimal size of 25. 3) The Tm was set to be 10°C higher than the primers to saturate the amount of probe molecules bound to the target sequence before the primers amplify the product, thus guaranteeing the specificity of the qPCR assay. 3) Similarly, with the primer sequences, the GC content of the probe was set to be from 35-65% with the optimal content being 50%. In addition, any generated probe with a G at the 5' end, was not selected to avoid the quenching of the 5' fluorophore. 4) Internal Oligo Max Poly-X function was set to allow 5 mononucleotide repeats.

For amplicons: 1) Amplicon length was set to be 75-150 bp to allow enough downstream nucleotide sequence within which appropriate primer and probe set with satisfactory criteria and Tm can be designed. This short length is easily amplified using standard universal qPCR cycling conditions, whilst longer lengths will need longer cycling conditions.

Finally, both primers and probe designs were screened for self-dimers and/or hetero-dimers against the primers as well as any potential hairpin formations, which could negatively affect the qPCR efficiency. Primer3 software automatically runs these screens after primer selection.

Once generated, potential primer and probe sets were tested for their qPCR efficiencies using vDNA extracted from corresponding MVA viral dilutions or with the use of a BAC-MVA plasmid that contains the entire genome of MVA. Some primer/probe pairs had to be discarded due to inadequate qPCR efficiencies and were replaced by the most suitable one having an efficiency between 90-100% in accordance to MIQE criteria[205].

2.4.36 Viral DNA extraction

Viral nucleic acids were extracted using a Purelink Viral RNA/DNA extraction kit according to manufacturer's instructions (ThermoFisher). In brief, 25µl Proteinase K were added into a sterile microcentrifuge tube, along with 200µl of cell-free sample. After addition of 200µl lysis buffer, samples were vortexed for 15 seconds and incubated at 56˚C for 15 minutes in a heat block. Then 250µl pure ethanol were added to each sample, vortexed for 15 seconds followed by a 5 minutes incubation at RT. Viral lysates were added to viral spin columns, centrifuged for 1 minute at 6800x g, discarding the flow through and re-spun at 6800x g after addition of 500µl wash buffer to the spin column. After discarding the flow through, spin columns were centrifuged at maximum speed (20000x g) for 1 minutes to dry the membrane. Lastly, viral spin columns were added to sterile 1.5ml centrifuge tube where the vDNA was eluted with the addition of sterile RNase free water in 50µl volume. The extracted vDNA samples were finally stored at -20˚C until they were required.

2.4.37 qPCR setup

To avoid potential cross contamination dedicated pipettes were used just for the generation of 10-fold MVA viral dilutions and different dedicated pipettes in a different room were used for diluting vDNA and for the plating of the samples and standards. Pipettes were routinely UV sterilised in the hood before usage and all equipment (racks) and consumables (gloves/filter tips/tubes) were of DNAse free quality. Plating of samples and standard was also routinely

done at a specified bench area, which had previously been DNAsed. MicroAmp Optical 96 well plates (Thermo) were used and in each plate samples, standards and no template control (NTC) were plated in triplicate. For the purposes of reducing pipetting errors, 5µl of vDNA were added to each well. Reactions were performed with 10µl enzymatic mastermix along with appropriate amounts of the primer/probe set for Taqman reactions or just primer set for SYBR green reactions and filled up with nuclease free water to a final volume of 20µl. All qPCR assays were performed using an Applied Biosystems StepOne Plus qPCR machine and data analysed with using StepOne software version 2.3.

2.4.38 SYBR green based qPCR protocol

A universal SYBR green mastermix solution (Applied Biosystems, UK) was used. The cycling conditions were as follows: enzyme pre-activation for 2 minutes at 50°C, then initial denaturation step for 10 minutes at 95°C, followed by 40 amplification cycles including denaturation at 95°C for 15 seconds and annealing/extension for 1 minute at 60°C. At the end of 40 PCR cycles, a melt curve step was additionally created by continuously recording the fluorescence during progressive heating up to 95°C with ramp rates of 0.3°C/s increments. This analysis assesses whether the DNA intercalating dye used in the assay has produced single specific products, which is a concern with intercalating dye assays rather than Taqman probe-based assays. This is due to the fact, SYBR green binds to any double stranded DNA product, which includes the primers themselves, during the amplification stages and thus it is not sequence specific.

2.4.39 Taqman probe based qPCR protocol

Unlike intercalating dye-based assays, with probe-based assays the same primers get an added level of specificity which stems from the probe. The probe, which is an additional 3rd DNA sequence is required to bind within the target sequence and in between the 2 primers. Once this takes place, only then this generates a fluorescent signal.

Universal qPCR cycling conditions were used with an initial hot start activation for 10 minutes at 95°C, followed by 15 seconds denaturation at 95°C and 1 minute annealing/extension at 60°C for 40 cycles enzyme step for 2 minutes at 50°C followed by an initial denaturation step for 10 minutes.

Some probes were using the FAM-TAMRA chemistry while others were using the FAM-MGB. Once the experiment was finished, values were extrapolated from the standard curve and presented as pfu/mg of lysed MPs to calculate the encapsulated viral load and encapsulation efficiency for each manufactured batch.

Primers and probe sequences used in this thesis:

		5'-3' DNA sequence	Algorithm used
	Forward	CAACCACATATCTGCGACGGA	Primer3
	Reverse	TCAGTCATTGTCTCCTCCTCCA	
	Probe	AGTTCTCATCTTTCCCAACGGCCCTCGCA	
	Forward	GCGTTTCTTTGGCTCTTCTATC	IDT technologies
	Reverse	GTCATTGTCTCCTCCTCCATTT	
	Probe	AGTTCTCATCTTTCCCAACGGCCT	
	Forward	TTGGCTCTTCTATCAACC	Sigma Aldrich
	Reverse	TCCTCATTACTTTTATTACGTAG	
	Probe	AATGGAGGAGGAGACAATGACTGAT	
	Forward	CGGCTAAGAGTTGCACATCCA	Baker et al
	Reverse	CTCTGCTCCATTTAGTACCGATTCT	
	Probe	AGGACGTAGAATGATCTTGTA	
	Forward	GAACATTTTTGGCAGAGAGAGCC	Pan orthopox paper
	Reverse	CAACTCTTAGCCGAAGCGTATGAG	
	Probe	CAGGCTACCAGTTCAA	
		Sequences not provided due to patented software	Applied Biosystems

Table 2.3 Primer/probe sets used in this thesis

Chapter 3
MVA virus encapsulation and quantification

3 Chapter 3: MVA virus encapsulation & quantification

Statement of authorship

All microparticles (MPs) were manufactured by CK. All in vitro and in vivo experiments including animal procedures, sample collection and immunological work, their associated analysis, optical microscopy, fluorescent microscopy, ultracentrifugation, viral plaque assays, SEM, 80% of TEM, 80% of immunogold labelling for TEM, were done by CK. The rest 20% of TEM and 20% immunogold labelling for TEM were purchased as a service. FFE procedure was done by Dr. Joshua Blight.

3.1 Introduction

In a seminal study conducted in the 1990s, the recombinant MVA viral vector was used for the first time in the setting of malaria as a part of a DNA-MVA prime boost regime stimulating CD8+ T-cells. Mice were sterilely protected in *P.berghei* sporozoite challenge by TRAP and CSP liver antigens[206]. When adenovirus replaced DNA as the priming vaccine in a heterologous adenoviral-MVA prime boost regime instead, even higher T-cells were induced which added more credibility to the notion that MVA viral vectors have superb immune boosting abilities but not very good priming abilities[207].

It has been shown that protection from irradiated sporozoites infection in mice and non-human primates is mediated by cytotoxic CD8+ T-cells targeting the liver stage of the disease[208–210].

At the Jenner Institute, there is a major goal of developing and improving new vaccination regimes against malaria with a particular focus on optimising T-cell inducing vaccines for the liver stage of malaria. One of the main vaccine platforms at the Jenner Institute is an adenoviral-MVA prime boost regime.

An 8 week interval heterologous adenovirus – MVA regime using ME-TRAP as the encoding antigen has shown good results in our group[211], where CD8+ T-cell responses have been associated with clinical efficacy. Even more recently, the same heterologous regime was used in the setting of an Ebola vaccine where comparable cellular and humoral immunity was achieved with prime-boost intervals as short as 1 or 2 weeks[212].

In this setting, the adenoviral-MVA prime boost regime requires two injections separated by 1 - 8 week interval. As previously mentioned in general, vaccines require more than one injection in order to provide robust immune responses and this can cause insufficient coverage due to non-compliance. Single dose immunisation using fabricated biodegradable polyester microparticles has been suggested as an approach to address this issue. The shared vision of increasing compliance worldwide, led the WHO and the Children's Vaccine initiative in the 1990s to sponsor research for the development of such fabricated microdevices using tetanus toxoid as a model vaccine[213]. Fast-forward 20 years, this particular idea was revisited in order to introduce the microencapsulation technology and transform Jenner Institute's established adenovirus – MVA prime boost regime from 2 injections into a single dose.

Studies in the past have demonstrated pulsatile release from PLGA microparticles in vitro[214], however in vitro release kinetics do not correspond with what happens in vivo[215,216]. The reason behind such discrepancy could be explained by biological factors (inflammation, presence of enzymes, organic constituents e.g. lipids) and by physicochemical factors (surrounding fluid volumes, inherent pH buffering systems) present at the MP administration area, which combined can affect the drug release rates from MPs[215]. Only recently there was an attempt for a pulsatile release in vivo, using inactivated polio virus (IPV) as the encapsulated vaccine[217].

To tackle the gap of knowledge and the clinical need presented in the introduction, we sought to develop a technology that would allow the transformation of the current adenoviral prime

and MVA boost regime, from a 2-injection regime into a single injection by encapsulating the MVA booster dose. Our general strategy to achieve this goal was to encapsulate MVA virus using current methodologies and practices in the field of drug microencapsulation, followed by a suitable method to measure encapsulated infectious MVA virus and then testing different MVA-loaded MP formulations with in vivo immunogenicity studies.

3.2 Vaccine encapsulation into polymeric microparticles

The main purpose of this thesis was to evaluate the feasibility and potential use of a pulsatile release technology in our current heterologous adenovirus prime and MVA virus boost regime with an 8-week interval (Figure 3.1). Tunable MVA virus loaded core-shell microparticles were proposed to be engineered to create a delayed/pulsatile release of the encapsulated MVA. This would enable a single administration prime-boost methodology, in which the prime vaccine is given alongside the encapsulated booster vaccine, which is tuned to be released with an 8-week delay release profile in vivo.

3.3 BSA-FITC loaded microparticles

To begin with, standard BSA-FITC loaded microparticles were made using the double emulsion technique. PLGA MPs were prepared using a standard water-in-oil-in-water ($W_1/O/W_2$) emulsion/solvent evaporation technique or in the case of double walled particles, a $W_1/O_1/O_2/W_2$ emulsion both shown in Figure 3.2. BSA-FITC was encapsulated initially as a model antigen as described in Methods (2.4.20 & 2.4.21). Briefly, the inner waster phase W_1 consists of the BSA-FITC protein disolved in solution. The oil phase (O) contains the dissolved PLGA polymer in DCM (organic solvent), which will form the polymeric mesh. After the BSA-FITC solution (W_1) is added to the oil phase (O) forming the primary emulsion (W_1/O), this is then transferred to the external aqueous phase (W_2) containing the stabiliser PVA forming the double emulsion ($W_1/O/W_2$), or ($W_1/O_1/O_2/W_2$) if PLA polymer is used as the

second oil phase (O_2). Evaporation of DCM solvent from the final emulsion, leads to a critical point causing the polymer to precipitate and encapsulating the protein of interest. In the case of encapsulating lyophilised protein instead of dissolved protein, the emulsions now includes a solid dispersion (S) instead of W_1 thus forming $S/O/W_2$ or $S/O_1/O_2/W_2$ respectively.

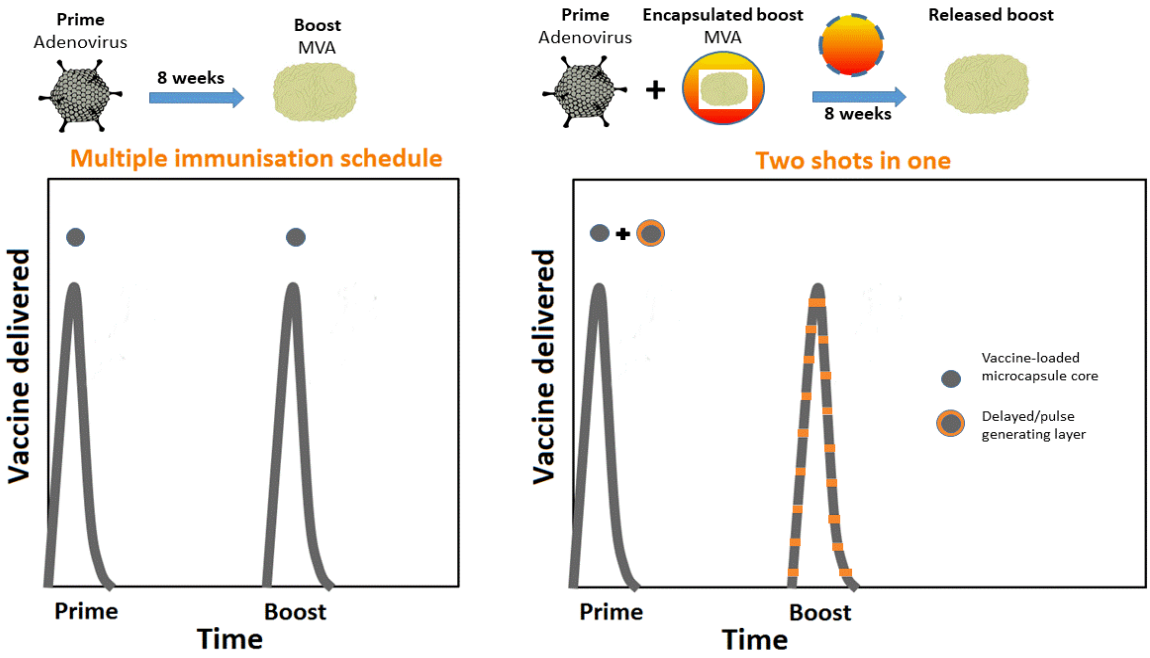


Figure 3.1 Graphical thesis concept for a single administration prime-boost regime
Many commercial vaccines require multiple injections spaced weeks/months/years apart. At the Jenner Institute, the current leading approach for CD8+ T cell induction is an Adenovirus prime encoding the Ag of interest followed by a second booster injection of an MVA virus encoding the same Ag.

BSA-FITC PLGA MPs were synthesised and following washing and freeze-drying (Methods 2.4.14), microparticles were visualised in order to evaluate microparticle morphology. Photographs were taken using light microscopy (Methods 2.4.24), scanning electron microscopy (SEM) (Methods 2.4.10) and fluorescent microscopy collated in Figure 3.3. The MPs were of spherical nature with a porous morphology. Particle size analysis was performed using an Accusizer particle size analyser (Methods 2.4.24) and size distributions for each MP batch is shown in a table format in Figure 3.3D, ranging from 2-95µm in size.

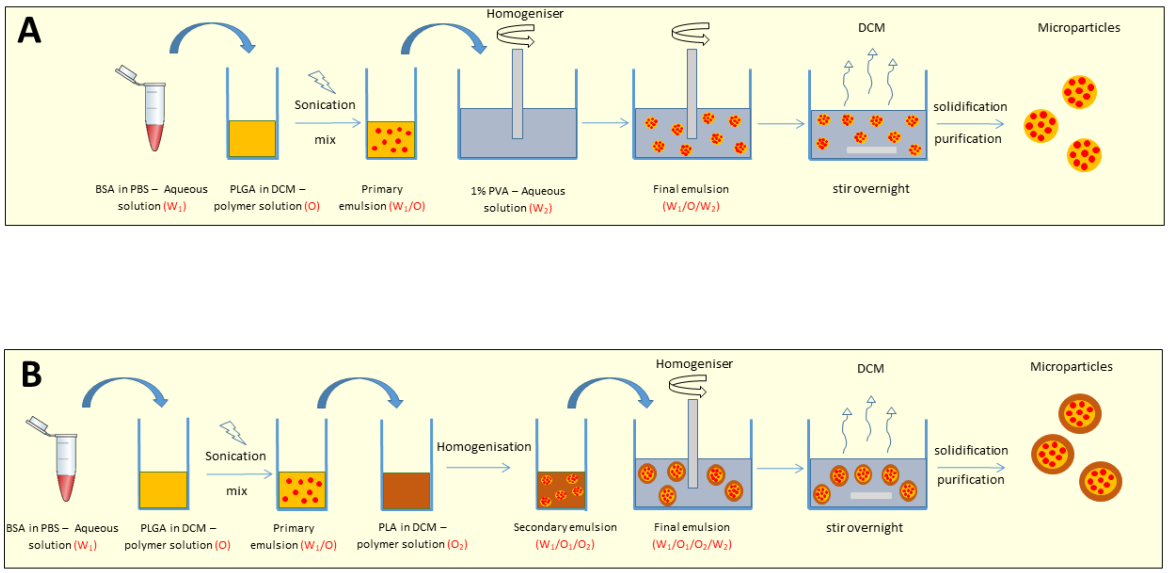
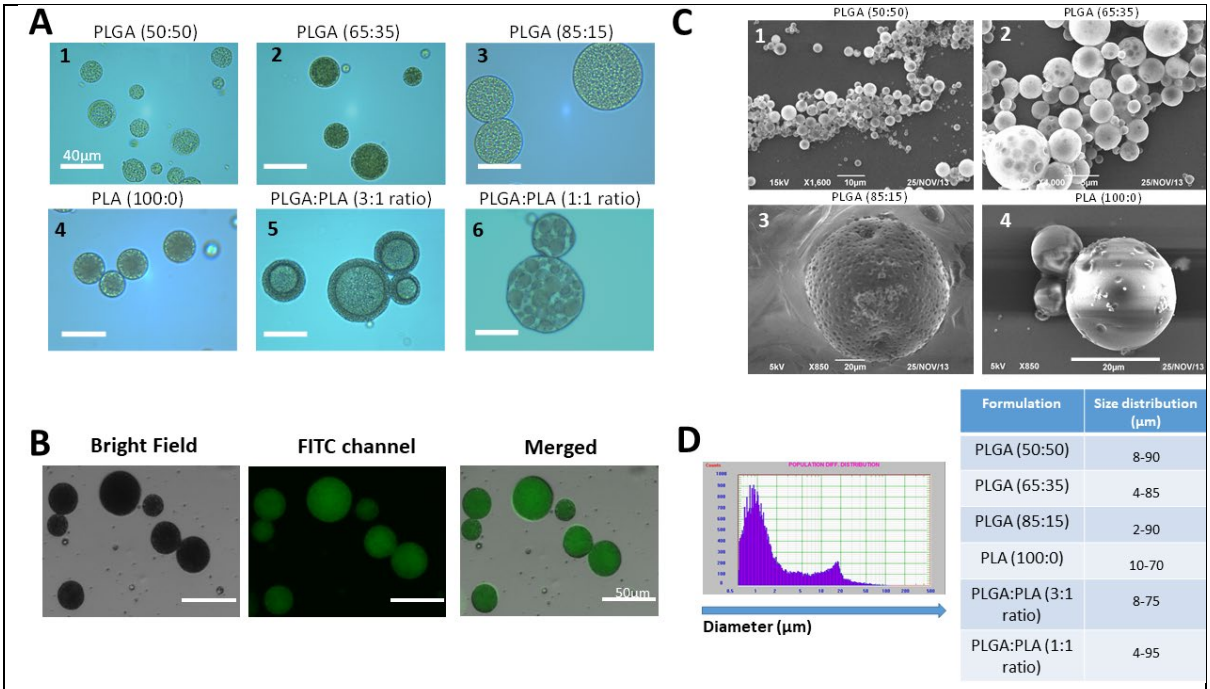


Figure 3.2 Preparation of microparticles by double emulsion solvent evaporation

A) Protein/vaccine is dispersed in organic solvent containing PLGA by 30 second sonication or homogenisation. This forms the primary water-in-oil emulsion (W_1/O). The primary emulsion is then transferred to a larger aqueous phase containing the polyvinyl alcohol (PVA) stabiliser (W_2).

B) Similarly with A, to form double walled MPs protein/vaccine solution is mixed with PLGA polymer solution and then dispersed into organic solvent containing PLA by sonication or homogenisation. The resultant polymer W_1/O emulsion containing mixed PLGA and PLA is then transferred into a larger aqueous phase containing the PVA stabiliser forming the final $W_1/O_1/O_2/W_2$ emulsion.

In both settings, once the final emulsions have been formed, the volatile solvent (DCM) is allowed to evaporate at either reduced (rotary evaporator) or normal atmospheric pressure (mechanical stirring overnight). This causes the hardening of the MPs. MPs are then purified by centrifugation and washed several times to remove the stabiliser PVA, before being lyophilised.



Formulation	Size distribution (µm)
PLGA (50:50)	8-90
PLGA (65:35)	4-85
PLGA (85:15)	2-90
PLA (100:0)	10-70
PLGA:PLA (3:1 ratio)	8-75
PLGA:PLA (1:1 ratio)	4-95

Figure 3.3 Microparticle morphology

A) Optical microscopy images (40x magnification) of biodegradable MPs with different ratios between lactic and glycolic acid of PLGA. A1-A4 were made using $W_1/O/W_2$ double emulsion method where O is dissolved PLGA. A5&A6 were made using $W_1/O_1/O_2/W_2$ double emulsion method where O_1 is dissolved PLGA and O_2 is dissolved PLA. A1) PLGA (50:50); A2) PLGA (65:35); A3) PLGA (85:15); A4) PLA (100:0); A5) PLGA:PLA (3:1 ratio to each polymer); A6) PLGA:PLA (1:1 ratio to each polymer). Scale bar = 40µm.

B) Representative fluorescent images using the 40x objective, confirming the presence of BSA-FITC within the MP matrix and revealing its intra-particle distribution. Scale bar = 50µm.

C) Representative SEM imaging of lyophilised MPs containing BSA-FITC. MPs were made using double emulsion. Specimens were placed onto metal stubs coated with lysine, dried, sputter coated with gold and then visualised. C1) PLGA (50:50); C2) PLGA (65:35); C3) PLGA (85:15); C4) PLA.

D) Representative size distribution data based on mean volume diameter of the microparticles using an Accusizer diffractometer. A table showing the size distribution in µm for each MP batch is at the bottom right.

3.4 MVA encapsulation processing stability studies

For the microparticle-based pulsatile release technology to be effective, MVA virus needs to survive the encapsulation process. This includes steps such as contact with organic solvents, high energy sonication and mechanical stress which are both used to disperse the primary emulsions into the secondary emulsion during the double emulsion procedure. Lastly, a lyophilisation step is included where MPs containing MVA are lyophilised to form a dried and stable MP product that can be used to vaccinate mice.

Known amounts of MVA were subjected to each of the aforementioned steps and to determine the amount of MVA that survived the encapsulation emulsion simulation, MVA was quantified with the plaque assay technique (Figure 3.4), described in detail in Methods 2.4.9.

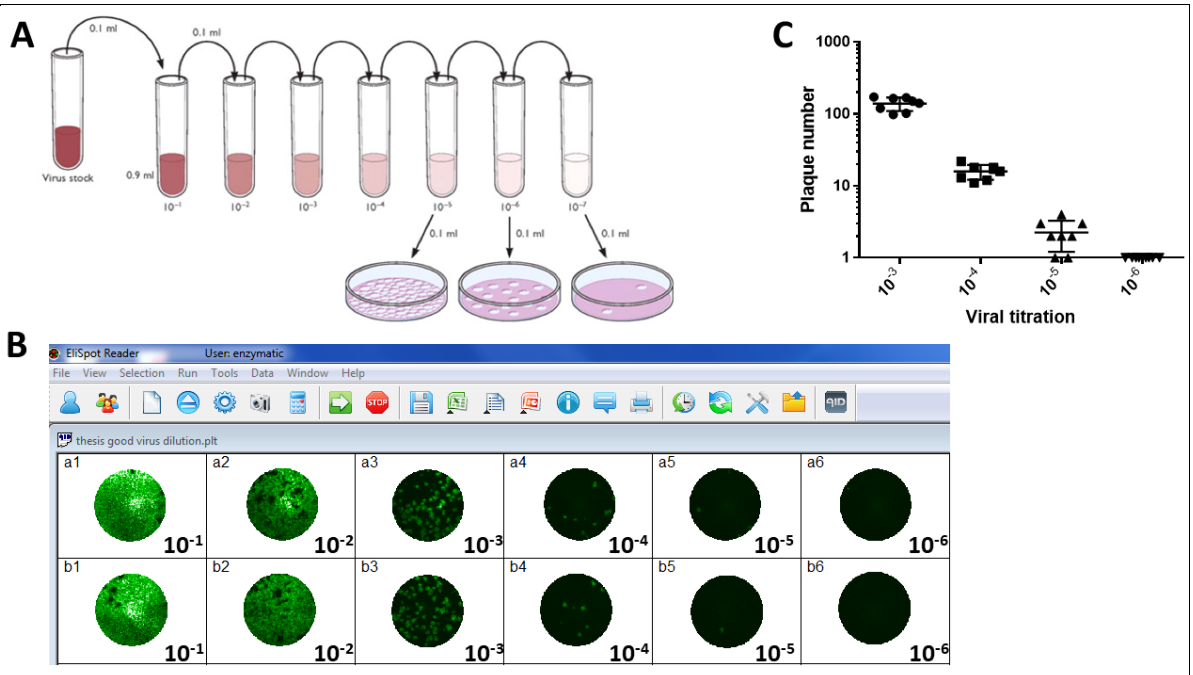


Figure 3.4 Quantification of bioactive MVA with plaque assay

A) Schematic overview of principle of plaque-based viral quantification in terms of infectious dose. To measure the concentration of MVA in a sample, 10 fold dilutions were prepared and 100µl were added to susceptible DF-1 chicken fibroblast cell monolayers. After 1.5 hours incubation time, where the virus attaches to DF-1 cells, the monolayers are covered with medium containing carboxymethylcellulose that limits the spread of MVA. When an infectious virion infects a cell, a viral plaque is formed. This lytic event is then used to determine the titre of the original stock in plaque-forming units (pfu) by back-calculating based on the number of plaques visible and the dilution factor.

B) An example of viral plaque assay used to determine the amount of MVA surviving the encapsulation process. MVA used encodes GFP protein hence fluorescent plaques were visible after 30 hours post infection under a microscope. A fluorescent ELISPOT reader was used to take microphotographs on FITC channel from 96 well plates containing the fluorescent plaques. Microphotographs show dilutions at which virus has completely infected the whole cell monolayer (dilution 10^{-1} and 10^{-2}) and there were too many plaques to count. Dilution with 10^{-3} and 10^{-4} plaques were countable and no plaques were developed at dilutions 10^{-5} and 10^{-6} because too few or no virions were present.

C) Representative dataset from a highly concentrated MVA virus encoding GFP that was bulked up, and titrated with plaque assay using 8 different aliquots (n=8). Plaque numbers are shown as the median from dilutions that plaques were distinct and countable starting from 10^{-3} dilution. This graph shows consistent titration of MVA virus adding credibility to operator's skill for any generated plaque assay-based data. Data shown are the mean plus standard deviation.

We sought to determine whether MVA virus could be encapsulated into polymeric MPs while retaining its bioactivity and hence infectivity. The aim of the following in vitro studies was to establish which stage of the encapsulation process could be deleterious for MVA virus. All tests were carried out in the absence of PLGA polymer. To test solvent suitability we selected 7 solvents which have previously been used to make PLGA MPs[32,218–221], namely DMSO, acetone, DCM, ethyl acetate (EtAc), acetonitrile (AcN), tetrahydrofuran (THF) and triacetin. MVATIPeGFP was exposed to each solvent for 30 seconds (Methods 2.4.26i), corresponding to the exposure time during formulation and MVA bioactivity/infectivity was assessed by plaque assay quantification in DF-1 cells (Figure 3.5A). Figure 3.5A shows that 30 second solvent exposure led to a significant loss of MVA bioactivity with DMSO, Acetone, DCM, EtAc, AcN and THF. Addition of 15% (w/v) trehalose did not improve MVA viability when EtAc was used. On the other hand, when MVA was exposed to triacetin there was no significant reduction in bioactivity after 30 seconds when compared to the MVA in PBS control. Similar results were obtained when the virus was exposed for 4 hours and 24 hours respectively at room temperature, even though there was a very slight reduction but was not statistically significant. Figure 3.5D shows a snapshot of generated fluorescent plaques from MVA in PBS for 24 hours vs the MVA incubated for 24 hours in triacetin.

Similarly, the effect of brief sonication on MVA virus was investigated and compared with homogenisation according to Methods 2.4.26ii. MVA virus was either sonicated or homogenised for 30 seconds and then plaque assay was performed. No statistically significant difference was found after homogenisation at 13k rpm (Figure 3.5B). However, MVA virus lost significant bioactivity after sonication at 4 Watts or sonicated in a waterbath at room temperature for 30 seconds.

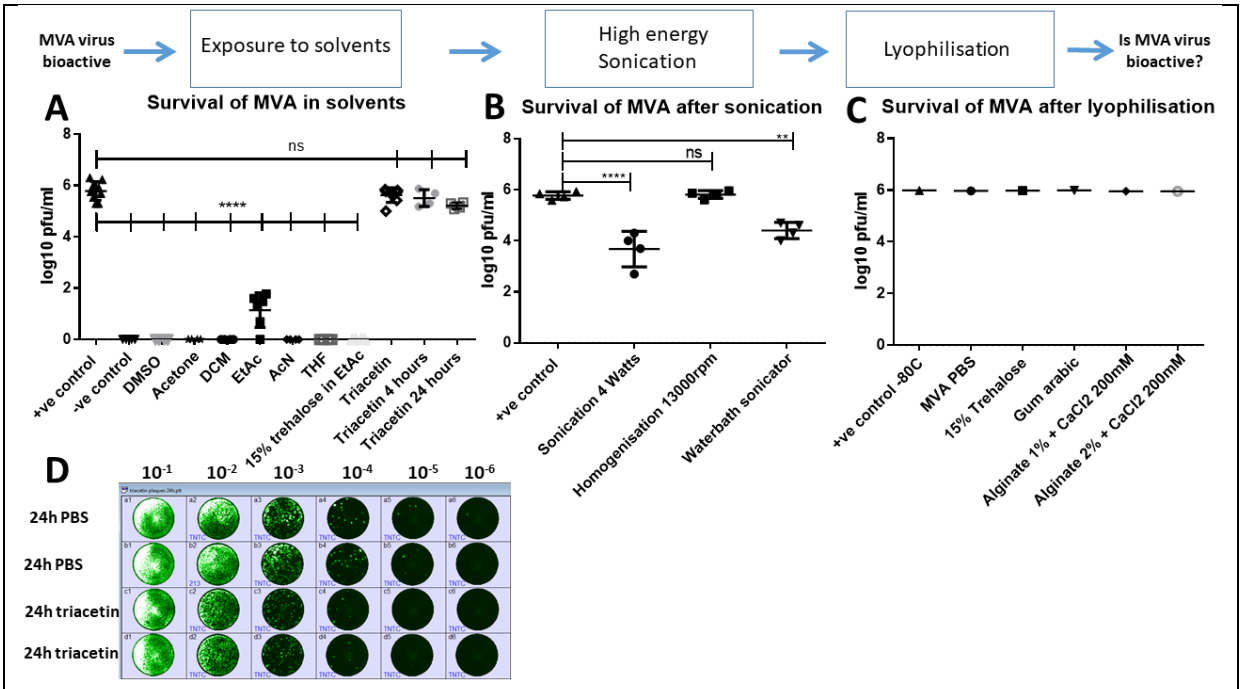


Figure 3.5 Stability of MVA virus during encapsulation procedure in the absence of PLGA polymer

A) 10^6 pfu were exposed to different solvents for 30 seconds unless otherwise specified in the legend (n= 4-10): DMSO, Acetone, Dichloromethane (DCM), Ethyl Acetate (EtAc), Acetonitrile (AcN), Tetrahydrofuran (THF) and triacetin. Solvents were then diluted with PBS buffer and evaporated with reduced pressure. An aliquot from the exposed resuspended virus was then used for plaque assay quantification. In the case of triacetin which is not a volatile solvent, the aliquot was taken immediately after resuspension with PBS.

B) 10^6 pfu were either sonicated with a probe sonicator at 4 watts or homogenised at 13k rpm or sonicated in a standard waterbath for 30 seconds (n=4). An aliquot from treated viruses was used for plaque assay quantification.

C) 10^6 pfu were lyophilised with and without cryoprotectant (trehalose) or with other excipients such as gum Arabic and alginate that has been ionically gelated with Calcium salts. After rehydration with PBS, an aliquot from each batch was used for plaque assay quantification.

D) Photographs of plaques assay with diluted MVA virus that has been exposed to triacetin for 24 hours in comparison to MVA virus that has been in PBS for 24 hours.

Statistical analysis was performed using one-way ANOVA with Bonferroni's multiple comparison post-hoc test (*p<0.05; **p<0.01; ***p<0.001; ****p<0.0001). Data shown are the mean plus standard deviation.

Microparticles are lyophilised at the last step of the manufacturing process in order to form a dried product that can be measured in weight. Three different excipients were tested namely gum Arabic which has been used to stabilise Tetanus toxoid[222], trehalose and lastly alginate which has been used to stabilise bovine insulin[223]. As expected, Figure 3.5C shows that bioactivity of lyophilised MVA compared to unlyophilised MVA has no significant difference (Methods 2.4.26iii). Presence of different excipients made no difference to MVA bioactivity either.

MVA virus had now been tested for each of the 3 encapsulation steps but in an isolated manner. To independently validate the in vitro results and whether MVA virus would behave in a similar fashion after being exposed to all 3 encapsulation steps consecutively, we chose to demonstrate bioactivity by measuring immunogenicity in vivo.

Three groups of female Balb/c mice (n=5 per group) were immunised according to the schedule described in Table 3.1.

Table 3.1 Immunogenicity from MVA exposed to solvent, homogenisation and lyophilisation

Group (n=5)	Description (solvent exposure, homogenised and lastly lyophilised)
1	10^6 pfu MVATIPeGFP in PBS
2	10^6 pfu MVATIPeGFP in triacetin 4 hours and then resuspended in PBS
3	10^6 pfu MVATIPeGFP in DCM 30 seconds, then DCM evaporated and resuspended in PBS

It is known that after a single dose of MVA virus in mice, T-cell immune response peaks 1-week post immunisation[224]. To ensure that the encapsulation steps did not affect the ability of

the exposed virus to induce cellular responses, T-cell responses in the spleen were assessed after 1 week. To test this, ex-vivo IFN-γ ELISpot to Pb9 was measured using splenocytes at 1-week post immunisation (Figure 3.1A), with appropriate internal controls validating the ELISpot assay (Figure 3.6B). Splenocytes were isolated according to Methods 2.4.4 and IFN-γ responses were measured according to Methods 2.4.6. Mice immunised with MVATIPeGFP exposed to DCM solvent showed no T cell responses to Pb9. Reassuringly, no significant difference was detected between mice immunised with MVATIPeGFP after exposure to triacetin, supporting our previous in vitro plaque assays results.

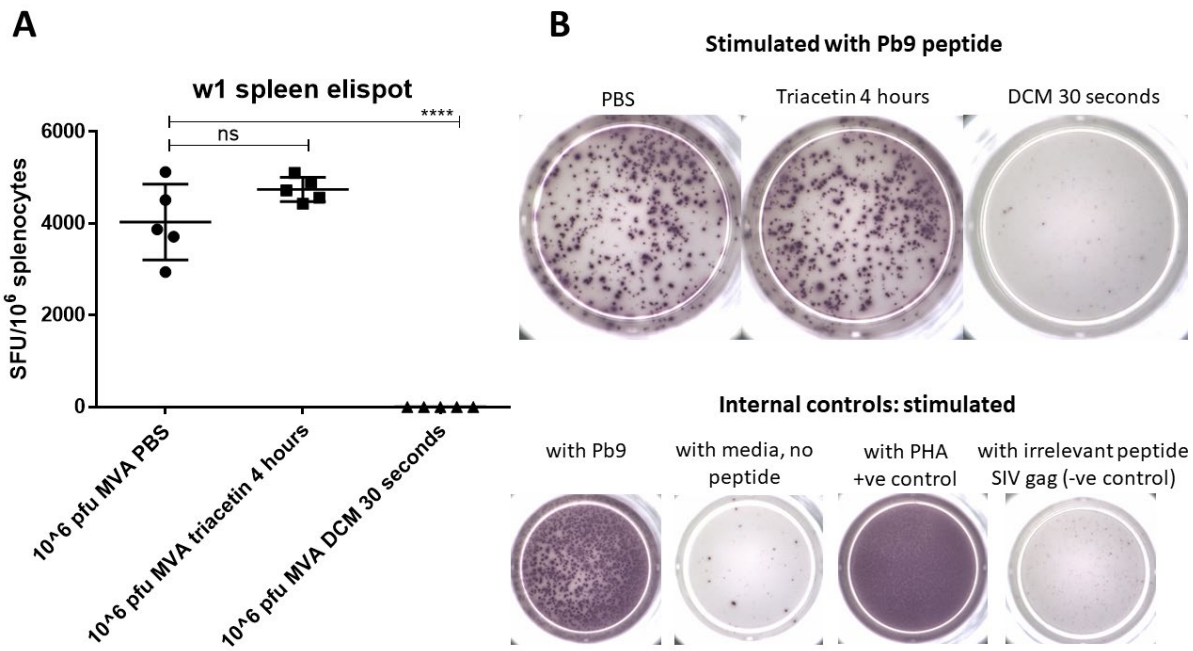


Figure 3.6 In vivo immunogenicity from MVA exposed to solvents, homogenisation and lyophilisation

A) Mice were immunised with MVATIPeGFP encoding the Pb9 immunodominant T-cell epitope found within the TIP epitope string. MVA viruses were exposed to either DCM or triacetin solvents for 30 seconds and 4 hours respectively, reflecting and replicating the incubation times used with the in vitro studies. After solvent exposure, samples were homogenised. Viral batches were then resuspended in PBS and solvents were removed (reduced pressure for DCM). Batches were placed into the -80°C freezer for 20 minutes before they were freeze-dried overnight. Lyophilised batches were resuspended with an appropriate volume of PBS so that it matched with 10^6 pfu/ 50µl injection volume per mouse. T-cell responses were assayed by ex-vivo IFN-γ ELISPOT in mouse splenocytes at 1-week post-immunisation. Splenocytes were stimulated with Pb9 peptide. Each symbol represents an individual mouse and data shown are the mean plus standard deviation. (*p<0.05; **p<0.01; ***p<0.001; ****p<0.0001) by one-way ANOVA with Bonferroni's multiple comparison post-hoc test.

B) Representative images from the plate scan generated by the ELISPOT reader system are shown for each vaccinated group stimulated with Pb9 peptide in top row (62.5k cells/well). Internal controls from left to right having 250k cells/well: 1) stimulated with Pb9 peptide to show Ag-specific IFN-γ release 2) unstimulated with just media 3) stimulated with Phytohemagglutinin (PHA) that acts as a polyclonal T-cell activator with non-specific IFN-γ release showing that assay works and that splenocyte secreted IFN-γ is detectable 4) stimulated with an irrelevant peptide SIVgag.

To determine why MVA gets deactivated after short exposure with DCM solvent but not with triacetin, Transmission Electron Microscopy (TEM) imaging was performed to investigate whether any severe structural changes occur on the viral particles themselves (Methods 2.4.11). Immunogold labelling was performed as described in detail in Methods 2.4.12, using commercial polyclonal antibody against the A27L vaccinia surface protein (Figure 3.8A&B). MVA viruses were exposed to DCM and triacetin, then placed onto TEM grids, processed for imaging and visualised (Figure 3.8C,D,E). All treated samples were of the same viral particle concentration and volume. After DCM exposure (Figure 3.8D), no intact virions were found throughout the TEM grid apart from some protein artefacts. In comparison triacetin-exposed MVA virions looked the same as the PBS control (Figure 3.8E&C).

Based on the insights produced so far the MVA encapsulation procedure was updated as shown in Figure 3.9 by altering steps that were shown to affect viral bioactivity. PLGA polymer was now dissolved in triacetin instead of DCM solvent and homogenisation was preferred over the use of sonication for the creation of the primary emulsion (W_1/O).

With this new MP manufacturing protocol we wanted to establish: 1) whether MPs can still be produced since triacetin has different physical and chemical properties than DCM and 2) examine their morphology. Particle size analysis using the AccuSizer diffractometer (Methods 2.4.24), revealed similar size distribution for both triacetin and DCM based batches (Figure 3.7A&B), ranging from 5-80μm and 5-90μm in size. Morphologically however they were markedly different as shown in Figure 3.10. DCM MPs had a very smooth surface whereas triacetin MPs had a porous-like morphology with several indentations around the surface.

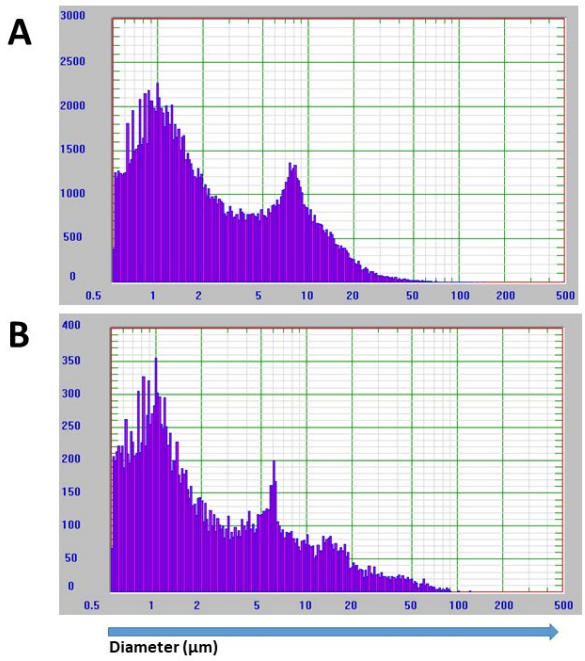


Figure 3.7 Particle size analysis using Accusizer diffractometer
A) Population sizes for triacetin based MPs (5-80µm)
B) Population sizes for DCM based MPs (5-90µm)
Background noise is anything below 2µm.

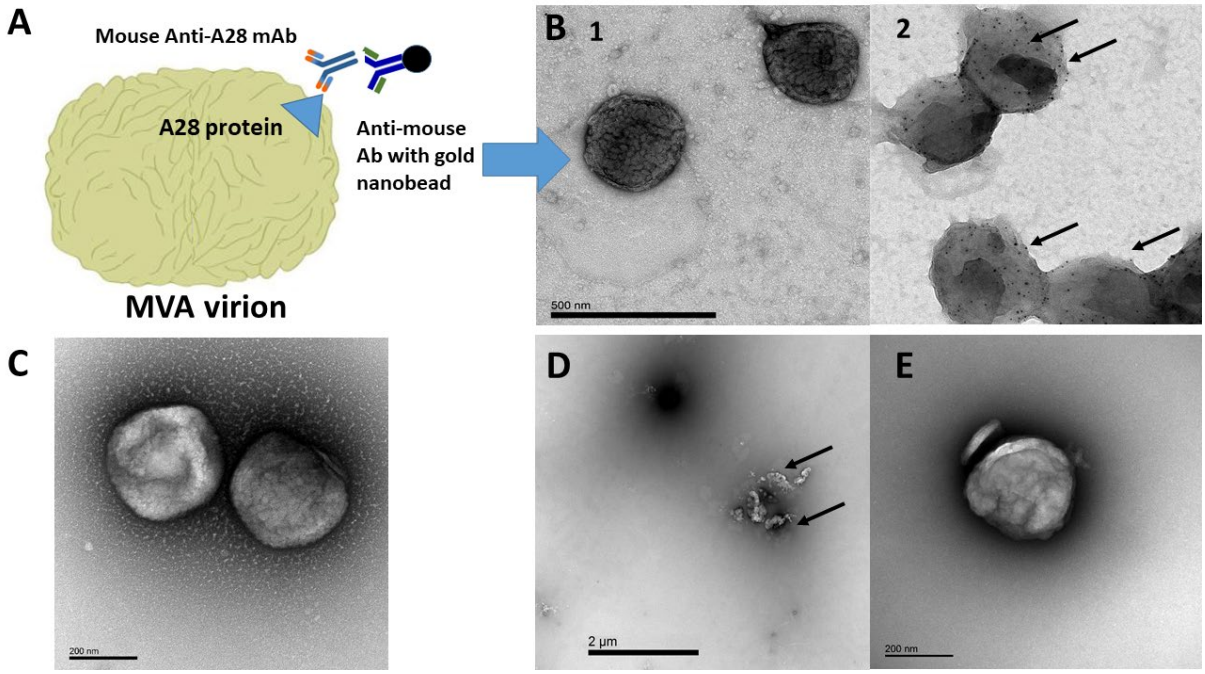


Figure 3.8 Diagnostic TEM images of negatively stained MVA virus exposed to DCM and triacetin solvents

A) Schematic representation of immunogold labelling. A27L protein was detected on MVA virions with anti-A27L mouse antibody, followed successively by a secondary rabbit anti-mouse IgG antibody conjugated to gold nanoparticles. Gold nanoparticles have high electron density and appear as 'dark dots' when imaged with TEM.

B) Primary antibody concentration was optimised to 1:20, after comparing to 1:100 and 1:200 dilutions (not shown). B1) internal control for background purpose with only secondary antibody but no primary antibody present. B2) Negatively stained MVA virions for A27L protein shown as dark dots. Scale bar for both images is 500nm.

C) Representative images of MVA virions in PBS that have been homogenised. Scale bar is 200nm.

D) MVA virions that have been exposed for 30 seconds to DCM while being homogenised for 30 seconds and then resuspended in PBS and visualised. DCM was evaporated under reduced pressure for 2 hours to ensure complete solvent evaporated to avoid reaction of solvent with electron beam.

E) MVA virions that have been exposed for 4 hours to triacetin while being homogenised for 30 seconds, then resuspended in PBS and visualised.

Note for B,C,&D: Virions were not lyophilised, to get a cleaner background devoid from any crystals that might be formed during freeze-drying.

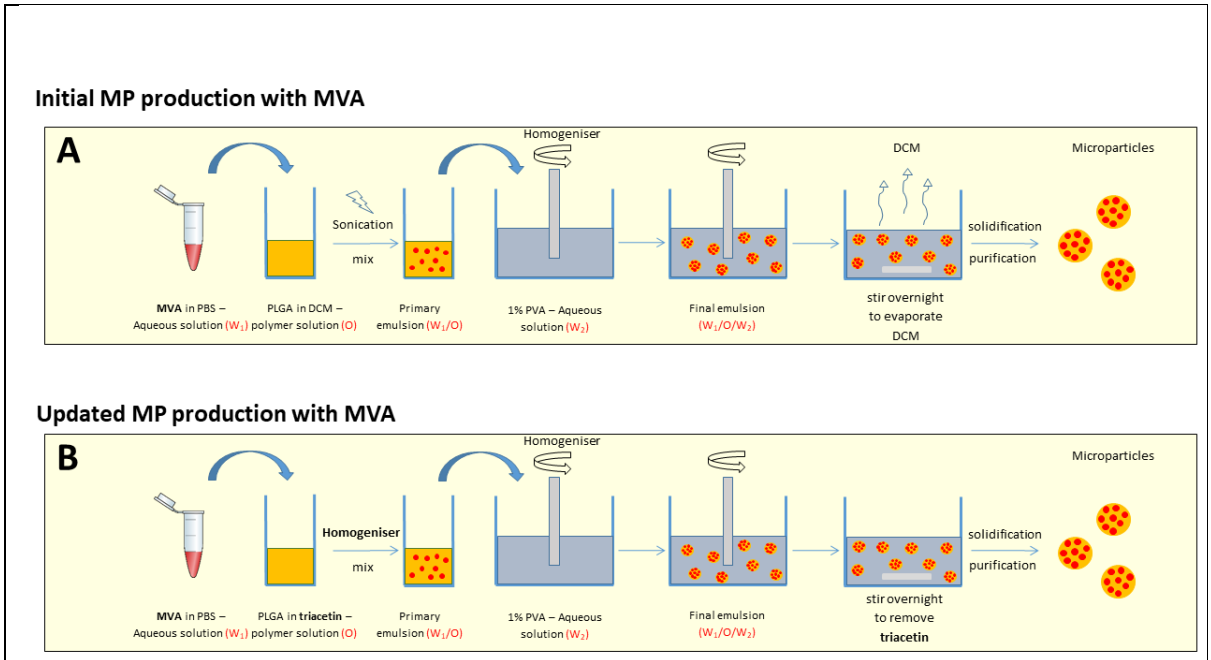


Figure 3.9 Updated MP formulation procedure for bioactive MVA virus

A) Original recipe used to generate MVA loaded MPs using DCM to dissolve the PLGA polymer and sonication to adequately mix MVA with dissolved polymer to form the primary emulsion (W_1/O).

B) Updated formulation recipe taking in consideration steps during the encapsulation where MVA virus had partial (sonication step) or complete deactivation (DCM solvent exposure step). Changing these parameters would ensure the bioactivity of the MVA virus throughout the encapsulation procedure. DCM solvent was replaced by triacetin to dissolve PLGA polymer and sonication was eliminated and replaced by homogenisation to form the primary emulsion (W_1/O).

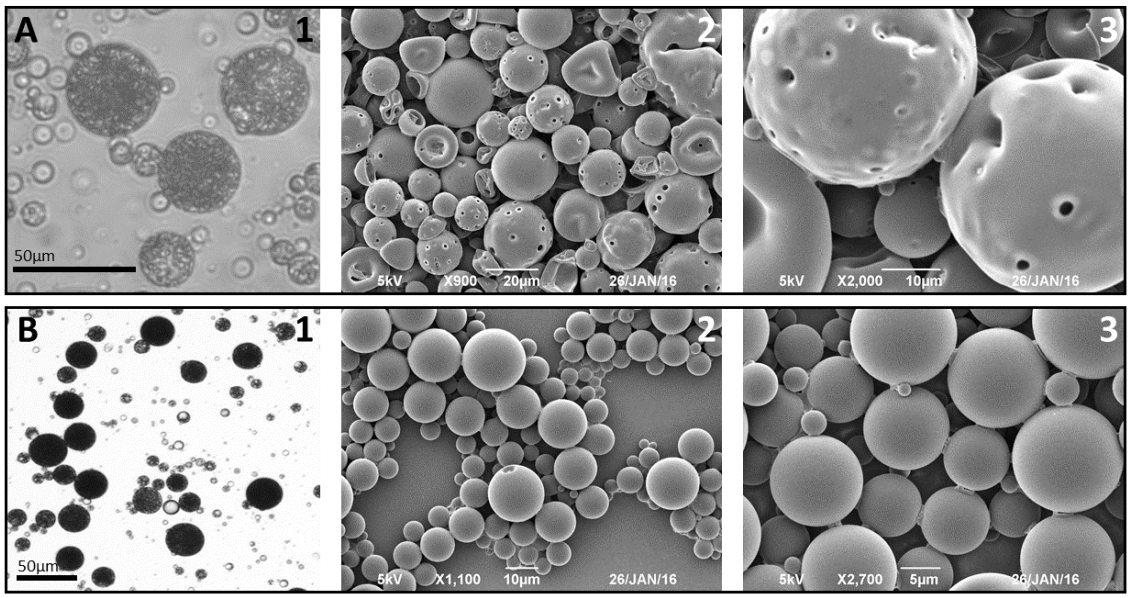


Figure 3.10 Morphology of triacetin based MPs and DCM based MPs
PLGA 50:50 24-38kDa MPs were manufactured based on the updated protocol using triacetin and were morphologically characterised and compared to the morphology of DCM based MPs.

A) 1) Representative optical microscopy image (40x magnification) of triacetin based MPs. Scale bar = 50µm. 2&3) Representative SEM microscopy image of MP population followed by a close-up image. Specimens were placed onto metal stubs, dried, sputter coated with gold and then visualised. Scale bar = 20µm and 10µm respectively.

B) 1) Representative optical microscopy image (20x magnification) of DCM based MPs. Scale bar = 50µm. 2&3) Representative SEM microscopy images of MP population followed by a close-up image. Scale bar = 10µm and 5µm respectively.

3.5 MVA extraction strategies for quantification of infectious virions

Triacetin-based MVA loaded MPs were successfully made (Methods 2.4.23). A small amount of lyophilised MPs was washed with PBS to remove the cryoprotectant trehalose, used during lyophilisation. This was then spun down to form a pellet inside an Eppendorf tube and then incubated with 1ml of triacetin at room temperature on a shaking platform for 6-8 hours, until all MPs have been dissolved (Figure 3.11). An aliquot from the dissolved polymer solution containing extracted MVA viruses, was used to perform the viral titrations and trituration on a separate 96 well plate containing media, before being added onto DF-1 cells for the 1.5 hours

incubation time required for viral cell adhering. When viewed under the microscope before the medium was switched to CMC media, it was found that the medium containing the first 2 viral titrations (10^{-1}&10^{-2}) contained reformed MPs which were sedimented on top of the DF-1 cells (Figure 3.11B).

3.5.1 Molecular weight based separation

We sought to test whether it was possible to separate the extracted MVA viruses from the polymeric solution based on Mw differences between the virions themselves and the polymer. For this purpose, centrifugal Amicon Ultra filters with a 100kDa cut-off filter were used according to the manufacturer's instructions. Dissolved polymer solution containing extracted MVA viruses, was placed in the centrifugal filters, span down and washed twice with fresh triacetin and an aliquot was used for plaque assay quantification. No plaques were observed (Figure 3.11A).

Furthermore, we tested whether the filtering act itself had any effect on MVA's bioactivity. When unencapsulated soluble MVA virus in PBS was concentrated using centrifugal filters, we noticed a significant loss in titre by procedure itself (Figure 3.11A).

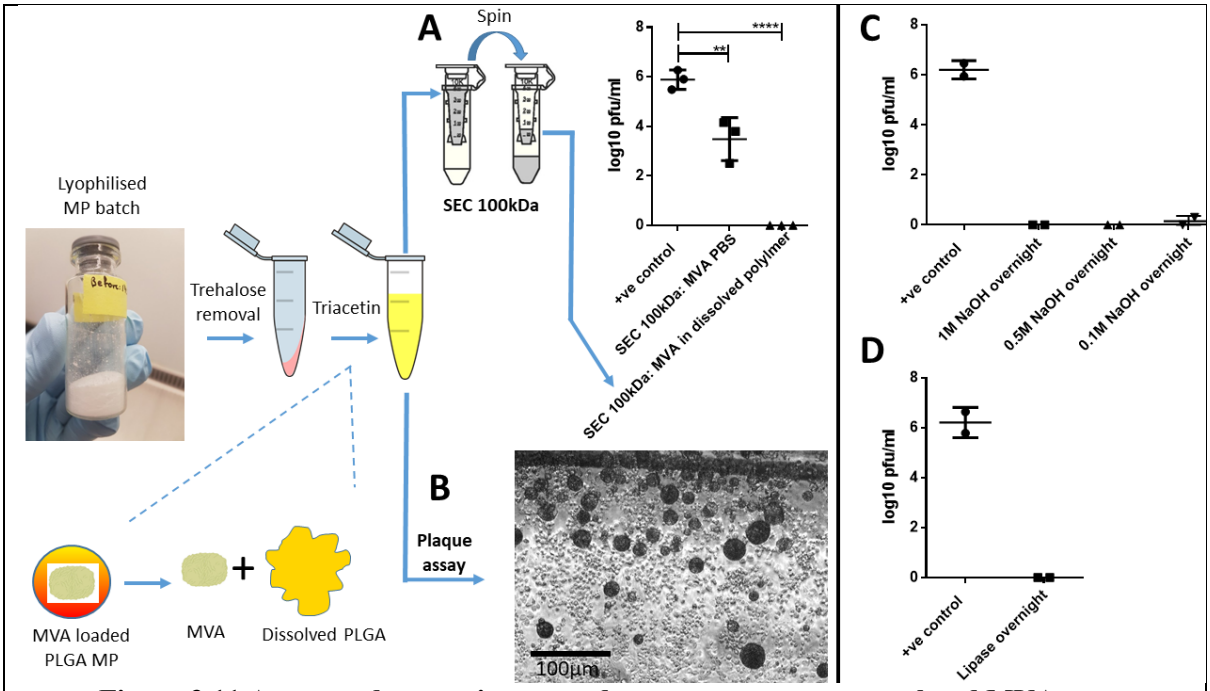


Figure 3.11 Attempted extraction procedures to separate encapsulated MVA virus from PLGA polymer and measure infectious virus

A known amount of lyophilised PLGA 50:50 24-38 kDa MPs was scooped out, resuspended in PBS and span down to pellet the MPs, removing the trehalose that was used as a cryoprotectant during lyophilisation. MPs were then dissolved with 1ml triacetin for 6-8 hours at room temperature on a shaking platform until no visible MPs were present. This would liberate MVA viruses encased within the MPs and be in a soluble form within the polymer solution. This was then used to test 2 extraction protocols with the aim to extract MVA viruses and use them to measure their quantity using the plaque assay procedure.

A) Amicon Ultra 0.5ml centrifugal filters - Size exclusion columns (SEC) – with a 100 kDa cut-off filter was used to separate extracted MVA virus from polymer solution. Dissolved polymer solution containing extracted MVA viruses was ran through the filters with additional fresh triacetin to wash away any residual polymer. MVA viruses due to their size would be retained within the filter while the polymer would flow through due to its size. Then the recovered MVA virus solution was used to perform a plaque assay to quantify it. An internal control was also done using unencapsulated MVA virus in PBS to demonstrate whether the act of filtering had any side effects on MVA bioactivity. (*$p<0.05$; **$p<0.01$; ***$p<0.001$; ****$p<0.0001$) by one-way ANOVA with Bonferroni's multiple comparison post-hoc test. Data shown are the mean plus standard deviation.

B) Representative optical microscopy image (10x magnification) of a well from 24 well plate with 90% confluent DF-1 cells used for plaque assay quantification. This image was taken during the incubation period with the 10^{-1} titration from an aliquot taken from the dissolved solution containing extracted MVA virus, before CMC media was added. Newly formed microparticles were noticeable on top of the DF-1 cells. Scale bar = 100µm

C) Plaque assay results after incubation overnight at 37˚C of unencapsulated MVA virus with diluted concentrations of NaOH on a shaking incubator. Data shown are the mean plus standard deviation. Statistics could not be done due to n=2.

D) Plaque assay results after incubation overnight at 37˚C of unencapsulated MVA virus with 1mg/ml *C.antarctica* lipase on a shaking incubator. Data shown are the mean plus standard deviation. Statistics could not be done due to n=2.

3.5.2 Chemical and enzymatic extraction

We then focussed to chemically extract encapsulated MVA viruses with diluted NaOH, sufficient to digest the polymer matrix of the MPs but leaving the MVA viruses intact. As shown in Figure 3.11C where unencapsulated MVA virus was incubated with different NaOH concentrations, it was evident that MVA virus itself gets deactivated overnight even with 0.1M NaOH.

Despite this, we attempted to measure viral protein content of NaOH hydrolysed MVA virus by BCA assay to simulate the overnight hydrolysis conditions of MPs containing MVA. A standard curve using hydrolysed titrated MVA virus was created (Methods 2.4.27). Comparison between BCA assay (detection range for model BSA protein: 20-2000µg/ml) and micro-BCA assay (detection range for BSA protein: 0.5-20µg/ml) showed that both assays had a LOD of 10^4 pfu/ml (Figure 3.12A&B).

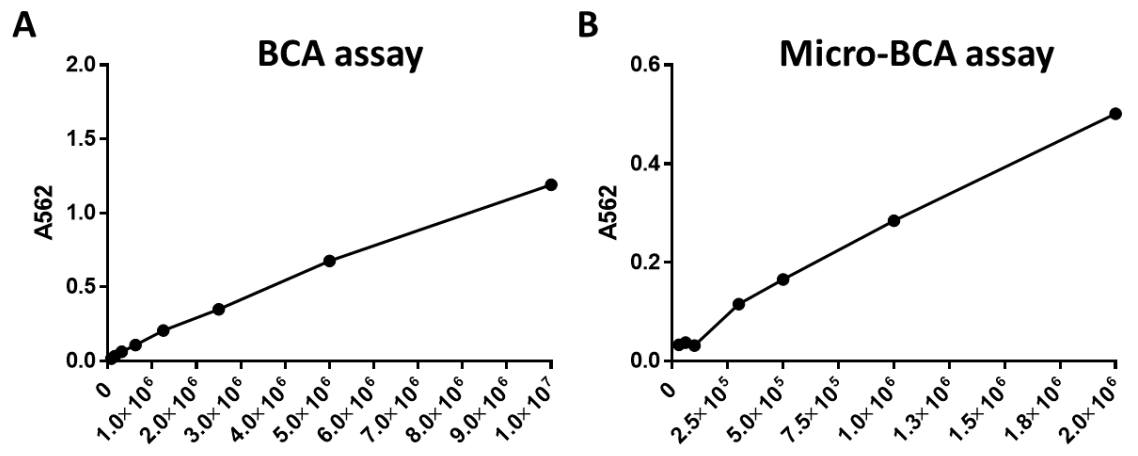


Figure 3.12 Detection limit of titrated NaOH lysed MVA virus using BCA and micro-BCA assays
Standard curves generated with 2-fold dilutions of MVA virus
A) BCA assay standard curve. Detection range: 20-2000µg/ml
B) Micro-BCA assay standard curve. Detection range: 0.5-20µg/ml

In addition, degradation behaviour of PLGA polymers under enzymatic digestion has previously been monitored using lipases that randomly cleave ester-bonds within the PLGA substrate[225]. To test the idea of lipase enzymatic digestion as an extraction strategy and whether this procedure would affect the bioactivity of MVA virus under the same conditions, unencapsulated MVA virus was incubated overnight with 1mg/ml *C.antarctica* lipase at 37˚C. This led to deactivation of MVA virus (Figure 3.11D).

3.6 Ultracentrifugation and separation on sucrose gradient based on buoyancy

Utilising the difference in densities between the MVA virus and the dissolved polymer, we wanted to explore whether using a sucrose cushion and ultracentrifugation would lead to successful pelleting of MVA virus away from the dissolved polymer. A similar approach is followed using zonal sucrose gradient ultracentrifugation to separate MVA from cell debris as depicted in Figure 3.13A. Based on this principle we employed a discontinuous sucrose gradient having 4 distinct and denser regions within the ultracentifuge tube to separate the MVA virus from PLGA polymer.

A discontinuous sucrose gradient with 4 sucrose regions (60%, 40% 30% and 8% w/v sucrose) was created inside a sterile ultracentrifuge tube starting with the most dense sucrose region at the bottom and then moving on to the least dense sucrose solutions (Figure 3.13B). Half the batch of MVA loaded triacetin- based MPs made from PLGA 50:50, 24-38 kDa, was dissolved in triacetin. This polymeric solution containing the MVA was layered on top of the sucrose gradient and this was then ultracentrifuged for 1 hour at 13k rpm at 4˚C in a fixed angle ultracentrifuge. When the run was finished, the tube was taken out carefully and inspected. A thin solidified polymeric membrane was noticable between the top two sucrose bands (Figure 3.13C). A plaque assay was performed using aliquots from the supernatants above and below the polymeric membrane in the 30% sucrose region without disturbing the 40% and 60% sucrose layers in order to quantify extracted infectious virions, but with no visible plaques (data not shown).

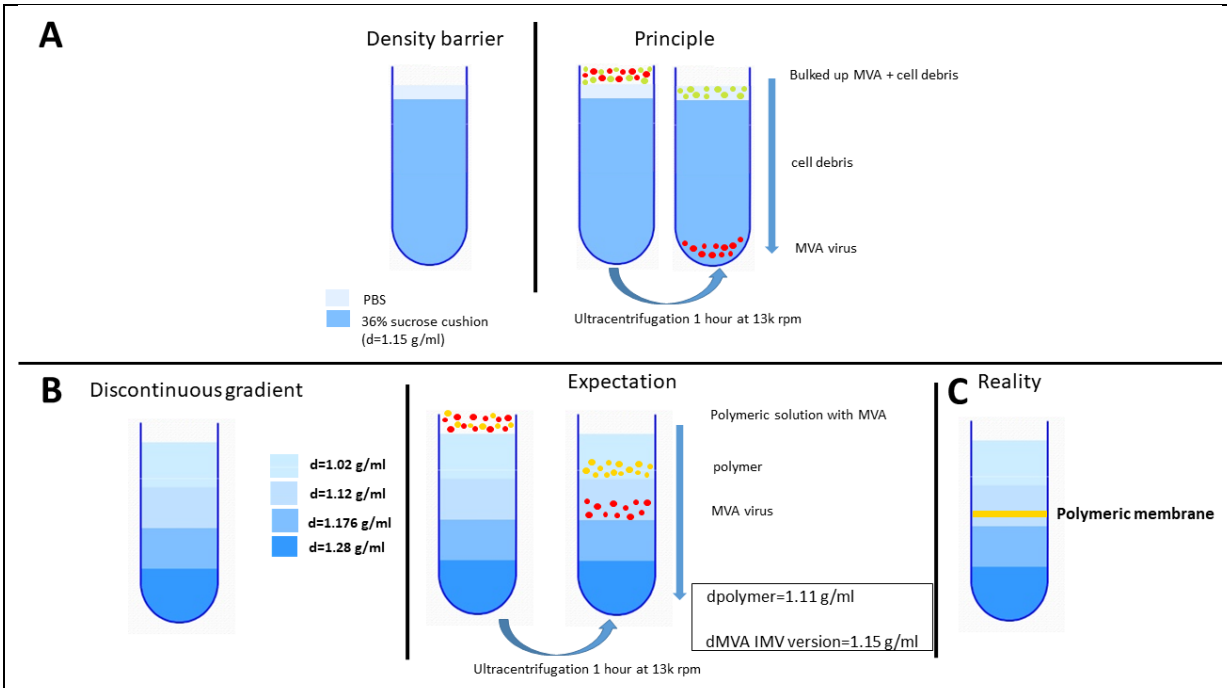


Figure 3.13 Separation of encapsulated MVA from PLGA polymer using ultracentrifugation in sucrose gradient

A known quantity of lyophilised PLGA 50:50 24-38 kDa MPs with encapsulated MVA was treated by removing trehalose with PBS and dissolving the MPs in triacetin to release MVA. This was then used to test the idea of using ultracentrifugation in a sucrose gradient to separate MVA from the polymer, with the aim to recover infectious virions to be quantified with a plaque assay.

A) MVA virus is usually purified by sucrose cushion ultracentrifugation to obtain purified/high titre viral MVA stock devoid of major cell debris. This is a graphical representation of the procedure. The cell lysate is carefully layered onto a 3ml sucrose cushion 36% (w/v) in a sterile ultracentrifuge tube. This is then ultracentrifuged for 1 hour at 13k rpm at 4˚C. Based on the basis of buoyant density, cell debris is separated from the MVA and a clear pellet is formed at the bottom of the tube containing purified MVA.

B) A discontinuous sucrose gradient was prepared starting from the one with the highest density from the bottom 60% (w/v), followed by 40%, 30% and 8% cushions having densities of 1.28, 1.17, 1.12 and 1.02 g/ml respectively. Density of polymeric solution without MVA was identified using the $\rho = m/v$ formula taking an aliquot from polymer solution and measuring its weight. The density of the IMV version of MVA was established to be ~ 1.15g/ml from literature[226]. Polymeric solution was layered on top of discontinuous gradient. Theoretically the polymer solution would not be able to migrate into the 30% sucrose gradient whereas MVA would progress and stop before the 40% sucrose gradient.

3.7 Ultracentrifugation and separation based on buoyancy in water-free environment in pure triacetin

We then decided to move away from using sucrose gradients containing water and instead add the polymer solution containing MVA directly into pure triacetin and then ultracentrifuge the sample as shown in Figure 3.14A.

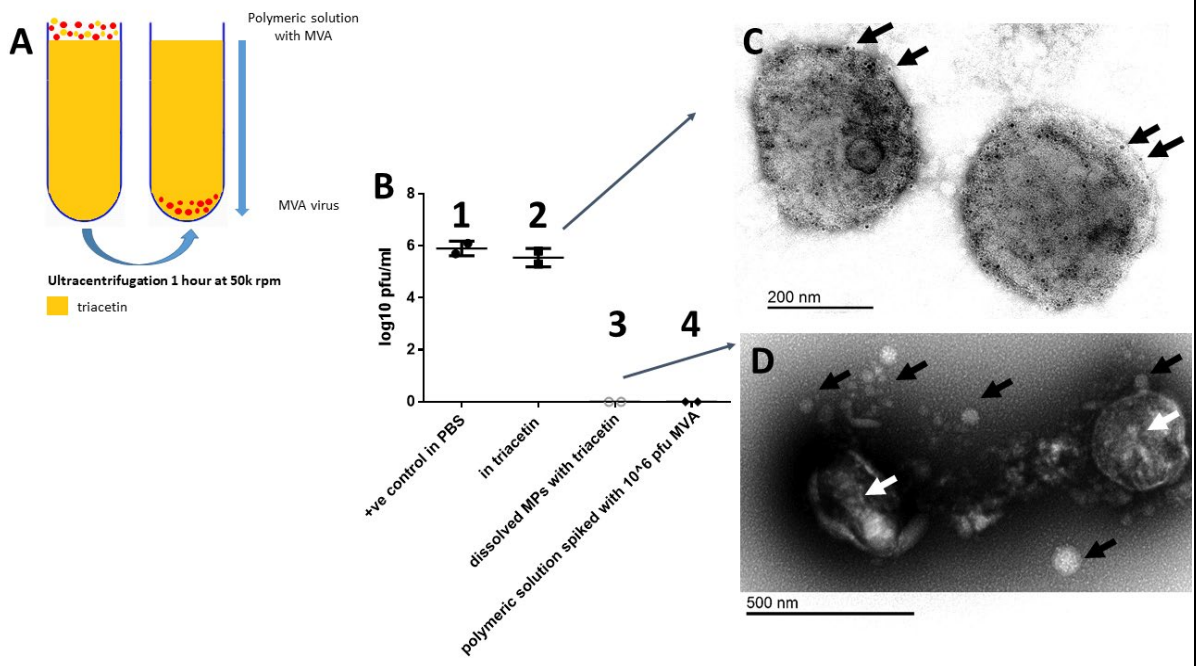


Figure 3.14 Separation of encapsulated MVA from PLGA polymer using ultracentrifugation in pure triacetin

A known quantity of lyophilised PLGA 50:50 24-38 kDa MPs with encapsulated MVA was dissolved in triacetin to release MVA. The idea of using ultracentrifugation in pure triacetin rather than a sucrose gradient in order to separate MVA from the polymer, was tested. Ultimate aim was to recover infectious virions to be quantified with a plaque assay.

A) Graphical representation of ultracentrifugation in excess triacetin. Dissolved MPs in triacetin containing MVA were carefully layered onto 3ml triacetin in a sterile ultracentrifuge tube. This was then ultracentrifuged at 50k rpm for 1 hour at 4˚C.

B) Plaque assay results. 1) Positive internal control in PBS after 50k rpm spin; 2) internal control for effect of triacetin on bioactivity of unencapsulated MVA combined with the act of high speed ultracentrifugal force; 3) Dissolved MVA loaded MPs after 50k rpm spin; 4) Spiked polymer solution with 10^6 pfu MVA after 50k rpm spin. Data shown are the mean plus standard deviation. Statistics could not be done due to n=2.

C) TEM image of immunogold labelled MVA virions for A27L protein, retrieved after spinning at 50k rpm in triacetin. Sample was from B2. Black arrows show the dark dots which is A27L protein. Image has been digitally enhanced in terms of brightness by 41% for better visualisation. Scale bar is 200nm.

D) TEM image of immunogold labelled MVA virions for A27L protein, retrieved after spinning at 50k rpm in triacetin from dissolved MPs. Black arrows show polymeric remnants and in some cases polymeric nanoparticles being reformed. White arrows show MVA virions based on their size and shape. Sample is representative for B3. Image has been digitally enhanced to have increased brightness by 41% for better visualisation. Scale bar is 500nm.

Before proceeding with this, we wanted to confirm whether unencapsulated MVA virus retains its bioactivity while being incubated in pure triacetin for 1 hour at 4˚C and enduring high speed ultracentrifugation. As shown in Figure 3.14 B2 the act of ultracentrifugation while bathed in triacetin had no detrimental effect on MVA's bioactivity.

Following this confirmatory test, MVA loaded triacetin-based MPs made from PLGA 50:50 24-38 kDa polymer were dissolved in triacetin. We proceeded by layering this polymeric solution on top of 3ml of triacetin and then ultracentrifuged it for 1 hour at 50k rpm at 4˚C. Once the run had finished, the tubes were taken out with care and the supernatant was removed very carefully. Then 100µl of PBS were added to collect the pelleted sample and a plaque assay was performed. Unfortunately, no visible plaques were seen (Figure 3.14 B3).

We also tested a 'simulated' MP batch which was essentially a polymeric solution spiked with the total 10^7 pfu starting material simulating a 100% loading efficiency batch. The same ultracentrifugation process was repeated with this spiked polymeric solution and a plaque assay was performed. Surprisingly, despite having maximum loading in this 'simulated' MP batch no plaques were seen either (Figure 3.14 B4).

To validate the presence of MVA virions at the bottom of the tube and that they were indeed recovered with this procedure, we performed TEM imaging from the samples used to perform plaque assay with, namely the MVA-loaded MPs and the spiked 'simulated' MP version. Interestingly as seen in Figure 3.14D, which is the spun down sample from dissolved MVA-loaded MPs, MVA virions are visible (white arrows) alongside with polymer remnants and some reformed polymeric nanoparticles.

To answer the question why the recovered MVA virions are not infectious and thus not detected by a plaque assay, immunogold labelling against the A27L protein was performed and samples

were imaged with TEM. Figure 3.14C shows successful immunogold labelling in the absence of any polymer (sample was spun in pure triacetin). However when polymer was present in the mixture as seen in Figure 3.14D, be it the dissolved MPs or the spiked MP version, there was no successful immunogold labelling. Both samples looked similar as well with a messy background of polymeric remnants.

3.8 Separation based on surface polarity

Another method we tested was Free Flow Electrophoresis (FFE). This lesser known electrophoresis technique is a high throughput method, which separates molecules based on their surface charge differences without loss of functionality. It has been around for 60 years and used before for separation of cells[227], proteins[228], enzymes[229] and peptides[230]. An overview of the FFE procedure is shown in Figure 3.15A. The FFE chamber was first conditioned with deionised water and then filled up with carrier buffer and FFE setup was handled according to Methods 2.4.33. A sample trial run was performed using SPADNS, a red water-soluble dye to illustrate the principle of the FFE in Figure 3.15 B-D. SPADNS was injected into the FFE chamber and then collected in 96 fractions in a deep 96 well plate.

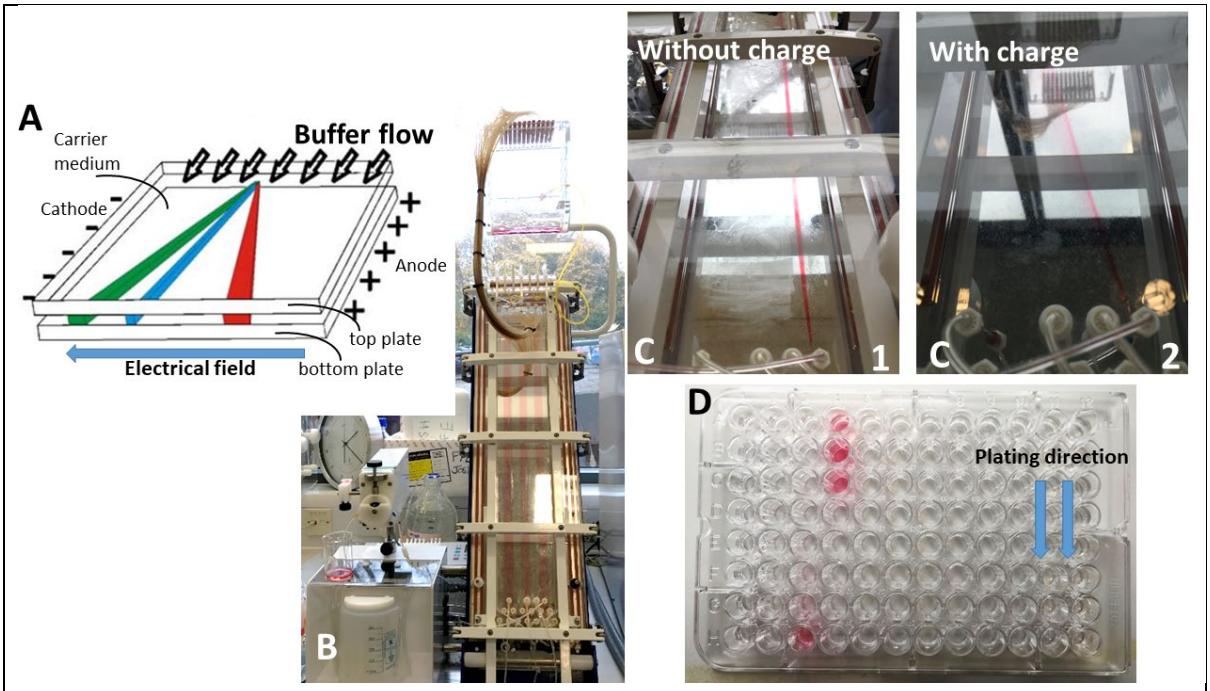


Figure 3.15 Free flow electrophoresis (FFE) procedure overview

A) Graphical representation of how continuous separation and purification occurs in FFE. Sample migrates down the chamber filled with a carrier buffer, by pressure driven buffer flow. The electric field is applied perpendicularly to the flow. Sample is then deflected laterally by the electric field into analyte streams based on their electrophoretic mobility. Once at the end of the chamber, separated samples are collected in 96 fractions and plated in a 96 well plate with preserved functionality due to native conditions used in the electrophoretic chamber.

B) Image of the FFE machine demonstrating the long chamber during conditioning stage before the carrier medium was added. The starting point of the chamber is at the bottom of the image with the sample injector point visible. At the very top is the end of the chamber with the 96 fraction collector hanging from the top.

C) Trial run for demonstration purposes using a red water soluble dye called SPADNS illustrating the FFE principle in action. C1) Without an electric field being applied SPADNS retains the same position from where it was injected into the chamber. C2) Once an electric field was applied the sample was deflected and moved towards its isoelectric point and then collected in 96 well in fractions.

D) Image of the fractions collected showing the plating direction and the wells containing the recovered SPADNS starting from well E3 moving downwards and peaking at well C4.

We first wanted to test the hypothesis that FFE itself with the applied electric field was not hazardous for MVA's bioactivity. For this purpose, a $5x10^7$/ml viral solution was fed into the FFE setup. Once processed and 96 well fractions were collected, small aliquots were taken and a plaque assay was performed in a 96 well plate.

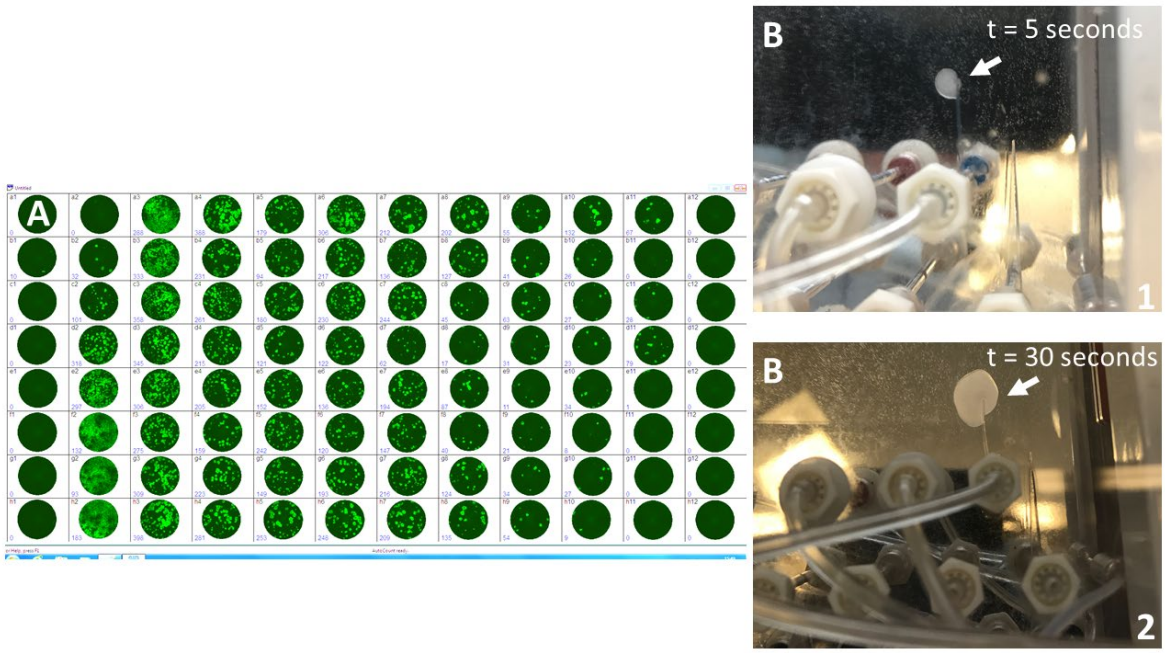


Figure 3.16 Separation of encapsulated MVA from PLGA polymer using Free Flow electrophoresis (FFE)

A) Unencapsulated MVA virus solution $5x10^7$/ml was run through the FFE machine and collected in 96 well fractions after the run was finished. All 96 well fractions were used to perform plaque assay in a 96 well plate. After 30 hours post infection microphotographs were taken with a fluorescent ELISPOT reader on a FITC channel showing the individual plaques in each well.

B) Attempt using FFE to extract MVA from polymeric solution. Sample was injected as normally into the FFE chamber and was observed for the first 2 minutes. B1 shows a snapshot after 5 seconds post injection showing the location of the polymer solution in the chamber. B2 shows the build-up of polymeric solution with no downward stream movement.

Once imaged with the fluorescent ELISPOT reader, there were fluorescent plaques present (Figure 3.16A). However, it was against our expectations to find out that MVA was present in every single one of the 96 fractions shown again in Figure 3.16A – excluding the fractions in columns 1 & 12 on the 96 well plate as they are devoid from samples by default.

With then performed an experiment where a spiked polymer solution was used with 10^7 pfu MVA simulating a dissolved MP batch having a 100% loading efficiency and tested whether MVA can be successfully extracted and quantified in infectious units. Figure 3.16B1 shows a snapshot at the injection point inside the FFE chamber 5 seconds after sample injection while

Figure 3.16B2 after 30 seconds. There was no visible movement downstream the chamber, apart from a polymeric bubble forming at the injection site causing a build up.

3.9 Discussion

For work presented in this thesis, we have used an established technique for the synthesis of MPs[231]. BSA-FITC has been used extensively in encapsulation studies by other groups in order to characterise in more detail the double emulsion procedure[232–234].

Initial batches of BSA-FITC using DCM as the solvent were similar in shape and size but their surface morphology varied between smooth, smooth with indentations or porous (Figure 3.3). It has been shown that porosity of MPs plays an important role in the initial burst stage[235], where the higher levels of porosity and rougher surfaces, the faster the biodegradation rate of the MPs[236]. Therefore, surface porosity was an important factor to consider at the later stage of MP optimisation.

To ensure that MVA bioactivity is not affected during the encapsulation procedure, we split the encapsulation procedure into 3 stages (solvent exposure, sonication and lyophilisation) in order to elucidate if and at which step MVA virus could potentially be deactivated. We on purposely chose to expose low amounts of MVA virus (10^6 pfu) but not higher e.g. 10^8 pfu, so that if there was a deactivation effect it would be more prominent while avoiding the scenario of a 'shielding' effect from the solvent, due to the vast number of MVA virions. All tests were carried out in the absence of PLGA polymer because the polymer was interfering with the plaque assay quantification.

We showed that solvent interaction with the virion results in loss of MVA bioactivity during processing (Figure 3.5A) along with the use of high-energy sonication during emulsion dispersion (Figure 3.5B). There is evidence that organic solvents, sonication and high shearing

forces used during encapsulation do result in protein denaturation/aggregation[237]. Although use of DCM, DMSO, acetone, EtAc, AcN and THF solvents led to a significant deactivation of MVA virus in vitro, triacetin did not. This was first shown with our in vitro studies (Figure 3.5A) and then in vivo with MVA retaining the ability to induce immunogenicity after exposure to triacetin (Figure 3.6). This in vivo study made use of the immunodominant epitope Pb9 to measure T-cell specific Ag-mediated immune responses. Pb9 which is included in the multi-epitope string TIP present in the MVATIPeGFP construct, is a 9 amino-acid long sequence from *P.berghei* circumsporozoite protein, shown to be protective against sporozoite murine malaria challenges[194].

Addition of 15% trehalose, an excipient which has been shown to reduce protein denaturation during MP formulation[238] did not improve MVA viability. On the other hand, inherent polarity and properties of each solvent could explain their compatibility with MVA. According to solvents used, in order of decreasing dielectric constant (polarity)[239]: DMSO (46.68)>AcN>Acetone>DCM>THF>Triacetin (7.01)>EtAc (6.02); EtAc shouldn't be affecting the MVA since it has lower polarity than triacetin. This means that overall properties of the solvent play an important role as well. Triacetin having 3 glycerol chains merged with acetic acid[240] might be beneficial to MVA virus, as it resembles a bulky fatty acid or a form of triglycerides, which are abundantly present in cell membranes[241]. This made sense with our next experiment where we exposed MVA to DCM or triacetin and viewed the samples with TEM. To validate the presence of MVA virus under TEM imaging, immunogold labelling against the A27L was performed, which is critical for virus-to-cell interactions[242] and viral spreading[243] .Virion structure was decimated after DCM treatment (Figure 3.8D) but when treated with triacetin MVA virions were intact and comparable to the PBS control (Figure

3.8E). These results indicate that MVA virions lose their bioactivity and hence immunogenicity after DCM exposure, due to destruction of the virion structure.

Review of the literature highlighted that viral inactivation could indeed occur due to: A) solvent exposure leading to a stressful interfacial environment between the organic and aqueous phase during the emulsion stage, which could cause protein aggregation or even denaturation[244]; and B) sonication time and intensity which was shown to negatively affect protein activity[245]. In contrast, lyophilisation of MVA virus should not in theory affect its bioactivity, which was indeed the case (Figure 3.5C), since lyophilisation of vaccinia virus – parental virus of MVA virus – has been used since the 1970s for the preservation of the smallpox vaccine[246].

Recombinant viruses have gathered much interest as vaccine carriers for antigen delivery in recent years[247–249]. Originally mainly used for gene therapy[250], there has been an interest to utilise MPs to encapsulate recombinant adenoviruses for vaccination purposes[251–254]. Unlike adenovirus, MVA is an enveloped virus with membrane derived from host cell membrane during the budding stage[179]. It is possible that this property is the sole reason why MVA is more vulnerable to routinely used organic solvents such as DCM, which could dissolve the membrane lipids and deactivate MVA. This could serve as an additional explanation why MVA was deactivated in vitro (Figure 3.5A) and for the structural damage seen under TEM (Figure 3.8D).

A recent report by Kern et al[255], demonstrated encapsulation of live-viral vaccinia vector in Eudragit pH-sensitive polymer MP, providing protection in mice against the causative agent of Lyme disease, *B.Burgdorferi*. It is encouraging to see that our in vitro solvent studies with MVA (Figure 3.5A) are in accordance to the results of this report, confirming that brief exposure to DCM, DMSO and others led to complete deactivation of MVA[255]. Authors demonstrated that exposure of vaccinia to toluene for 15 minutes was not detrimental for its

infectivity but after 3 hours exposure there was a 60% loss of infectivity. A fundamental common ground with the report from Kern et al[255], was that we ensured that MVA infectivity was indeed not affected throughout the timeframe of vaccine preparation, which in our case was the preparation of the MPs over the 24 hour solidification stage. This is why we exposed MVA to triacetin for 24 hours in order to simulate the 24 hour incubation period required to remove triacetin (Figure 3.5A) from the MPs leading to their solidification. With this data, it was clear that for MVA encapsulation, the encapsulation procedure had to be tailored to the properties of the MVA virus in order to preserve its bioactivity. For this reason we updated our manufacturing protocol accordingly, which is reflected in Figure 3.9.

Triacetin is not routinely used for polymeric MP production and not much work has been done in terms of optimising the double emulsion procedure using triacetin. Only 3 reports exist demonstrating work with in-situ formed 'pre-microspheres', which harden only when in contact with water or physiological fluid, encapsulating cytochrome-c[256], myoglobin[257] and anti-asthma drug montelukast[219]. In all 3 studies the encapsulated material was stable and retained its bioactivity which were promising findings for MVA virus encapsulation. MPs in Figure 3.10 looked similar to the ones in those 3 studies. However, the porous morphology of triacetin MPs was not a desirable feature since this allows the possibility of MVA virus leaking from the MPs and being presented to the immune system prematurely.

We have previously demonstrated in Figure 3.5A that 24 hour exposure of MVA virus to triacetin in the absence of polymer, did not affect its bioactivity. Infectious viruses are routinely quantified with the plaque assay. A requirement for the plaque assay is to have MVA virus in a solution so it can adhere to the cell monolayer, infect and then produce plaques. Thefore we had to extract MVA virus from particle formulations without affecting its bioactivity during the extraction process, so that we could proced with plaque assay quantification. The obvious

experiment to do was to reintroduce triacetin onto the solidified polymeric MVA loaded MPs. This would dissolve the MPs thus liberating the entrapped MVA viruses into the dissolved polymer solution. The re-introduction of triacetin to dissolve the MPs and performing a plaque assay from a direct aliquot, was not successful due to the reformation of MPs as shown in Figure 3.11B.

Separating MVA virions from the PLGA polymer with a centrifugal 100kDa filter based on differences on Mw proved unsuccessful, as well as losing viral titre due to adsorption of unencapsulated MVA virus with the internal cellulose filter membrane (Figure 3.11A). MVA virus should not be able to pass through the 100kDa cut-off filter (a single viral core polypeptide has 76 kDa Mw[258]). Whereas the PLGA 50:50, 24-38kDa polymer used to make the MPs should pass through, separating the extracted MVA viruses from the dissolved polymer.

Critically reflecting back on this situation, a solution to the loss of unencapsulated viral titre due to adsorption on the filter membrane, would have been to incubate the membrane with a protein solution e.g. casein or BSA to coat and reduce the interactive forces between the MVA virus and the cellulose filter. However when polymeric MVA solution is used, this would not have made any difference as the presence of polymer prevented MVA infection in DF-1 cells (Figure 3.11A&B).

The preferred procedure amongst the protein/drug encapsulation scientific community for quantifying encapsulated material is hydrolysis of the polymer with NaOH followed by a protein-based assay (BCA assay). The process of incubation of unencapsulated MVA virus with decreasing amounts of NaOH overnight to simulate hydrolysis of the PLGA polymer overnight (Figure 3.11C), deactivated the MVA virus. This is consistent with findings that even 5 minutes incubation with 0.25M NaOH can be virucidal for MVA virus[259].

The reason why we were not in favour of using the routine BCA protein assay to measure encapsulated viral protein content (Figure 3.12) was because MVA virus provided by viral vector core is in reality semi-purified after sucrose purification, meaning that the resulting viral sample is mostly purified MVA virions plus some cellular debris. This posed the question whether cellular debris is also encapsulated into the PLGA MPs along with MVA, and whether the BCA protein assay measures the cellular by-products as well, leading to misleading results.

MVA loaded triacetin-based MPs were made out of PLGA 50:50 24-38 kDa which polymer has been shown to be degraded enzymatically by 95% after 48 hours incubation at 37˚C with 1mg/ml *C.antarctica* lipase. Similarly incubation of unencapsulated MVA with *C.antarctica* lipase to simulate the enzymatic digestion of the PLGA ester bonds, led to the complete deactivation of MVA (Figure 3.11D). It is possible that esterase (lipase) enzyme specifically cleaves all ester linkages within the phospholipids[260] present within the MVA lipid envelope, rendering it non-infectious.

Critically reflecting on this work, another way would have been to use high-performance liquid chromatography, which has been used in the past for PLGA protein microencapsulation[261]. Nevertheless, this would not be advantageous as MVA virus is a multi-protein complex rather than a single protein and harsh solvents e.g. AcN are used during this procedure, which would have led to the deactivation of MVA virus. Therefore, we had to devise a methodology that allowed to safely extract MVA virus from the PLGA MPs and be able to quantify it with an infectivity plaque assay. This was crucial for future in vivo immunogenicity experiments since dosages of infectious encapsulated MVA in MPs had to be reflective of the soluble boosting dose of MVA.

We then attempted to separate the polymer from the MVA virus based on their buoyancies. It is possible to separate distinct cellular and sub cellular components based on their densities

independently of their size and shape, using a gradient of different sucrose concentrations[262]. With density gradient centrifugation, each particulate population will migrate to a position where their densities match the density of the surrounding sucrose concentration while under centrifugal force. Although density ultracentrifugation has been used to separate VLPs and viruses in solution[263] this principle has not been tested in such conditions.

We first figured out the density (ρ) of our polymer solution using the formula ρ = m/v, by weighing 100µl of polymer solution that did not contain MVA which was found to be 1.11 g/ml. We then scouted the literature and found that the vaccinia virus IMV version has ρ = ~ 1.15 g/ml[226]. In theory based on these densities, MVA virus present in the polymer solution would be able to migrate past the first and second regions of 8% and 30% sucrose but would stop before the 40% sucrose region. Similarly the polymer would in theory be able to migrate through the first region of 8% but stop before the second region of 30% sucrose (Figure 3.13B). Dissolved MPs solution containing MVA was added on top of a sucrose density gradient and was ultracentrifuged but with no successful recovery of infectious MVA (Figure 3.13). The polymeric membrane formed inside the centrifugal tube probably re-entrapped the virus. When in contact with water, triacetin diffused out of the polymer solution, acting in a similar way to the 'pre-microspheres' triacetin based MPs mentioned earlier.

Because of the formation of the polymeric membrane due to a solidification reaction between the polymer solution and water inside the ultracentrifuge tube, we avoided using sucrose cushions containing water. This would enable us to have a water-free environment and by having excess triacetin instead, this would dilute the polymer even further liberating MVA virions and potentially concentrating MVA at the bottom of the ultracentrifuge tube. We have demonstrated earlier in this thesis that incubation of unencapsulated MVA virus with pure triacetin in vitro for 4 hours and 24 hours made no significant statistical difference on MVA's

bioactivity (Figure 3.5A). Similar results were obtained in vivo in terms of immunogenicity (Figure 3.6), however it remained to be seen what was the combinatory effect of ultracentrifugation and triacetin incubation. We showed that the combinatory act of spinning down unencapsulated MVA while in triacetin, had no effect on virus bioactivity when compared to PBS control (Figure 3.14 B1 & 2). In addition to exclude the possibility that we did not see any plaques because of circumstantial low MVA loading during encapsulation resulting in very few to no extracted MVA viruses, we also tested a spiked 'simulated' MP batch, containing high numbers of MVA (Figure 3.14 B4).

Under these conditions (Figure 3.14B3&D), we showed with the help of TEM that the virus was successfully recovered intact but could not be quantified by plaque assay. To elucidate why MVA was not infectious despite being recovered intact by ultracentrifugation, we then performed TEM with immunogold labelling against the viral surface antigen A27L. The only difference between samples on Figure 3.14 B2 &B3 is the presence of polymer. Our experimental design with TEM immunogol labelling confirmed our hypothesis that MVA virus was covered with a polymer layer (Figure 3.14C&D). Recovered MVA virus from polymeric solution did not get immunolabelled, most likely due to the unavailability of the A27L antigen covered with the polymer, thus ultimately preventing the virions from infecting when used in plaque assays for quantification purposes.

We then decided to use the FFE approach to separate MVA virus from the polymer based on its surface polarity. A trial run of polymeric solution led to unsuccessful separation since a polymer bubble started forming within 30 seconds inside the FFE system re-entrapping the MVA virus (Figure 3.16B). Nevertheless, an unexpected result was documented when unencapsulated MVA virus was exposed to FFE and then recovered in 96 fractions for usage in plaque assay. Although, the FFE did not affect MVA bioactivity (Figure 3.16A), we

expected to recover the unencapsulated MVA virus in 5-10 fractions similar to Figure 3.15D with the SPADNS red dye, but instead MVA virus was present in almost all fractions (Figure 3.16A). This result most probably happened due to differences in the polarity of the envelope membrane surrounding each MVA virion, causing them to separate into multiple fractions. It is known, that MVA during its intracellular assembly stages acquires membrane(s) from the endoplasmic reticulum (ER) and/or trans-Golgi network before budding off the cell acquiring its external membrane envelope from the host cell[264]. Differences in surface charge have been used to successfully isolate ER vesicles from Golgi vesicles[265] and plasma membrane vesicles[266] for each cell compartment, thus MVA acquiring membrane from each cellular network would have different surface charge and hence migrate to different fractions.

To summarise using standard protein encapsulation protocols led to the inactivation of MVA virus thus a tailored encapsulation protocol had to be devised to ensure its bioactivity. Lastly, several extraction strategies were attempted to recover infectious MVA virus from microparticles but with no success.

Chapter 4

Development of a qPCR based protocol for quantification of infectious encapsulated MVA

4 Chapter 4: Development of a qPCR based protocol for quantification of infectious encapsulated MVA

Statement of authorship

All microparticles (MPs) were manufactured by CK. All in vitro experiments in this chapter associated with the qPCR method, plaque assays and their corresponding analysis were done by CK.

4.1 Introduction

From the available literature, work on encapsulation of viral vectors in polymeric microparticles was limited. No agreed consensus or methodology existed that permitted confident estimations of encapsulated infectious virions. Wang D. et al, encapsulated a radio-labelled ^{125}I-Adenovirus and encapsulation efficiency was determined by % of adenovirus encapsulated in PLGA MPs vs the radio-labelled adenovirus present in supernatants[252]. Radiolabelling however, would not indicate what % of adenoviruses got deactivated during the encapsulation process, as both infectious and non-infectious adenoviral virions would retain their radioactive ^{125}I. The only other work involving adenovirus encapsulation using a double emulsion technique was a report by Guillermo del Barrio et al[251]. In this report total adenoviral particles per mg of lyophilised MPs, were estimated based on chemilluminescent detection of DNA. A known mass of MPs was dissolved with solvent and a DNA dot plot technique was utilised with an adenoviral DNA standard curve. Despite their best efforts, they did not test the effect of solvent exposure on adenovirus infectivity hence proving that all encapsulated adenoviruses did retain their native infectivity. We were in agreement however with their observation that: 1) their method measured both infective and non-infective adenoviral particles and 2) that by reversing the encapsulation procedure by re-adding the same solvent

and dissolving the MPs, it was not possible to measure infective adenovirus as the extraction process led to inactivation of the infective adenoviruses.

Work from Mittal et al[254], showed encapsulation of bovine adenovirus type 3 in sodium alginate microspheres by alginate-Ca^{+} ionic crosslinking with similar work by Sailaja et al[253], but neither of them provided a robust explanation on how they derived the amount of encapsulated viruses in their MP formulations. Lastly infectious salmon anemia virus (ISAV) was also encapsulated in PLGA nanoparticles and then incorporated into larger alginate microparticles and although authors demonstrated the presence of ISAV inside the microparticles, they did not provide any encapsulation efficiency estimates nor any proposals for its determination[267]. It is important to note that encapsulation into alginate microparticles via ionic gelation is a reversible process that does not involve harsh solvents or high-energy processes, thus it is easier to measure infectious encapsulated viruses from such formulations than it is to extract infectious viruses from polymeric microparticles after they have solidified by solvent evaporation.

4.2 Universal viral quantification methods

Collectively, it proved practically impossible to extract successfully bioactive MVA to be used for quantification of infectious units using the plaque assay method. We reviewed the current literature for viral quantification methods that are universally and scientifically acceptable. Frequently used methods for viral quantification that are relevant to vaccinia, are summarised in Table 4.1. After careful consideration, we decided to choose the quantitative PCR (qPCR) method to quantify and estimate the loading of MVA viruses in each MP batch.

Method	Detection	Time	Reproducibility	Labour	Costly	Reference
Plaque assay	infectious units	days	poor	high	no	[268]
Immunofluorecent Focus assay	infectious units	days	poor	high	yes	[269]
TCI_{50}	infectious units	days	poor	high	no	[270]
qPCR	DNA	hours	excellent	high	yes	[271]
Immunoblotting	protein	days	good	moderate	no	[272]
ELISA	protein	hours	good	moderate	no	[273]
Immunoprecipitation	protein	days	good	moderate	no	[274]
Heamagglutination assay	protein	hours	good	moderate	no	[275]
Viral flowcytometry	viral particles	hours	excellent	high	yes	[276]
TEM microscopy	viral particles	days	excellent	high	yes	[277]

Table 4.1 Most commonly used viral quantification protocols

4.3 Quantification of encapsulated MVA with qPCR

The strategy we followed to quantify encapsulated MVA within each MP batch is shown in Figure 3.1A. Briefly, once the MPs are hydrolysed overnight with NaOH and balanced with HCl, DNA could be extracted and purified with a commercial viral DNA extraction kit. This

would then be titrated using a standard curve of diluted genetic material from corresponding diluted MVA quantities.

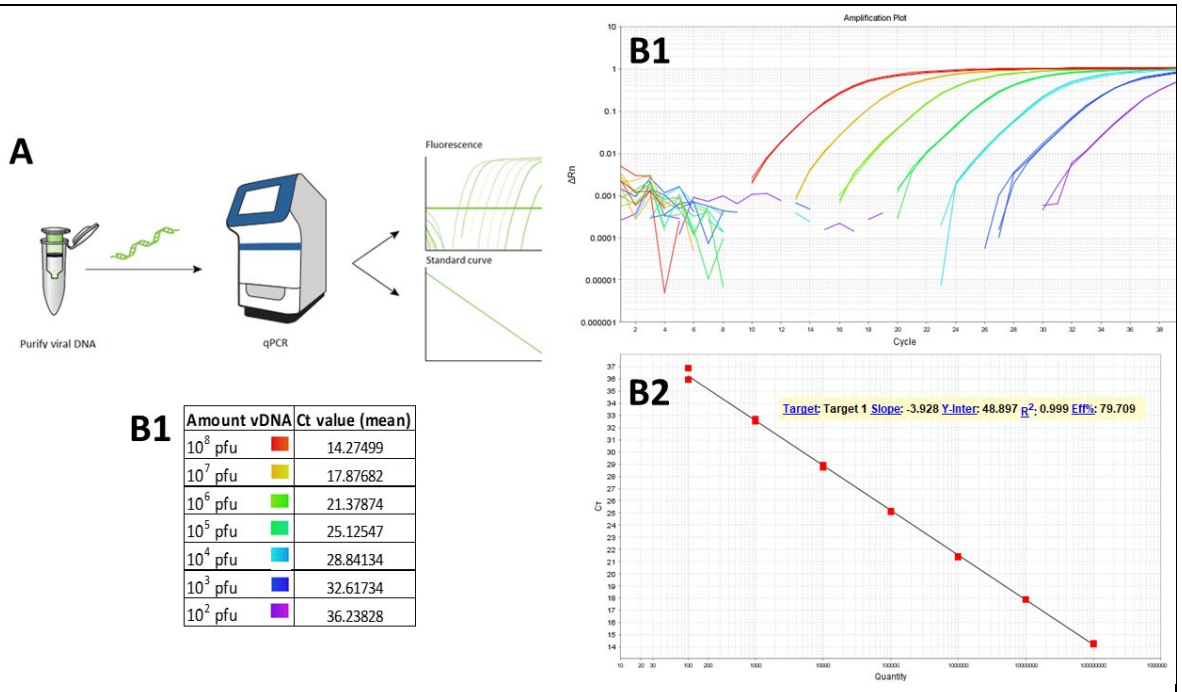


Figure 4.1 Quantitative PCR (qPCR) for determination of encapsulated MVA virus within MP batch

A) Flowchart of the proposed procedure for titrating and quantifying the encapsulated amount of MVA virus based on genetic material. Once part of the MP batch is hydrolysed with NaOH overnight and then balanced with HCl, 200µl volume is used to extract and purify viral DNA (vDNA). This vDNA, would then be subjected to qPCR, generating a fluorescent signal based on Taqman-chemistry, which is used to determine the threshold cycle (Ct). The amount of MVA pfu would be determined from a standard curve generated by plotting the Ct values against the corresponding amount of pfu.

B) 1) Ct values and the corresponding amount of pfu from extracted vDNA. Colours indicate on the fluorescent plot the amount of pfu for each curve. 2) Standard curve for qPCR reaction. 10-fold dilutions of extracted vDNA were assayed and generated Ct values were plotted against the corresponding amount of pfu for each viral dilution. R^2 value and Efficiency values of reaction are shown. Non-template control (NTC) with just DNAse/RNAse free water was used as a negative control.

We used the following primer and probe sequences that target the E9L DNA polymerase in the MVA genome: 1) E9L forward primer: CGGCTAAGAGTTGCACATCCA 2) E9L reverse primer: CTCTGCTCCATTTAGTACCGATTCT and 3) E9L probe Taqman Minor Groove

Binding (MGB) from Applied Biosystems with sequence AGGACGTAGAATGATCTTGTA, all of which were designed and used by Baker et al[278].

To validate the above primer and probe against the E9L DNA polymerase sequence, 10-fold viral dilutions were first made starting from 10^8 pfu down to 10^2 pfu. vDNA was then extracted from each viral dilution and purified with Purelink's Viral RNA/DNA extraction kit according to manufacturer's instructions (Methods 2.4.36). Real time qPCR was then performed in triplicate for each of the extracted viral dilutions to test the efficiency and sensitivity of the qPCR (Methods 2.4.37 & 2.4.39). These parameters were assessed by serial logarithmic dilutions covering a range of ≥ 7 logs. Following the PCR amplification, the generated Ct values were plotted against the initial pfu amounts from the viral dilutions leading to a standard curve (Figure 4.1B1/2/3). The standard curve provided insights on the consistency of the replicate reactions, the amplification efficiency and finally the detection limit of this assay. A linear regression line was automatically generated and the consistency of the replicates was measured by the correlation efficiency (R^2), which indicated the linearity of the generated Ct values in the standard curve. The R^2 value of 0.999 (Figure 4.1B2) indicated a strong linearity over ≥7 logs range down to 10^2 pfu value which in turn indicated the limit of detection for the assay (LOD) or sensitivity, as shown in Figure 4.1B1&B2. Lastly, the amplification efficiency which is defined by the slope of the standard which is -3.928, the efficiency of the qPCR reaction was 79.7% (Figure 4.1B2) calculated with the following formula: $10^{(-1/slope)}$-1.

We then used another primer/probe set targeting the E9L DNA polymerase from another manuscript for smallpox and pan-orthopox virus detection[279], having the following sequences: 1) forward primer: 5′-GAA CAT TTT TGG CAG AGA GAG CC-3′; 2) reverse primer: 5′-CAA CTC TTA GCC GAA GCG TAT GAG-3′ and Taqman probe: 3) 6′FAM-CAG GCT

ACC AGT TCA A-MGBNFQ-3′ with MGB chemistry. Despite following the manuscript's protocols and conditions the qPCR efficiency was only 68.67% (Figure 4.2A1).

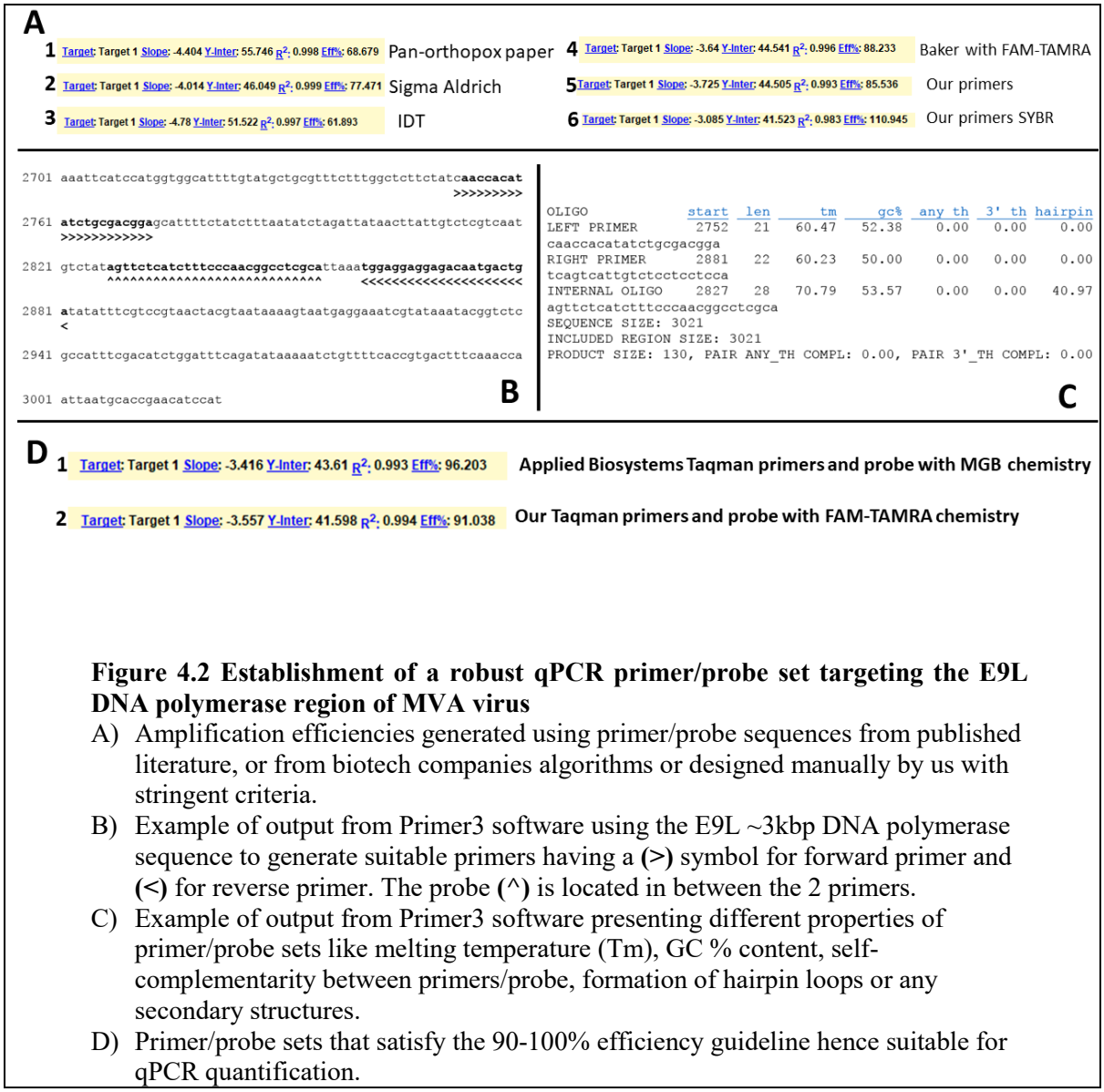


Figure 4.2 Establishment of a robust qPCR primer/probe set targeting the E9L DNA polymerase region of MVA virus

A) Amplification efficiencies generated using primer/probe sequences from published literature, or from biotech companies algorithms or designed manually by us with stringent criteria.
B) Example of output from Primer3 software using the E9L ~3kbp DNA polymerase sequence to generate suitable primers having a **(>)** symbol for forward primer and **(<)** for reverse primer. The probe **(^)** is located in between the 2 primers.
C) Example of output from Primer3 software presenting different properties of primer/probe sets like melting temperature (Tm), GC % content, self-complementarity between primers/probe, formation of hairpin loops or any secondary structures.
D) Primer/probe sets that satisfy the 90-100% efficiency guideline hence suitable for qPCR quantification.

Based on these inadequate qPCR efficiencies from the published domain we went forward and designed our own primer and probe sets. We retrieved the E9L DNA polymerase gene from the Uniprot database with ascension number P06856 and used automated algorithms from Sigma Aldrich and IDT Technologies to generate 2 primer/probe sets. Primer sequences were

of HPLC grade purity and the probe sequence contained MGB chemistry. These were then experimentally tested for validation.

Primer/probe sequences are shown in Table 2.3. When tested the primer/probe generated from website algorithms used in Sigma Aldrich and IDT technologies websites, they had an efficiency of 77.47% and 61.89% respectively (Figure 4.2A2/A3).

We then considered changing the dye chemistry for the sequences from the Baker et al manuscript from non-fluorescent quencher (NFQ)-MGB to a fluorescent TAMRA quencher chemistry. The same probe sequence was used but with a FAM-TAMRA chemistry and the efficiency increased from 79.7% efficiency to 88.33% (Figure 4.2A4).

Based on these events, we decided to manually design suitable primer/probe sequences. The institutional Primer3 website was used where the entire E9L DNA polymerase sequence was entered. Primer/probes were designed with stringent criteria and properties, described in detail in Methods 2.4.35. Figure 4.2 B&C show examples of how Primer3 website displays the binding location of the generated primer/probe within the E9L DNA polymerase region and the properties of the individual primers/probes. In Figure 4.2C, generated primers and probe had excellent properties as seen by their Tm, GC % content and no self-annealing and no hairpin formations. These sequences were ordered with HPLC grade purity while probe was ordered with MBG-NFQ chemistry. When experimentally tested these primer/probe set resulted in an efficiency of 85.53% (Figure 4.2A5).

We also considered using only the primer set, rather the primers with the probe in a SYBR qPCR reaction (Methods 2.4.38). When the SYBR was conducted under universal conditions with the same primer set but without the probe, the efficiency was 110% (Figure 4.2A6).

We also re-tried using the primers that we generated but changed the MGB-NFQ chemistry of the probe to TAMRA. When experimentally tested, surprisingly the efficiency became 91% (Figure 4.2D2).

We then outsourced the design of a primer/probe set with MBG chemistry from Applied Biosystem with MGB chemistry. When we tested their primers with a purified BAC-MVA plasmid containing the entire MVA genome, the qPCR efficiency was 96.2% (Figure 4.2 D1). This primer/probe set was then used for all downstream qPCR applications with consistent and reliable results using different MVA viruses encoding different antigens as shown in Figure 4.3.

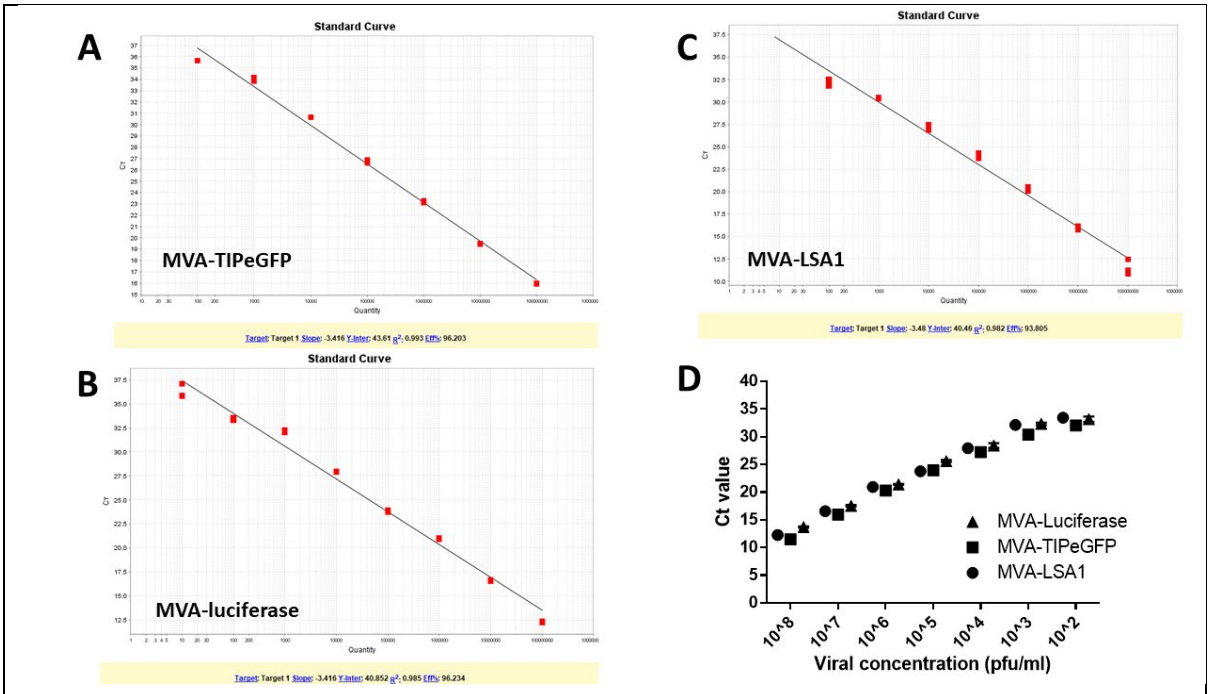


Figure 4.3 Standard curves for quantification and titration of encapsulated MVA viruses in polymeric MPs
Collated standard curves for MVA viruses encoding different antigens used throughout the project for measurement of encapsulated content, demonstrating consistency and reliability across experiments. Efficiencies shown are as following: A) MVA-TIPeGFP: 96.20%, B) MVA-luciferase: 96.23%, C) MVA-LSA1: 93.80%
D) Pooled data from A, B, C indicating consistency between pfu numbers and measured Ct across different MVA viruses arising from different stock concentrations. Data shown are the mean plus standard deviation.

4.4 Quality controls for qPCR methodology

Before proceeding with measuring the encapsulated MVA virus content of lysed MPs samples, we wanted to establish the validity of this qPCR methodology with quality control testing.

First, we took the opportunity to examine whether any viral DNA loss occurs during extraction, as well as the absence of PCR inhibitors in the lysed MPs that might distort results. To confirm that no substantial DNA loss occurs because of manufacturing inconsistencies between DNA binding columns, we tested the DNA binding quality of the commercial columns. To document this, 3 DNA binding columns were randomly chosen from the provided batch. Each binding column was used to purify vDNA, using 200µl from the same viral dilution and treated according to manufacturer's instructions (Figure 4.4A). We found that there were no significant differences between extracted DNA from different DNA columns whilst constant levels of MVA genome were detected (Figure 4.4A).

We then checked for the possibility of inherent inhibitors being carried over from the polymer itself into the lysed MP samples. Empty PLA MPs containing only PBS were manufactured. These were then lysed overnight and an aliquot was used to purify vDNA. After that, the extracted genetic sample from empty MPs was spiked with a known amount of vDNA. This was compared to a positive control to monitor for the presence of polymer inhibitors. Figure 4.4B confirmed the absence of PCR inhibitors associated with the PLA polymer with no vDNA. A similar experiment was done with PLGA polymer MPs (Figure 4.4B).

We then wanted to validate that we were able to regenerate reliable standard curves from viral stocks and get consistent Ct values for comparable MP loading estimations. To experimentally test for any day-to-day variations using the same virus stock in order to create 10-fold viral dilutions and then extract vDNA from them, we prepared over 3 days, a single 10^6 pfu/ml viral dilution every day directly from stock. This was kept in the -80˚C freezer until required. Viral

DNA was extracted as usual, tested by qPCR and then Ct values were compared. Figure 4.4C illustrates that it was possible to regenerate samples of equal genetic quantity on different days to be used in standard curves.

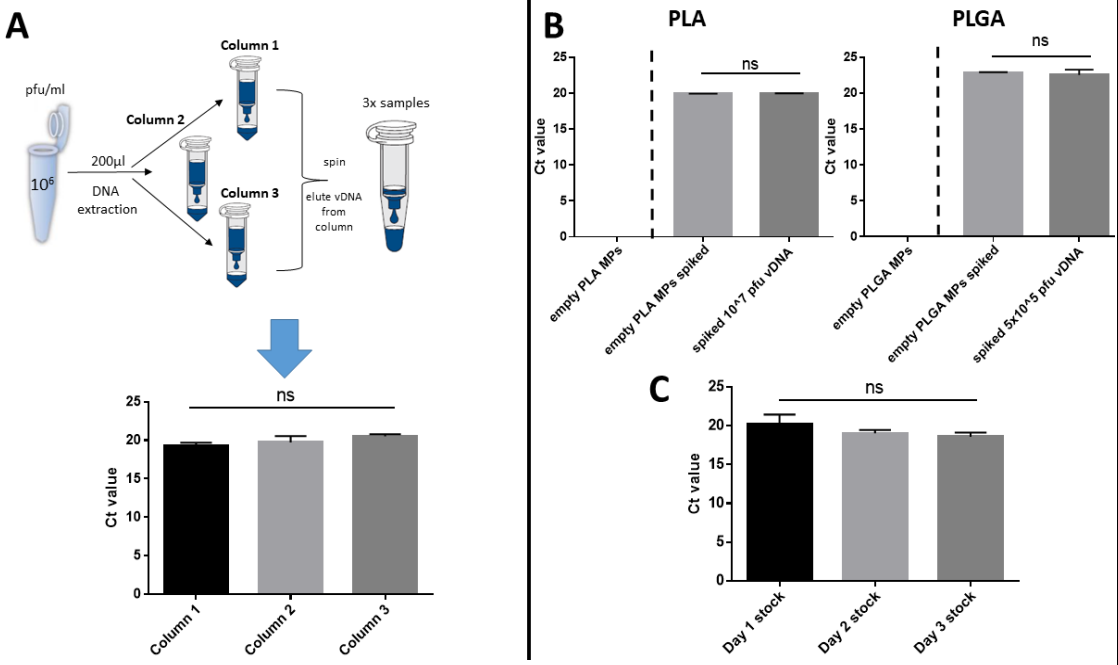


Figure 4.4 Establishment of quality controls before planned qPCR work

A) Commercial DNA binding columns were tested for DNA binding efficiencies to avoid having any discrepancies for the amounts of recovered vDNA. A single MVA dilution was prepared and then 3 aliquots were taken and used with 3 randomly chosen binding columns provided with the kit. vDNA was processed, purified, eluted and tested with qPCR to find whether similar vDNA amounts are recovered from the same tube.

B) Empty PLA or PLGA MPs were carefully prepared encapsulating PBS, lysed with NaOH overnight and balanced with HCl. Then an aliquot was taken and purified using the commercial DNA extraction kit. The eluded sample was then spiked with a known amount of vDNA and compared to the same sample without lysed polymer to indicate if an inhibitory effect occurs in the qPCR reaction from the polymer.

C) For the purpose of regenerating consistent standard curves from viral stocks, a single MVA dilution was prepared on 3 different days directly from stock, and processed similarly to A. vDNA was tested by qPCR and compared across the 3 days.

Statistically confirmed non-significant (ns) by one-way ANOVA with Bonferroni's multiple comparison post-hoc test. Data shown are the mean plus standard deviation.

We then compared two methods of generating an appropriate standard curve. The first option was to make a range of 10-fold viral dilutions from stock and then extract vDNA (Figure 4.5A). The second, was to create a single viral dilution, extract vDNA and then proceed creating 10-fold dilutions from the extracted vDNA (Figure 4.5B). As seen in Figure 4.5C when compared, theoretically equivalent samples were statistically different in terms of Ct value.

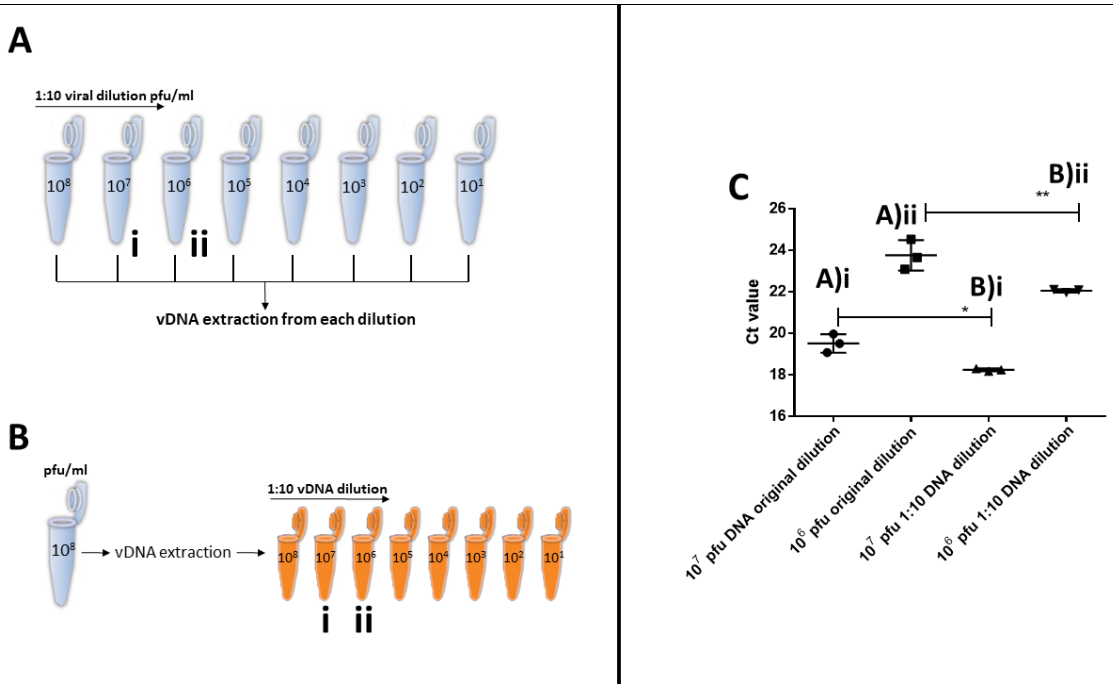


Figure 4.5 Determination on which standard curve preparation procedure to use for proposed qPCR work

A) Standard curve preparation where serial logarithmic viral dilutions (pfu/ml) were made covering a range of 8 logs. Then vDNA extraction was done for each dilution and samples were stored in -20˚C freezer until required.

B) An alternative standard curve approach. A single viral dilution (pfu/ml) is made and viral nucleic acid is extracted and then serial logarithmic vDNA dilutions are prepared covering a range of 7 logs.

C) qPCR data showing the difference in Ct value for theoretically matched vDNA samples. Samples shown and compared are from A (i&ii) and B (i&ii). A Ct value is inversely proportional to the amount of vDNA detected i.e. a high Ct value indicates that the detected product is of low abundance since it needs more amplification cycles (Ct) to reach the detectable signal above threshold.

Statistical significance (*p<0.05; **p<0.01; ***p<0.001; ****p<0.0001) by one-way ANOVA with Bonferroni's multiple comparison post-hoc test. Data shown are the mean plus standard deviation.

4.5 Discussion

In our view, there was no official nor scientifically robust method in the published domain to measure infectious encapsulated viruses from PLGA microparticles. For this project, it was necessary to balance encapsulated infectious MVA dose to the unencapsulated booster MVA dose before proceeding with in vivo studies.

In the previous chapter we showed that it was indeed impossible to separate safely infectious MVA virions from the polymer. To refresh, we tried reintroducing the MVA-compatible solvent triacetin to remobilise the entrapped MVA virus from the polymer mesh with no avail. Using the Mw difference between the MVA virions and polymer itself using a 100kDa cut-off protein filter as well as chemically extracting MVA by hydrolysing the PLGA polymer with diluted amounts of NaOH, also proved ineffective. Enzymatic degradation of polymer with lipases was shown to deactivate the virus itself. Taking advantage of the different physicochemical properties of the MVA virus such as density and membrane surface charge and then venturing on to ultracentrifugation and FFE respectively, proved to be fruitless.

We then compiled a table with the most commonly used viral quantification protocols (Table 4.1) and based on the process of elimination we chose to utilise the qPCR approach and measure the encapsulated vDNA content. Genetic material could be harvested and used for quantification of MVA viruses right after MP hydrolysis with NaOH overnight and HCl balancing, followed by qPCR measurement. As shown in Table 4.1, methods measuring viral protein do not have excellent reproducibility but qPCR has. In addition, it was clear that protein-based colorimetric assays e.g. BCA is not an internationally accepted method to quantify viruses in the virology field like it is in the field of protein encapsulation.

Based on the data gathered so far in this project it was physically impossible to recover virions that are able to infect and hence be used in any method which readout is infectious units.

Automatically the plaque, immunofluorescent focus (similar to plaque assay but uses immunostaining to detect infected cells and/or infectious viral particles) and TCI_{50} assays (similar to plaque assay but quantifies amount of virus needed to produce a 50% cytopathic effect in cultured cells), were excluded. TEM microscopy, which we had already used was not a viable option either to quantify routinely MVA viral particles as the presence of the polymer made it hard to distinguish between viral particles themselves and images were full of background noise (Figure 3.14). Viral flowcytometry on the other hand, which was first reported with baculoviruses[276] and later on with several viruses of different morphology and genomes[280], has excellent reproducibility and can be done within hours. However when feeding the polymeric solution containing the MVA viruses from the dissolved MPs into the flowcytometer, it would have blocked it with the instant solidification of the polymer like we have seen with FFE in Figure 3.16B. Similarly, based on Figure 3.14D where we have shown that due to polymer coating the surface of the virions immunogold labelling failed by preventing access of the immunogold labelled antibodies to their viral protein target, we excluded the protocols requiring binding to a viral protein/virions in order to produce a quantifiable signal i.e. ELISA, immunoprecipitation and immunoblotting. Likewise, with heamagglutination, MVA virions wouldn't be able to bind and agglutinate susceptible chicken erythrocytes via their heamagglutinin.

As of 2017, quantitative PCR is widely accepted as the gold standard for detecting and quantifying nucleic acids from a plethora of origins[281]. Today qPCR routinely used in scientific and diagnostic laboratories for detection of different kinds of viruses like influenza, herpes simplex, adenoviruses, Epstein-Barr, enteroviruses and many more[271] as well as more tropical viral diseases like Dengue virus[282]. However in the field of encapsulation, qPCR has not been

used to quantify genetic material inside MPs but has been used only for the purposes of quantification/monitoring of induced genes by MP administration in specific tissues in vivo[283].

We tested 2 published sets of Taqman probe + primers targeting the E9L DNA polymerase in the MVA genome according to the manuscript's protocols and conditions. We could not reproduce the published 99% qPCR efficiency, as it turned out that the efficiency value of the qPCR reactions was inadequate (<90% efficiencies - Figure 4.1B2 & Figure 4.2A). Based on the instructions of Applied Biosystems[284] and the *M*inimum *I*nformation for Publication of *Q*uantitative Real time PCR *E*xperiments (MIQE)[205] criteria, which is a universal consensus providing guidelines to promote consistency and reliability of results between laboratories; having efficiencies of <90% was alarming. Acceptable amplification efficiency should be between 90% and up to 100% with theoretical 100% indicating that the amount of amplicons is doubled with each cycle. Therefore the published primers and probe from Baker et al[278] & Kulesh et al[279] did not appear to be useful.

To interpret results of qPCR measurements, it is imperative to have high amplification efficiency. Even a small error in the assumed qPCR efficiency could cause large errors in the estimated amounts of amplicons due to the cycling and exponential nature occurring during a qPCR reaction[285]. It has been experimentally shown that even a 5% difference in qPCR efficiencies can produce a substantial 50% difference in the number of amplicons produced after only 25 cycles, due to accumulation effects[285].

TAMRA probes are usually longer than MGF-NFQ by an average 35bp and this reduces specificity of the probe[286]. MGB is the recommended quencher by Applied Biosystems for Taqman assays, as it provides higher signal and lower background when compared to non-MGB assays[287,288]. MGB-NFQ when chemically conjugated into the probe it modifies the DNA, increases stability and generates short a probes with high Tm and substantial quenching.

But this modification has the drawback of making it very challenging to design such probes as Tm prediction algorithms for such modification are not extensively known[287,289].

We initially used MGB as the quencher in the probe, which proved to be scientifically unsuitable (Figure 4.2A2/3/5/6 with 77.4%, 61.89%, 85.53% and 110.94% respectively). However we ended up with a primer/probe set with TAMRA as the quencher within the probe resulting in a 91% qPCR efficiency (Figure 4.2D2), which was above the acceptable limit. After consultation with Applied Biosystems, a primer/probe set having MGB as the quencher was created and was experimentally validated having a 96% efficiency (Figure 4.2D1). Due to its exceptional efficiency, this primer/probe set was preferred for all downstream qPCR experiments. Standard curves generated from MVA viruses encoding different antigens showed that the limit of detection limit (LOD) was 10^2 pfu/ml (Figure 4.3). This qPCR LOD value was a 100-fold improvement in sensitivity for quantifying encapsulated MVA viruses, when compared to the protein BCA assay LOD value of 10^4 pfu/ml (Figure 3.12).

By choosing to have the conserved and universal E9L DNA polymerase sequence as the amplicon target, different MVA viruses could be tested and presented in 'pfu' since pfu is a universal viral quantification output for MVA (Figure 4.3). Therefore, the E9L DNA polymerase primer/probe pairs were suitable for any antigen-enconding MVA that we wanted to encapsulate.

It is important to note at this point that by default qPCR measures total viral genetic material, whether the virions are viable or not after the encapsulation procedure. However, we made substantial effort in the previous chapter confirming both in vitro and in vivo and adapted the encapsulation procedure, so that the encapsulation itself does not affect the bioactivity of the virus (Figure 3.5 & Figure 3.6). Because of this virus-tailored encapsulation, encapsulated MVA should still be infectious with no loss of bioactivity. Therefore, extrapolated amounts of

genetic ‘pfu’ would be reflective of a true pfu value once encapsulation is finished. If there was some loss of bioactivity at any point of the encapsulation procedure, we would not be able to continue using this qPCR approach, since genetic material from non-infectious MVA virus would be quantified by the qPCR as well in addition to the vDNA from any infectious MVA virions.

Before proceeding to establish MP encapsulation efficiencies based on viral genetic material, we also thoroughly tested our methodology with quality controls. We have shown that there was no significant DNA loss occurring during the extraction process using the kit-provided DNA binding columns (Figure 4.4A).

It is a known fact that PCR amplification is prone to the presence of inhibitors[290], which is especially true when dealing with biological samples, that frequently contain for example heparin[291], or with food/microbial samples[292]. Our proposed workflow using qPCR involves multiple steps and stages, all of which can introduce inhibitors during sample handling, nucleic acid isolation and the qPCR reaction. Many starting materials could contain high levels of inhibitors and in our case, inherent inhibitors could be present or carried over from the polymer itself. By spiking the samples with known amounts of vDNA, we demonstrated that after hydrolysis of the PLGA or PLA polymer, carry-over lysed polymer had no significant interference effect on the qPCR reaction and primer/probe chemistries (Figure 4.4B). Spiking[293] is a useful way for detecting inhibition but it is not routinely included as an internal control in many real time PCR assays. This experimental design confirmed the absence of PCR inhibitors that could originate from the PLA or PLGA polymers itself and that no co-purification of vDNA with inhibitors occurs.

We also showed that a reliable and reproducible standard curve could be regenerated at will using viral stock solutions on different days, meaning that MP batches could be compared directly across measurements (Figure 4.4C).

Our last quality control was to decide the most appropriate standard curve and its generation. We initially considered using genome copies as a measurement, since it is believed that there is only 1 copy of the MVA genome in each MVA particle with an estimated particle to pfu ratio[278] of 408:1. For simplification, we decided to avoid using genome copies as our measurement output and illustrate instead a direct relationship between extracted vDNA and pfu. To achieve this we compared two ways of generating a standard curve: 1) we made 10-fold serial viral dilutions and vDNA was extracted from each dilution; 2) from a single viral dilution, vDNA was extracted and from this vDNA 10-fold dilutions were made. When experimentally tested there was a statistical difference between them (Figure 4.5) and we chose to generate 10-fold viral dilutions first and then extract vDNA from each of them, to utilise in future MP batch loading measurements. This approach was more representative of the viral genetic material present in lysed MVA-loaded MP batches. This preparatory method produced viral dilutions in a 1ml volume from which 200µl was used to extract vDNA, which coincides with the routine digestion method for MPs. MPs are hydrolysed with 500µl of 1M NaOH overnight followed by 500µl of 1M HCl, making it a 1ml total volume, from which 200µl is used to extract vDNA. Therefore, the extrapolated value from the qPCR assay would represent the pfu amount present in the 1ml of lysed MVA-loaded MPs.

To summarise, quantification of encapsulated infectious MVA virus was possible with qPCR thus paving the way for the initiation of in vivo studies. Reflecting back on work from this chapter, it would have been a better investment of time to design our own primer/probe sets with stringent criteria from the very start rather than spending time reproducing published

primers/probes that proved inadequate based on international standardisation criteria. To the best of our knowledge, there was no previous example in the literature of applying qPCR for measurement of vDNA material directly from polymer matrices or polymeric substances.

Chapter 5

Microparticle preparation, optimisation & characterisation

5 Chapter 5: Microparticle preparation, optimisation & characterisation

Statement of authorship

All microparticles (MP) were manufactured by CK. All in vitro experiments, qPCR, SEM, fluorescent microscropy, viral plaque assays and their associated analysis were done by CK. MVA-D8-GFP virus was genetically engineered by Dr. Vincent Pavot and donated to CK who bulked it up.

5.1 Introduction

In the field of viral vector encapsulation only 2 studies have attempted to encapsulate a viral vector (adenovirus) within solid polymeric microparticles[251,252]. Neither of them provided a robust way for the measurement of encapsulated infectious virions. Additionally, in the context of prime-boost immunisation only one study involved adenovirus and polymeric microparticles. This entailed mouse studies where microparticles coated with ovalbumin were given as a prime followed by a boost with unencapsulated adenovirus encoding ovalbumin protein[294].

5.2 Quantification of encapsulated viral content

From the previous chapter we established a reliable and sensitive qPCR approach to quantify encapsulated infectious units present within MVA-loaded MP batches. Table 5.1 shows the formula used to determine the amount of MVA content in the MP batch with an example calculation from a batch that was used later on with in vivo studies.

$$Total\ viral\ loading\ (1) = \frac{virus\ (pfu)\ in\ lysed\ MPs}{mass\ of\ lysed\ MPs\ (mg)}\ x\ total\ mass\ of batch\ (mg)$$

$$Encapsulation\ Efficiency\ (EE\%) = \frac{total\ viral\ loading\ (1)}{starting\ virus\ (pfu)}\ x\ 100$$

Name (replicates)	Extrapolated PFU	Amount of lysed MPs (mg)	PFU/mg	Average PFU/mg	Total mass of batch (mg)	Total viral loading (PFU)	Starting amount (PFU)	Encapsulation Efficiency (EE%)
PLGA A	393984.5313	12.9	30541.44	36486.62405	494.9	1.81E+07	5.00E+07	36.11
PLGA B	580392.6875	12	48366.06					
PLGA C	400236.1563	13.1	30552.38					

Table 5.1 Formula for determination of MVA content in MPs
Actual viral loading and encapsulation efficiency (EE%) values were calculated according to the above equations. A part of the MP batch was measured for its mass and then lysed overnight with 500µl NaOH. Equal volume of HCl was added to counter balance NaOH and from this 200µl were used to extract viral DNA. This viral DNA was measured and amounts of theoretical pfu based on genetic material were extrapolated with an appropriate standard curve. EE% was calculated with the formula shown above. Underneath is one example of a MP batch that was used in an in vivo immunogenicity study having an EE % of 36.

Following the protocol illustrated earlier in Figure 3.9B using triacetin as the base manufacturing solvent, our next experiment focused on determining the degree of encapsulation efficiency for generated MP batches. In addition, we sought to optimise encapsulation efficiencies by changing processing conditions during the double emulsion procedure, so that sufficient amounts of MVA were encapsulated for in vivo studies.

5.3 Microparticle batch optimisation and characterisation

We manufactured 7 MP batches demonstrated in Table 5.2. We kept a base MP formulation as a reference particle and experimented with different processing conditions as described in Table 5.2. Interestingly increasing the W_1 phase with PBS led to a decrease in EE% (Formulations F to H) while MP population size was relatively similar. Doubling the PLGA concentration from 100mg/ml to 200mg/ml, as well as reducing by half the homogenisation speeds between different emulsions, led to a decrease in EE% (Formulations J & I). On the

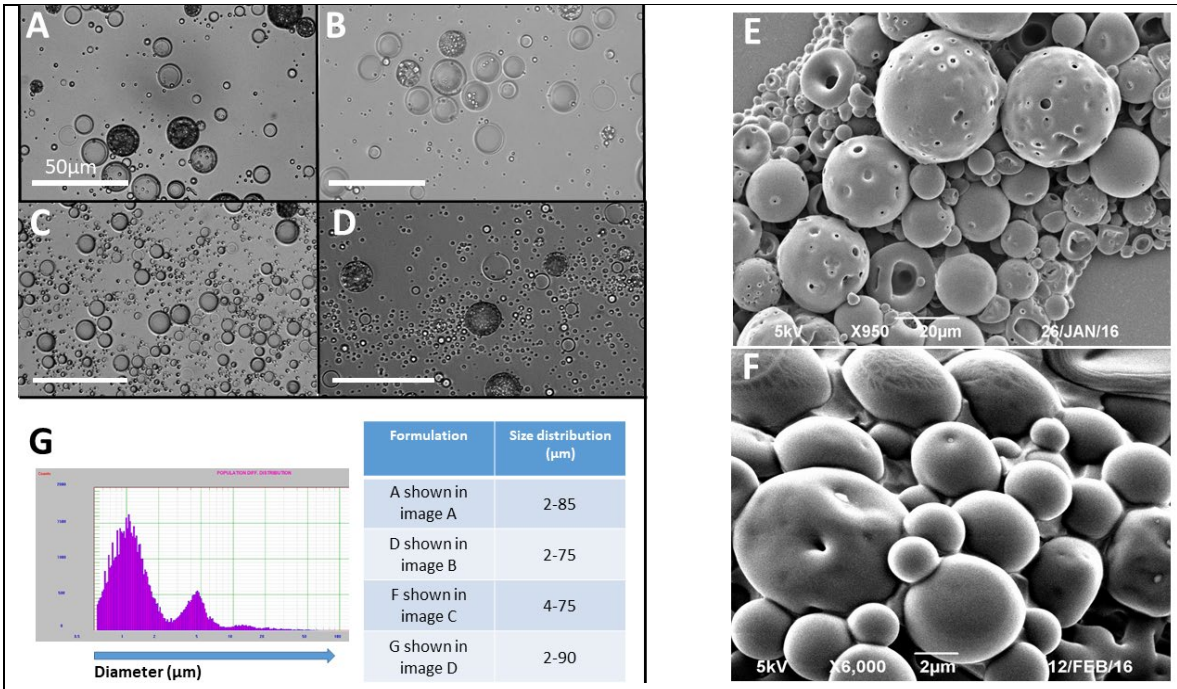
other hand, addition of EtOH in the W_2 phase of 1% PVA having a final concentration of 5% EtOH increased EE%.

Optical imaging of the produced MPs confirmed the similarity of MPs in terms overall appearance (Figure 5.1A-D). Furthermore, samples A and D from Table 5.2 were observed under SEM to check their surface morphology. The addition of EtOH in the W_2 phase smoothened the MP surface throughout for formulation D (Figure 5.1F), while formulation A was porous with indentations (Figure 5.1E). Triacetin based PLGA MPs from the SEM images (Figure 5.1E&F) were mostly irregular in shape rather than spherical. Particle size analysis was performed using an Accusizer particle size analyser (Methods 2.4.24) and size distributions for each MP batch is shown in a table format in Figure 5.1G, ranging from 2-90μm in size.

Processing conditions									
Formulation	Polymer concentration (mg/ml)	Homogenisation speed (rpm)	W_1 volume (µl)	O volume (ml)	W_2 volume 1% PVA (ml)	EtOH addition to W_2 1% PVA 5% EtOH	Stirring rate (rpm)	MPs size (µm)	Encapsulation Efficiency (EE%)
A	100	25000	6.6	1	15	No	800	2-85	7.9
D	100	25000	6.6	1	15	**Yes**	800	2-75	13.6
F	100	25000	**50**	1	15	No	800	4-75	1.3
G	100	25000	**100**	1	15	No	800	2-90	0.3
H	100	25000	**200**	1	15	No	800	4-70	0.1
I	100	**12000**	6.6	1	15	No	800	2-70	0
J	**200**	25000	6.6	1	15	No	800	4-80	0.2

Table 5.2 Table of optimisation steps for encapsulation efficiency with varying processing conditions

Different MP batches were manufactured using PLGA with Lactic/Glycolic acid ratio 65:35 and polymer Mw of 24-38 kDa. More than 14 MP batches were initially manufactured for optimisation purposes. This table shows 7 of them where addition of EtOH to W_2 phase, increasing W_1 volumes, homogenisation speeds between phases and polymer concentration were tested. All batches were compared to a base formulation (A) changing 1 parameter at a time while keeping other parameters constant. Values **in bold** were the ones changed in each respective recipe.



Formulation	Size distribution (µm)
A shown in image A	2-85
D shown in image B	2-75
F shown in image C	4-75
G shown in image D	2-90

Figure 5.1 Images of the first 4 MP batches from Table 5.2
Top left quadrant are representative optical microscopy images (40x magnification) of A) Formulation A; B) Formulation D; C) Formulation F; D) Formulation G. Scale bar = 50µm.
On the right side are representative SEM microscopy images. E) Formulation A; F) Formulation D. Scale bars are as shown.
Bottom left (G) is a representative size distribution based on mean volume diameter of the microparticles using an Accusizer diffractometer. A table showing the size distribution in µm for the 4 MP batches is shown ranging from 2-90µm.

We then updated our MP manufacturing procedure by having the MPs stir overnight in a 50ml volume of 1% PVA, rather than 15ml, after the final emulsion $W_1/O/W_2$ had been formed (Figure 5.2A).

We also assessed whether increasing the concentration of the stabiliser from 1% to 5% PVA for the W_2, provided more stability to MP formulations. Based on empirical observations under optical microscopy, MP having 5% PVA as a W_2 stabiliser looked better than the ones with 1% PVA. For this reason, we had the primary emulsion (W_1/O) form the final double emulsion inside 10ml of 5% PVA and then transferred this into 50ml 1% PVA to be stirred overnight (Figure 5.2A). Comparison in EE% between double emulsions formed in 10ml 1% PVA vs in

10ml 5% PVA showed that increasing the concentration of PVA improved the EE% (Figure 5.2B). After this, we updated once again our MP procedure using 5% instead of 1% PVA.

Utilising the most updated protocol (Figure 5.2) we then fabricated formulations from not only PLGA, but also PLA and mixtures of PLGA/PLA with 3:1 ratio and PLA/PLGA with 3:1 ratio (Figure 5.2C). Another variant formulation was PLA MPs that were exposed to 20% (v/v) EtOH for 2 minutes after being stirred overnight in 50ml 1% PVA. All formulations were tested for their EE% which is shown in Figure 5.2C, with PLA formulation having the highest EE%.

SEM was performed again to investigate the surface texture of the MP formulations using the most up-to-date triacetin based protocol. Basic particles manufactured with the protocol looked spherical with majority having smooth surfaces with some pores and/or indentations (Figure 5.3A). Building on this, we then tested whether increasing concentrations of EtOH would have any effect on the MP surfaces. For this purpose, 3 batches were made where the final emulsion ($W_1/O/W_2$) was added to 50ml 1% (w/v) PVA containing either 20%, 30% or 40% (v/v) EtOH and left to be stirred overnight. As seen in Figure 5.3 B,C,D corresponding to 20%, 30% and 40% EtOH, the higher the EtOH concentration the rougher the MP surface with increasing number of pores and 'wrinkles'.

Moreover, we also examined how the MPs look like with short exposure to 20% (v/v) EtOH after they have been stirred overnight and solidified. Once the stirring was finished, MPs were collected by centrifugation and then exposed to 10ml of 20% of EtOH for 2 minutes before being washed three times with water to remove the EtOH. Figure 5.3E shows that short treatment with 20% EtOH transformed the base MP formulation (Figure 5.3A) from having few pores/indentations to having none with a smooth surface throughout.

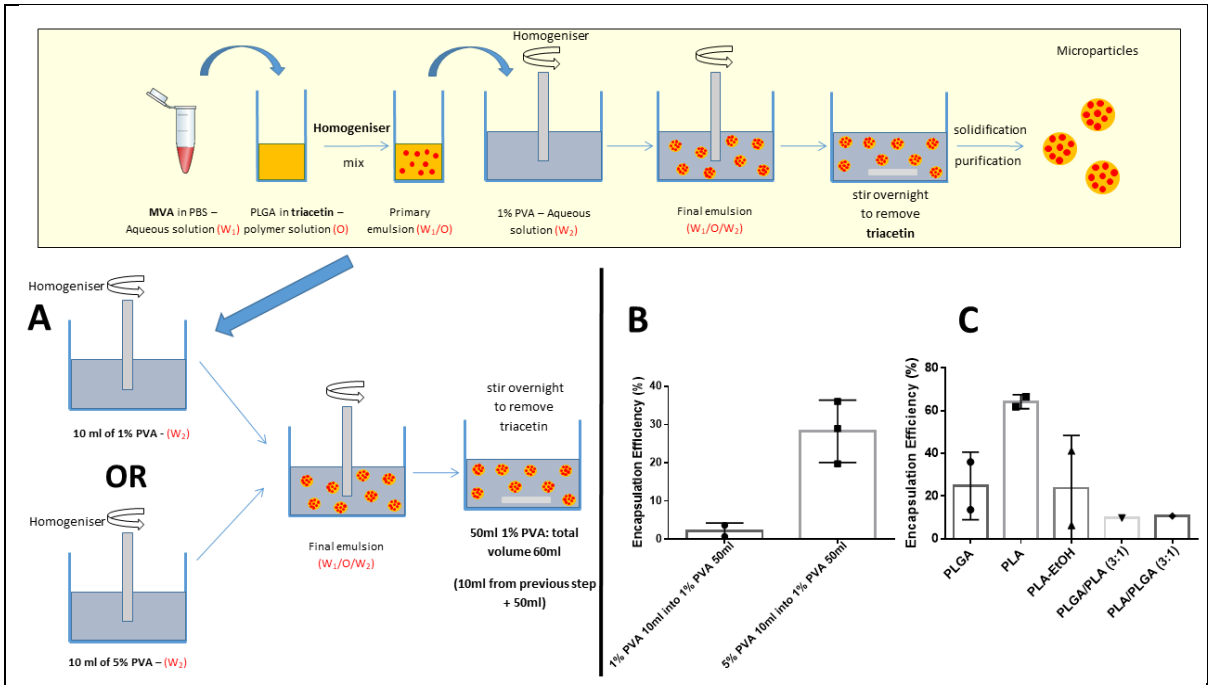


Figure 5.2 Updated MP procedure with encapsulation efficiencies (EE%) for different polymer formulations

Reminder illustration about the MP manufacturing procedure using triacetin.

A) Introduction of new steps for better MP stabilisation: Primary emulsion (W_1/O) was transferred into either 10ml of 1% PVA (W_2) or 10ml of 5% PVA to make the final double emulsion ($W_1/O/W_2$), both of which were finally transferred into 50ml of 1% PVA, making 60ml total volume and was left to stir overnight. The extra volume of 1% PVA provided enough water for complete removal of triacetin from polymer. MPs would be solidified throughout ensuring a spherical shape.

B) Comparison in EE% between transferring the primary W_1/O emulsion into either 10ml of 1% PVA or 10ml of 5% PVA and then transferred to 50ml of 1% PVA. Data shown are the mean plus standard deviation. Statistics could not be done due to n <=3.

C) Comparison in EE% between different polymers and formulations. Data shown are the mean plus standard deviation. Statistics could not be done due to n<=2.

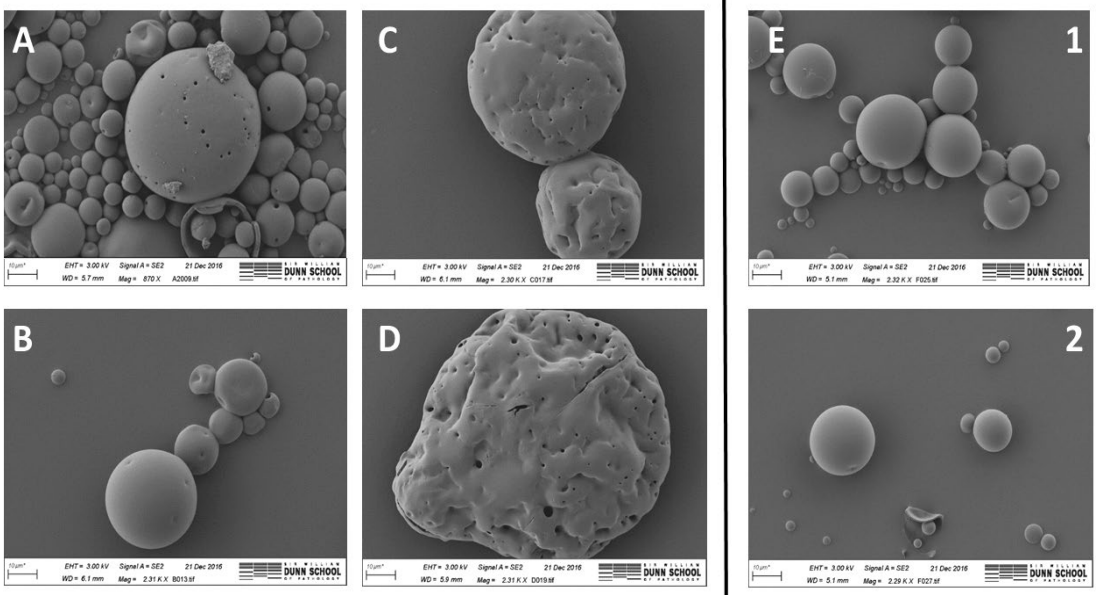


Figure 5.3 SEM Morphology of optimised triacetin based MPs
Blank MP with PBS were manufactured with the most up-to-date triacetin based protocol using 5% PVA as the stabiliser and then visualised with SEM. Effect of overnight and short-term exposure to EtOH was investigated.

A) Morphology of base MP formulation using the most updated protocol.
B) Same to formulation A but exposed to 20% (v/v) 1% (w/v) PVA and stirred overnight.
C) Same to formulation A but exposed to 30% (v/v) 1% (w/v) PVA and stirred overnight.
D) Same to formulation A but exposed to 40% (v/v) 1% (w/v) PVA and stirred overnight.
E) 1&2 Same to formulation A but exposed briefly for 2 minutes after MPs have been stirred overnight and solidified followed by a final wash in water.

We then proceeded to study the relationship effect of adding EtOH into the MP fabrication process in terms of EE% for each formulation. However, we had to first confirm whether exposure to EtOH had any effect on MVA bioactivity. To document this we exposed a known amount of intact MVATIPeGFP to 20%, 30% and 40% (v/v) EtOH for 24 hours as well as 10 minutes only with 20% (v/v) EtOH and then compared it to the PBS control (Figure 5.4A). It was evident that exposure of MVA virus to EtOH for more than 10 minutes had a detrimental effect on its bioactivity. When MVA virus was exposed for less than 10 minutes to 20% (v/v)

EtOH for bioactivity was not affected. When experimentally measured, the EE% of the MP formulation with short 2 minute EtOH exposure was illustrated earlier in Figure 5.2C.

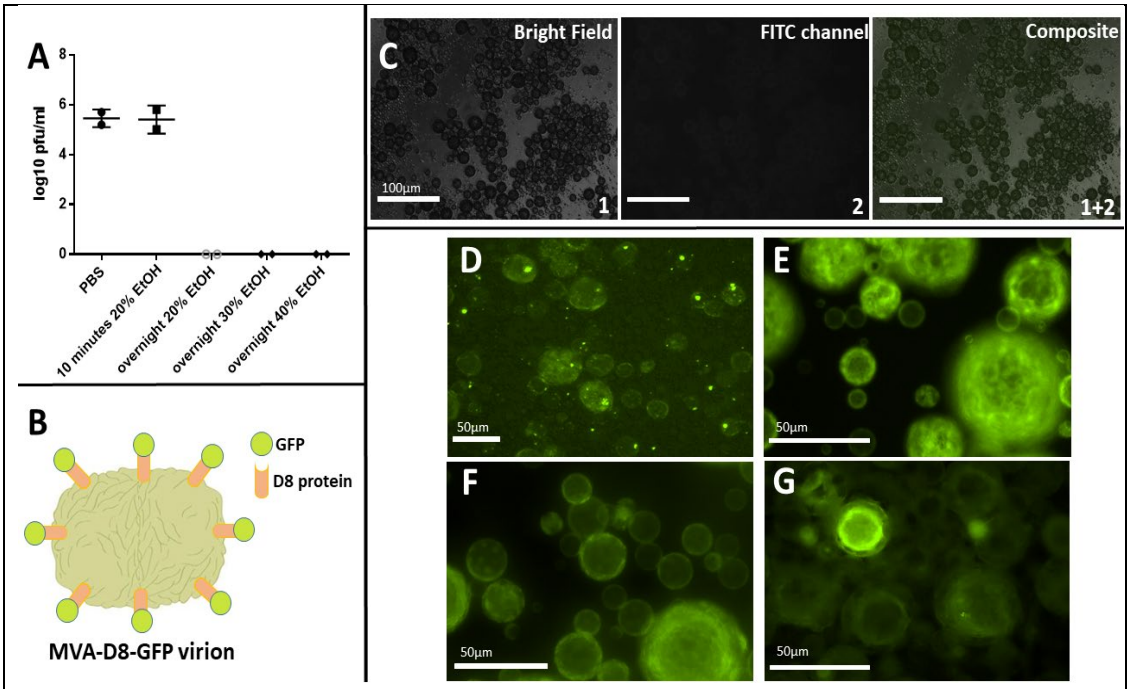


Figure 5.4 Effect of long vs short exposure to EtOH on MVA bioactivity and MVA intraparticle distribution

A) 10^6 pfu were exposed for 24 hours to increasing amounts of 20%, 30% and 40% (v/v) EtOH (n= 2) to simulate what happens when the primary emulsion W_1/O containing MVA is added into the W_2 phase containing EtOH. In addition 10^6 pfu were exposed for 10 minutes to 20% EtOH. An aliquot from each condition was then used for plaque assay quantification. Data shown are the mean plus standard deviation. Statistics could not be done due to n=2.

B) Directly fluorescent infectious MVA virus with genetic modification by fusing GFP molecule to the structural D8 protein of the MVA virion. This was used for the determination of intraparticle distribution of encapsulated MVA virus using fluorescent microscopy.

C) Blank PLGA MPs containing PBS were imaged to demonstrate the background fluorescent of blank MPs as the polymer autofluoresces when viewed under FITC channel.

D) PLGA MPs with encapsulated MVA-D8-GFP virus in FITC channel.

E) PLA MPs with encapsulated MVA-D8-GFP virus in FITC channel.

F) PLGA/PLA 3:1 ratio MPs with encapsulated MVA-D8-GFP virus in FITC channel.

G) PLA/PLGA 3:1 ratio MPs with encapsulated MVA-D8-GFP virus in FITC channel.

5.4 Intraparticle location of MVA virus after encapsulation

We then sought to understand the intraparticle distribution and location of MVA within the MPs themselves. To gain insight we encapsulated a genetically modified MVA virus that had been engineered to be directly fluorescent by addition of a GFP molecule to its structural D8 protein (Figure 5.4B). MVA-D8-GFP virus was bulked up (Methods 2.4.31 & 2.4.32), encapsulated in MPs using double emulsion and visualised with fluorescence microscopy (Methods 2.4.13). PLGA, PLA, PLGA/PLA with 3:1 ratio and PLA/PLGA with 3:1 ratio with 10^7 pfu MVA-D8-GFP as starting material were manufactured and visualised (Figure 5.4D-G). Blank PLGA MPs containing only PBS were also visualised to show the background autofluorescent levels from PLGA polymer in the FITC channel and distinguish it from true GFP signal (Figure 5.4C). We found that the intraparticle distribution of MVA virus was different depending on what polymer was used to manufacture the MPs. Within PLGA MPs MVA virus seemed to be accumulated in distinct puncta or pockets within the polymeric matrix, whereas when PLA polymer was used MVA virus appeared to be distributed throughout the MP (Figure 5.4D&E). PLGA/PLA with 3:1 ratio and PLA/PLGA 3:1 ratio MPs similar to the MPs formed but with DCM described earlier (Figure 3.3A5), were compared. MVA seemed to be localised in the outer layer PLA layer of the PLGA/PLA 3:1 MPs (Figure 5.4F) whereas in the PLA/PLGA 3:1 MPs MVA localised more frequently in the inner layer containing PLA (Figure 5.4G). Pooled together, when viewed at a MP population level, MVA loading differed between MPs as shown by the difference of fluorescence from individual MPs.

5.5 Discussion

Having demonstrated in Chapter 4 a qPCR-based method to quantify infectious units of encapsulated MVA virus, we then proceeded to estimate the degree of encapsulation within MP formulations. To achieve this we established a loading formula reflecting the encapsulated MVA in pfu based on available formula from the literature used for protein encapsulation (Table 5.1).

It has been shown that technical variables during the microencapsulation procedure have a significant effect on the resulting encapsulation efficiency[295]. The success of microencapsulation is multifactorial and parameters such as increasing polymer concentration in the oil phase[296], the ratios between the $W_1/O/W_2$[295] phases volumes, mixing and stirring rates[297] to name a few, do affect the encapsulation efficiency for each batch. Using our formula we did some early optimisation for triacetin-based PLGA MPs by altering parameters such as the W_1 volume containing MVA, homogenisation speed and polymer concentration with disappointing encapsulation efficiency (EE%) as shown in Table 5.2.

Nevertheless, introduction of 5% EtOH into the W_2 phase containing 1% PVA almost doubled the EE%. A possible explanation for this is that because triacetin is soluble in EtOH[298], at the moment of contact with the W_2 containing EtOH, triacetin moves out from the polymer causing fast solidification of the MPs entrapping more MVA with an increased rate during the process of polymer precipitation. EtOH has been used as a co-solvent in combination with DCM to dissolve PLGA for MP preparation[299], but using it as a way to remove triacetin and cause fast solidification of the MPs is a novel observation. We found that when MPs exposed to EtOH in the W_2 phase were viewed under SEM, they had a smoothened surface with fewer pores/indentations in comparison to without EtOH exposure (Figure 5.1E&D). A smoother MP surface with less porosity could prove beneficial in delaying even more the release of MVA

from the MPs, as well as providing perhaps an immunological benefit to the encapsulated MVA by having a smooth rather than rough surface. It is a fact that when acting as drug delivery vehicles besides size and polymer chemistry, surface morphology and roughness can significantly affect the drug-release behaviour in vitro and in vivo since release of the encapsulated material depends on the wrinkle features and shell thickness of the MPs[300].

After reviewing our manufacturing protocols we realised that we did not take in account the solubility of triacetin in water which is 6%[298]. The PLGA polymer was dissolved in 1ml of triacetin (Oil phase) and the W_2 volume was kept constant at 15ml (Table 5.2). For this 1ml of triacetin to be fully removed and have complete solidification of the MPs, we needed to have at least 16.66ml of aqueous W_2 volume. With a W_2 volume of 15ml, this meant that triacetin was not fully removed from the precipitated MPs, which could explain the irregular MP shapes seen in Figure 5.1E. It was therefore evident that the triacetin-based MP protocol had to be updated, that is why we included a larger aqueous W_2 volume (50ml of 1% PVA W_2) to provide enough water and ensure complete removal of triacetin from the MP population (Figure 5.2A).

Empirical visual observation of the produced MPs, using a more concentrated 5% PVA solution as the stabiliser followed by transfer into a diluted 1% PVA solution, which was later confirmed by having higher EE% (Figure 5.2A&B), was also added into the triacetin-based MP protocol. When different polymers and their combinations were used for generation of MPs, we observed batch-to-batch variability although MVA EE% seemed to be higher in PLA formulations when compared to others (Figure 5.2C). This preference of MVA for PLA, could be explained due to the fact that PLA is more hydrophobic than PLGA, thus MVA preferentially gets more hydrophobic interactions.

Further work with increasing amounts of EtOH (20-40%) in the W_2 phase with the help of SEM, showed that there was a correlation between MP surface texture and EtOH concentration,

leading to rougher MP surface with increasing amounts of EtOH in the W_2 (Figure 5.3A-D). However, increasing numbers of pores and wrinkles were not desirable features for our MP technology. Short EtOH exposure (20%) for 2 minutes to already solidified MPs, reproduced the smooth surface (Figure 5.3E). This meant that we could just expose the MPs after they have solidified and still induce smoothened MPs surfaces, rather than having EtOH present overnight in the W_2 phase.

Before we went on to compare the effect of EtOH on the EE% for each formulation, we simulated the effect of EtOH exposure on MVA infectivity using unencapsulated MVA. It was clear that 24 hour incubation overnight with increasing amounts of EtOH led to the deactivation of MVA, whereas exposure to 20% EtOH for 10 minutes did not affect virus infectivity (Figure 5.4A). This experiment indicated that we could not proceed to determine the EE% using qPCR for the formulations where EtOH was present in the W_2 (Figure 5.4B-D). Since overnight exposure to EtOH deactivated MVA, this suggested that some of the MVA virus encapsulated in those formulations with EtOH would be non-infectious. Therefore, the qPCR measurement would not be able to distinguish vDNA from infectious and non-infectious MVA as explained in the previous chapter. In contrast, EE% was possible to be estimated with qPCR for the formulation having brief exposure to EtOH to smoothen the outer MP surface following overnight stirring (Figure 5.3E), since according to the simulation study MVA was not deactivated after 10 minutes exposure to 20% EtOH (Figure 5.4A). These results are consistent with work by Rabenau et al[301], where both vaccinia and MVA virus after being exposed to 40-60% EtOH for 1 minute, were significantly deactivated but with 30% EtOH this was not the case.

Intraparticle distribution of encapsulated MVA was also an important area to investigate as the relative location of MVA inside each MP could have a significant effect on the immune

response. Ideally, the encapsulated MVA booster dose had to be 'hidden' from immune system detection until it was required, in order to provide a faster and more robust immune response to the encoded Ag that has been primed with adenovirus. Early presentation of MVA to the immune system by being located near/on the surface of the MP would reduce the overall boosting efficacy of the MP technology by leading to an unwanted booster immune exposure during the priming stage with adenovirus. To validate this, an engineered MVA virus fused with a GFP reporter molecule on its D8 structural protein was encapsulated into different MP formulations for visualisation purposes (Figure 5.4C-G). These images gave important insight to the behaviour of MVA once within the MPs. Firstly it was apparent that there was no equal loading between MPs. Another interesting conclusion is the visual evidence that MVA-D8-GFP had a preference to be integrated with PLA polymer. As seen in Figure 5.4D, MVA was focussed in pockets within the PLGA matrix, but was spread throughout when in PLA matrix (Figure 5.4E). This was also in agreement with the higher EE% seen in the PLA MPs vs PLGA shown earlier (Figure 5.2C). When double layered MPs using different mixture ratios between PLGA and PLA were manufactured, MVA is seen predominantly present in the outer PLA layer (Figure 5.4F) and within the inner PLA layer (Figure 5.4G), indicating the hydrophobicity preference of MVA.

To summarise, MP batches were examined for their content using qPCR and encapsulation efficiencies were determined and optimised. We found out that exposure of MPs to EtOH produced a smooth surface appearance. Lastly, with the use of a directly fluorescent MVA virus we observed the intra-particle distribution of MVA once encapsulated.

Chapter 6
In vivo & in vitro studies with MP technology

6 Chapter 6: In vivo & in vitro studies with MP technology

Statement of authorship

All microparticles (MP) were manufactured by CK. All in vivo murine experiments including animal procedures, sample collection, immunological assays, flowcytometry, plaque assays and all in vitro work, were done by CK. In vivo imaging as well as image analysis was done by Dr. Ahmed Salman. Malaria challenge experiment with sporozoites generation, infection via i.v. route, blood film readings and ICS pre-challenge along with their analyses, were done by Dr. Ahmed Salman. Electrospraying procedure was done by DPhil candidate Tayo Sanders II.

6.1 Introduction

In 2016, Tzeng et al [217] designed PLGA MPs encapsulating inactivated polio virus (IPV) and claimed a pulsatile release in vivo based on the detected humoral response from the MPs. In 2017, true pulsatile release was achieved in vivo with advanced 3-dimensional microfabrication technique for MPs by McHugh *et al*[302] from MIT. Cubic PLGA microdevices with a hollow centre were filled with a pico-liter dispensing apparatus and then sealed, encapsulating a model fluorescent drug. When tested with in vivo imaging for real time kinetics, they had excellent reproducibility with on-demand pulse release kinetics.

6.2 In vivo immunogenicity studies

For our first in vivo experiment, we wanted to study the immune response arising from the encapsulated MVA and follow the humoral immune kinetics in isolation rather than in combination with an adenovirus prime regime. Figure 6.1 illustrates this concept.

To investigate the antibody immune response, mice were immunised first with 2μg recombinant GFP protein co-formulated with commercial 2% (w/v) alhydrogel adjuvant (aluminium hydroxide) to achieve seropositivity. Mouse handling and immunisation was

according to Methods 2.4.1. After 2 weeks 7 groups of Balb/c mice (n=5) were immunised i.m. with different MVA-loaded MP formulations according to the schedule described in Table 6.1. Serum samples were taken every 2 weeks and assessed by ELISA (Figure 6.2A). All groups that received MP formulations had heightened detectable anti-GFP Abs peaking after 6 weeks post administration, when compared to mice receiving no MVA (Figure 6.2B). Mice receiving no MVA in either soluble or encapsulated form displayed the least amounts of anti-GFP Abs.

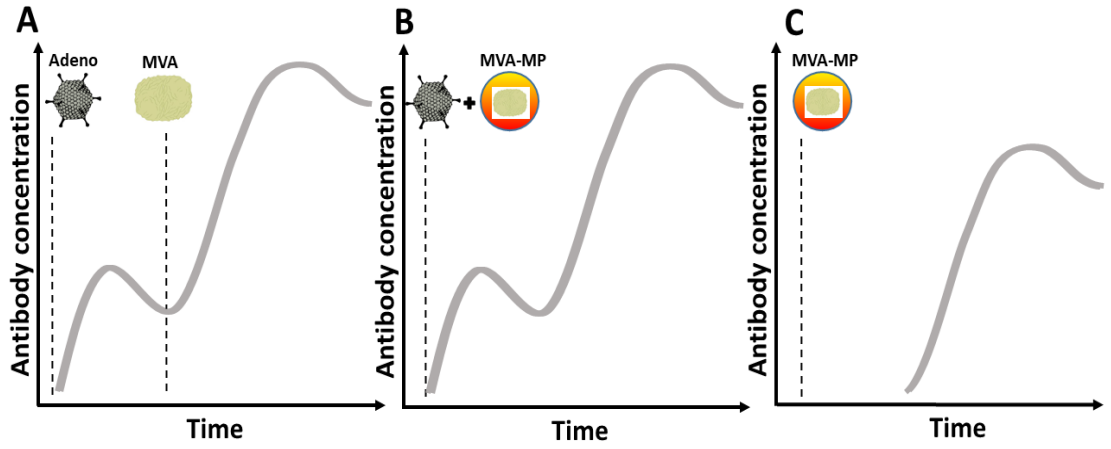


Figure 6.1 Scheme to dissect the humoral immune response generated from MVA-loaded MP technology
Overview showing antibody immune response kinetics in 3 different scenarios following the standard prime-boost vaccination regime of Adenovirus and MVA and proposed strategies with MP technology.
A) Adenovirus used as a prime followed by an MVA boost a few weeks later.
B) Proposed theoretical behaviour of antibody kinetics when adenovirus is co-vaccinated with encapsulated MVA in MPs. In this scenario, changes in humoral response at different timepoints would be blurred and thus hard to attribute any changes to a specific virus.
C) Proposed strategy using only the MVA-loaded MPs by themselves. This would provide information on MVA release from the MP by translation into antibody kinetics.

Group (n=5)	Day 0	Day 14
1	2µg GFP protein + 2% Alhydrogel (Alum)	No MVATIPeGFP
2	2µg GFP protein + 2% Alhydrogel (Alum)	$2x10^4$ pfu MVATIPeGFP unencapsulated
3	2µg GFP protein + 2% Alhydrogel (Alum)	$2x10^6$ pfu MVATIPeGFP unencapsulated
4	2µg GFP protein + 2% Alhydrogel (Alum)	PLGA with encapsulated $2x10^6$ MVATIPeGFP
5	2µg GFP protein + 2% Alhydrogel (Alum)	PLA with encapsulated $2x10^6$ MVATIPeGFP
6	2µg GFP protein + 2% Alhydrogel (Alum)	PLGA/PLA (3:1) with encapsulated $2x10^6$ MVATIPeGFP
7	2µg GFP protein + 2% Alhydrogel (Alum)	PLA/PLGA (3:1) with encapsulated $2x10^6$ MVATIPeGFP

Table 6.1 Vaccination regime for MVA-loaded MPs only without Adenovirus prime

In addition to measuring the humoral response, we also assessed T-cell responses in the spleen to test the effect of the MVA microparticulate technology on the T-cell responses. To verify this, spleen IFN-γ ELISPOT responses to the Pb9 peptide were measured at week 14. Mice immunised with no MVA (control), PLGA-MVA, PLA/PLGA-MVA showed no detectable IFN-γ responses, whereas mice immunised with $2x10^4$ pfu MVA, $2x10^6$ pfu MVA, PLA-MVA and PLGA/PLA (3:1)-MVA had detectable IFN-γ responses (Figure 6.2C). Interestingly from the MVA-encapsulated MP groups only the PLA-MVA group had significantly higher T-cell responses than the soluble $2x10^6$ pfu MVA control (Figure 6.2C).

Furthermore, we characterised the T-cell immune response by measuring cytokine production of CD4+ and CD8+ T-cells in response to the Pb15 & Pb9 epitopes present in the TIP insert of the MVA viral vector. Splenocytes from the terminal timepoint at week 14, were stimulated for 6 hours with Pb9 & Pb15 peptides as described in Methods section 2.4.8 and then stained

for surface and intracellular markers. Gating strategy is shown in Figure 6.3 and background responses from unstimulated splenocytes were subtracted from stimulated responses before statistical analysis.

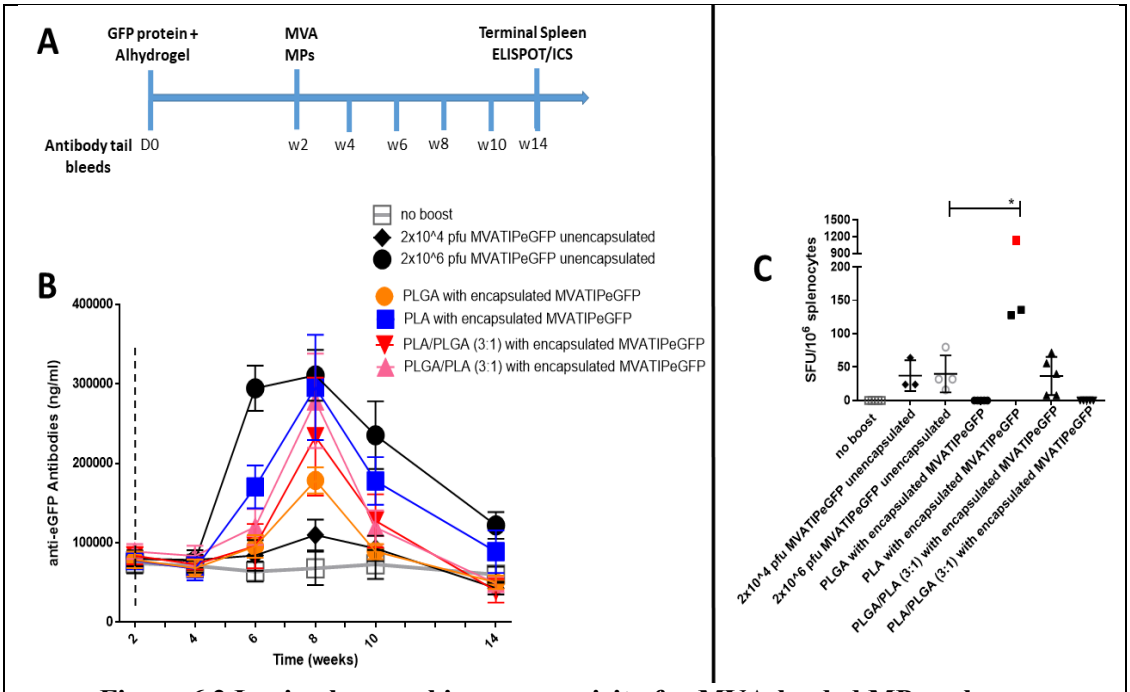


Figure 6.2 In vivo humoral immunogenicity for MVA-loaded MPs only without Adenovirus prime

Balb/c mice (n=5) were immunised i.m. with recombinant GFP protein mixed with alhydrogel and after 2 weeks administrated MVA in encapsulated or soluble forms. Total IgG titres were measured in the serum in response to GFP by ELISA.

A) Illustrated timeline of procedures with tail bleeds on a 2-week interval and take down at week 14 with terminal spleen ICS and ELISPOT.
B) Antibody time course of IgG titres in mice for each group. Vertical dotted line represents immunisation with encapsulated or unencapsulated MVA.
C) At week 14, T-cell responses were assayed by ex vivo IFN-γ ELISPOT in mouse splenocytes at 12 weeks after the administration of MP groups and soluble MVA controls. Cells were stimulated with Pb9 peptide. Each dot represents an individual mouse and error bars represent the standard deviation. Some groups by week 14 had fewer than 5 mice due to animals developing spontaneous cancers and had to be culled. Red square denotes an outlier.

Statistical significance (*p<0.05; **p<0.01; ***p<0.001; ****p<0.0001) by one-way ANOVA with Bonferroni's multiple comparison post-hoc test.

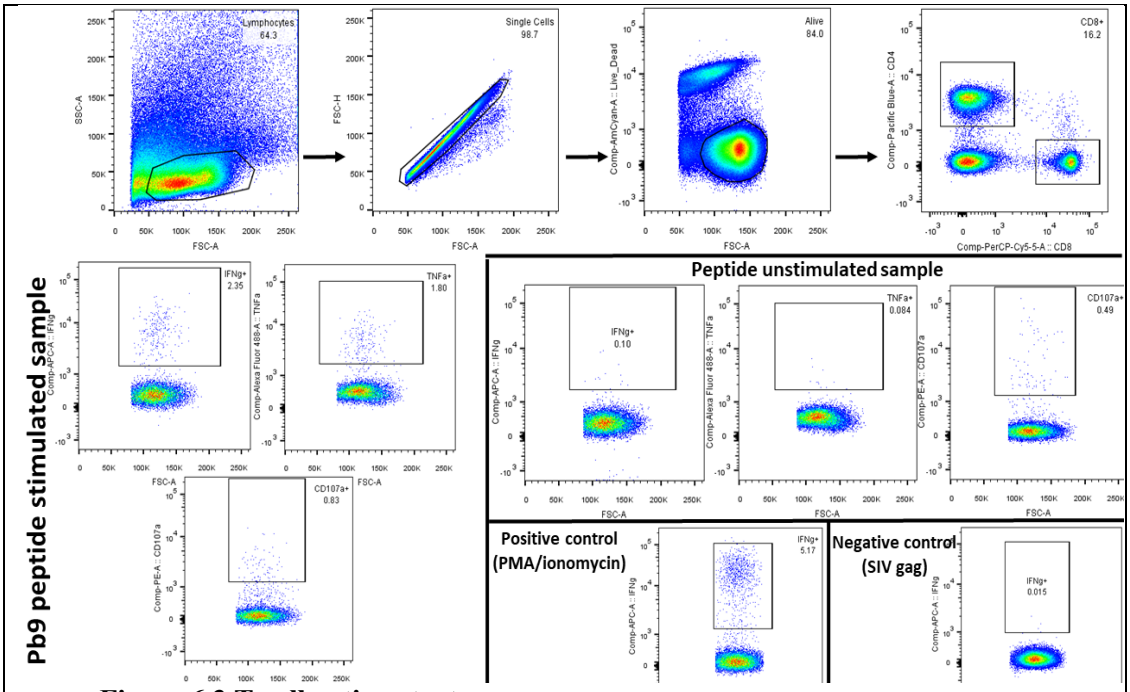


Figure 6.3 T-cell gating strategy

ICS gating strategy used throughout project to further dissect T-cell immune responses. Lymphocytes were gated based on side scatter and forward scatter, followed by specific gates focussing only on singlet population.

A live/dead stain Aqua, was used to gate only on alive cells that did not take up the viability dye. T-cells were identified as CD4+ or CD8+ and each population was further characterised to determine the frequency of IFN-γ+, TNF-α+ and CD107α+ (degranulation marker) for CD8+ population, and IFN-γ+, TNF-α+ for CD4+ population.

A representative sample is shown (PLA-MVA immunised mouse, 12 weeks after administration). The top 3 and far left panels illustrate responses in a Pb9 peptide stimulated well. The far right panels are the peptide unstimulated control for the same sample. A positive control stimulated with PMA (20ng/ml) and ionomycin (1μg/ml) and a negative control with irrelevant peptide from SIV-gag were also used to validate the ICS assay (bottom right panels).

In response to stimulation with Pb9 and Pb15 peptides, no significant changes were observed in the percentage of CD4+ T-cell producing IFN-γ or CD4+ T-cell producing TNF-α (Figure 6.4A&B). Analysis of the CD8+ T-cell population, revealed no significant differences in the percentage of CD8+ IFN-γ and CD8+TNF-α between MVA-loaded PLA MP groups and soluble $2x10^6$ MVA (Figure 6.5A&B). The only MP group that was consistently above 1%

frequency was the PLA-MVA loaded MP for CD8+IFN-γ and CD8+TNF-α. However for CD8+CD107α+ T cells (Figure 6.5C), a significantly superior percentage of CD8+ T cells were found to produce CD107α with the $2x10^6$ soluble MVA, when compared to all other groups including all MP formulations.

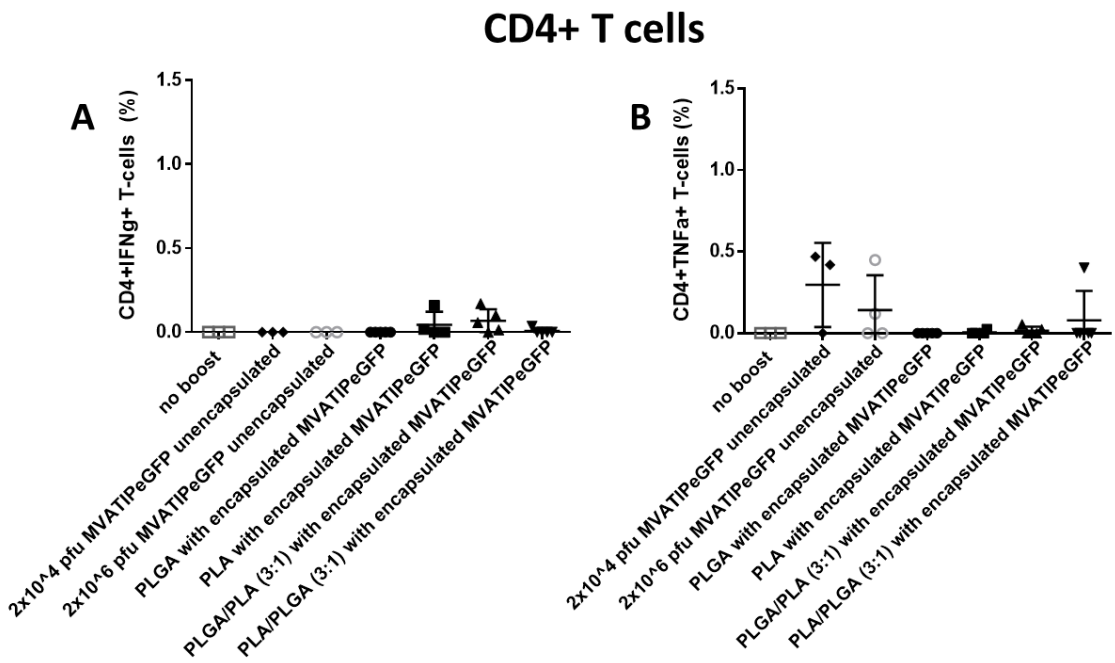


Figure 6.4 Characterisation of CD4+ T-cell responses induced following administration of MVA-loaded MPs in mice

T-cell responses were assayed by flowcytometry from splenocytes at week 12 post administration of MVA-loaded MPs. Cells were stimulated with Pb9 & Pb15 peptides for 6 hours before surface and intracellular straining as described in Materials and Methods 2.4.8. Lymphocyte populations were dissected as demonstrated in Figure 6.3 and cytokine producing cells were analysed. Statistical analysis was performed using one-way ANOVA with Bonferroni's multiple comparison post-hoc test (*$p<0.05$; **$p<0.01$; ***$p<0.001$; ****$p<0.0001$) with no significant changes in either A or B. Data shown are the mean plus standard deviation.

A) Percentage of CD4+ cells expressing IFN-γ is shown.
B) Percentage of CD4+ cells expressing TNF-α is shown.

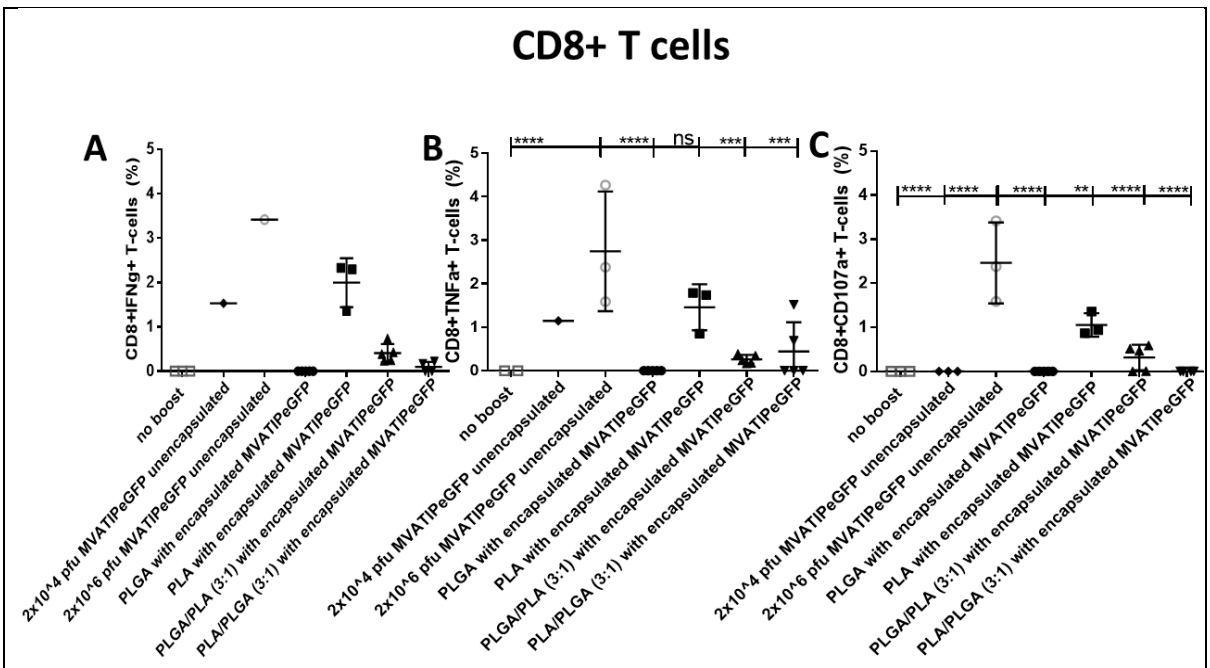


Figure 6.5 Characterisation of CD8+ T-cell responses induced following administration of MVA-loaded MPs in mice

T-cell responses were assayed by flowcytometry from splenocytes at week 12 post administration of MVA-loaded MPs. Cells were stimulated with Pb9 & Pb 15 peptides for 6 hours before surface and intracellular straining as described in Materials and Methods 2.4.8. Lymphocyte populations were dissected as demonstrated in Figure 6.3 and cytokine producing cells were analysed. Statistical analysis was performed using one-way ANOVA with Bonferroni's multiple comparison post-hoc test (*$p<0.05$; **$p<0.01$; ***$p<0.001$; ****$p<0.0001$). Data shown are the mean plus standard deviation.

A) Percentage of CD8+ cells expressing IFN-γ is shown. For groups with $2x10^4$ & $2x10^6$ pfu unencapsulated MVA, some samples did not stain well. Statistics could not be done due to n=1-2 in some groups.
B) Percentage of CD8+ cells expressing TNF-α is shown.
C) Percentage of CD8+ cells expressing CD107α is shown.

6.3 In vivo MP biodistribution and real time release kinetics using in vivo imaging

Another interesting question we wanted to answer was to investigate in more detail the biodistribution of the MPs once injected intramuscularly. For this purpose, we employed an in vivo optical imaging system (IVIS).

Before manufacturing MVA luciferase loaded MPs we sought to verify the lowest luciferase detection signal of the IVIS imaging system. Previous research on the kinetics of luciferase engineered vaccinia virus, showed that luciferase signal peaked 24 hours post i.m. inoculation before vanishing by 72 hours[303]. In vivo imaging procedure is detailed in Methods 2.4.15. To evaluate the fate of the MVA derived luciferase signal and determine the limit of detection, 5 groups of female Balb/c mice (n=5) were inoculated i.m. with decreasing amounts of soluble MVA luciferase according to the schedule described in Table 6.2.

Group (n=5)	**Regime per mouse**
1	10^1 pfu MVA luciferase
2	10^2 pfu MVA luciferase
3	10^3 pfu MVA luciferase
4	10^4 pfu MVA luciferase
5	10^6 pfu MVA luciferase

Table 6.2 Vaccination regime for determination of LOD of luciferase signal for IVIS 200 imaging system

Mice were vaccinated i.m. with the corresponding amounts of MVA luciferase and after 24 hours, they were sedated with isofluorane and imaged on an IVIS 200 imaging system. Uniform luciferase signal was present at the muscle injection site for each group which was directly proportional to the amount of MVA luciferase (Figure 6.6). We found that the IVIS system was able to detect down to 10^2 pfu dose per mouse.

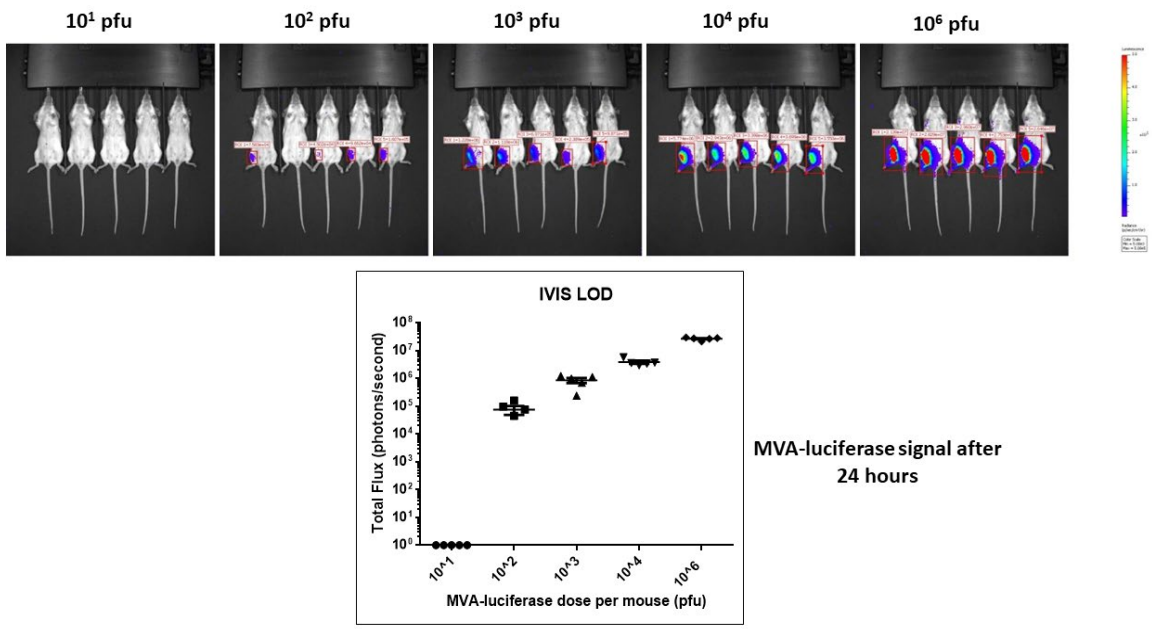


Figure 6.6 Limit of detection (LOD) for luciferase signal for in vivo imaging system
In vivo imaging was performed using the IVIS 200 imaging system to quantify MVA luciferase signal 24 hours post i.m. inoculation. Mice were immunised according to Table 6.2. Luciferase whole body images are shown and results are presented as the total flux of photos measured per second. Light intensity scale bar is depicted on the right. Individual data points are shown as median with standard deviation.

With the next biodistribution experiment with MVA luciferase loaded MPs the aim was two-fold: 1) observe the retention and/or migration of MPs from i.m. injection and 2) monitor in real time active MVA release kinetics from MPs. In order to answer these questions 3 groups of female Balb/c mice (n=5) were ear-nothced for identification to ensure consistend documentation of signal progression from the same mouse. Mice were administered the formulations described in Table 6.3, sedated and imaged on Days 1, 3, 6, 10, 25, 31 and 36 (Figure 6.7A). As expected, for soluble MVA luciferase in PBS, luciferase signal peaked at Day 1, followed by reduced intensity at Day 3 and a completely faded signal by Day 6 (Figure 6.7B). MVA luciferase loaded PLGA MPs had a relatively strong signal on Day 1 (Figure 6.8). Signal was dramatically reduced at Day 3 (72 hours) and was no longer detectable at Day 6

similar to Figure 6.7B. Disappointingly, all imaging time points past Day 6 were devoid of any luciferase signal for the PLGA group (Figure 6.8).

Group (n=5)	**Regime per mouse**
1	10^6 pfu MVA luciferase in PBS
2	10^6 pfu MVA luciferase in PLGA 50:50 7-17 kDa (100mg/ml)
3	10^6 pfu MVA luciferase in PLA 18-28 kDa (100mg/ml)

Table 6.3 Vaccination regime for biodistribution of MVA-loaded MPs

At the earliest timepoint, mice immunised with MVA luciferase-loaded PLA MPs also showed a relatively strong signal like in the previous 2 groups, however at Day 3 no signal was detected (Figure 6.9). Even more intriguing, at Day 25 and Day 31 a luciferase signal was observed although markedly reduced in intensity when compared to Day 1 (Figure 6.9). This signal was primarily located in the abdominal area of the mice.

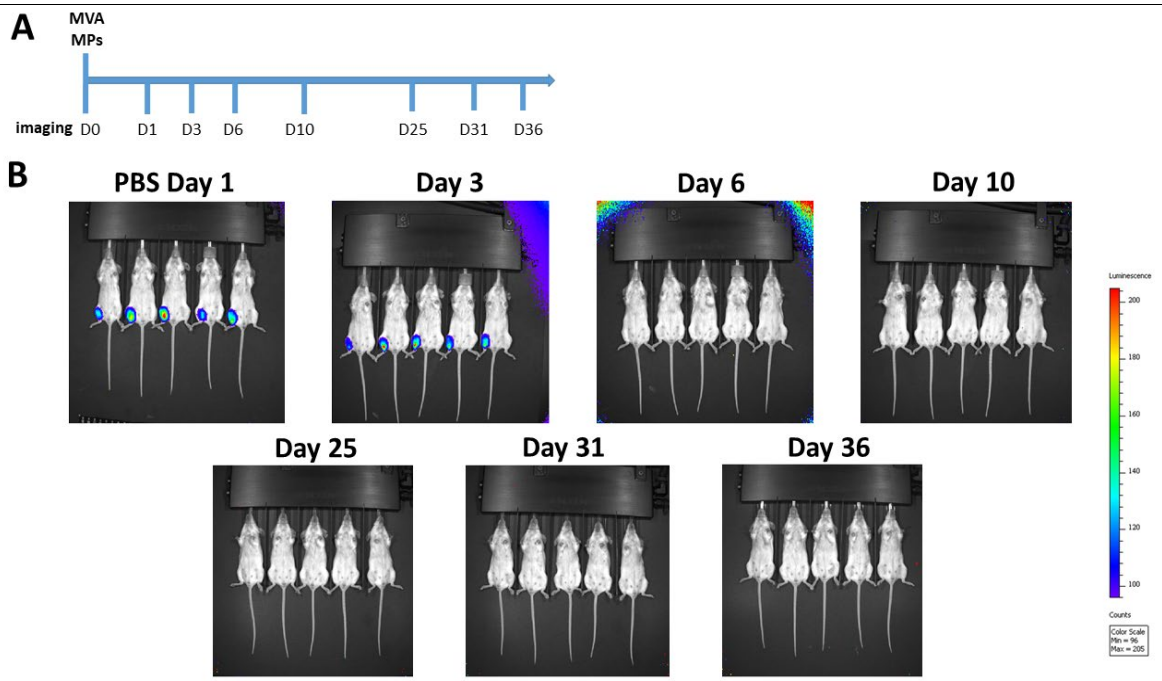


Figure 6.7 In vivo imaging following intramuscular administration of MVA luciferase-loaded MPs (Part I - PBS)

A) Experimental timeline of in vivo imaging.

B) Mice were injected i.m. with 10^6 pfu MVA luciferase in PBS and followed for 36 days in a whole-animal imaging study with luciferase signal being quantified. Light intensity scale bar is depicted on the right.

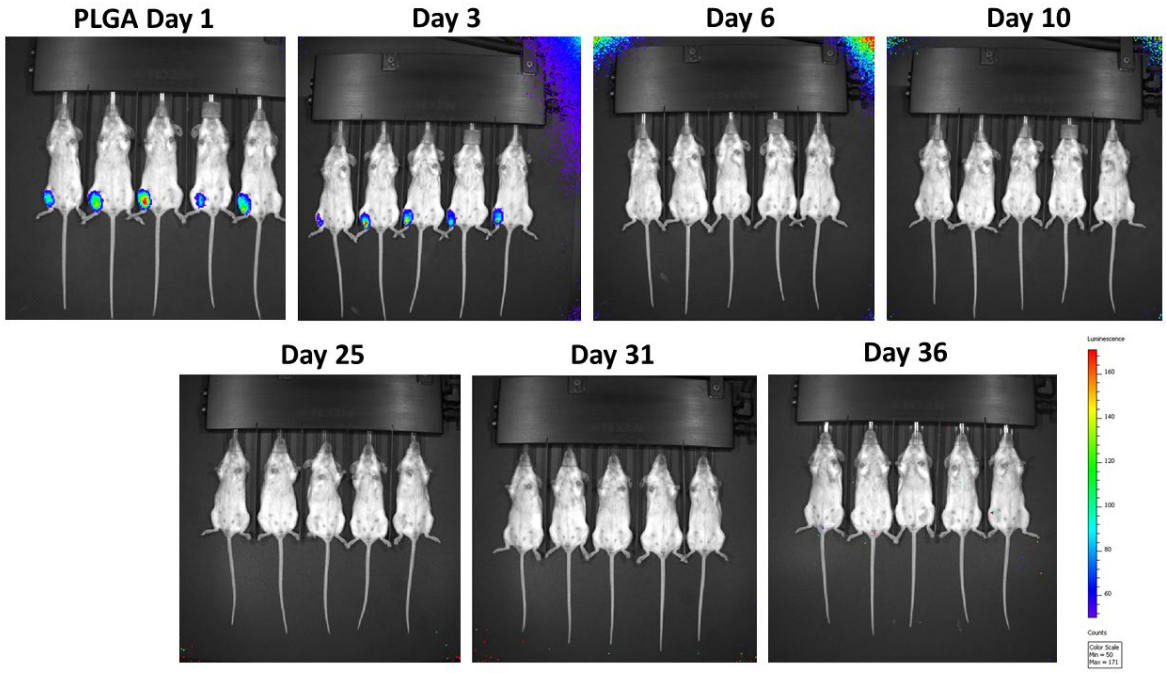


Figure 6.8 In vivo imaging following intramuscular administration of MVA luciferase-loaded MPs (Part II - PLGA)

Mice were injected i.m. with 10^6 pfu encapsulated MVA luciferase in PLGA MPs and followed for 36 days in a whole-animal imaging study with luciferase signal being quantified. Light intensity scale bar is depicted on the right.

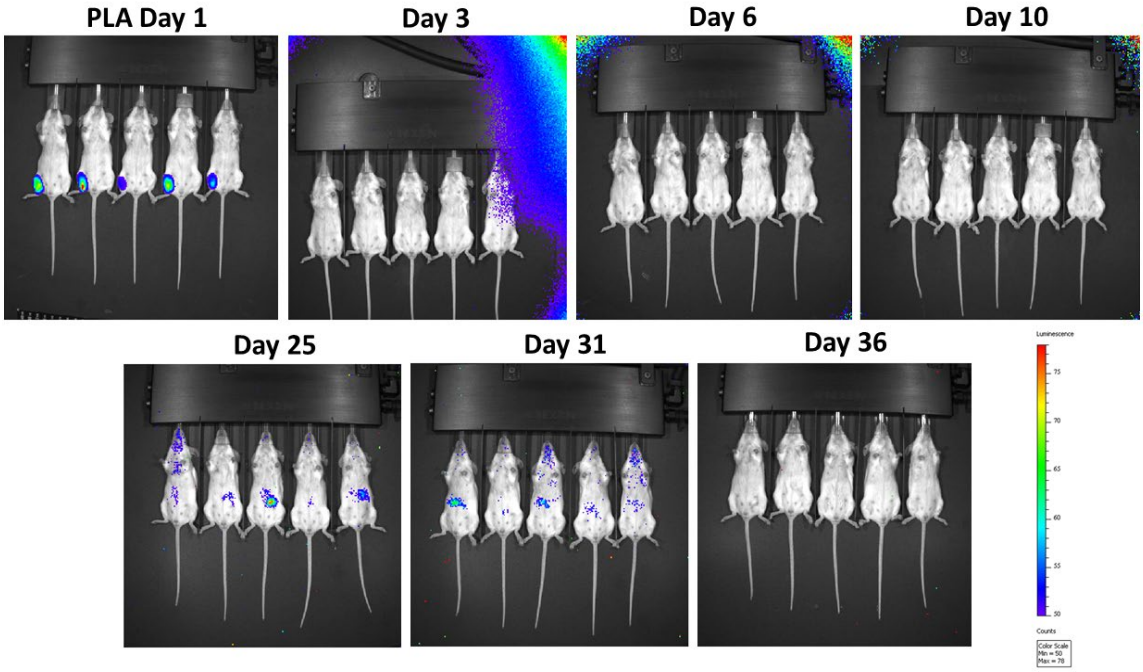


Figure 6.9 In vivo imaging following intramuscular administration of MVA luciferase-loaded MPs (Part III - PLA)
Mice were injected i.m. with 10^6 pfu encapsulated MVA luciferase in PLA MPs and followed for 36 days in a whole-animal imaging study with luciferase signal being quantified. Light intensity scale bar is depicted on the right.

Despite the low signal, the PLA group seemed a potential formulation exhibiting pulsatile release kinetics during the course of 5 weeks (Figure 6.10A). Documented luciferase signals from all groups were analysed, quantified and plotted as a function of time elapsed from the MP injection. This is summarised in Figure 6.10B.

We repeated the same experiment with the addition of a PLA-MVA luciferase formulation exposed to EtOH. An extra PLA-MVA luciferase group was also included to clarify the organ distribution of the MPs after migration from the injection site. At the timepoint where a delayed luciferase signal was expected to emerge, mice would be sacrificed and dissected and have their major internal organs (spleen, liver, kidneys, lungs) isolated and imaged separately.

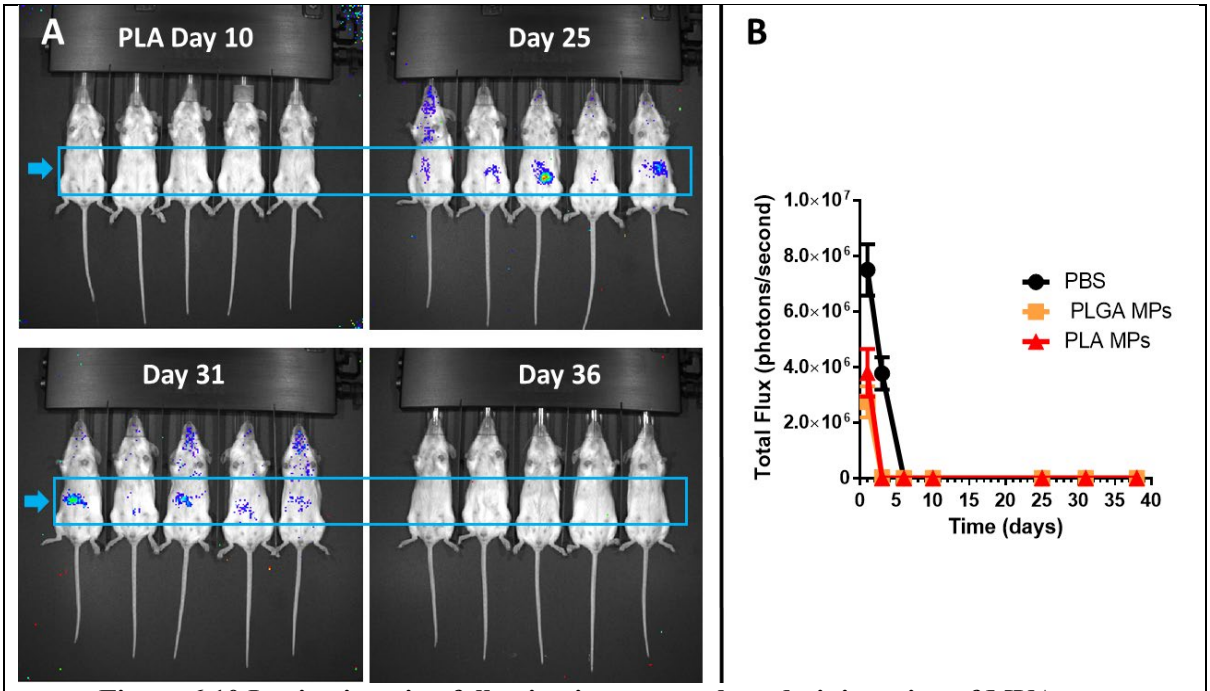


Figure 6.10 In vivo imaging following intramuscular administration of MVA luciferase-loaded MPs (Part IV - Summary)
A) Enlarged images of Day 10 and onwards from Figure 6.9. Blue rectangle highlights the 'off-on-off' progression of the detected luciferase signal.
B) Summary plot of quantified luciferase activity presented as total photon flux per second. Data shown are the mean plus standard deviation.

Group (n=5)	Regime per mouse
1	10^6 pfu MVA luciferase in PBS
2	10^6 pfu MVA luciferase in PLGA 50:50 7-17 kDa (100mg/ml)
3	10^6 pfu MVA luciferase in PLA 18-28 kDa (100mg/ml)
4	10^6 pfu MVA luciferase in PLA 18-28 kDa Repeat (100mg/ml)
5	10^6 pfu MVA luciferase in PLA-EtOH 18-28 kDa (100mg/ml)

Table 6.4 Vaccination regime for repeat in vivo biodistribution of MVA-loaded MPs

Mice were vaccinated with corresponding formulations shown in Table 6.4 and imaged more frequently on Days 1, 3, 5, 14, 24, 28, 31, 35, 38 and 45 (Figure 6.11A) in order to generate a more complete release kinetics curve.

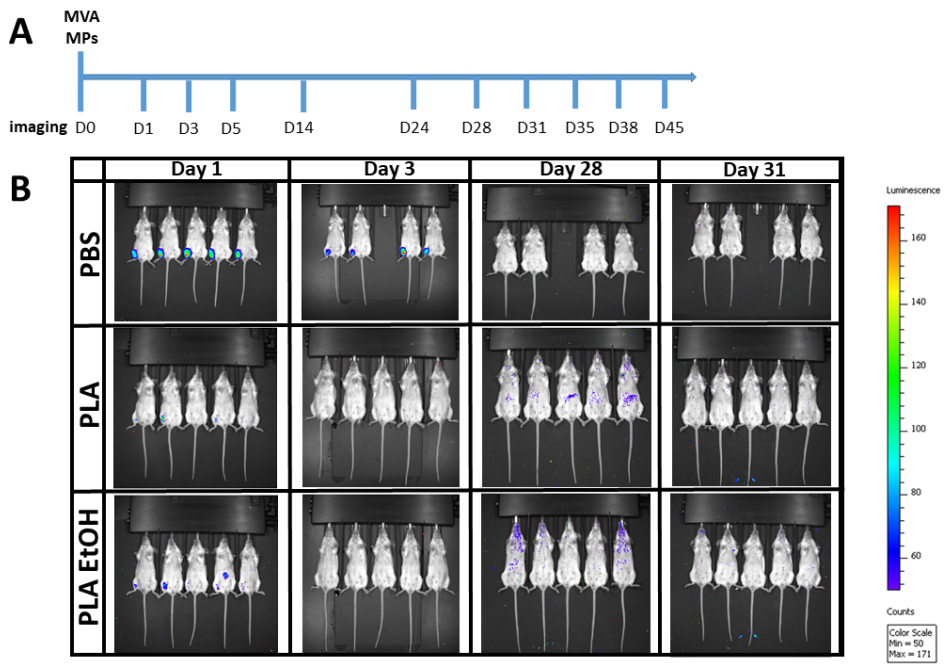


Figure 6.11 Repeat in vivo imaging following intramuscular administration of MVA luciferase-loaded MPs
Mice were injected i.m. with 10^6 pfu soluble in PBS or encapsulated MVA luciferase in PLGA, PLA (2x repeats), and PLA exposed to EtOH formulations. They were followed more frequently over 45 days in a whole-animal imaging study with luciferase signal being quantified. Light intensity scale bar is depicted on the right.
A) Experimental timeline of in vivo imaging.
B) Illustrating the off-on-off principle suggesting a pulse release, PLA (one of them), PLA-EtOH and PBS groups are shown only. For PBS group we started with 5 mice in total but on Day 3 one mouse had to be culled due to spontaneous tumour formation.

At Day 1, some luciferase gene expression was observed in both PLA groups. By Day 3 it had faded, but reappeared on Day 28 (Figure 6.11B) and was undetectable after that until the last timepoint. However due to clash with priority booking users mice were not imaged between Days 14-24 as originally planned and by the time they were imaged at Day 31 no signal was observed.

Therefore we were not able to sacrifice the extra PLA mouse group and have post-mortem evaluation of the accumulated luciferase signal to pinpoint the exact organ destination of the MPs after i.m. injection. On the other hand, at the earliest timepoint the PLA-EtOH group had mild luciferase gene expression at the injection site and also elsewhere in the abdominal area in some mice (Figure 6.11). By Day 3 there was the expected damping of gene expression until Day 28 when signal was detected, which faded by Day 31 and was lastly undetectable by Day 45. Captured luciferase signals from all groups were analysed, quantified and plotted as a function of time elapsed from the MP injection and were striking similar to Figure 6.10B (data not shown for repeat experiment).

This specific PLA formulation with or without exposure to EtOH, demonstrated a release at around 4 weeks (Figure 6.10A & Figure 6.11B).

6.4 Proof-of-concept immunogenicity study: single injection vs routine double injection

Taken into account the presented information so far, the proof-of-concept was initiated having the groups shown in Table 6.5.

Group (n=6)	Day 0	Week 4
1	10^8 i.u. AdenoHu5TIPeGFP	-
2	10^8 i.u. AdenoHu5TIPeGFP + empty PLA MPs	-
3	10^8 i.u. AdenoHu5TIPeGFP + 10^6 pfu encapsulated MVATIPeGFP in PLA MPs	-
4	10^8 i.u. AdenoHu5TIPeGFP + 10^6 pfu encapsulated MVATIPeGFP in PLA-EtOH MPs	-
5	10^8 i.u. AdenoHu5TIPeGFP	10^6 pfu encapsulated MVATIPeGFP
6	10^8 i.u. AdenoHu5TIPeGFP mixed with 10^6 pfu MVATIPeGFP	-

Table 6.5 Vaccination regime for proof-of-concept immunogenicity experiment

To test the feasibility of the MVA-MP technology as a replacement methodology for normal prime-boost regimes, 6 groups of female Balb/c mice (n=6) were vaccinated and followed up over the course of 8 weeks. MPs size was between 4-70μm (data not shown). An overview of the experimental timeline is shown on Figure 6.12A. On odd weeks IFN-γ responses to Pb9 peptide using PBMCs were measured by ex vivo IFN-γ ELISPOT (Methods 2.4.3 & 2.4.5). T-cell responses induced by the MVA-loaded MP formulations are illustrated in Figure 6.12B. Ag specific IFN-γ T-cell responses showed steady increase until week 3 after the Adenovirus priming, however in groups without an MVA boost in either soluble or encapsulated form T-cell responses fell by the end of week 7. Group receiving Adenovirus mixed with MVA had a peak IFN-γ T-cell response at week 5 before also decreasing. There was a noticeable boosting effect in mice receiving MVA-loaded MPs, but by week 7 the standard prime-boost approach with soluble MVA boost proved superior to the MP formulations.

On even weeks serum IgG titres were assayed in response to GFP by ELISA (Figure 6.12C) with minimum blood sampling to adhere to animal welfare regulations. A peak Ab response was observed at 6 weeks in the PLA/EtOH group but for groups receiving the normal week 4 soluble MVA booster shot and the PLA MPs, a peak was seen at the end of the experiment (Figure 6.12C). Groups receiving no MVA boost in either soluble or encapsulated form along with the mixture of Adenovirus with MVA, the Ab levels were maintained by week 8.

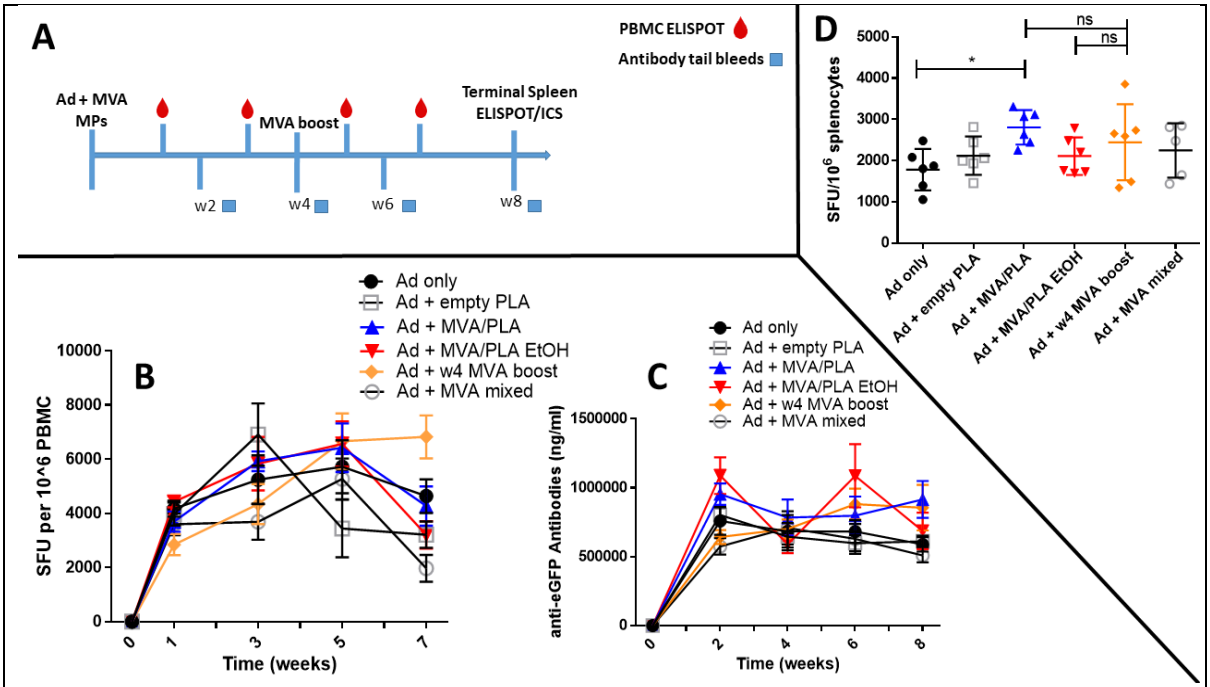


Figure 6.12 Proof-of-concept immunogenicity experiment replacing the prime-boost regime with MVA-loaded MPs

A) Experimental timeline showing the procedures at each timepoint.
Mice were immunised as previously described in Table 6.5.

B) T-cells responses in blood were assayed by ex vivo IFN-γ ELISPOT in PBMCs on weeks 1, 3, 5 and 7 post immunisation. Cells were stimulated with Pb9 peptide and the mean T-cell responses to Pb9 for all groups are shown as a time course.

C) Total serum IgG titres against GFP were measured by ELISA on weeks 2, 4, 6 and 8. A time course is shown of mean Ab titres for all groups at each time point.

D) T-cells responses were assayed post-mortem in spleen samples by ex vivo IFN-γ ELISPOT on week 8. Cells were stimulated with Pb9 peptide and mean group responses are shown.

Statistical analysis was performed using one-way ANOVA with Bonferroni's multiple comparison post-hoc test (*p<0.05; **p<0.01; ***p<0.001; ****p<0.0001). Data shown are the mean plus standard deviation.

At week 8 post-mortem spleens were harvested. Responses to Pb9 peptides were measured in splenocytes by ex-vivo IFN-γ ELISPOT (Figure 6.12D). Animals receiving soluble or encapsulated MVA in MPs displayed higher T-cells responses to Pb9, than mice immunised with no MVA or mixed with Adenovirus. The difference in T-cell responses between group receiving MVA-loaded PLA MPs achieved statistical significance when compared to Adenovirus only group. Most importantly, there was no significant difference between MVA-loaded in PLA or PLA-EtOH MPs when compared to week 4 soluble MVA boost.

We also looked at the cytokine production profile of CD4+ and CD8+ T-cells generated from the vaccination schedule. Splenocytes from week 8, were stimulated for 6 hours with Pb9 & Pb15 peptides as described in Methods section 2.4.8, stained for surface and intracellular markers and then analysed with a flowcytometer.

After stimulation, no significant changes were observed between experimental groups in terms of percentage of CD4+ producing IFN-γ or TNF-α T-cells (Figure 6.13A&B). On the other hand within the CD8+ T-cell population, there were no significant changes between frequencies of CD8+ IFN-γ+ T-cells apart from the group having Adenovirus only and the group that got boosted at 4 weeks with soluble MVA (Figure 6.14A). Significantly higher proportion of CD8+ T-cells was found to produce TNF-α in the group with 4 week MVA boost and PLA-MVA group when compared to Adenovirus only group (Figure 6.14B).

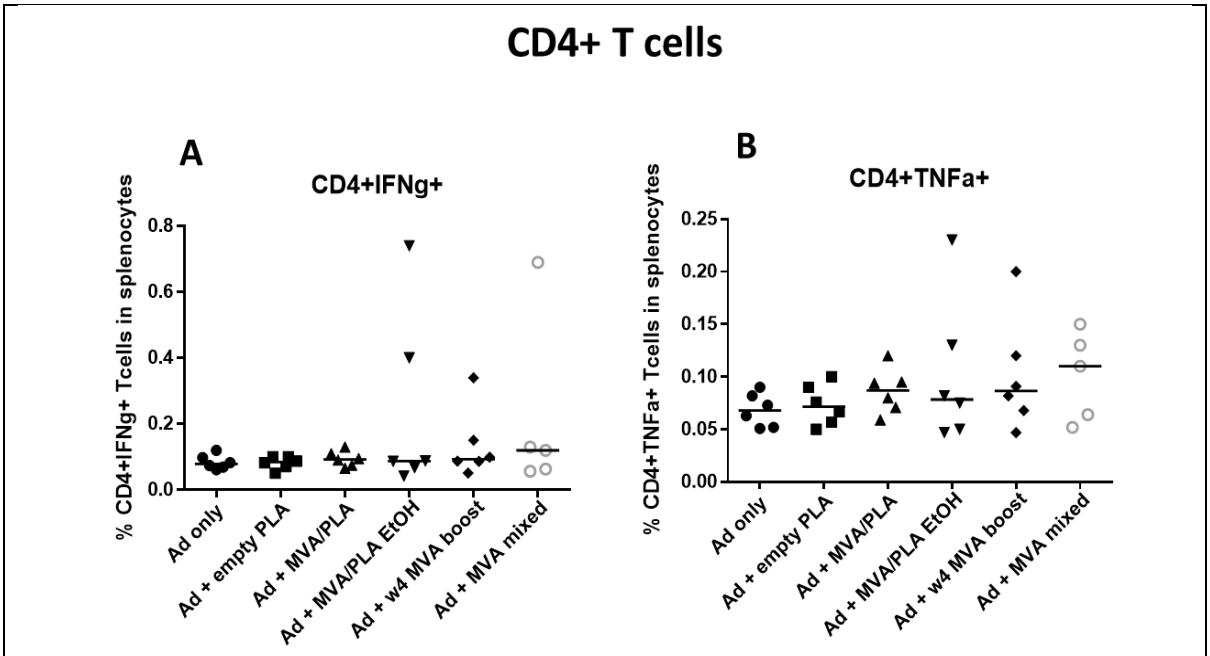


Figure 6.13 Characterisation of CD4+ T-cell responses induced following administration of MVA-loaded MPs in mice for proof-of-concept experiment
T-cell responses were assayed by flowcytometry from splenocytes 8 weeks post vaccination. Cells were stimulated with Pb9 & Pb15 peptides for 6 hours before surface and intracellular straining as described in Materials and Methods 2.4.8. Lymphocyte populations were gated as demonstrated in Figure 6.3 and cytokine producing cells were analysed. Statistical analysis was performed using one-way ANOVA with Bonferroni's multiple comparison post-hoc test (*p<0.05; **p<0.01; ***p<0.001; ****p<0.0001) with no significant changes in either A or B.
Data shown are the mean plus standard deviation.
A) Percentage of CD4+ cells expressing IFN-γ.
B) Percentage of CD4+ cells expressing TNF-α.

Similar trends were also found in the CD8+CD107α+ with groups receiving MVA in MPs and normal prime boost exhibiting higher percentages of T-cells than all other groups, however they did not reach statistical significance (Figure 6.14C).

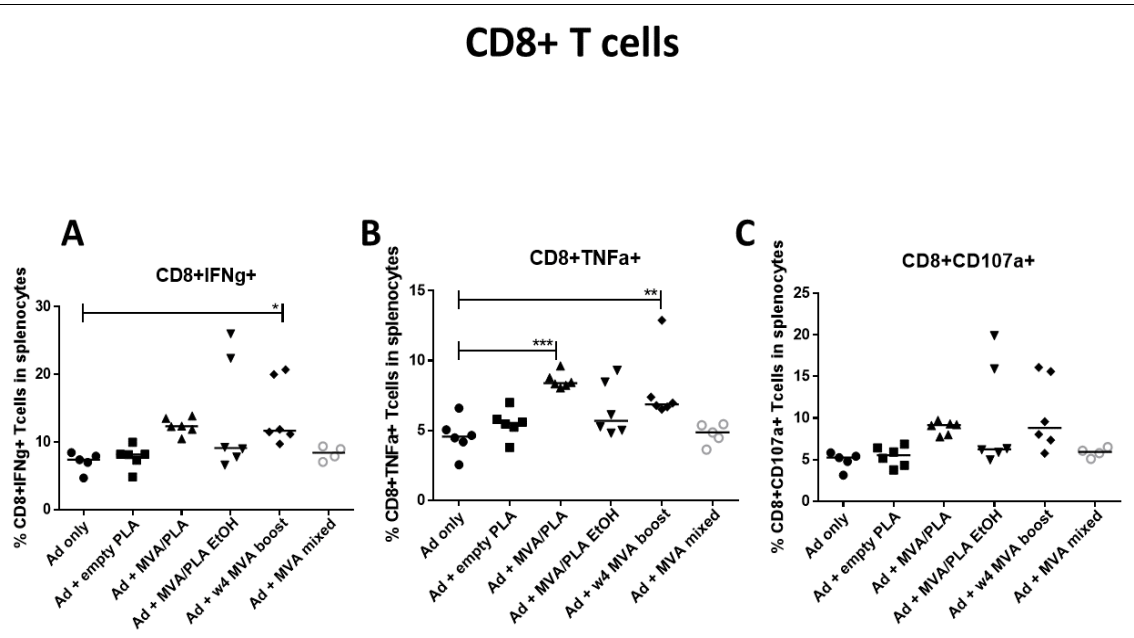


Figure 6.14 Characterisation of CD8+ T-cell responses induced following administration of MVA-loaded MPs in mice for proof-of-concept experiment
T-cell responses were assayed by flowcytometry from splenocytes at 8 weeks post vaccination. Cells were stimulated with Pb9 & Pb15 peptide for 6 hours before surface and intracellular straining. Lymphocyte populations were gated as demonstrated in Figure 6.3 and CD8+ T-cells were analysed. Statistical analysis was performed using one-way ANOVA with Bonferroni's multiple comparison post-hoc test (*p<0.05; **p<0.01; ***p<0.001; ****p<0.0001).
Data shown are the mean plus standard deviation.
A) Percentage of CD8+ cells expressing IFN-γ.
B) Percentage of CD8+ cells expressing TNF-α.
C) Percentage of CD8+ cells expressing CD107α.

6.5 In vivo protective efficacy of single injection technology with sporozoite challenge

In parallel with the above experiment, we also assessed the protective efficacy of the PLA-MVA and PLA-EtOH-MVA loaded formulations and compared them to the routine Adenovirus prime followed by MVA boost approach in inbred mice. MVA encoding the *P.Falciparum* (Pf) liver stage antigen 1 (LSA1), which was shown to provide 87.5% sterile protection in a heterologous prime-boost approach in the past[304], was encapsulated in these

MPs. Four groups of inbred Balb/c female mice (n=8) were vaccinated according to the schedule shown in Table 6.6.

Mice were bled on week 5 for ICS to get a snapshot of the immune response before they were challenged intravenously (i.v.) with transgenic sporozoites displaying Pf-LSA1 on their surface (Figure 6.15A) as described in Methods 2.4.18.

Group (n=8)	Day 0	Week 4	Week 5
1 (naïve)	-	-	1000 transgenic sporozoites expressing LSA1 (i.v.)
2	10^8 i.u. AdCh63-LSA1	10^6 pfu MVA-LSA1	1000 transgenic sporozoites expressing LSA1 (i.v.)
3	10^8 i.u. AdCh63-LSA1 + 10^6 pfu MVA-LSA1 in PLA MPs	-	1000 transgenic sporozoites expressing LSA1 (i.v.)
4	10^8 i.u. AdCh63-LSA1 + 10^6 pfu MVA-LSA1 in PLA-EtOH MPs	-	1000 transgenic sporozoites expressing LSA1 (i.v.)

Table 6.6 Vaccination schedule for challenge experiment

PBMCs were isolated from blood samples and stimulated for 6 hours with 5 μg/ml of Pf-LSA1 protein overlapping peptide pool. Pre-challenge cellular immune responses were characterised with flowcytometry and CD4+ and CD8+ T-cells subsets were quantified for expression of IFN-γ, TNF-α, CD107α and IL-2 cytokines. Encouragingly there were no statistically significant changes between MP formulations and the normal prime boost approach in all CD4+ T-cell subset populations (Figure 6.15B) and in all CD8+ T-cell subset populations (Figure 6.16A). Challenge study then followed using transgenic murine sporozoites expressing LSA-1 which were prepared in advance according to Methods 2.4.16. After 5 weeks post immunisation all mice were infected with 1000 sporozoites via the intravenous route and

monitored daily with thin blood film slides for level of parasitaemia (Methods 2.4.17). The Kaplan-Meier survival curve (Figure 6.16B) illustrates the projected time needed to progress to 1% blood parasitaemia.

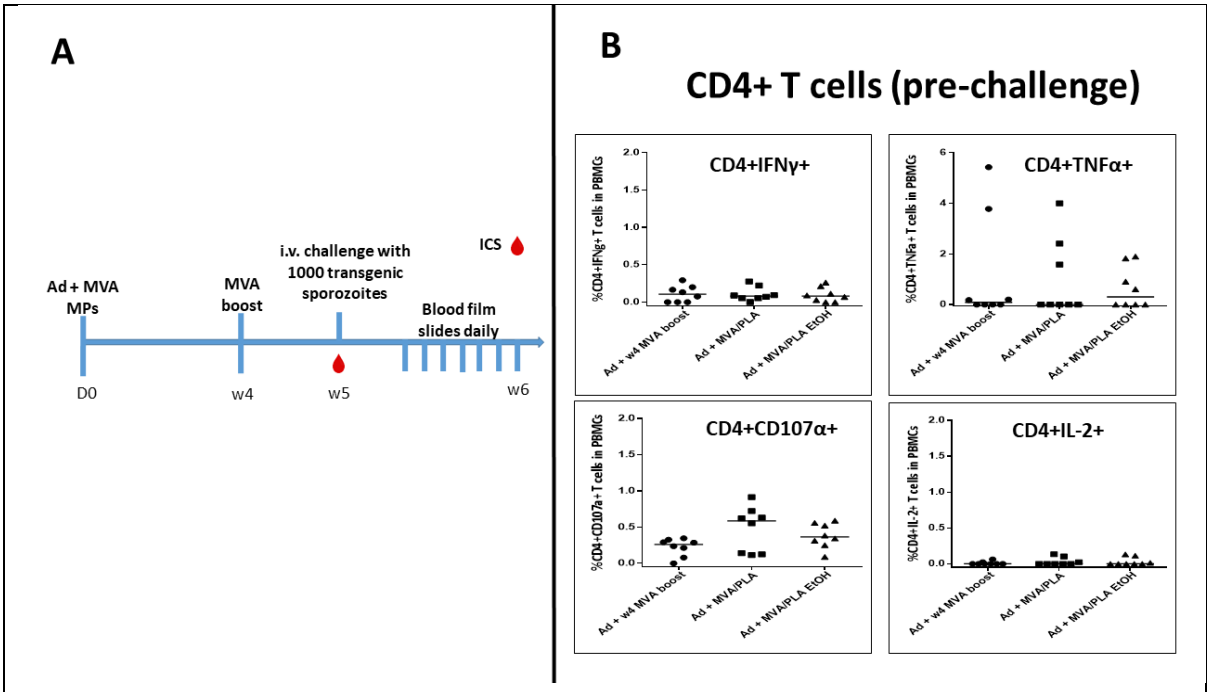


Figure 6.15 Characterisation of CD4+ T-cell responses induced following administration of MVA-loaded MPs, pre-challenge in mice.

A) Experimental timeline for challenge study with ICS staining at week 5 before challenge and then inoculation of transgenic sporozoites i.v. displaying the LSA1 protein on their surface. Mice were monitored daily and blood film slides were done to measure levels of parasiteamia.

B) T-cell responses were assayed by flowcytometry from PBMCs 5 weeks post vaccination according to schedule in Table 6.6. Isolated PBMCs were stimulated with 5µg/ml of Pf-LSA1 protein overlapping peptide pool for 6 hours before surface and intracellular straining. Lymphocyte populations were gated as demonstrated in Figure 6.3 and the immunological markers of IFN-γ, TNF-α, CD107α and IL2 were analysed. Statistical analysis was performed using one-way ANOVA with Bonferroni's multiple comparison post-hoc test (*p<0.05; **p<0.01; ***p<0.001; ****p<0.0001) with no significant changes in frequencies of cytokine producing T cells between different groups and for each T-cell subset.

Data shown are the mean plus standard deviation.

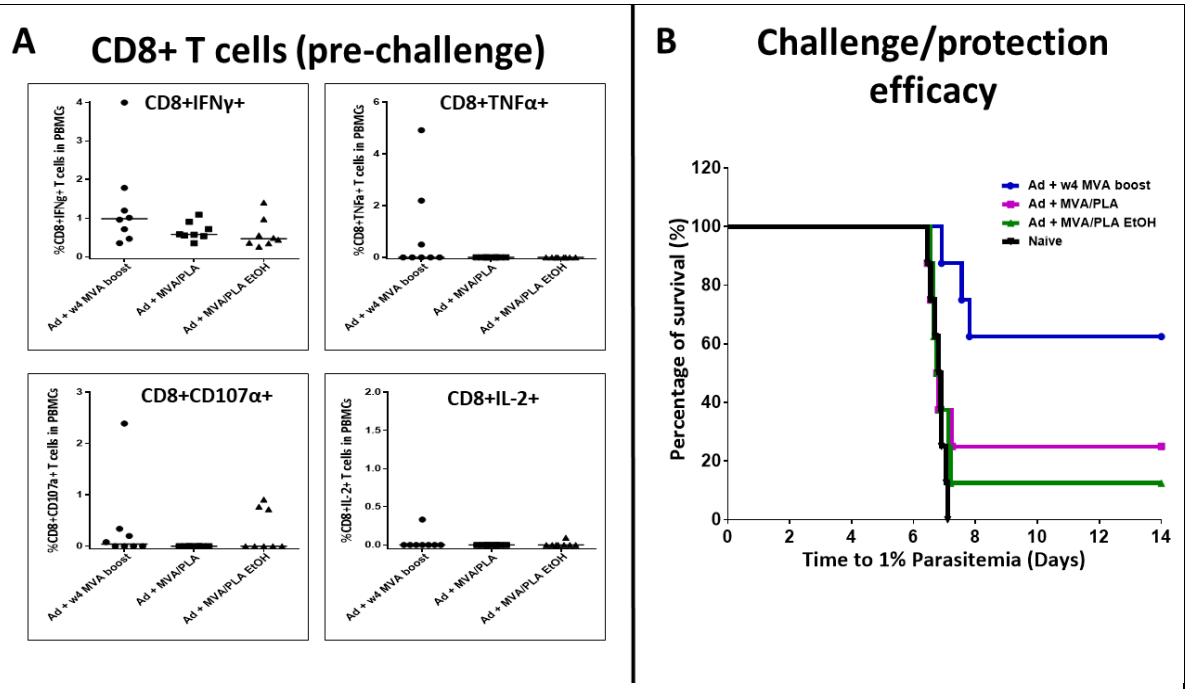


Figure 6.16 Characterisation of CD8+ T-cell responses before challenge and survival curve after challenge.

A) T-cell responses were assayed by flowcytometry from PBMCs 5 weeks post vaccination according to schedule in Table 6.6. Isolated PBMCs were stimulated with 5µg/ml of Pf-LSA1 protein overlapping peptide pool for 6 hours before surface and intracellular straining. CD8+ lymphocyte populations were gated as demonstrated in Figure 6.3 and the immunological markers IFN-γ, TNF-α, CD107α and IL2 were analysed (A). Statistical analysis was performed using one-way ANOVA with Bonferroni's multiple comparison post-hoc test (*$p<0.05$; **$p<0.01$; ***$p<0.001$; ****$p<0.0001$) with no significant changes in frequencies of cytokine producing T cells between different groups and for each T-cell subset. Data shown are the mean plus standard deviation.

B) Balb/c mice (n=8) per groups, were challenged with 1000 transgenic parasites i.v. 5 weeks after immunisation with AdC63-LSA1 followed by MVA-LSA1 or the AdC63-LSA1 with MVA-LSA1 encapsulated in MPs. Naïve mice were used as an internal control to demonstrate that the parasites were viable and able to cause infection. Mice were monitored daily to enable calculation of the time to 1% parasitaemia. Thin blood film slides were taken daily to monitor levels of parasitemia. Mice that were slide-negative at 14 days post-challenge were considered sterily protected. The Kaplan-Meier survival curves illustrate the time to 1% parasitaemia, whilst statistical significance between the vaccinated groups' survival curves compared to the naïve, was assessed with the Mantel-Cox test: i) Ad + w4 MVA boost (p-value =0.0002 (***)); ii) Ad + MVA-PLA (p-value = 0.3347 (ns)); iii) Ad + MVA-PLA-EtOH (p-value = 0.2998 (ns)).

Vaccination using MVA-loaded PLA-EtOH MPs protected 1/8 mice (12.5% protection) whilst vaccination using MVA-loaded PLA MPs protected 2/8 mice (25% protection). Both MP groups did not have a significant delay in the time to 1% parasitaemia compared to naïve controls (p-value=0.3347 MVA-PLA MP and p-value= 0.2998 MVA-PLA-EtOH MP). In comparison, vaccination with normal prime boost approach was able to protect 5/8 mice (62.5% protection) which was a statistically significant level of induced sterile protection compared to naïve controls (p-value= 0.0002).

6.6 In vitro release kinetics of MP batches

We documented so far the kinetics of MVA being released from MPs with immunogenicity studies and in vivo imaging studies monitoring the expressed luciferase signal. We also generated in vitro release kinetics of the same MP formulations encasing MVA and compared them to the obtained in vivo release kinetics.

Three formulations were made encapsulating MVA-TIPGFP: 1) PLGA 50:50 38-54 kDa, PLA 18-28 kDa and PLA 18-28 kDa that has been exposed to 20% EtOH after overnight solidification, all at 100mg/ml polymer concentration. These were the same formulations used in the most recent in vivo studies. To determine the effect of these particular formulations on MVA release rates, in vitro release studies were carried out as described in Methods 2.4.19. Encapsulated content of MVA-loaded MP was determined with qPCR and MPs were matched by content containing 10^6 MVATIPeGFP. MPs were dispersed in 1ml PBS and incubated at 37ºC under constant shaking. At weekly timepoints, MPs were span down, 800µl were removed and then replaced by fresh buffer, without disturbing or removing MPs when sampling. From aliquots sampled, plaque assays were performed and cumulative release profiles were generated for each formulation which are shown in Figure 6.17A. It was disappointing to find that over the course of 5 weeks no viral plaques were detected from either formulation.

While titrating the weekly viral aliquots from the MP supernatants to perform the plaque assays in a separate 96 well plate containing DMEM medium, we noticed that the media pH indicator (phenol red), was changing colour from red to orange indicating a shift from pH 7 to more acidic pH (Figure 6.17B).

Based on literature information about the pH microclimate distribution inside PLGA microparticles[305], we used the pH values of 5.8, 4.5 and 3.9 and tested whether acidic pH had a detrimental effect on MVA bioactivity. A known amount of MVATIPeGFP was added to 1ml of PBS having different acidic pHs or pH 7 at 37°C in duplicates. Over the course of 2 weeks plaque assays were performed using aliquots from these samples. Interestingly even after 24 hours there was a log reduction in viral titre at pH 5.8 when compared to pH 7, while at lower pHs of 4.5 and 3.9 MVA could not infect (Figure 6.17C). Over the course of 2 weeks MVA in pH 7 started decreasing in titre and by the end of 2 weeks at pH 5.8 the virus was rendered non-infectious.

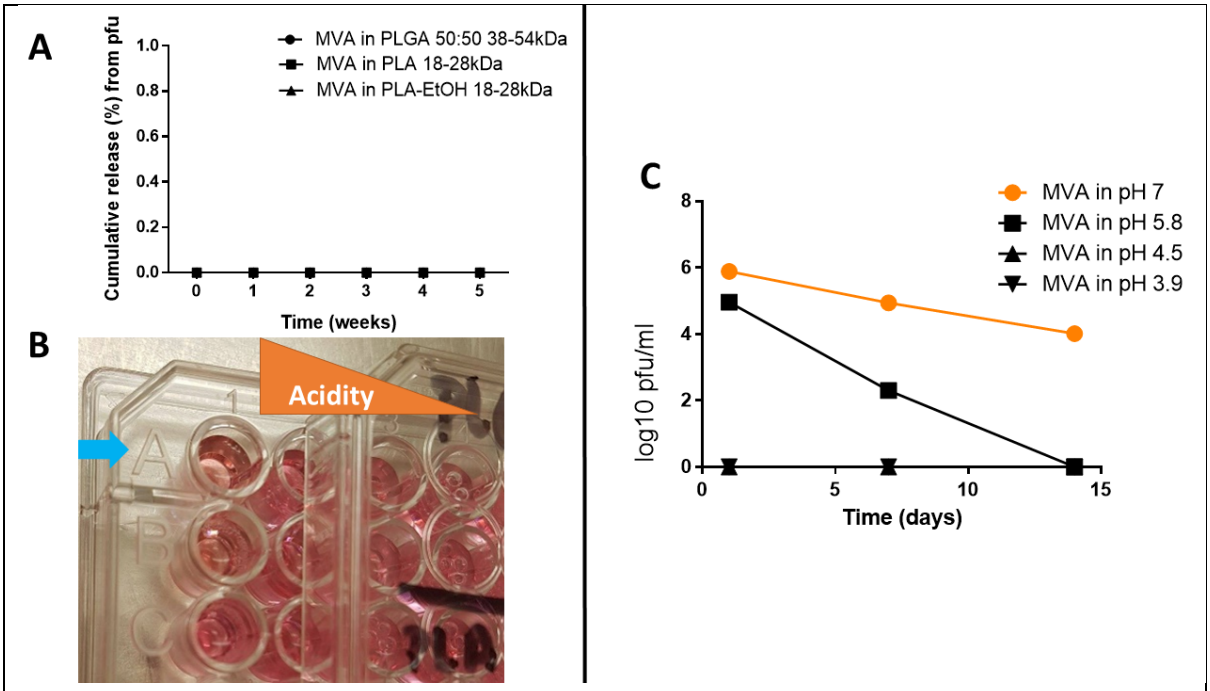


Figure 6.17 Cumulative release profiles of MVATIPeGFP from MPs and bioactivity of MVA in acidic environments

MVA was encapsulated using the same formulations used for the in vivo studies outlined previously. MPs were lysed and quantified for MVA content and dose matched to have 10^6 pfu theoretical starting amount of encapsulated MVA. Experimental groups were in duplicates (n=2).

A) Cumulative release profiles of MVA. MPs were placed in PBS at 37˚C under constant agitation. Weekly aliquots were taken and plaque assay was performed and the cumulative release of pfu is shown.

B) Photograph of 96 well plate used to titrate down viral aliquots from in vitro release studies for plaque assay quantification. Indicated on A1 and B1 are aliquots used to form the 10^{-1} dilution where a change in the cell medium to orange indicated a low pH.

C) 10^6 pfu of MVATIPeGFP were added to 1ml having different pH values (7, 5.8, 4.5 and 3.9) and the bioactivity of the virus was monitored for 2 weeks, in duplicates.

6.7 MVA encapsulation by electrospraying

We also examined a more sophisticated method for particle production, called electrospraying. The underlying principle of electrospraying is liquid atomisation and this generates microparticles under high electric field. Simply put, it consists of a high voltage supplier, a syringe pump containing the dissolved polymer and a grounded collector container (Figure 6.18A). Keeping in line with the methodology presented so far in this thesis, before considering

this method for production of triacetin based polymeric MPs we wanted to confirm that the process of electrospraying with high electric field application did not affect the bioactivity of the MVA virus.

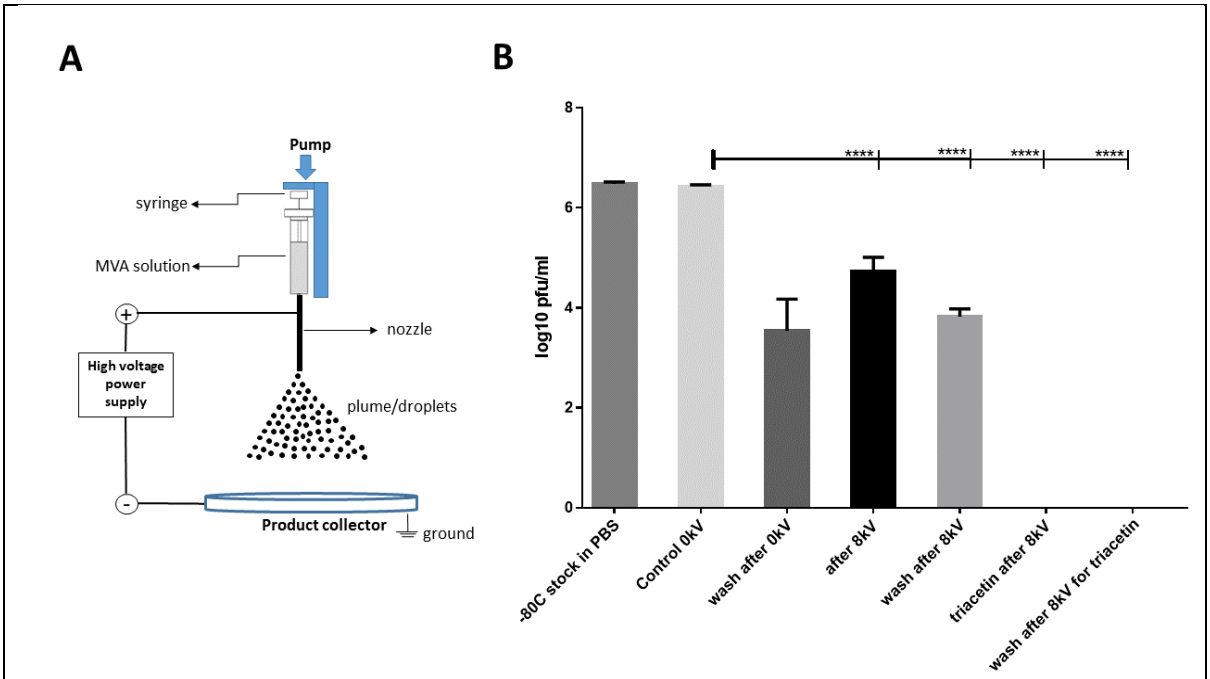


Figure 6.18 Electrospraying method for MVA encapsulation

A) Graphical representation of the experimental electrospraying configuration used for MVA encapsulation studies. Briefly, 10^6 pfu/ml solution MVATIPeGFP was added into a syringe and pumped through a high voltage 8kV-charged metallic nozzle at a constant rate. At the end of the experiment, MVA was collected in a grounded container and was titred using traditional plaque assay.

B) Results from plaque assay comparing effects of applied voltage to MVA's infectivity. -80C stock and internal control with virus exposed to no voltage was compared to virus exposed to 8kV in PBS or in pure triacetin. Washes were collected with an additional PBS run to establish the presence of leftover virus inside the tubing. Tubing was then disinfected with pure ethanol followed by PBS.

To test this, known amounts of unencapsulated MVA virus in PBS were fed into the electrospraying system and collected after application of 8kV, as described in more detail in Methods 2.4.30. A PBS wash followed to collect any remaining virus present in the tubing. Both collections were then quantified for infectivity using plaque assays. Results of the plaque assays are shown in Figure 6.18B. We found a significant reduction in MVA titre after

application of 8kV when compared to no voltage application (0kV). To simulate the encapsulation condition where MVA is contained within the polymeric solution, a known amount of unencapsulated MVA virus in pure triacetin was exposed to 8kV. When tested, MVA lost completely its infectivity (Figure 6.18B).

6.8 Discussion

To examine the ability of encapsulated MVA to induce an immune response, mice pre-immunised with adjuvanted GFP protein were administered MVATIPeGFP encapsulated in different MP formulations (Figure 6.2). MVA virus when given as a single dose is weak in producing high antibody titres[306]. By pre-immunising mice with adjuvanted GFP protein, this would make the murine immune system more sensitive to GFP protein produced by infectious MVA being released from the MPs, enhancing the detection limit of anti-GFP antibodies whilst allowing detection of minute immunological differences between MP formulations. There was a noticeable increase in antibody titres against GFP protein in all groups receiving encapsulated MVA virus. The induction of an increased humoral response provided indication that MVA-loaded MPs were immunogenic (Figure 6.2B). However neither MP formulation led to a delayed humoral immune response (Figure 6.2B). T-cell responses in the spleen 12 weeks post-immunisation showed a significant increase for mice immunised with the PLA formulation when compared to the corresponding PBS unencapsulated control (Figure 6.2C). When Ag-specific T-cell responses in the spleen were characterised there was no significant increase in the frequency of the CD4+ T cell populations (Figure 6.4). For the CD8+ T cell sub-populations, PLA formulation induced higher responses in comparison to all other MP formulations and CD8+TNF-α+ was comparable to the PBS unencapsulated MVA control group (Figure 6.5).

In order to initiate the proof-of-concept immunogenicity experiment, we had to determine first in which week MVA was being released in order to correctly time our unencapsulated booster shot and compare it to our MP formulations. The problem with following the humoral response in order to determine the exact week of MVA release, is that detectable antibody responses take a minimum of 2 weeks to generate once antigen is presented to the immune system[307].

Since there is a time-delay required to generate antibodies from Ab-secreting plasma cells, this meant that in terms of release kinetics the release happened 2 weeks before.

A better approach to determine the exact week of MVA release from MPs was to combine an MVA vector encoding luciferase with in vivo photon imaging to visualise the MVA release kinetics from the MPs. Kinetics of vaccine antigen expression from MVA viral vectors in real time have been examined in the past utilising in vivo imaging[303]. The underlying principle of the photon imaging process is the detection of light-producing catalysis event of luciferin by the expressed luciferase from the viral vector[308]. Luciferin is injected into the animals and the produced light is quantified in real time. In addition, by using an encapsulated MVA luciferase virus we could also follow at the same time the biodistribution of the intramuscularly injected MPs relative to the whole mouse body and clarify whether MPs were migrating to any other body areas/organs after i.m injection.

A trial in vivo imaging experiment to determine the lowest detectable amount of MVA luciferase virus, showed that the in vivo imaging system was able to detect signal arising from as low as 10^2 pfu inoculated virus 24 hours post inoculation (Figure 6.6). Such sensitivity would ensure that any detectable luciferase signal from the MPs was from at least 10^2 pfu (Figure 6.6) and that it was expressed within 72 hours upon release (Figure 6.7B Days 1-3 kinetics).

With this in mind PLGA and PLA formulations were administered intramuscularly and followed for 36 Days, where early strong signal was detected on Day 1 for both formulations (Figure 6.8&Figure 6.9) respectively indicating the presence of MVA on the surface or near the surface of the MPs. No signal was detected past Day 6 for PLGA indicating that this formulation did not exhibit a pulse release kinetic (Figure 6.8). However, in the PLA formulation there was a potential pulse release kinetic with signal showing up predominantly in the intestinal area and some underneath the neck on Days 25 &31, before fading away by

Day 36 (Figure 6.9&Figure 6.10A). Even though the signal was not as intense in magnitude as in Day 1 (Figure 6.10B), it was a promising formulation indicating a potential release of MVA 4 weeks post administration.

A repeat experiment was performed with the addition of two groups: 1) an additional PLA MP group to clarify the organ distribution of the detected signal and 2) smooth surface PLA-EtOH MPs. This time for the PLA group there was less signal detected on Day 1 suggesting lower amounts of MVA luciferase on surface of the MPs, but with a reproducible signal being detected at Day 28 and gone by Day 31 (Figure 6.11B). Based on in-house expertise with in vivo imaging, the predominant signal was most likely arising from the spleen based on its location of the mouse body. The PLA-EtOH group exhibited signals both at the injection site and in the intestinal area from Day 1, a feature that was not shared with the previous PLA group and similarly on Day 28, a pulsatile release kinetic was seen being predominantly in the area underneath the neck and some in the intestinal area.

Our reflection on this experiment is the following: it would have been useful to pinpoint in which organ(s) both PLA and PLA-EtOH formulations end up after intramuscular immunisation with in vivo imaging. The approach of using MVA luciferase virus as the reporter molecule having a 3-day detection window span was not ideal as it was in reality a 'hit or miss' strategy. A better approach would have been to encapsulate a more stable reporter molecule such as quantum dots. Quantum dots (nanoprobes) have superior optical properties and long-term luminescence stability and they have been used extensively in the past for monitoring in real time biodistribution in vivo[309,310], therefore the signal would still be there allowing for a definite answer to this question.

Following intramuscular administration of the MPs with encapsulated MVA luciferase it was interesting to see migration occurring from the muscle injection area to other areas of the animal body. In the case of PLA MPs this was predominantly in the intestinal area with some underneath neck area whereas with PLA-EtOH MPs, signal was predominantly from the neck and less from the intestinal area. This suggests a possible role for rough/porous vs smooth MP surface and their respective destinations. It is highly likely that MPs are phagocytosed by either resident or circulating phagocytic cells and migrate with their help via the lymphatic network to lymphatic areas. Studies have shown that optimal range for phagocytosis is around 2-3μm[311] while bigger MPs (6-10μm) can also be phagocytosed but less efficiently[312]. Despite having a MP size distribution ranging from 4-70μm, it's possible to speculate that once injected into the muscle area MPs over 10μm size get mechanically broken down into smaller phagocytosable parts due to the mechanical stress from within the constantly moving leg muscle. Then these smaller polymeric parts containing MVA, are taken up by phagocytic cells and trafficked to areas of immunological importance such as lymph nodes. This could prove beneficial in enhancing the potency of released MVA virus in boosting the immune response by presenting MVA directly to antigen presenting cells, T-cells and B-cells in the lymph node. This hypothesis is scientifically supported based on findings with direct deposition of biodegradable particles by intra-lymph node injection in mice[313,314].

Through the combined in vivo imaging experiments datasets illustrated above, we gained not only valuable insights about the biodistribution behaviour of the MPs but also when the unencapsulated soluble MVA booster dose needed to be administered in order to be comparable to the MVA-loaded MP formulations. Moving forward, with the proof-of-concept experiment we compared the immunogenicity induced by the single dose of Adenovirus + MVA loaded MPs vs Adenovirus followed by a 4 weeks soluble MVA boost. T-cell response in blood did

show a boosting effect in both groups receiving MPs comparable at their peak on week 5, but by week 7 the standard 2 injections prime-boost regime was superior to the MPs (Figure 6.12B). When the humoral response kinetics were analysed, mice immunised with the PLA-EtOH demonstrated a pulse-release Ab response, while the PLA group showed a relatively stable antibody titre followed by the normal prime boost regime with a steady increase (Figure 6.12C). At week 8 T-cells responses in spleen showed a significant increase in IFN-γ secreting lymphocytes in the group receiving the PLA MP formulation indicating a boosting effect, whilst there was no significant difference between both MP formulations and the normal prime boost approach (Figure 6.12D). This was promising as it meant that MP vaccinated groups after a single injection, had similar T-cell responses to the routine prime boost achieved with 2 independent injections spaced 4 weeks apart.

Mice given adenovirus with blank MPs had no statistical difference compared to mice given adenovirus only (Figure 6.12D), indicating that the presence and size of the MPs did not have an adjuvanting effect on the adenoviral priming stage as initially expected[315]. In addition, the early presence of detectable luciferase gene expression arising from injected MPs at Day 1 (Figure 6.9 & Figure 6.11) suggested the need for a control group to be added to the proof-of-concept experiment (Group 6 in Table 6.5). The adenovirus mixed with soluble MVA would control for MVA's presence on the surface of the MPs and its potential effect on the immune response induced by the priming Adenoviral vector. When tested this group behaved as expected (Figure 6.12D). Previous work at the Jenner has shown that co-administration of adenovirus with MVA induced weaker T-cell responses than given separately[316]. However, we were expecting a higher T-cell response induced by the normal adenovirus prime followed by week 4 MVA boost (Figure 6.12D). This made us to suspect that perhaps repeated freeze thawing of the viral stock tube, that we have been using throughout our last in vitro and in vivo

experiments, might have caused the MVA virus to lose some of its potency. In addition, the difference in the T-cell response induced by the PLA-EtOH group with the smooth surface MPs compared to the more porous PLA group, was thought provoking (Figure 6.12D). This result suggested that perhaps the immune system responds better when the MP surface has indentations/pores rather than being smooth. Surface roughness/morphology in biomaterials and their influence on the cell behaviour has been extensively studied[317]. Although still controversial, microscale roughness (irregularities distanced from 1μm to 100μm) and nanoscale roughness (irregularities distanced from 100nm to 1μm), have been shown to have a positive influence on cell adhesion and maturation[318]. In terms of this project, it is possible that scavenging or resident APCs, when in contact with rough surface MPs, spend more time surveying them due to their rough surface. In turn, the surface of the MP material could prolong contact time of released MVA to APCs thus maximising their interaction and influencing the potency of the encapsulating vaccine. Examination of in vitro phagocytosis with nanoparticles by HeLa cells, showed that surface roughness isn't as important as the overall charge of the nanoparticles with negatively charged nanoparticles are taken up to a higher extent than positively charged ones[319]. Nevertheless, it is an interesting concept on what the immune system detects with its germline-encoded receptors when it encounters the rough and smooth MP formulations and how it chooses to respond. This information could be useful in the future for engineering smarter and better-defined microdevices.

When T-cell responses in the spleen 8 weeks post immunisation were further dissected there was no significant changes within the CD4+ Ag-specific T-cell population (Figure 6.13) for all groups. When the CD8+ T-cell subset populations were analysed for cytokine production, there was significant increase in the frequency of CD8+IFN-γ+ and CD8+TNF-α+ T-cells induced by the standard prime boost approach, compared to Adenovirus only group (Figure 6.14A&B).

CD8+TNF-α+ T-cells were also significantly different in the PLA group when compared to the Adenovirus only group (Figure 6.14B). However, there was a consistent trend of the 2 MP formulations, PLA and PLA-EtOH, to have comparable frequencies of CD8+IFN-γ+, CD8+TNF-α+, CD8+CD107α+ T-cells and be higher than the Adenovirus only group, indicating a boosting effect (Figure 6.14A&B&C). This further supported the notion that the MVA-MP technology could confer similar cellular and humoral immune responses generated by a single immunisation rather than two immunisations.

In order to determine the relative protective efficacy of T-cell response induced by the standard prime boost approach and the single injection containing the MVA-loaded MPs, we carried out a challenge experiment using chimeric *P.berghei* sporozoites expressing the *P.falciparum* LSA1 antigen. Five weeks post-immunisation and after the soluble MVALSA1 boost from week 4, flowcytometry revealed no significant differences between frequencies of CD4+T-cell subsets expressing IFN-γ, TNF-α, CD107α and IL-2 (Figure 6.15B), with similar immunological profiles of CD8+ T-cell population expressing IFN-γ, TNF-α, CD107α and IL-2 (Figure 6.16A). However, the routine prime boost approach was more protective by sterilely protecting 62.5% of Balb/c mice, when compared to the 12.5% and 25% efficacy for PLA-EtOH and PLA MPs respectively (Figure 6.16B). This challenge study was running in parallel with the proof-of concept experiment.

We also attempted to generate an in vitro release profile from the same MP formulations used in the last in vivo immunogenicity and challenge studies. However, we were not able to generate a cumulative release profile because no plaques were detectable (Figure 6.17A). The change in colour of phenol red (pH indicator) from pink to orange when viruses were titrated (Figure 6.17B), suggested that the aliquots from the in vitro release samples had a low pH. Disintegration of PLA and the simultaneous increase in the release of acidic by-products most

likely is responsible[320], causing the deactivation of MVA virus. It is known that biodegradable polymers such as PLGA and PLA which are made from acidic monomers could result in build up of acidic byproducts when they start degrading[321].

Further investigation with exposure of MVA virus to neutral and acidic pHs over time (Figure 6.17C) in order to simulate the acidic microenvironment encountered by MVA virus within the MPs, revealed that MVA is acid labile. This provided an explanation as to why no viral plaques were detected during the in vitro release studies, because the low pH had a detrimental effect on MVA. Stability at neutral pH at 37˚C over time was consistent with previous work at the Jenner institute[322], despite having tested only 2 samples. Behaviour of vaccinia virus at various pH levels has been examined decades ago[323] and it has been shown that vaccinia gets inactivated quickly and completely at pH 1 and 2.05, and between 8-17 hours at pH 3.5 while having good short-term persistence in pH 4 to 8. The result from the cumulative release (Figure 6.17A) also suggested a possibility of a buffering system in vivo which balances the acidity created from the PLA microparticles, thus allowing viable infectious virus to be released, adding more evidence to the 'in vivo veritas'[324] conundrum.

Our reflection to this experiment is the following: incubating the MPs in a suitable pH buffer or the direct inclusion of basic salts like $Mg(OH)_2$ in the MP formulations[325] might have resolved the problem of no viral plaques during the cumulative in vitro release assay. However, the condition for the inclusion of a basic salt in the MP formulation would have been to first confirm that the added salt does not inhibit/interfere with the qPCR reaction required to estimate encapsulated content. Additionally, incorporation of basic salts to counterbalance the acidity produced or a buffering system might sound useful but this would skew the data towards a non-physiological environment and would not be reflective of what happens in vivo.

Despite MVA getting deactivated by the low pH during in vitro release studies, cumulative release could possibly still be generated with qPCR by extracting the vDNA present in the shaking supernatants.

As a side project, we were also interested to produce a more tightly controlled and uniform population of MPs. This decision stemmed from the fact that the double emulsion technique used so far generated MPs having a broad range of sizes and also suffered from batch to batch variability, which ultimately could delay the clinical use of this technology. More sophisticated methods that provided this kind of precision manufacturing involve microfluidics[326] and electrospraying[204]. The single step procedure of electrospraying could overcome these limitations by providing better control on MP preparation with reproducible, monodisperse size and high loading[327]. Electrospraying works with the application of an electric field that highly charges the solution being pumped through. At the end of the metallic needle this solution stretches due to electrostatic forces and becomes aerosolised, which generates a uniform population of droplets (plume)[328]. When using volatile solvents like DCM, these droplets travel towards the grounded collector and while travelling the DCM gets evaporated trigerring the solidification of the droplets. However in our case using triacetin, the produced triacetin-based MPs would have to be stirred overnight in 1% PVA in high volume to remove the triacetin.

Before starting encapsulating MVA virus using the electrospraying method, we tested whether MVA virus could survive the high electric field exposure associated with electrospraying. In PBS buffer there was significant reduction at 8kV (Figure 6.18B). However due to the fact that MVA would be inside a polymeric solution, the most representative sample was MVA virus in pure triacetin, which when exposed to 8kV it rendered MVA virus non-infectious. This simulation study suggested that using electrospraying method would result in complete deactivation of MVA while being pumped in a polymeric solution with triacetin. Whole living

cells have been encapsulated in biomaterials using the technique commonly referred to as bio-electrospraying without losing their viability[329–331]. It seems however, that when similar viruses are exposed to high electric fields like equine herpes virus, which is a lipid enveloped virus as well, they sustain structural core and envelope damages[332].

To summarise, we showed that MVA retains its immunogenicity and can generate an immune response after it has been encapsulated. In vivo imaging studies provided an insight to the biodistribution of MPs after injection as well as a promising MP formulation with a pulsatile release behaviour at 4 weeks. Proof of concept experiment with single dose vaccination showed encouraging findings with comparable immune responses to two independent boluses, but the same formulations were not equally protective when tested in malaria challenge setting. Attempts to generate in vitro release kinetics for the MP formulation were not successful and likewise an attempt to make reproducible MPs with electrospraying showed deactivation of MVA virus.

Chapter 7:
Concluding Remarks

7 Chapter 7: Thesis summary, future prospects & conclusion

This project began with the specific aim of developing a technology that would allow the transformation of the current adenoviral prime and MVA boost regime, from a 2-injection regime into a single injection by encapsulating the MVA booster dose. This was theoretically feasible with the use of microparticulate drug delivery systems already existing for other applications.

7.1 Microparticulate delivery system for MVA virus

7.1.1 In vitro studies

Single injection vaccinations are of paramount importance in global health to satisfy the growing need to improve compliance amongst vaccinees and push forward worldwide eradication campaigns to reach their goals.

Encapsulation of model protein BSA-FITC initially showed that different microparticulate formulations could be produced exhibiting different structural properties and forms. MVA virus when encapsulated using standard protein encapsulation protocols was deactivated and a tailored encapsulation protocol had to be devised to retain its bioactivity. Harsh solvents like DCM and high-energy processes like sonication, were excluded from the encapsulation protocol and replaced with triacetin solvent and plain homogenisation.

Not much work has been done manufacturing triacetin-based microparticulate formulations and additional effort was required to further optimise their protocol for a more homogenous population with better appearance and overall forms.

The biggest hurdle in this project was the establishment of a quantification method of MVA infectious dose as previous published work was unsatisfactory and in some cases anecdotal in nature, apart from respectable work from Guillermo Garcia del Barrio *et al*[251]. In this study

encapsulated adenovirus was quantified using a southern DNA blot technique which measured total adenoviral particles based on genetic material but not infectious adenovirus.

Early attempts in this project were employed to extract infectious encapsulated MVA from the polymeric MPs based on differences on Mw, density, surface charges, or chemical and enzymatic separation. We showed that it was impossible to retrieve infectious virus for quantification with an infectivity-based assay. Following this, we employed qPCR to measure viral genetic material, which a widely acceptable virological quantification method. We simulated the encapsulation conditions of MVA virus and established that the microencapsulation strategy did not result in any MVA loss due to deactivation. Thus, genetic material quantified with qPCR would correspond only to infectious virus, rather than measuring genetic material from infectious and non-infectious virus that might have been deactivated by the microencapsulation procedure.

For the qPCR method, an efficient prime/probe set was created satisfying specific internationally set performance criteria, which allowed for the sensitive detection of MVA amounts as low as 10^2 pfu/ml. In addition, with the help of internal quality controls we established that the there was no DNA loss during the extraction process using commercial DNA extraction kit columns. Additionaly, the dissolved polymer did not affect in any way the qPCR reaction and reproducible standard curves could be made on different days ensuring cross-validity between MP batches. Lastly, an appropriate standard curve was established by titrating known viral amounts and then extracting viral DNA from each dilution.

7.1.2 In vivo studies using encapsulated MVA

Using the established qPCR method, MP batches were examined for their content and encapsulation efficiencies were determined. Based on this, MP formulations were optimised and encapsulation efficiency was increased from less than 10% to more than 40% for PLGA

based formulations, with even higher encapsulation efficiencies for PLA formulations. Exposure of MPs to ethanol was shown to produce less porous MPs with smooth surface throughout. Insights about the intra-particle distribution of MVA once encapsulated in different formulations, was possible with the use of a directly fluorescent MVA virus having GFP molecules on its surface.

Early in vivo immunogenicity results with antibodies as the readout indicated a successful MVA encapsulation, with MVA retaining its immunogenicity and able to generate a response. A PLA based formulation was the only one able to induce heightened T-cell responses in the spleen 14 weeks post administration.

In vivo imaging studies with a detection sensitivity of 10^2 pfu using encapsulated MVA luciferase in MPs, showed a pulsatile release behaviour at 4 weeks post administration with the PLA formulation in the intestinal area. Albeit less intense luciferase signal, this formulation was repeated with reproducible behaviour in vivo, however the exact organ location where MPs accumulated was not deciphered. Furthermore, PLA-EtOH MPs with a smooth surface also exhibited a pulsatile release behaviour at 4 weeks but mostly concentrated in areas of the neck rather than intestinal areas in comparison to the non EtOH-exposed PLA formulation. These experiments not only demonstrated the fate of the MPs once injected intramuscularly but also provided real time kinetics indicating the time when the unencapsulated booster shot had to be delivered in order to be compared to the encapsulated MVA booster version.

When the adenoviral-MVA routine prime boost regime was compared to the single injection technology using MPs simulating a 4 week boost interval, by the end of week 8 both mouse groups had comparable generated immune responses in terms of Ag-specific induced T-cells and Ag-specific antibodies produced. Apart from the exception of PLA-EtOH group that showed a pulse release kinetics in terms of antibodies, based on the T-cell kinetics and antibody

kinetics, MP formulations did not exhibit a true pulsatile release. Despite that, both groups receiving the single dose MP approach were not significantly different from the normal prime-boost regime, which was an encouraging finding. However, the immune response from the normal prime boost was lower than expected. Even though the same MVA virus stock was used for this experiment, we have some concerns that the MVA virus used might have lost some of its potency due to several repeated freeze-thawing cycles.

In a challenge study with transgenic sporozoites, mice immunised with the standard prime boost approach showed higher protection rates than the single injection approach. However, challenge occurred at 5 weeks post immunisation rather than 8 weeks which was the duration of the proof-of-concept immunogenicity experiment.

When MPs were evaluated for their in vitro release kinetic, it was shown that the low pH produced by the PLA biodegradation deactivated the released MVA thus cumulative release could not be generated.

Lastly, when electrospraying was attempted as a more sophisticated method to produce MPs, MVA was incompatible with this method based on the simulation studies using MVA inside pure triacetin, simulating the polymeric solution.

7.2 Future prospects

7.2.1 Microparticulate delivery of MVA in Adenovirus-MVA prime boost regime (Chapters 5&6)

- The work presented in this thesis is the first study of its kind to monitor both T-cells and B-cells with microparticulate devices entrapping a viral vector. This can provide the opportunity for more detailed immunological studies to dissect further the multi-functionality of T-cells generated with this technology. This would also enable to scout for differences in the generation of long-term memory immune cell populations for both T-cells and B-cells.

- Because double emulsion techniques create a broad range of MPs it would be also worth mechanically sieving the MPs based on size and then inject similar size particles in increasing size orders e.g. only 10μm, 20μm, 30μm etc. This would allow to examine the effect of the microparticle size on the immune response induced by the encapsulated MVA virus.

- Of paramount importance is the generation reproducible MPs with more precise control while also controlling the immobilisation positions of MVA within each MP. This would also reduce the batch-to-batch variability and produce uniform single size MPs rather than a broad range of sizes like in the case of double emulsion method. McHugh *et al*[302] have recently achieved this in 2017, where they used microfabrication techniques to manufacture consistent and reproducible injectable PLGA microdevices for vaccination purposes. A follow-up report is expected using the same technology combined with experimental vaccines illustrating T-cell and B-cell induced kinetics.

- ID Milligan *et al*[333] in a Phase I human trial using Adenovirus type 26 vector encoding an Ebola glycoprotein and MVA vector encoding 4 different viral nucleoproteins from

different viruses, showed similar immune response whether Adenovirus-MVA or MVA-Adenovirus prime boost approach was utilised. Thefore there is the potential to encapsulate adenovirus in microparticles following the methodology developed in this thesis and test the MVA-Adenovirus prime boost approach instead.

7.3 Overall conclusion

In the grander scheme of things, the methodology produced and demonstrated in this thesis could be used for the encapsulation of any living material containing DNA or RNA, like viruses and bacteria and be used for different purposes such as vaccination[166], anti-tumour approaches[334] or even encapsulation for probiotic bacteria for inflammatory bowel diseases[335].

Encapsulating the vaccines into microparticles which are then lyophilised could also improve their shelf life and avoid the need for constant refrigeration. This might be an effective alternative solution to the long-term refrigeration reliance of vaccines[336,337].

This promising microscopic solution (microparticles) to a macroscopic problem (vaccine compliance) indeed has potential. In the future, microencapsulation technology might be routinely used for human vaccination however there have been concerns raised about the long-term feasibility of this idea. For booster vaccines that have to be given after several years rather than months, there will be a need to coat this microdevice with anti-fibrotic substances. Assuming that the microdevice won't be affected by constant mechanical stresses from human muscle movement, this device won't be able to be cleared by the human body naturally. Because of the inability of the human body to clear this foreign object, it might activate fibrotic responses creating a fibrous membrane around it or initiate granulation tissue development by forming a macrophage-derived multinucleated giant cell formation[338–340]. Ultimately, both scenarios could potentially retard or even stop the release of the booster vaccine.

References

8 References

1. Smith, K. A. Smallpox: can we still learn from the journey to eradication? *The Indian journal of medical research* **137,** 895–899 (2013).
2. Moutou, F. The second eradication: Rinderpest. *Bull. la Société Pathol. Exot.* **107,** 137–138 (2014).
3. Centers for Disease Control and Prevention (CDC). *Ten great public health achievements--worldwide, 2001-2010. MMWR. Morbidity and mortality weekly report* **60,** (2011).
4. Baxby, D. Edward Jenner's inquiry; a bicentenary analysis. *Vaccine* **17,** 301–307 (1999).
5. Smith, K. A. Louis Pasteur, the father of immunology? *Frontiers in Immunology* **3,** (2012).
6. Murray, K., Stahl, S. & Ashton-Rickardt, P. G. Genetic engineering applied to the development of vaccines. *Philos. Trans. R. Soc. Lond. B. Biol. Sci.* **324,** 461–76 (1989).
7. Ura, T., Okuda, K. & Shimada, M. Developments in Viral Vector-Based Vaccines. *Vaccines* **2,** 624–641 (2014).
8. NHS. UK's immunisation schedule. Available at: https://www.nhs.uk/conditions/vaccinations/. (Accessed: 2nd September 2018)
9. WHO. WHO global immunisation. Available at: http://www.who.int/immunization/monitoring_surveillance/data/en/. (Accessed: 5th January 2018)
10. Falagas, M. E. & Zarkadoulia, E. Factors associated with suboptimal compliance to vaccinations in children in developed countries: a systematic review. *Curr. Med. Res. Opin.* **24,** 1719–1741 (2008).
11. Mutua, M. K., Kimani-Murage, E. & Ettarh, R. R. Childhood vaccination in informal urban settlements in Nairobi, Kenya: Who gets vaccinated? *BMC Public Health* **11,** (2011).
12. Walters, A. A., Krastev, C., Hill, A. V. S. & Milicic, A. Next generation vaccines: Single-dose encapsulated vaccines for improved global immunisation coverage and efficacy. *Journal of Pharmacy and Pharmacology* **67,** 400–408 (2015).
13. Raslan, R. *et al.* Re-Emerging Vaccine-Preventable Diseases in War-Affected Peoples of the Eastern Mediterranean Region—An Update. *Front. Public Heal.* **5,** (2017).
14. Aguado, M. T. Future approaches to vaccine development: Single-dose vaccines using controlled-release delivery systems. *Vaccine* **11,** 596–597 (1993).
15. Cleland, J. L. Single-administration vaccines: Controlled-release technology to mimic repeated immunizations. *Trends in Biotechnology* **17,** 25–29 (1999).
16. Preis, I. & Langer, R. S. A single-step immunization by sustained antigen release. *J. Immunol. Methods* **28,** 193–197 (1979).
17. Edlund, U. & Albertsson, a. Degradable Polymer Microspheres for Controlled Drug Delivery. *Adv. Polym. Sci.* **157,** 67–112 (2002).
18. Silva, A. L., Soema, P. C., Slütter, B., Ossendorp, F. & Jiskoot, W. PLGA particulate delivery systems for subunit vaccines: Linking particle properties to immunogenicity. *Human Vaccines and Immunotherapeutics* **12,** 1056–1069 (2016).
19. Johansen, P. *et al.* Towards clinical testing of a single-administration tetanus vaccine based on PLA/PLGA microspheres. *Vaccine* **19,** 1047–54 (2000).
20. Men, Y., Thomasin, C., Merkle, H. P., Gander, B. & Corradin, G. A single administration of tetanus toxoid in biodegradable microspheres elicits T cell and antibody responses similar or superior to those obtained with aluminum hydroxide. *Vaccine* **13,** 683–689 (1995).
21. Nair, L. S. & Laurencin, C. T. Biodegradable polymers as biomaterials. *Progress in Polymer Science (Oxford)* **32,** 762–798 (2007).
22. Uhrich, K. E., Cannizzaro, S. M., Langer, R. S. & Shakesheff, K. M. Polymeric Systems for Controlled Drug Release. *Chem. Rev.* **99,** 3181–3198 (1999).
23. Crotts, G. & Park, T. G. Protein delivery from poly(lactic-co-glycolic acid) biodegradable microspheres: release kinetics and stability issues. *J. Microencapsul.* **15,** 699–713 (1998).
24. Makadia, H. K. & Siegel, S. J. Poly Lactic-co-Glycolic Acid (PLGA) as biodegradable

controlled drug delivery carrier. *Polymers (Basel).* **3,** 1377–1397 (2011).
25. Wu, X. S. & Wang, N. Synthesis, characterization, biodegradation, and drug delivery application of biodegradable lactic/glycolic acid polymers. Part II: biodegradation. *J. Biomater. Sci. Polym. Ed.* **12,** 21–34 (2001).
26. Siegel, S. J. *et al.* Effect of drug type on the degradation rate of PLGA matrices. *Eur. J. Pharm. Biopharm.* **64,** 287–293 (2006).
27. Singh, M. N., Hemant, K. S. Y., Ram, M. & Shivakumar, H. G. Microencapsulation: A promising technique for controlled drug delivery. *Research in Pharmaceutical Sciences* **5,** 65–77 (2010).
28. Berkland, C., Kipper, M. J., Narasimhan, B., Kim, K. & Pack, D. W. Microsphere size, precipitation kinetics and drug distribution control drug release from biodegradable polyanhydride microspheres. *J. Control. Release* **94,** 129–141 (2004).
29. Gupta, A. & Dey, B. Microencapsulation for controlled drug delivery: a comprehensive review. *Sunsari Tech. Coll. J.* **1,** 48–54 (2013).
30. Arshady, R. Microspheres and microcapsules, a survey of manufacturing techniques Part II: Coacervation. *Polym. Eng. Sci.* **30,** 905–914 (1990).
31. Hua, F. J., Park, T. G. & Lee, D. S. A facile preparation of highly interconnected macroporous poly(D,L-lactic acid-co-glycolic acid) (PLGA) scaffolds by liquid-liquid phase separation of a PLGA-dioxane-water ternary system. *Polymer (Guildf).* **44,** 1911–1920 (2003).
32. Wan, F. *et al.* One-Step Production of Protein-Loaded PLGA Microparticles via Spray Drying Using 3-Fluid Nozzle. *Pharm. Res.* **31,** 1967–1977 (2014).
33. Bock, N., Woodruff, M. A., Hutmacher, D. W. & Dargaville, T. R. Electrospraying, a reproducible method for production of polymeric microspheres for biomedical applications. *Polymers (Basel).* **3,** 131–149 (2011).
34. Ahirrao, S. P., Gide, P. S., Shrivastav, B. & Sharma, P. Ionotropic Gelation : A Promising Cross Linking Technique for Hydrogels. *J. Pharm. Nanotechnol.* **2,** 1–6 (2014).
35. Khanna, O., Larson, J. C., Moya, M. L., Opara, E. C. & Brey, E. M. Generation of alginate microspheres for biomedical applications. *J. Vis. Exp.* (2012). doi:10.3791/3388
36. Badwan, A. A., Abumalooh, A., Sallam, E., Abukalaf, A. & Jawan, O. A sustained release drug delivery system using calcium alginate beads. *Drug Dev. Ind. Pharm.* **11,** 239–256 (1985).
37. Flajnik, M. F. & Kasahara, M. Origin and evolution of the adaptive immune system: Genetic events and selective pressures. *Nature Reviews Genetics* **11,** 47–59 (2010).
38. Palm, N. W. & Medzhitov, R. Pattern recognition receptors and control of adaptive immunity. *Immunological Reviews* **227,** 221–233 (2009).
39. Kumar, H., Kawai, T. & Akira, S. Pathogen recognition by the innate immune system. *Int Rev Immunol* **30,** 16–34 (2011).
40. Mogensen, T. H. Pathogen recognition and inflammatory signaling in innate immune defenses. *Clinical Microbiology Reviews* **22,** 240–273 (2009).
41. Janeway, C. A. Approaching the asymptote? Evolution and revolution in immunology. in *Cold Spring Harbor Symposia on Quantitative Biology* **54,** 1–13 (1989).
42. St. John, A. L. & Abraham, S. N. Innate Immunity and Its Regulation by Mast Cells. *J. Immunol.* **190,** 4458–4463 (2013).
43. Acharya, K. R. & Ackerman, S. J. Eosinophil granule proteins: Form and function. *Journal of Biological Chemistry* **289,** 17406–17415 (2014).
44. Sokol, C. L. & Medzhitov, R. Emerging functions of basophils in protective and allergic immune responses. *Mucosal Immunology* **3,** 129–137 (2010).
45. Topham, N. J. & Hewitt, E. W. Natural killer cell cytotoxicity: How do they pull the trigger? *Immunology* **128,** 7–15 (2009).
46. Flannagan, R. S., Cosío, G. & Grinstein, S. Antimicrobial mechanisms of phagocytes and bacterial evasion strategies. *Nature Reviews Microbiology* **7,** 355–366 (2009).
47. Epelman, S., Lavine, K. J. & Randolph, G. J. Origin and Functions of Tissue Macrophages. *Immunity* **41,** 21–35 (2014).

48. Kruger, P. *et al.* Neutrophils: Between Host Defence, Immune Modulation, and Tissue Injury. *PLoS Pathogens* **11,** 1–22 (2015).
49. Howard, C. J., Charleston, B., Stephens, S. A., Sopp, P. & Hope, J. C. The role of dendritic cells in shaping the immune response. *Anim. Heal. Res. Rev.* **5,** 191–195 (2004).
50. Dieu, M. C. *et al.* Selective recruitment of immature and mature dendritic cells by distinct chemokines expressed in different anatomic sites. *J. Exp. Med.* **188,** 373–386 (1998).
51. Lee, H. K. & Iwasaki, A. Innate control of adaptive immunity: dendritic cells and beyond. *Semin Immunol* **19,** 48–55 (2007).
52. Warren, R. L. *et al.* Exhaustive T-cell repertoire sequencing of human peripheral blood samples reveals signatures of antigen selection and a directly measured repertoire size of at least 1 million clonotypes. *Genome Res.* **21,** 790–797 (2011).
53. Ogle, B. M. *et al.* Direct measurement of lymphocyte receptor diversity. *Nucleic Acids Res.* **31,** e139 (2003).
54. Pennock, N. D. *et al.* T cell responses: naive to memory and everything in between. *Adv. Physiol. Educ.* **37,** 273–83 (2013).
55. Germain, R. N. T-cell development and the CD4–CD8 lineage decision. *Nat. Rev. Immunol.* **2,** 309–322 (2002).
56. Ra, J.-S., Shin, H.-H., Kang, S. & Do, Y. Lumazine synthase protein cage nanoparticles as antigen delivery nanoplatforms for dendritic cell-based vaccine development. *Clin. Exp. Vaccine Res.* **3,** 227 (2014).
57. Newton, K. & Dixit, V. M. Signaling in innate immunity and inflammation. *Cold Spring Harb. Perspect. Biol.* **4,** (2012).
58. Mosmann, T. R., Cherwinski, H., Bond, M. W., Giedlin, M. A. & Coffman, R. L. Two types of murine helper T cell clone. I. Definition according to profiles of lymphokine activities and secreted proteins. *J. Immunol.* (1986). doi:10.1111/j.1442-9071.2011.02672.x
59. Coffman, R. L. & Carty, J. A T cell activity that enhances polyclonal IgE production and its inhibition by interferon-gamma. *J. Immunol.* (1986).
60. Trinchieri, G., Pflanz, S. & Kastelein, R. A. The IL-12 family of heterodimeric cytokines: New players in the regulation of T cell responses. *Immunity* **19,** 641–644 (2003).
61. Kidd, P. Th1/Th2 balance: the hypothesis, its limitations, and implications for health and disease. *Altern. Med. Rev.* **8,** 223–46 (2003).
62. Liew, F. Y. TH1 and TH2 cells: A historical perspective. *Nature Reviews Immunology* (2002). doi:10.1038/nri705
63. Golubovskaya, V. & Wu, L. Different subsets of T cells, memory, effector functions, and CAR-T immunotherapy. *Cancers* (2016). doi:10.3390/cancers8030036
64. Deng, Y. *et al.* Th9 cells and IL-9 in autoimmune disorders: Pathogenesis and therapeutic potentials. *Human Immunology* (2017). doi:10.1016/j.humimm.2016.12.010
65. Zhao, H., Liao, X. & Kang, Y. Tregs: Where We Are and What Comes Next? *Front. Immunol.* **8,** 1578 (2017).
66. Harty, J. T., Tvinnereim, A. R. & White, D. W. CD8+ T cell effector mechanisms in resistance to infection. *Annu Rev Immunol* **18,** 275–308 (2000).
67. Berke, G. The CTL's kiss of death. *Cell* **81,** 9–12 (1995).
68. Shresta, S., Pham, C. T., Thomas, D. A., Graubert, T. A. & Ley, T. J. How do cytotoxic lymphocytes kill their targets? *Current Opinion in Immunology* **10,** 581–587 (1998).
69. Harty, J. T. & Bevan, M. J. Responses of CD8(+) T cells to intracellular bacteria. *Curr. Opin. Immunol.* **11,** 89–93 (1999).
70. Schoenberger, S. P., Toes, R. E. M., Van der Voort, E. I. H., Offringa, R. & Melief, C. J. M. T-cell help for cytotoxic T-lymphocytes is mediated by CD40-CD40L interactions. *Nature* **393,** 480–483 (1998).
71. Mittrücker, H.-W., Visekruna, A. & Huber, M. Heterogeneity in the Differentiation and Function of CD8+ T Cells. *Arch. Immunol. Ther. Exp. (Warsz).* (2014). doi:10.1007/s00005-014-0293-y
72. Dobrzanski, M. J., Reome, J. B., Hollenbaugh, J. A. & Dutton, R. W. Tc1 and Tc2 Effector

Cell Therapy Elicit Long-Term Tumor Immunity by Contrasting Mechanisms That Result in Complementary Endogenous Type 1 Antitumor Responses. *J. Immunol.* (2004). doi:10.4049/jimmunol.172.3.1380
73. Yu, Y. *et al.* Recent advances in CD8+ regulatory T cell research. *Oncol. Lett.* (2018). doi:10.3892/ol.2018.8378
74. Kim, H.-J., Verbinnen, B., Tang, X., Lu, L. & Cantor, H. Inhibition of follicular T-helper cells by CD8(+) regulatory T cells is essential for self tolerance. *Nature* **467,** 328–32 (2010).
75. Vantourout, P. & Hayday, A. Six-of-the-best: Unique contributions of γδ T cells to immunology. *Nature Reviews Immunology* (2013). doi:10.1038/nri3384
76. Steele, C. R., Oppenheim, D. E. & Hayday, A. C. γ δ T cells: Non-classical ligands for non-classical cells. *Curr. Biol.* (2000). doi:10.1016/S0960-9822(00)00408-5
77. Tanaka, Y. *et al.* Natural and synthetic non-peptide antigens recognized by human γδ T cells. *Nature* (1995). doi:10.1038/375155a0
78. Rincon-Orozco, B. *et al.* Activation of V 9V 2 T Cells by NKG2D. *J. Immunol.* (2005). doi:10.4049/jimmunol.175.4.2144
79. Bauer, S. *et al.* Activation of NK cells and T cells by NKG2D, a receptor for stress-lnducible MICA. *J. Immunol.* (2018). doi:10.1126/science.285.5428.727
80. Todaro, M. *et al.* Efficient Killing of Human Colon Cancer Stem Cells by T Lymphocytes. *J. Immunol.* (2009). doi:10.4049/jimmunol.0804288
81. Rhodes, K. A., Andrew, E. M., Newton, D. J., Tramonti, D. & Carding, S. R. A subset of IL-10-producing γδ T cells protect the liver from Listeria-elicited, CD8+T cell-mediated injury. *Eur. J. Immunol.* (2008). doi:10.1002/eji.200838354
82. Michel, M.-L. *et al.* Interleukin 7 (IL-7) selectively promotes mouse and human IL-17-producing cells. *Proc. Natl. Acad. Sci.* (2012). doi:10.1073/pnas.1204327109
83. Lawand, M., Déchanet-Merville, J. & Dieu-Nosjean, M. C. Key features of gamma-delta T-cell subsets in human diseases and their immunotherapeutic implications. *Frontiers in Immunology* (2017). doi:10.3389/fimmu.2017.00761
84. Ferrick, D. A. *et al.* Differential production of interferon-γ and interleukin-4 in response to Th1- and Th2-stimulating pathogens by γδ T cells in vivo. *Nature* **373,** 255 (1995).
85. Chien, Y., Meyer, C. & Bonneville, M. <scp>γδ</scp> T Cells: First Line of Defense and Beyond. *Annu. Rev. Immunol.* (2014). doi:10.1146/annurev-immunol-032713-120216
86. Khan, M. W. A., Eberl, M. & Moser, B. Potential Use of γδ T Cell-Based Vaccines in Cancer Immunotherapy. *Front. Immunol.* **5,** 512 (2014).
87. Zaidi, I. *et al.* γδ T Cells Are Required for the Induction of Sterile Immunity during Irradiated Sporozoite Vaccinations. *J. Immunol.* (2017). doi:10.4049/jimmunol.1700314
88. Godfrey, D. I., Stankovic, S. & Baxter, A. G. Raising the NKT cell family. *Nature Immunology* (2010). doi:10.1038/ni.1841
89. Lantz, O. & Bendelac, A. An invariant T cell receptor alpha chain is used by a unique subset of major histocompatibility complex class I-specific CD4+ and CD4-8- T cells in mice and humans. *J. Exp. Med.* (1994). doi:10.1084/jem.180.3.1097
90. Gapin, L. Development of invariant natural killer T cells. *Current Opinion in Immunology* (2016). doi:10.1016/j.coi.2016.01.001
91. Barral, P., Sénchez-Nieo, M. D., Van Rooijen, N., Cerundolo, V. & Batista, F. D. The location of splenic NKT cells favours their rapid activation by blood-borne antigen. *EMBO J.* (2012). doi:10.1038/emboj.2012.87
92. Van Kaer, L., Parekh, V. V. & Wu, L. The response of CD1d-restricted invariant NKT cells to microbial pathogens and their products. *Frontiers in Immunology* (2015). doi:10.3389/fimmu.2015.00226
93. Le Bourhis, L. *et al.* Mucosal-associated invariant T cells: Unconventional development and function. *Trends in Immunology* (2011). doi:10.1016/j.it.2011.02.005
94. Kjer-Nielsen, L. *et al.* MR1 presents microbial vitamin B metabolites to MAIT cells. *Nature* (2012). doi:10.1038/nature11605
95. Napier, R. J., Adams, E. J., Gold, M. C. & Lewinsohn, D. M. The role of mucosal associated

invariant T cells in antimicrobial immunity. *Front. Immunol.* (2015). doi:10.3389/fimmu.2015.00344
96. Le Bourhis, L. *et al.* MAIT Cells Detect and Efficiently Lyse Bacterially-Infected Epithelial Cells. *PLoS Pathog.* (2013). doi:10.1371/journal.ppat.1003681
97. Salou, M., Franciszkiewicz, K. & Lantz, O. MAIT cells in infectious diseases. *Current Opinion in Immunology* (2017). doi:10.1016/j.coi.2017.07.009
98. Wong, E. B., Ndung'u, T. & Kasprowicz, V. O. The role of mucosal-associated invariant T cells in infectious diseases. *Immunology* (2017). doi:10.1111/imm.12673
99. Yang, G., Richt, J. A. & Driver, J. P. Harnessing invariant NKT cells to improve influenza vaccines: A pig perspective. *International Journal of Molecular Sciences* (2018). doi:10.3390/ijms19010068
100. Leung, D. T. *et al.* Circulating Mucosal Associated Invariant T Cells Are Activated in Vibrio cholerae O1 Infection and Associated with Lipopolysaccharide Antibody Responses. *PLoS Negl. Trop. Dis.* (2014). doi:10.1371/journal.pntd.0003076
101. Blattman, J. N. *et al.* Estimating the Precursor Frequency of Naive Antigen-specific CD8 T Cells. *J. Exp. Med.* (2002). doi:10.1084/jem.20001021
102. Stemberger, C. *et al.* A Single Naive CD8+ T Cell Precursor Can Develop into Diverse Effector and Memory Subsets. *Immunity* (2007). doi:10.1016/j.immuni.2007.10.012
103. Gerlach, C. *et al.* Heterogeneous differentiation patterns of individual CD8+T cells. *Science (80-.).* (2013). doi:10.1126/science.1235487
104. Macallan, D., Borghans, J. & Asquith, B. Human T Cell Memory: A Dynamic View. *Vaccines* (2017). doi:10.3390/vaccines5010005
105. Farber, D. L., Yudanin, N. A. & Restifo, N. P. Human memory T cells: Generation, compartmentalization and homeostasis. *Nature Reviews Immunology* (2014). doi:10.1038/nri3567
106. MacLennan, I. C. Germinal centers. *Annu Rev Immunol* **12,** 117–139 (1994).
107. Doyle, C. & Strominger, J. L. Interaction between CD4 and class II MHC molecules mediates cell adhesion. *Nature* **330,** 256–259 (1987).
108. Norment, A. M., Salter, R. D., Parham, P., Engelhard, V. H. & Littman, D. R. Cell-cell adhesion mediated by CD8 and MHC class I molecules. *Nature* **336,** 79–81 (1988).
109. Kloetzel, P. M. Generation of major histocompatibility complex class I antigens: functional interplay between proteasomes and TPPII. *Nat. Immunol.* **5,** 661 (2004).
110. Jensen, P. E. Recent advances in antigen processing and presentation. *Nat. Immunol.* **8,** 1041–1048 (2007).
111. Holling, T. M., Schooten, E. & van Den Elsen, P. J. Function and regulation of MHC class II molecules in T-lymphocytes: of mice and men. *Hum. Immunol.* **65,** 282–290 (2004).
112. Roche, P. A. & Furuta, K. The ins and outs of MHC class II-mediated antigen processing and presentation. *Nat. Rev. Immunol.* **15,** 203 (2015).
113. Landsverk, O. J. B., Bakke, O. & Gregers, T. F. MHC II and the endocytic pathway: Regulation by invariant chain. *Scandinavian Journal of Immunology* (2009). doi:10.1111/j.1365-3083.2009.02301.x
114. Riese, R. J. *et al.* Essential role for cathepsin S in MHC class II-associated invariant chain processing and peptide loading. *Immunity* (1996). doi:10.1016/S1074-7613(00)80249-6
115. Denzin, L. K. & Cresswell, P. HLA-DM induces clip dissociation from MHC class II αβ dimers and facilitates peptide loading. *Cell* (1995). doi:10.1016/0092-8674(95)90061-6
116. Murat, P. & Tellam, J. Effects of messenger RNA structure and other translational control mechanisms on major histocompatibility complex-I mediated antigen presentation. *Wiley Interdiscip. Rev. RNA* **6,** 157–171 (2015).
117. Neefjes, J., Jongsma, M. L. M., Paul, P. & Bakke, O. Towards a systems understanding of MHC class I and MHC class II antigen presentation. *Nat. Rev. Immunol.* **11,** 823–836 (2011).
118. Rock, K. L. & Shen, L. *Cross-presentation: underlying mechanisms and role in immune surveillance*.
119. Segura, E., Durand, M. & Amigorena, S. Similar antigen cross-presentation capacity and

phagocytic functions in all freshly isolated human lymphoid organ–resident dendritic cells. *J. Exp. Med.* (2013). doi:10.1084/jem.20121103
120. Fehres, C. M., Unger, W. W. J., Garcia-Vallejo, J. J. & van Kooyk, Y. Understanding the biology of antigen cross-presentation for the design of vaccines against cancer. *Front. Immunol.* **5,** 149 (2014).
121. Münz, C. Autophagy Beyond Intracellular MHC Class II Antigen Presentation. *Trends Immunol.* **37,** 755–763 (2016).
122. Crotzer, V. L. & Blum, J. S. Autophagy and its role in MHC-mediated antigen presentation. *J. Immunol.* **182,** 3335–41 (2009).
123. Ahmed, R. & Gray, D. Immunological Memory and Protective Immunity: Understanding Their Relation. *Science (80-.).* **272,** 54–60 (1996).
124. Awate, S., Babiuk, L. A. & Mutwiri, G. Mechanisms of action of adjuvants. *Frontiers in Immunology* **4,** (2013).
125. Mantegazza, A. R., Magalhaes, J. G., Amigorena, S. & Marks, M. S. Presentation of Phagocytosed Antigens by MHC Class I and II. *Traffic* **14,** 135–152 (2013).
126. History, V. Vaccinology. Available at: https://www.historyofvaccines.org/gallery. (Accessed: 5th January 2018)
127. Baxter, D. Active and passive immunity, vaccine types, excipients and licensing. *Occupational Medicine* **57,** 552–556 (2007).
128. Clem, A. Fundamentals of vaccine immunology. *J. Glob. Infect. Dis.* **3,** 73 (2011).
129. Vaccine types. Available at: https://www.vaccines.gov/basics/types/index.html. (Accessed: 4th January 2018)
130. Choi, Y. & Chang, J. Viral vectors for vaccine applications. *Clin. Exp. Vaccine Res.* **2,** 97 (2013).
131. Knudsen, N. P. H. *et al.* Different human vaccine adjuvants promote distinct antigen-independent immunological signatures tailored to different pathogens. *Sci. Rep.* (2016). doi:10.1038/srep19570
132. Carter, D. & Reed, S. G. Role of adjuvants in modeling the immune response. *Current Opinion in HIV and AIDS* (2010). doi:10.1097/COH.0b013e32833d2cdb
133. van Aalst, S. *et al.* Dynamics of APC recruitment at the site of injection following injection of vaccine adjuvants. *Vaccine* (2017). doi:10.1016/j.vaccine.2017.02.005
134. Harris, J., Sharp, F. A. & Lavelle, E. C. The role of inflammasomes in the immunostimulatory effects of particulate vaccine adjuvants. *European Journal of Immunology* (2010). doi:10.1002/eji.200940172
135. Gupta, A. & Chaphalkar, S. R. Vaccine adjuvants: The current necessity of life. *Shiraz E Medical Journal* (2015). doi:10.17795/semj28061
136. Didierlaurent, A. M. *et al.* Enhancement of Adaptive Immunity by the Human Vaccine Adjuvant AS01 Depends on Activated Dendritic Cells. *J. Immunol.* (2014). doi:10.4049/jimmunol.1400948
137. Aucouturier, J., Dupuis, L., Deville, S., Ascarateil, S. & Ganne, V. Montanide ISA 720 and 51: A new generation of water in oil emulsions as adjuvants for human vaccines. *Expert Review of Vaccines* (2002). doi:10.1586/14760584.1.1.111
138. Del Giudice, G., Rappuoli, R. & Didierlaurent, A. M. Correlates of adjuvanticity: A review on adjuvants in licensed vaccines. *Seminars in Immunology* (2018). doi:10.1016/j.smim.2018.05.001
139. Sjölander, A., Cox, J. C. & Barr, I. G. ISCOMs: An adjuvant with multiple functions. *Journal of Leukocyte Biology* (1998). doi:10.1002/jlb.64.6.713
140. Schmidt, S. T., Foged, C., Korsholm, K. S., Rades, T. & Christensen, D. Liposome-based adjuvants for subunit vaccines: Formulation strategies for subunit antigens and immunostimulators. *Pharmaceutics* (2016). doi:10.3390/pharmaceutics8010007
141. Scheinberg, D. A. *et al.* Carbon nanotubes as vaccine scaffolds. *Advanced Drug Delivery Reviews* (2013). doi:10.1016/j.addr.2013.07.013
142. Guillén, G. *et al.* Virus-Like Particles as vaccine antigens and adjuvants: Application to

chronic disease, cancer immunotherapy and infectious disease preventive strategies. in *Procedia in Vaccinology* (2010). doi:10.1016/j.provac.2010.07.004
143. Akagi, T., Baba, M. & Akashi, M. Biodegradable nanoparticles as vaccine adjuvants and delivery systems: Regulation of immune responses by nanoparticle-based vaccine. *Advances in Polymer Science* (2012). doi:10.1007/12_2011_150
144. Gutjahr, A. *et al.* Biodegradable Polymeric Nanoparticles-Based Vaccine Adjuvants for Lymph Nodes Targeting. *Vaccines* (2016). doi:10.3390/vaccines4040034
145. Adams, J. R. & Mallapragada, S. K. Enhancing the immune response through next generation polymeric vaccine adjuvants. *TECHNOLOGY* (2014). doi:10.1142/S2339547814300017
146. Pichichero, M. E. Protein carriers of conjugate vaccines Characteristics, development, and clinical trials. *Human Vaccines and Immunotherapeutics* (2013). doi:10.4161/hv.26109
147. Barrett, D. J. Human immune responses to polysaccharide antigens: an analysis of bacterial polysaccharide vaccines in infants. *Adv Pediatr* (1985).
148. Micoli, F., Adamo, R. & Costantino, P. Protein carriers for glycoconjugate vaccines: History, selection criteria, characterization and new trends. *Molecules* (2018). doi:10.3390/molecules23061451
149. Tillett, W. S., Avery, O. T. & Goebel, W. F. Chemo-immunological studies in conjugated carbohydrate-proteins : III. Active and passive anaphylaxis with synthetic sugar-proteins. *J. Exp. Med.* (1929). doi:10.1084/jem.50.4.533
150. Durando, P., Faust, S. N. & Torres, A. Immunological features and clinical benefits of conjugate vaccines against bacteria. *Journal of Immunology Research* (2015). doi:10.1155/2015/934504
151. Pollard, A. J., Perrett, K. P. & Beverley, P. C. Maintaining protection against invasive bacteria with protein- polysaccharide conjugate vaccines. *Nature Reviews Immunology* (2009). doi:10.1038/nri2494
152. Bröker, M., Berti, F., Schneider, J. & Vojtek, I. Polysaccharide conjugate vaccine protein carriers as a "neglected valency" – Potential and limitations. *Vaccine* (2017). doi:10.1016/j.vaccine.2017.04.078
153. Kushnir, N., Streatfield, S. J. & Yusibov, V. Virus-like particles as a highly efficient vaccine platform: Diversity of targets and production systems and advances in clinical development. *Vaccine* (2012). doi:10.1016/j.vaccine.2012.10.083
154. Lua, L. H. L. *et al.* Bioengineering virus-like particles as vaccines. *Biotechnology and Bioengineering* (2014). doi:10.1002/bit.25159
155. Crisci, E., Bárcena, J. & Montoya, M. Virus-like particles: The new frontier of vaccines for animal viral infections. *Veterinary Immunology and Immunopathology* (2012). doi:10.1016/j.vetimm.2012.04.026
156. Huang, X., Wang, X., Zhang, J., Xia, N. & Zhao, Q. Escherichia coli-derived virus-like particles in vaccine development. *npj Vaccines* (2017). doi:10.1038/s41541-017-0006-8
157. Mohsen, M. O., Zha, L., Cabral-Miranda, G. & Bachmann, M. F. Major findings and recent advances in virus–like particle (VLP)-based vaccines. *Semin. Immunol.* **34,** 123–132 (2017).
158. Hu, G. *et al.* Generation and immunogenicity of porcine circovirus type 2 chimeric virus-like particles displaying porcine reproductive and respiratory syndrome virus GP5 epitope B. *Vaccine* (2016). doi:10.1016/j.vaccine.2016.02.047
159. Perri, S. *et al.* An Alphavirus Replicon Particle Chimera Derived from Venezuelan Equine Encephalitis and Sindbis Viruses Is a Potent Gene-Based Vaccine Delivery Vector. *J. Virol.* (2003). doi:10.1128/JVI.77.19.10394-10403.2003
160. Iavarone, C., O'hagan, D. T., Yu, D., Delahaye, N. F. & Ulmer, J. B. Mechanism of action of mRNA-based vaccines. *Expert Review of Vaccines* (2017). doi:10.1080/14760584.2017.1355245
161. Lundstrom, K. Latest development on RNA-based drugs and vaccines. *Futur. Sci. OA* (2018). doi:10.4155/fsoa-2017-0151
162. Pardi, N., Hogan, M. J., Porter, F. W. & Weissman, D. mRNA vaccines-a new era in vaccinology. *Nature Reviews Drug Discovery* (2018). doi:10.1038/nrd.2017.243

163. Schlake, T., Thess, A., Fotin-Mleczek, M. & Kallen, K. J. Developing mRNA-vaccine technologies. *RNA Biology* (2012). doi:10.4161/rna.22269
164. Pollard, C., De Koker, S., Saelens, X., Vanham, G. & Grooten, J. Challenges and advances towards the rational design of mRNA vaccines. *Trends in Molecular Medicine* (2013). doi:10.1016/j.molmed.2013.09.002
165. Moss, B., Smith, G. L., Gerin, J. L. & Purcell, R. H. Live recombinant vaccinia virus protects chimpanzees against hepatitis B. *Nature* **311,** 67–69 (1984).
166. Ramezanpour, B., Haan, I., Osterhaus, A. & Claassen, E. Vector-based genetically modified vaccines: Exploiting Jenner's legacy. *Vaccine* **34,** 6436–6448 (2016).
167. Humphreys, I. R. & Sebastian, S. Novel viral vectors in infectious diseases. *Immunology* (2017). doi:10.1111/imm.12829
168. Russell, W. C. Adenoviruses: update on structure and function. *J. Gen. Virol.* **90,** 1–20 (2009).
169. Bangari, D. S. & Mittal, S. K. Development of nonhuman adenoviruses as vaccine vectors. *Vaccine* **24,** 849–862 (2006).
170. Gutiérrez-Martínez, E. *et al.* Cross-presentation of cell-associated antigens by MHC class I in dendritic cell subsets. *Frontiers in Immunology* **6,** (2015).
171. Ertl, H. C. Viral vectors as vaccine carriers. *Curr. Opin. Virol.* **21,** 1–8 (2016).
172. Shott, J. P. *et al.* Adenovirus 5 and 35 vectors expressing Plasmodium falciparum circumsporozoite surface protein elicit potent antigen-specific cellular IFN-γ and antibody responses in mice. *Vaccine* **26,** 2818–2823 (2008).
173. Gabitzsch, E. S. *et al.* Novel Adenovirus type 5 vaccine platform induces cellular immunity against HIV-1 Gag, Pol, Nef despite the presence of Ad5 immunity. *Vaccine* **27,** 6394–6398 (2009).
174. Ledgerwood, J. E. *et al.* Chimpanzee Adenovirus Vector Ebola Vaccine - Preliminary Report. *N. Engl. J. Med.* 1–9 (2014). doi:10.1056/NEJMoa1410863
175. Ledgerwood, J. E. *et al.* Chimpanzee Adenovirus Vector Ebola Vaccine. *N. Engl. J. Med.* **376,** 928–938 (2017).
176. Johnson, L., Gupta, A. K., Ghafoor, A., Akin, D. & Bashir, R. Characterization of vaccinia virus particles using microscale silicon cantilever resonators and atomic force microscopy. *Sensors Actuators, B Chem.* **115,** 189–197 (2006).
177. Moss, B. Poxviridae: the viruses and their replication. *Fields Virol.* 2637–2671 (1996).
178. Kim, J. W. & Gulley, J. L. Poxviral vectors for cancer immunotherapy. *Expert Opin. Biol. Ther.* **12,** 463–478 (2012).
179. Smith, G. L., Vanderplasschen, A. & Law, M. The formation and function of extracellular enveloped vaccinia virus. *Journal of General Virology* **83,** 2915–2931 (2002).
180. Mayr, A., Hochstein-Mintzel, V. & Stickl, H. Abstammung, Eigenschaften und Verwendung des attenuierten Vaccinia-Stammes MVA. *Infection* **3,** 6–14 (1975).
181. Mayr A, Stickl H, Müller HK, Danner K, S. H. The smallpox vaccination strain MVA: marker, genetic structure, experience gained with the parenteral vaccination and behavior in organisms with a debilitated defence mechanism. *Zentralbl. Bakteriol. B.* **167,** 375–390 (1978).
182. Harari, A. *et al.* An HIV-1 clade C DNA prime, NYVAC boost vaccine regimen induces reliable, polyfunctional, and long-lasting T cell responses. *J. Exp. Med.* **205,** 63–77 (2008).
183. Ibanga, H. B. *et al.* Early clinical trials with a new tuberculosis vaccine, MVA85A, in tuberculosis-endemic countries: issues in study design. *Lancet. Infect. Dis.* **6,** 522–8 (2006).
184. Webster, D. P. *et al.* Enhanced T cell-mediated protection against malaria in human challenges by using the recombinant poxviruses FP9 and modified vaccinia virus Ankara. *Proc. Natl. Acad. Sci.* **102,** 4836–4841 (2005).
185. WHO. WHO Malaria 2017. Available at: http://www.who.int/malaria/media/world-malaria-report-2017/en/. (Accessed: 5th January 2018)
186. Knox, D. P. & Redmond, D. L. Parasite vaccines - Recent progress and problems associated with their development. *Parasitology* **133,** (2006).
187. Flannery, E. L., Chatterjee, A. K. & Winzeler, E. A. Antimalarial drug discovery — approaches and progress towards new medicines. *Nat. Rev. Microbiol.* **12,** 70–70 (2013).

188. Kantele, A. & Jokiranta, T. S. Review of cases with the emerging fifth human malaria parasite, Plasmodium knowlesi. *Clin. Infect. Dis.* **52,** 1356–62 (2011).
189. Hollingdale, M. R., Nardin, E. H., Tharavanij, S., Schwartz, A. L. & Nussenzweig, R. S. Inhibition of entry of Plasmodium falciparum and P. vivax sporozoites into cultured cells; an in vitro assay of protective antibodies. *J Immunol* **132,** 909–913 (1984).
190. Kirkman, L. A. & Deitsch, K. W. Antigenic variation and the generation of diversity in malaria parasites. *Current Opinion in Microbiology* **15,** 456–462 (2012).
191. Janse, C. J. *et al.* A genotype and phenotype database of genetically modified malaria-parasites. *Trends in Parasitology* **27,** 31–39 (2011).
192. Bolad, A. & Berzins, K. Antigenic diversity of plasmodium falciparum and antibody-mediated parasite neutralization. *Scandinavian Journal of Immunology* **52,** 233–239 (2000).
193. Winzeler, E. A. Malaria research in the post-genomic era. *Nature* **455,** 751–756 (2008).
194. Romero, P. *et al.* Cloned cytotoxic T cells recognize an epitope in the circumsporozoite protein and protect against malaria. *Nature* **341,** 323–326 (1989).
195. Amselem, S., Alving, C. R. & Domb, A. J. Polymeric biodegradable lipospheres™ as vaccine delivery systems. *Polym. Adv. Technol.* **3,** 351–357 (1992).
196. Men, Y., Gander, B., Merkle, H. P. & Corradin, G. Induction of sustained and elevated immune responses to weakly immunogenic synthetic malarial peptides by encapsulation in biodegradable polymer microspheres. *Vaccine* (1996). doi:10.1016/S0264-410X(96)00074-6
197. Men, Y., Tamber, H., Audran, R., Gander, B. & Corradin, G. Induction of a cytotoxic T lymphocyte response by immunization with a malaria specific CTL peptide entrapped in biodegradable polymer microspheres. *Vaccine* (1997). doi:10.1016/S0264-410X(97)00047-9
198. Thomasin, C., Corradin, G., Men, Y., Merkle, H. P. & Gander, B. Tetanus toxoid and synthetic malaria antigen containing poly(lactide)/poly(lactide-co-glycolide) microspheres: importance of polymer degradation and antigen release for immune response. *J. Control. Release* **41,** 131–145 (1996).
199. Nixon, D. F. *et al.* Synthetic peptides entrapped in microparticles can elicit cytotoxic T cell activity. *Vaccine* (1996). doi:10.1016/S0264-410X(96)00099-0
200. Rosas, J. E. *et al.* Biodegradable PLGA microspheres as a delivery system for malaria synthetic peptide SPf66. *Vaccine* (2001). doi:10.1016/S0264-410X(01)00192-X
201. Rosas, J. E. *et al.* Remarkably high antibody levels and protection against P. falciparum malaria in Aotus monkeys after a single immunisation of SPf66 encapsulated in PLGA microspheres. *Vaccine* (2002). doi:10.1016/S0264-410X(01)00508-4
202. David, A. E. *et al.* BIODEGRADABLE POLYMERIC PARTICLES ENCAPSULATING AN ACTIVE AGENT, PHARMACEUTICAL COMPOSITIONS AND USES THEREOF. (2018).
203. Larsen, K. C. *et al.* Expression of tak1 and tram induces synergistic pro-inflammatory signalling and adjuvants DNA vaccines. *Vaccine* **27,** 5589–5598 (2009).
204. Nath, S. D., Son, S., Sadiasa, A., Min, Y. K. & Lee, B. T. Preparation and characterization of PLGA microspheres by the electrospraying method for delivering simvastatin for bone regeneration. *Int. J. Pharm.* **443,** 87–94 (2013).
205. Bustin, S. A. *et al.* The MIQE guidelines:Minimum Information for publication of quantitative real-time PCR experiments. *Clin. Chem.* **55,** 611–622 (2009).
206. Schneider, J. *et al.* Enhanced immunogenicity for CD8+ T cell induction and complete protective efficacy of malaria DNA vaccination by boosting with modified vaccinia virus Ankara. *Nat. Med.* **4,** 397–402 (1998).
207. Gilbert, S. C. *et al.* Enhanced CD8 T cell immunogenicity and protective efficacy in a mouse malaria model using a recombinant adenoviral vaccine in heterologous prime-boost immunisation regimes. *Vaccine* **20,** 1039–1045 (2002).
208. Weiss, W. R. & Jiang, C. G. Protective CD8+ T lymphocytes in primates immunized with malaria sporozoites. *PLoS One* **7,** (2012).
209. Hoffman, S. L. *et al.* Sporozoite vaccine induces genetically restricted T cell elimination of malaria from hepatocytes. *Science* **244,** 1078–81 (1989).
210. Weiss, W. R., Sedegah, M., Beaudoin, R. L., Miller, L. H. & Good, M. F. CD8+ T cells

(cytotoxic/suppressors) are required for protection in mice immunized with malaria sporozoites. *Proc. Natl. Acad. Sci. U. S. A.* **85,** 573–576 (1988).
211. Ewer, K. J. *et al.* Protective CD8 + T-cell immunity to human malaria induced by chimpanzee adenovirus-MVA immunisation. *Nat. Commun.* **4,** (2013).
212. Ewer, K. *et al.* A Monovalent Chimpanzee Adenovirus Ebola Vaccine Boosted with MVA. *N. Engl. J. Med.* **374,** 1635–1646 (2016).
213. Aguado, M. T. & Lambert, P. H. Controlled-Release Vaccines-Biodegradable Polylactide/Polyglycolide (PL/PG) Microspheres as Antigen Vehicles. *Immunobiology* **184,** 113–125 (1992).
214. Makino, K. *et al.* Pulsatile drug release from poly (lactide-co-glycolide) microspheres: How does the composition of the polymer matrices affect the time interval between the initial burst and the pulsatile release of drugs? *Colloids Surfaces B Biointerfaces* **19,** 173–179 (2000).
215. Doty, A. C. *et al.* Mechanisms of in vivo release of triamcinolone acetonide from PLGA microspheres. *J. Control. Release* **256,** 19–25 (2017).
216. Doty, A. C. *et al.* Validation of a cage implant system for assessing in vivo performance of long-acting release microspheres. *Biomaterials* **109,** 88–96 (2016).
217. Tzeng, S. Y. *et al.* Thermostabilization of inactivated polio vaccine in PLGA-based microspheres for pulsatile release. *J. Control. Release* **233,** 101–113 (2016).
218. Kranz, H. & Bodmeier, R. Structure formation and characterization of injectable drug loaded biodegradable devices: In situ implants versus in situ microparticles. *Eur. J. Pharm. Sci.* **34,** 164–172 (2008).
219. Ahmed, T. A. *et al.* Biodegradable Injectable In Situ Implants and Microparticles for Sustained Release of Montelukast: In Vitro Release, Pharmacokinetics, and Stability. *AAPS PharmSciTech* **15,** 772–780 (2014).
220. Tao Meng, F., Hui Ma, G., Qiu, W. & Guo Su, Z. W / O / W double emulsion technique using ethyl acetate as organic solvent: effects of its diffusion rate on the characteristics of microparticles. *J. Control. Release* **91,** 407–416 (2003).
221. Pang, J. *et al.* Ibuprofen-loaded poly(lactic-co-glycolic acid) films for controlled drug release. *Int. J. Nanomedicine* **6,** 659–665 (2011).
222. Sanchez, A., Gupta, R. K., Alonso, M. J., Siber, G. R. & Langer, R. Pulsed controlled-release system for potential use in vaccine delivery. *J. Pharm. Sci.* **85,** 547–552 (1996).
223. Schoubben, A. *et al.* Novel composite microparticles for protein stabilization and delivery. *Eur. J. Pharm. Sci.* **36,** 226–234 (2009).
224. Rollier, C. S., Hill, A. V. S. & Reyes-Sandoval, A. Influence of adenovirus and MVA vaccines on the breadth and hierarchy of T cell responses. *Vaccine* **34,** 4470–4474 (2016).
225. Kemme, M., Prokesch, I. & Heinzel-Wieland, R. Comparative study on the enzymatic degradation of poly(lactic-co-glycolic acid) by hydrolytic enzymes based on the colorimetric quantification of glycolic acid. *Polym. Test.* **30,** 743–748 (2011).
226. Shield, A. Axis Shield. Available at: http://www.axis-shield-density-gradient-media.com/virusindexes.htm. (Accessed: 4th January 2018)
227. Zeiller, K., Löser, R., Pascher, G. & Hannig, K. Free-flow electrophoresis ii: Analysis of the method with respect to preparative cell separation. *Hoppe. Seylers. Z. Physiol. Chem.* **356,** 1225–1244 (1975).
228. Poggel, M. & Melin, T. Free-flow zone electrophoresis: A novel approach and scale-up for preparative protein separation. *Electrophoresis* **22,** 1008–1015 (2001).
229. Hoffstetter-Kuhn, S. & Wagner, H. Scale-up of free-flow electrophoresis: II. Purification of alcohol dehydrogenase from a crude yeast extract by field step electrophoresis and combined field step-zone electrophoresis. *Electrophoresis* **11,** 457–462 (1990).
230. Prusik, Z. *et al.* Correlation of capillary zone electrophoresis with continuous free-flow zone electrophoresis: Application to the analysis and purification of synthetic growth hormone releasing peptide. *Electrophoresis* **11,** 932–936 (1990).
231. Tabata, Y., Gutta, S. & Langer, R. Controlled Delivery Systems for Proteins Using Polyanhydride Microspheres. *Pharm. Res. An Off. J. Am. Assoc. Pharm. Sci.* **10,** 487–496

(1993).
232. Wischke, C. & Borchert, H. H. Influence of the primary emulsification procedure on the characteristics of small protein-loaded PLGA microparticles for antigen delivery. *J. Microencapsul.* **23,** 435–448 (2006).
233. Zhou, X. L. *et al.* Effect of NaCl in outer water phase on the characteristics of BSA-loaded PLGA sustained-release microspheres fabricated by a solid-in-oil-in-water emulsion technique. *Yaoxue Xuebao* **45,** 1057–1063 (2010).
234. Porjazoska, A. *et al.* Poly(lactide-co-glycolide) microparticles as systems for controlled release of proteins -- preparation and characterization. *Acta Pharm.* **54,** 215–229 (2004).
235. Yeo, Y. & Park, K. Control of encapsulation efficiency and initial burst in polymeric microparticle systems. *Arch. Pharm. Res.* **27,** 1–12 (2004).
236. Ravivarapu, H. B., Burton, K. & DeLuca, P. P. Polymer and microsphere blending to alter the release of a peptide from PLGA microspheres. *Eur. J. Pharm. Biopharm.* **50,** 263–270 (2000).
237. Ye, M., Kim, S. & Park, K. Issues in long-term protein delivery using biodegradable microparticles. *Journal of Controlled Release* **146,** 241–260 (2010).
238. Wang, J., Chua, K. M. & Wang, C. H. Stabilization and encapsulation of human immunoglobulin G into biodegradable microspheres. *J. Colloid Interface Sci.* **271,** 92–101 (2004).
239. Dielectric constants solvents. Available at: http://macro.lsu.edu/HowTo/solvents/Dielectric Constant .htm. (Accessed: 4th January 2018)
240. Quinn, M. J. & Ziolkowski, D. Wildlife Toxicity Assessment for Triacetin. in *Wildlife Toxicity Assessments for Chemicals of Military Concern* 291–301 (Elsevier, 2015). doi:10.1016/B978-0-12-800020-5.00017-X
241. Lerique, B., Lepetit-Thévenin, J., Vérine, A., Delpéro, C. & Boyer, J. Triacylglycerol in biomembranes. *Life Sci.* **54,** 831–40 (1994).
242. Vázquez, M. I., Rivas, G., Cregut, D., Serrano, L. & Esteban, M. The vaccinia virus 14-kilodalton (A27L) fusion protein forms a triple coiled-coil structure and interacts with the 21-kilodalton (A17L) virus membrane protein through a C-terminal alpha-helix. *J. Virol.* **72,** 10126–37 (1998).
243. Chung, C. S., Hsiao, J. C., Chang, Y. S. & Chang, W. A27L protein mediates vaccinia virus interaction with cell surface heparan sulfate. *J. Virol.* **72,** 1577–1585 (1998).
244. van de Weert, M., Hennink, W. E. & Jiskoot, W. Protein instability in poly(lactic-co-glycolic acid) microparticles. *Pharm. Res.* **17,** 1159–1167 (2000).
245. Zambaux, M. F., Bonneaux, F., Gref, R., Dellacherie, E. & Vigneron, C. Preparation and characterization of protein C-loaded PLA nanoparticles. *J. Control. Release* **60,** 179–188 (1999).
246. Hekker, A. C., Bos, J. M. & Smith, L. A stable freeze-dried smallpox vaccine made in monolayer cultures of primary rabbit kidney cells. *J. Biol. Stand.* **1,** 21–32 (1973).
247. Rollier, C. S., Reyes-Sandoval, A., Cottingham, M. G., Ewer, K. & Hill, A. V. S. Viral vectors as vaccine platforms: Deployment in sight. *Curr. Opin. Immunol.* **23,** 377–382 (2011).
248. Schuldt, N. J. & Amalfitano, A. Malaria vaccines: Focus on adenovirus based vectors. *Vaccine* **30,** 5191–5198 (2012).
249. Pol, J. *et al.* Trial watch: Oncolytic viruses for cancer therapy. *OncoImmunology* **3,** (2014).
250. Ghosh, S. S., Gopinath, P. & Ramesh, A. Adenoviral vectors: A promising tool for gene therapy. *Applied Biochemistry and Biotechnology* **133,** 9–29 (2006).
251. García del Barrio, G., Hendry, J., Renedo, M. ., Irache, J. M. & Novo, F. J. In vivo sustained release of adenoviral vectors from poly(d,l-lactic-co-glycolic) acid microparticles prepared by TROMS. *J. Control. Release* **94,** 229–235 (2004).
252. Wang, D. *et al.* Poly(D,L-lactic-co-glycolic acid) microsphere delivery of adenovirus for vaccination. *J. Pharm. Pharm. Sci. a Publ. Can. Soc. Pharm. Sci. Soci??t?? Can. des Sci. Pharm.* **10,** 217–230 (2007).
253. Sailaja, G., HogenEsch, H., North, A., Hays, J. & Mittal, S. K. Encapsulation of recombinant adenovirus into alginate microspheres circumvents vector-specific immune response. *Gene*

Ther. **9,** 1722–9 (2002).
254. Mittal, S. K. *et al.* Immunization with DNA, adenovirus or both in biodegradable alginate microspheres: effect of route of inoculation on immune response. *Vaccine* **19,** 253–263 (2000).
255. Kern, A., Zhou, C. W., Jia, F., Xu, Q. & Hu, L. T. Live-vaccinia virus encapsulation in pH-sensitive polymer increases safety of a reservoir-targeted Lyme disease vaccine by targeting gastrointestinal release. *Vaccine* **34,** 4507–4513 (2016).
256. Jain, R. a, Rhodes, C. T., Railkar, a M., Malick, a W. & Shah, N. H. Controlled delivery of drugs from a novel injectable in situ formed biodegradable PLGA microsphere system. *J. Microencapsul.* **17,** 343–362 (1998).
257. Jain, R. A., Rhodes, C. T., Railkar, A. M., Malick, A. W. & Shah, N. H. Controlled release of drugs from injectable in situ formed biodegradable PLGA microspheres: Effect of various formulation variables. *Eur. J. Pharm. Biopharm.* **50,** 257–262 (2000).
258. Katz, E. & Moss, B. Formation of a vaccinia virus structural polypeptide from a higher molecular weight precursor: inhibition by rifampicin. *Proc. Natl. Acad. Sci. U. S. A.* **66,** 677–84 (1970).
259. Eterpi, M., McDonnell, G. & Thomas, V. Virucidal activity of disinfectants against parvoviruses and reference viruses. *Appl. Biosaf.* **15,** 165–171 (2010).
260. Guler, S. D. *et al.* Effects of ether vs. ester linkage on lipid bilayer structure and water permeability. *Chem. Phys. Lipids* **160,** 33–44 (2009).
261. Mahboubian, A., Hashemein, S. K., Moghadam, S., Atyabia, F. & Dinarvand, R. Preparation and in-vitro evaluation of controlled release PLGA microparticles containing triptoreline. *Iran. J. Pharm. Res.* **9,** 369–378 (2010).
262. Araùjo, M., Hube, L. A. & Stasyk, T. Isolation of Endocitic Organelles by Density Gradient Centrifugation. in *Methods in molecular biology (Clifton, N.J.)* **424,** 317–331 (2008).
263. Peyret, H. A protocol for the gentle purification of virus-like particles produced in plants. *Journal of Virological Methods* **225,** 59–63 (2015).
264. Harrison, S. C. *et al.* Discovery of antivirals against smallpox. *Proc. Natl. Acad. Sci. U. S. A.* **101,** 11178–11192 (2004).
265. Parsons, H. T. Preparation of highly enriched ER membranes using free-flow electrophoresis. in *Methods in Molecular Biology* **1691,** 103–115 (2018).
266. De Michele, R. *et al.* Free-Flow Electrophoresis of Plasma Membrane Vesicles Enriched by Two-Phase Partitioning Enhances the Quality of the Proteome from Arabidopsis Seedlings. *J. Proteome Res.* **15,** 900–913 (2016).
267. Ulanova, L. S. *et al.* Development of methods for encapsulation of viruses into polymeric nano- and microparticles for aquaculture vaccines. *J. Appl. Polym. Sci.* **131,** 8785–8796 (2014).
268. Baer, A. & Kehn-Hall, K. Viral Concentration Determination Through Plaque Assays: Using Traditional and Novel Overlay Systems. *J. Vis. Exp.* (2014). doi:10.3791/52065
269. ånestad, G. Surveillance of respiratory viral infections by rapid immunofluorescence diagnosis, with emphasis on virus interference. *Epidemiol. Infect.* **99,** 523–531 (1987).
270. Roldão, A., Oliveira, R., Carrondo, M. J. T. & Alves, P. M. Error assessment in recombinant baculovirus titration: Evaluation of different methods. *J. Virol. Methods* **159,** 69–80 (2009).
271. Watzinger, F. *et al.* Real-time quantitative PCR assays for detection and monitoring of pathogenic human viruses in immunosuppressed pediatric patients. *J. Clin. Microbiol.* **42,** 5189–5198 (2004).
272. Zaaijer, H. L. *et al.* Reliability of the third???generation recombinant immunoblot assay for hepatitis C virus. *Transfusion* **35,** 745–749 (1995).
273. Filice, G. *et al.* Sensitivity and specificity of anti-HIV ELISA employing recombinant (p24, p66, gp120) and synthetic (gp41) viral antigenic peptides. *Microbiologica* **14,** 185–94 (1991).
274. Bernstein, J. M. & Hruska, J. F. Respiratory syncytial virus proteins: identification by immunoprecipitation. *J. Virol.* **38,** 278–85 (1981).
275. Hirst, G. K. THE QUANTITATIVE DETERMINATION OF INFLUENZA VIRUS AND ANTIBODIES BY MEANS OF RED CELL AGGLUTINATION. *J. Exp. Med.* **75,** 49–64

(1942).
276. Shen, C. F., Meghrous, J. & Kamen, A. Quantitation of baculovirus particles by flow cytometry. *J. Virol. Methods* **105,** 321–330 (2002).
277. Goldsmith, C. S. & Miller, S. E. Modern uses of electron microscopy for detection of viruses. *Clinical Microbiology Reviews* **22,** 552–563 (2009).
278. Baker, J. L. & Ward, B. M. Development and comparison of a quantitative TaqMan-MGB real-time PCR assay to three other methods of quantifying vaccinia virions. *J. Virol. Methods* **196,** 126–132 (2014).
279. Kulesh, D. A. *et al.* Smallpox and pan-Orthopox Virus Detection by Real-Time 3???-Minor Groove Binder TaqMan Assays on the Roche LightCycler and the Cepheid Smart Cycler Platforms. *J. Clin. Microbiol.* **42,** 601–609 (2004).
280. Brussaard, C. P. D., Marie, D. & Bratbak, G. Flow cytometric detection of viruses. *J. Virol. Methods* **85,** 175–182 (2000).
281. Mackay, I. M. Real-time PCR in virology. *Nucleic Acids Res.* **30,** 1292–1305 (2002).
282. Gurukumar, K. R. *et al.* Development of real time PCR for detection and quantitation of dengue viruses. *Virol. J.* **6,** 10 (2009).
283. Park, J. S., Lim, H. J., Yi, S. W. & Park, K. H. Stem cell differentiation-related protein-loaded PLGA microspheres as a novel platform micro-typed scaffold for chondrogenesis. *Biomed. Mater.* **11,** (2016).
284. Biosystems, A. qPCR quidelines.
285. Ståhlberg, A., Aman, P., Ridell, B., Mostad, P. & Kubista, M. Quantitative real-time PCR method for detection of B-lymphocyte monoclonality by comparison of kappa and lambda immunoglobulin light chain expression. *Clin. Chem.* **49,** 51–9 (2003).
286. Biosystems, A. TAMRA. Available at: https://www.thermofisher.com/cy/en/home/products-and-services/product-types/primers-oligos-nucleotides/applied-biosystems-custom-primers-probes/custom-taqman-probes/taqman-tamra-probes.html. (Accessed: 4th January 2018)
287. Kutyavin, I. V *et al.* 3'-minor groove binder-DNA probes increase sequence specificity at PCR extension temperatures. *Nucleic Acids Res.* **28,** 655–61 (2000).
288. Biosystems, A. MGB. Available at: https://www.thermofisher.com/cy/en/home/products-and-services/product-types/primers-oligos-nucleotides/applied-biosystems-custom-primers-probes/custom-taqman-probes/taqman-mgb-probes.html. (Accessed: 4th January 2018)
289. Technologies, I. MGB Tm. Available at: https://eu.idtdna.com/pages/decoded/decoded-articles/product-spotlight/decoded/2012/01/10/qpcr-probes-high-tms-without-sacrificing-quenching. (Accessed: 4th January 2018)
290. Bustin, S. A. & Nolan, T. Pitfalls of quantitative real-time reverse-transcription polymerase chain reaction. *J. Biomol. Tech.* **15,** 155–66 (2004).
291. Izreli, S., Pfleiderer, C. & Lion, T. Detection of gene expression by PCR amplification of RNA derived from frozen heparinized whole blood. *Nucleic Acids Res.* **19,** 6051 (1991).
292. Rossen, L., Nørskov, P., Holmstrøm, K. & Rasmussen, O. F. Inhibition of PCR by components of food samples, microbial diagnostic assays and DNA-extraction solutions. *Int. J. Food Microbiol.* **17,** 37–45 (1992).
293. Nolan, T., Hands, R. E., Ogunkolade, W. & Bustin, S. A. SPUD: A quantitative PCR assay for the detection of inhibitors in nucleic acid preparations. *Anal. Biochem.* **351,** 308–310 (2006).
294. Lemke, C. D., Geary, S. M., Joshi, V. B. & Salem, A. K. Antigen-coated poly α-hydroxy acid based microparticles for heterologous prime-boost adenovirus based vaccinations. *Biomaterials* **34,** 2524–9 (2013).
295. Taghipour, B., Yakhchali, M., Haririan, I., Tamaddon, A. M. & Samani, S. M. The effects of technical and compositional variables on the size and release profile of bovine serum albumin from PLGA based particulate systems. *Res. Pharm. Sci.* **9,** 407–420 (2014).
296. Fu, X., Ping, Q. & Gao, Y. Effects of formulation factors on encapsulation efficiency and release behaviour in vitro of huperzine A-PLGA microspheres. *J. Microencapsul.* **22,** 705–714 (2005).
297. Sah, E. & Sah, H. Recent trends in preparation of poly(lactide-co-glycolide) nanoparticles by

mixing polymeric organic solution with antisolvent. *Journal of Nanomaterials* **2015,** (2015).
298. Cruz, S. Solubility of triacetin. Available at: https://www.scbt.com/scbt/product/glyceryl-triacetate-102-76-1. (Accessed: 5th January 2018)
299. Rawat, A. & Burgess, D. J. Effect of ethanol as a processing co-solvent on the PLGA microsphere characteristics. *Int. J. Pharm.* **394,** 99–105 (2010).
300. Hussain, M. *et al.* Regulation of Drug Release by Tuning Surface Textures of Biodegradable Polymer Microparticles. *ACS Appl. Mater. Interfaces* **9,** 14391–14400 (2017).
301. Rabenau, H. F., Rapp, I. & Steinmann, J. Can vaccinia virus be replaced by MVA virus for testing virucidal activity of chemical disinfectants? *BMC Infect. Dis.* **10,** (2010).
302. McHugh, K. J. *et al.* Fabrication of fillable microparticles and other complex 3D microstructures. *Science (80-.).* **357,** 1138–1142 (2017).
303. Geiben-Lynn, R., Greenland, J. R., Frimpong-Boateng, K. & Letvin, N. L. Kinetics of recombinant adenovirus type 5, vaccinia virus, modified vaccinia ankara virus, and DNA antigen expression in vivo and the induction of memory T-lymphocyte responses. *Clin. Vaccine Immunol.* **15,** 691–696 (2008).
304. Longley, R. J. *et al.* Comparative assessment of vaccine vectors encoding ten malaria antigens identifies two protective liver-stage candidates. *Sci. Rep.* **5,** (2015).
305. Ding, A. G. & Schwendeman, S. P. Acidic microclimate pH Distribution in PLGA microspheres monitored by confocal laser scanning microscopy. *Pharm. Res.* **25,** 2041–2052 (2008).
306. Wang, Z. *et al.* Recombinant modified vaccinia virus Ankara expressing a soluble form of glycoprotein B causes durable immunity and neutralizing antibodies against multiple strains of human cytomegalovirus. *J. Virol.* **78,** 3965–76 (2004).
307. Kafuye-Mlwilo, M. Y., Mukherjee, P. & Chauhan, V. S. Kinetics of humoral and memory B cell response induced by the plasmodium falciparum 19-kilodalton merozoite surface protein 1 in mice. *Infect. Immun.* **80,** 633–642 (2012).
308. Cook, S. H. & Griffin, D. E. Luciferase imaging of a neurotropic viral infection in intact animals. *J. Virol.* **77,** 5333–5338 (2003).
309. Kim, J. S. *et al.* In vivo NIR imaging with CdTe/CdSe quantum dots entrapped in PLGA nanospheres. *J. Colloid Interface Sci.* **353,** 363–371 (2011).
310. Gao, X. *et al.* In vivo molecular and cellular imaging with quantum dots. *Current Opinion in Biotechnology* **16,** 63–72 (2005).
311. Champion, J. A., Walker, A. & Mitragotri, S. Role of particle size in phagocytosis of polymeric microspheres. *Pharm. Res.* **25,** 1815–1821 (2008).
312. Hirota, K. *et al.* Optimum conditions for efficient phagocytosis of rifampicin-loaded PLGA microspheres by alveolar macrophages. *J. Control. Release* **119,** 69–76 (2007).
313. Jewell, C. M., Bustamante Lopez, S. C. & Irvine, D. J. In situ engineering of the lymph node microenvironment via intranodal injection of adjuvant-releasing polymer particles. *Proc. Natl. Acad. Sci.* **108,** 15745–15750 (2011).
314. Andorko, J. I., Tostanoski, L. H., Solano, E., Mukhamedova, M. & Jewell, C. M. Intra-lymph Node Injection of Biodegradable Polymer Particles. *J. Vis. Exp.* (2014). doi:10.3791/50984
315. O'Hagan, D. T. & Singh, M. Microparticles as vaccine adjuvants and delivery systems. *Expert Rev. Vaccines* **2,** 269–83 (2003).
316. Lambe, T. *et al.* Immunity against heterosubtypic influenza virus induced by adenovirus and mva expressing nucleoprotein and matrix protein-1. *Sci. Rep.* **3,** (2013).
317. Bacakova, L., Filova, E., Parizek, M., Ruml, T. & Svorcik, V. Modulation of cell adhesion, proliferation and differentiation on materials designed for body implants. *Biotechnology Advances* **29,** 739–767 (2011).
318. Stevens, M. M. & George, J. H. Exploring and engineering the cell surface interface. *Science* **310,** 1135–1138 (2005).
319. Schrade, A., Mailänder, V., Ritz, S., Landfester, K. & Ziener, U. Surface Roughness and Charge Influence the Uptake of Nanoparticles: Fluorescently Labeled Pickering-Type Versus Surfactant-Stabilized Nanoparticles. *Macromol. Biosci.* **12,** 1459–1471 (2012).

320. Agrawal, C. M. & Athanasiou, K. A. Technique to control pH in vicinity of biodegrading PLA-PGA implants. *J. Biomed. Mater. Res.* **38,** 105–114 (1997).
321. Fu, K., Pack, D. W., Klibanov, A. M. & Langer, R. Visual evidence of acidic environment within degrading poly(lactic-co- glycolic acid) (PLGA) microspheres. *Pharm. Res.* **17,** 100–106 (2000).
322. Alcock, R. *et al.* Long-term thermostabilization of live poxviral and adenoviral vaccine vectors at supraphysiological temperatures in carbohydrate glass. *Sci. Transl. Med.* **2,** (2010).
323. Hale, J. M. A Study of the pH Stability of Vaccinia Virus. *Yale J. Biol. Med.* **15,** 241–58 (1942).
324. Kosco-Vilbois, M. H., Imhof, B. A., Kosco-Vilbois, M. H. & Imhof, B. A. In vivo veritas. *Immunol. Today* **21,** 64–5 (2000).
325. Zhu, G., Mallery, S. R. & Schwendeman, S. P. Stabilization of proteins encapsulated in injectable poly (lactide-co- glycolide). *Nat. Biotechnol.* **18,** 52–57 (2000).
326. Xu, Q. *et al.* Preparation of monodisperse biodegradable polymer microparticles using a microfluidic flow-focusing device for controlled drug delivery. *Small* **5,** 1575–1581 (2009).
327. Valo, H. *et al.* Electrospray encapsulation of hydrophilic and hydrophobic drugs in poly(L-lactic acid) nanoparticles. *Small* **5,** 1791–1798 (2009).
328. Xie, J., Lim, L. K., Phua, Y., Hua, J. & Wang, C. H. Electrohydrodynamic atomization for biodegradable polymeric particle production. *J. Colloid Interface Sci.* **302,** 103–112 (2006).
329. Barron, C. & He, J. Q. Alginate-based microcapsules generated with the coaxial electrospray method for clinical application. *Journal of Biomaterials Science, Polymer Edition* **28,** 1245–1255 (2017).
330. Gasperini, L., Mano, J. F. & Reis, R. L. Natural polymers for the microencapsulation of cells. *J. R. Soc. Interface* **11,** 20140817–20140817 (2014).
331. Bartolovic, K., Mongkoldhumrongkul, N., Waddington, S. N., Jayasinghe, S. N. & Howe, S. J. The differentiation and engraftment potential of mouse hematopoietic stem cells is maintained after bio-electrospray. *Analyst* **135,** 157–164 (2010).
332. Mizuno, A. *et al.* Inactivation of viruses using pulsed high electric field. *Ind. Appl. Soc. Annu. Meet. 1990., Conf. Rec. 1990 IEEE* 713–719 vol.1 (1990). doi:10.1109/IAS.1990.152263
333. Milligan, I. D. *et al.* Safety and Immunogenicity of Novel Adenovirus Type 26– and Modified Vaccinia Ankara–Vectored Ebola Vaccines. *JAMA* **315,** 1610 (2016).
334. Fukuhara, H., Ino, Y. & Todo, T. Oncolytic virus therapy: A new era of cancer treatment at dawn. *Cancer Sci.* **107,** 1373–1379 (2016).
335. Cook, M. T., Tzortzis, G., Charalampopoulos, D. & Khutoryanskiy, V. V. Microencapsulation of a synbiotic into PLGA/alginate multiparticulate gels. *Int. J. Pharm.* **466,** 400–408 (2014).
336. Kartoglu, U. & Milstien, J. Tools and approaches to ensure quality of vaccines throughout the cold chain. *Expert Review of Vaccines* **13,** 843–854 (2014).
337. Milstien, J. B., Galazka, A. M., Kartoglu, U. & Zaffran, M. Temperature sensitivity of vaccines. *World Heal. Organ. Dept Immunization, Vaccines Biol.* 1–58 (2006). doi:WHO/IVB/06.10
338. McNally, A. K. & Anderson, J. M. Macrophage fusion and multinucleated giant cells of inflammation. *Adv. Exp. Med. Biol.* **713,** 97–111 (2011).
339. Luttikhuizen, D. T., Harmsen, M. C. & Van Luyn, M. J. A. Cellular and molecular dynamics in the foreign body reaction. *Tissue Eng.* **12,** 1955–1970 (2006).
340. Gretzer, C., Emanuelsson, L., Liljensten, E. & Thomsen, P. The inflammatory cell influx and cytokines changes during transition from acute inflammation to fibrous repair around implanted materials. *J. Biomater. Sci. Polym. Ed.* **17,** 669–687 (2006).